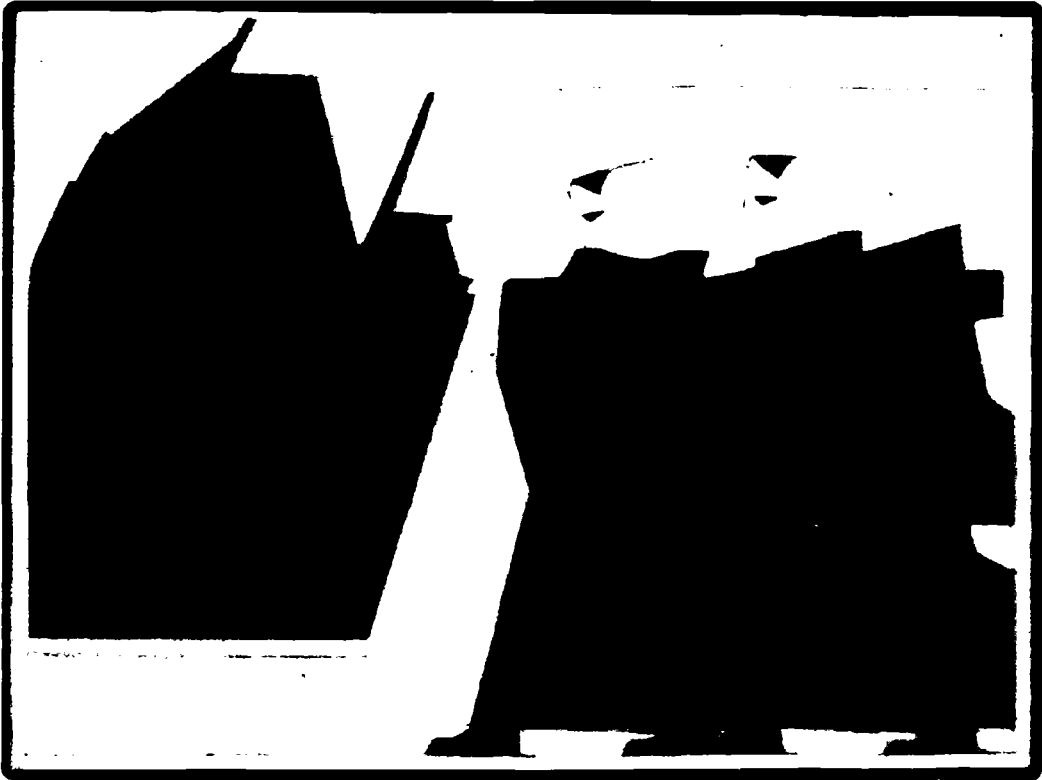


Green Water on Ship-type Offshore Structures



**Delft University of Technology
Ship Hydromechanics Laboratory
Library**

**Mekelweg 2, 2628 CD Delft
The Netherlands**

Phone: +31 15 2786873 - Fax: +31 15 2781836

Bas Buchner

Green Water

on

Ship-type Offshore Structures

On the cover:

'The Tempest', Bart van der Leck, 1916

120 x 60 cm, oil painting

Kröller-Müller Museum

©*Bart van der Leck, The Tempest, 2002 c/o Beeldrecht Hoofddorp*

Printed by:

Grafisch Bedrijf Ponsen & Looijen bv, Wageningen, The Netherlands

Green Water

on

Ship-type Offshore Structures

Proefschrift

ter verkrijging van de graad van doctor
aan de Technische Universiteit Delft,
op gezag van de Rector Magnificus Prof. dr. ir. J.T. Fokkema,
voorzitter van het College van Promoties,
in het openbaar te verdedigen op dinsdag 5 november 2002 te 16.00 uur

door

Bastiaan BUCHNER

scheepsbouwkundig ingenieur
geboren te Sliedrecht

Dit proefschrift is goedgekeurd door de promotor:

Prof.dr.ir. J.A. Pinkster

Samenstelling promotiecommissie:

Rector Magnificus,	voorzitter
Prof.dr.ir. J.A. Pinkster,	Technische Universiteit Delft, promotor
Prof.ir. J. Meek,	Technische Universiteit Delft
Prof. A. Incecik,	University of Newcastle
Prof. J. Juncher Jensen,	Technical University of Denmark
Prof.dr. A.E.P. Veldman,	Rijksuniversiteit Groningen
Prof.dr.ir. A.J. Hermans,	Technische Universiteit Delft
Dr.ing. C.T. Stansberg,	Marintek

ISBN: 90-4646-883-X

Copyright © Bas Buchner, 2002. All rights reserved.

***“And behold, there arose a great storm on the sea,
so that the boat was being swamped by the waves...”***

Matthew 8.24

CONTENTS

1. INTRODUCTION	1
1.1 The problem	1
1.1.1 The problem of 'green water'	1
1.1.2 The problem of green water for ship-type offshore units	2
1.2 Historical overview of green water research	5
1.2.1 Early studies	5
1.2.2 Experimental studies, focussing on relative wave motions	5
1.2.3 Experimental studies, focussing on loads on deck	6
1.2.4 Effect of bow shapes	7
1.2.5 Stability of fishing vessels	8
1.2.6 Prediction methods	8
1.3 Problem definition and objective of this study	9
1.4 Outline of the thesis	10
1.5 Model tests and their interpretation	11
2. THE PHYSICS OF GREEN WATER ON THE BOW	13
2.1 Introduction	13
2.2 Model tests	14
2.2.1 Test Series A: Pilot tests FPSO with traditional full bow	14
2.2.2 Test Series B: Comparative tests traditional full bow and alternative thin bow	16
2.3 Observations	17
2.3.1 Visualisation techniques applied	17
2.3.2 Summary of observations	20
2.4 Motions and relative wave motions	22
2.4.1 Ship motions	23
2.4.2 Relative wave motions	28
2.5 Water flow onto the deck	33
2.6 Effect of above water hull shape	34
2.7 Water behaviour and loading on the deck	35
2.8 Green water impact on structures	39
2.9 Summary of the physics of green water on the bow	43
3. SYSTEMATIC MODEL TESTING	45
3.1 Introduction	45
3.2 Structure of the semi-empirical design evaluation method	46
3.3 Systematic model series	47
3.3.1 Bow shape variations	48
3.3.2 Bow flare variations	49
3.3.3 Stern shapes	50
3.3.4 Summary of basic hull models	51
3.4 Structures at the bow	51
3.5 Protective breakwaters	53
3.6 Set-up: soft spring mooring system	53

3.7	Environmental conditions	54
3.8	Analysis of combined extremes	55
4.	NON-LINEAR RELATIVE WAVE MOTIONS AT THE BOW	57
4.1	Introduction	57
4.2	Description of non-linearities	58
4.3	Physical background of non-linearities	63
4.3.1	The effect of the water on deck on the ship motions	64
4.3.2	The effect of the above water hull shape	65
4.3.3	The effect of the non-linearity in the waves	68
4.4	Review of existing descriptions of non-linearities	69
4.5	Proposed method for the prediction of relative wave motion extremes	72
4.5.1	Introduction	72
4.5.2	Relative wave motions below the freeboard	73
4.5.3	Relative wave motions above the freeboard	77
4.6	Validation of the developed expression	84
4.6.1	Variations available for validation	84
4.6.2	Validation results	85
4.7	Effect of current	86
4.8	Summary of the development of the modified Rayleigh distribution	90
5.	WATER FLOW ONTO AND ON THE BOW DECK	93
5.1	Introduction	93
5.2	Observation of the flow onto the deck for different flare angles	94
5.3	Relation between relative motions and water height on the deck	95
5.4	Flow patterns and velocities over the deck	102
6.	GREEN WATER IMPACT LOADING	109
6.1	Introduction	109
6.2	Relation freeboard exceedance and impact loading	110
6.3	Vertical and horizontal load profiles	122
6.3.1	Vertical load profile	122
6.3.2	Horizontal load profile	129
6.4	Effect of structural shape on impact loading	130
6.4.1	Method	130
6.4.2	Direct comparison between the different structural shapes	135
6.5	Effect of distance from the forward perpendicular	136
6.6	Summary of load prediction procedure for structures on the deck	137
6.7	Efficiency of protecting breakwaters	138
6.7.1	Design considerations	138
6.7.2	Observations	138
6.7.3	Quantification of breakwater efficiency	139
6.7.4	Loading on the breakwater	141

7.	GREEN WATER FROM THE SIDE AND STERN	143
7.1	Introduction	143
7.2	Model tests	144
7.3	Observations of relative wave motions along the side	145
7.4	Relative wave motions along the side of a hull	145
7.4.1	Calculated linear relative wave motions	145
7.4.2	Measured non-linear relative motions along the side	146
7.5	Physical background of observed behaviour	147
7.6	Description of non-linear relative wave motions	149
7.7	Green water flow and loading from the side	153
7.7.1	Transverse water flow onto the deck	153
7.7.2	Hydraulic models for green water flow from the side	155
7.7.3	Green water loading from the side on slender structures on the deck	158
7.8	Green water in stern area	162
7.8.1	Traditional tanker sterns with a relatively low freeboard	164
7.8.2	New design full and flat sterns with a high freeboard	164
8.	REVIEW AND APPLICATION OF THE METHOD	167
8.1	Introduction	167
8.2	Range of applicability of the method	169
8.3	Coupling with specific metocean data	172
8.3.1	Use of the contour of joint probabilities of wave height and period	172
8.3.2	Determination of the extreme heading angle with respect to the waves	174
8.4	Dynamic structural response	174
9.	NUMERICAL PREDICTION OF GREEN WATER	179
9.1	Introduction	179
9.2	Requirements for numerical methods	180
9.3	Evaluation of existing numerical methods	181
9.3.1	General	181
9.3.2	Method using height functions: Glimm's method	181
9.3.3	Method using line segments: non-linear boundary integral method	184
9.3.4	Method using fluid regions: VOF	188
9.3.5	Evaluation of a modified-VOF method	189
9.4	Mathematical and numerical model of the modified-VOF method	190
9.4.1	Mathematical model	190
9.4.2	Numerical model: geometry and free surface description	190
9.4.3	Discretisation of the Navier-Stokes equations	192
9.4.4	Other aspects in the numerical model	194

9.5	Case study 1: Flow onto a deck with impact on different structural shapes	195
9.5.1	General	195
9.5.2	Computational domain and initial conditions	195
9.5.3	Results	197
9.6	Case study 2: Water entry of a 2D wedge	202
9.6.1	General	202
9.6.2	Model tests	203
9.6.3	Modified-VOF simulation model	205
9.6.4	Results	205
9.7	Evaluation of Modified-VOF method related to the green water problem	209
9.8	Possibilities for the present application of the Modified-VOF method	210
10.	CONCLUSIONS AND RECOMMENDATIONS	213
10.1	Summary of objective	213
10.2	Conclusions	213
10.3	Recommendations for further research	217
	APPENDIX I: SCALING OF GREEN WATER PHYSICS	219
	APPENDIX II: EFFECT OF STRUCTURAL ELASTICITY	223
	APPENDIX A: Pilot tests traditional full bow (Test Series A)	235
	APPENDIX B: Comparative tests traditional full bow and alternative thin bow (Test Series B)	239
	APPENDIX C: Systematic test series with different hull shapes and flare angles (Test Series C)	243
	APPENDIX D: Pilot tests green water from the side (Test Series D)	257
	REFERENCES	259
	NOMENCALTURE	267
	SUMMARY	273
	SAMENVATTING	275
	ACKNOWLEDGEMENTS	277
	CURRICULUM VITAE	279

1. INTRODUCTION

1.1 The problem

1.1.1 The problem of 'green water'

In heavy storms, the waves and ship motions can become so large that water flows onto the deck of a ship. This problem is known as 'shipping of water', 'deck wetness' or 'green water loading'. The term 'green water' is used to distinguish between the spray (small amounts of water and foam) flying around and the real solid seawater on the deck. Because seawater is rather green than blue, the term 'green water' is widely used.

For a long time already, green water has been considered to be an important problem for the safety and operability of naval and merchant vessels. Tan (1969) noted that shipping of water was the most important reason for changing course and speed for Dutch merchant ships in order to avoid serious damage to the ships or their deck loads. Also the widely known accident with M.V. Derbyshire has shown the destructive force of green water loading and its fatal consequences, see for instance Faulkner (2001).

The same applies to naval vessels. Andrew and Lloyd (1980) quote Captain D. MacIntyre from his book 'The Battle of the Atlantic': "Their hulls whipped and shuddered in the huge Atlantic seas...solid green water swept destructively along their decks...For hour after hour this process repeated itself. Damage mounted, hull plates splitting, boats being smashed, men swept overboard and delicate anti-submarine devices put out of order..."

1.1.2 The problem of green water for ship-type offshore units

In recent decades the use of ship-type offshore units for the production and storage of oil has become a common method, even in harsh environments. Moored permanently at a certain location at sea, these Floating Production Storage and Offloading (FPSO) units should be able to survive the most critical environmental conditions occurring, see Photo 1-1.

This requires an adequate mooring system, but also attention to the problem of possible green water on the deck. Where tankers have an almost empty deck, FPSO decks per definition carry a lot of sensitive equipment. Because FPSOs are generally connected to their mooring system with a rotating turret at the bow, important equipment is also present close to the bow. Furthermore, the rotating turret results in a weather-vaning character of the vessel, exposing the bow to the most critical wave conditions. Consequently green water can cause damage to its equipment, such as the fluid swivels, piping, turret structure, control valves, emergency systems, fire detection/protection systems and cable trays. For FPSO units with the superstructure at the bow, the same applies to the front of the superstructure.

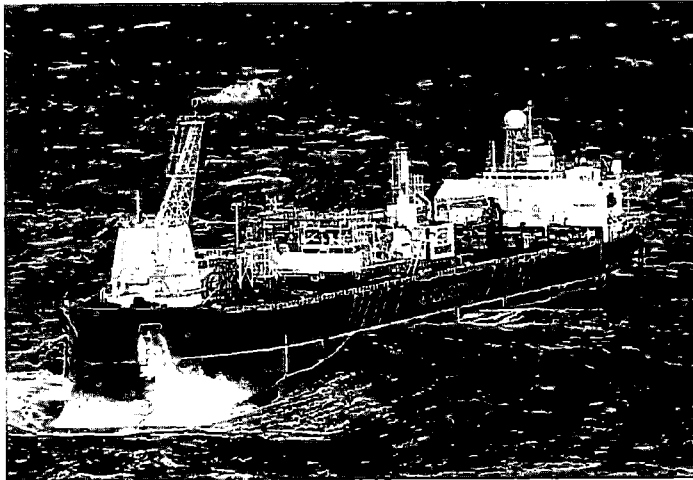


Photo 1-1
FPSO in heavy storm in the North Sea
(Courtesy Bluewater Energy Services)

Recent experience in the North Sea with UK and Norwegian FPSOs confirms the importance of the green water problem. As reported by Morris, Millar and Buchner (2000), from 1995 to date 17 green water incidents have been identified on 12 UK FPSOs/FSUs (Floating Storage Units). Some installations have experienced more than one incident. In a winter storm in January 1995 damage occurred for instance on the Emerald FSU, resulting in the destruction of a fire-fighting platform, as shown in the Photo 1-2.

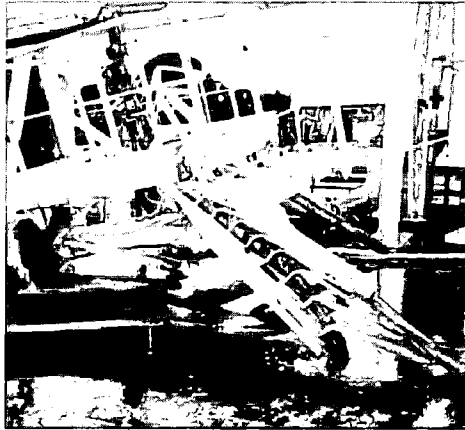


Photo 1-2

Damaged fire-fighting platform, completely pushed over by green water

Moreover, the Norwegian FPSOs also experienced damage, as reported by Ersdal and Kvitrud (2000). In January 2000 the living quarters on the bow of the Varg FPSO was hit by green water. This resulted in the damage of a window at the second floor, flooding the area behind it. The vessel was designed for green water loading, but an incorrect arrangement of the window resulted in the damage. The situation after the initial repair is shown in Photo 1-3.

It was also found that in slightly non-collinear wind, waves and current conditions, green water can come on the deck from the sides of the ship. As reported by Vestbøstad (1999), green water from the side of the Norne FPSO resulted in some minor damage to the piping system in 1998 (March 19). Evaluation of the vessel showed that also the bow was vulnerable to green water. This resulted in operational draft restrictions to minimise the chance of shipping green water. Photo 1-4 illustrates the green water loads that can be experienced by structures placed close to the side in heavy storms. On this FPSO two containers have clearly shifted from their initial position after being hit by green water from the side.

Finally, green water has been observed at the stern, particularly in the case of traditional converted tankers with no poop deck.



*Photo 1-3
Damage and first repair of a window on the Varg FPSO superstructure
(Courtesy PGS / Norsk Hydro)*



*Photo 1-4
Shifted containers after they have been hit by green water from the side*

This overview makes clear that FPSOs, designed according to existing class rules and regulations, still suffer from green water loading damage.

1.2 Historical overview of green water research

1.2.1 Early studies

Green water (or 'deck wetness') has been the subject of study and debate since the early days of research into ship behaviour at the end of the Nineteenth Century. However, the work by Newton (1959) is generally seen as the first large systematic study in this field. He fitted a destroyer with 5 different above-water bow forms and tested in regular head waves. His investigations were mainly based on visual observations of the deck wetness, which he categorised as 'dry', 'wet' or 'very wet'.

Also testing in regular head waves, Tasaki (1963) investigated the green water problem by measuring the amount of shipped water with a special water collection mechanism in his model. He pointed out the importance of the static and dynamic swell-up in front of the bow, as important factors in the relative wave motions.

Another important contribution came from Ochi (1964), who applied his statistical methods to the prediction of slamming and shipping of green water. He assumed that an exceedance of the freeboard by the relative wave motions resulted in the same height of green water on the deck and that the pressure on the deck was equal to the static water head.

1.2.2 Experimental studies, focussing on relative wave motions

In later years, a number of experimental studies have been carried out, focussing on the bows of naval and merchant vessels.

Some looked mainly to the relative wave motions, such as the work of Hoffman and Maclean (1970) and the studies presented by Hong, Lee and Gong (1993) and by Gu, Miao and Gu (1993). In general these methods were based on relative wave motion predictions with linear strip theory, corrected for the dynamic swell-up: the effect of water being pushed up around the bow, higher than can be accounted for by considering only heave and pitch motions versus the undisturbed incident wave. For the origin of the concept of dynamic swell-up, generally reference is made to Tasai (1961). Blok and Huisman (1984) investigated this concept in detail, using also free running tests in calm water to determine sinkage, trim and the static bow wave, captive tests to determine wave reflections and oscillation tests to determine radiated wave effects. Generally a swell-up-coefficient (SUC) is determined based on empirical data (Gu, Miao and Gu, 1993), which is used to correct the Response Amplitude Operator (RAO) of the relative wave motions for the effect of the dynamic swell-up of a specific hull shape.

A number of authors used this concept to come to recommendations for freeboard heights, based on the main vessel parameters and environmental conditions. Bales (1979) formulated minimum freeboard requirements for dry foredecks. Takaki and Takaishi (1993) developed an expression for the evaluation of the 1966 Load Line Convention based on the response characteristics of 67 existing ships, using a similar method.

In Watanabe, Ueno and Sawada (1989) and Watanabe (1990) a thorough study into the relative wave motions and deck wetness for a container ship is presented. They found a wave height dependence of the relative wave motion Response Amplitude Operators in regular waves. In irregular waves they identified a clear deviation of the distribution of extremes from the linear narrow banded Rayleigh distribution and a concentration of amplitudes at approximately the freeboard height.

1.2.3 Experimental studies, focussing on loads on deck

The loading of green water on forecastle decks and hatch covers has long been a major point of concern for merchant vessels. Consequently, a number of authors focussed their experimental research on this topic.

Fukuda, Ikegami and Mori (1973) developed a predicting method for the long term trends of the loads on the deck, based on the assumption that the load on the deck is given by the water head in excess of the freeboard.

However, this assumption is not supported by experiments of others. Kawakami (1969) for instance reported measured peak loads on the forecastle deck of 50 t/m^2 ($\sim 500 \text{ kPa}$) full scale in his tests in regular head waves, much higher than the static water head. The prediction method he developed is based on the assumption that piled up spray and swell-up waves around the bow are actually falling on the deck, resulting in impulsive pressures. A similar assumption was made by Takezawa, Hagino, Kobayashi and Sawada (1977). In later work Kawakami and Tanaka (1975, 1977) extended their work to a general expression for the impact pressure on the deck. This pressure is a function of draft, relative wave motion amplitude (including dynamic swell-up) and freeboard corrected for static swell-up.

According to Hansen (1972) the pressure on the deck is higher than the static water head because the vertical acceleration of the deck should be added to the gravity acceleration to find the correct pressure. He assumes in his calculation that the water height on the deck is equal to the undisturbed wave contour.

In a study evaluating existing green water methods with their assumptions, Buchner (1994) performed model tests in regular and irregular waves with a frigate of the Royal Netherlands Navy.

He observed a very strong dynamic amplification of the pressure on the deck of the frigate with respect to the static water head. A maximum amplification of 15.5 was found. He derived a new calculation method for the pressure of the water on the deck, based on the evaluation of Newton's momentum relations for a control volume on the deck. This accounts for the static water head, the vertical acceleration of the deck and an additional term related to the combination of vertical velocity of the deck and the rate of change of water height on the deck. This last term results in the large peak loads ('dynamic amplifications') observed. The method will be used in the present thesis and was validated by work carried out by Ogawa, Taguchi and Ishida (1998). Wang, Juncher Jensen and Xia (1998) extended this new method to determine the effect of green water on the hull girder bending, including the effect of vessel speed.

Dallinga and Gaillarde (2001) finally presented experimental results on the hatch cover loads on the M.V. Derbyshire in the Typhoon Orchid.

1.2.4 Effect of bow shapes

The effect of the bow shape on the occurrence of green water has always been a point of discussion between Naval Architects. Lloyd, Salsich and Zselezky (1985) give an interesting overview of this discussion since 1889. Together with the paper of O'Dea and Walden (1984), their work gives insight in the way the subject has been investigated for naval and merchant vessels. The results are, however, inconclusive. O'Dea and Walden report a decrease in deck wetness when a significant flare is applied for traditional ships, whereas Lloyd, Salsich and Zselezky find an increase in deck wetness with flare after studying nine different bow variations on one vessel.

This is probably due to the fact that the green water problem is highly complex and non-linear. It is a result of a very large number of parameters (freeboard, underwater hull shape, above water hull shape, draft, deck shape, loading conditions, ship speed, wave height, wave period, wave heading). This is confirmed by the work presented by Watanabe, Ueno and Sawada (1989) and Watanabe (1990) on the effect of bow flare shape of a container ship. They also point to the complex deformation of the incoming wave profile by the bow flare. A study of Takagi and Naito (1993) finally presents interesting observations on the effect of the hull shape on the final flow pattern on the deck.

Due to this complexity, a bow shape that is very effective to keep the deck dry in one condition can be less ideal in other environmental conditions.

1.2.5 Stability of fishing vessels

Beside the work on naval and merchant vessels, a lot of research has been carried out on the effect of water on deck of fishing vessels after a number of capsizing incidents. Dillingham (1981) was the first who studied the flow of the water on deck of small fishing vessels numerically. Later he was followed by others, such as Pantazopoulos (1988) and Huang and Hsiung (1996).

For the calculation of the water flow on the deck between the bulwarks they used Glimm's method (Glimm, 1965). It is assumed that the flow of the water on deck is a shallow water flow (constant velocity over the depth). The deck area can therefore be divided into a two-dimensional grid. In time domain the water flow between the grid points can now be calculated. This research resulted in a coupled equation of motion between the ship motions and the motions and loads of the water trapped on the deck. In this way the effect of the water on the ship's dynamic stability can be investigated.

1.2.6 Prediction methods

Mizoguchi (1988, 1989) successfully applied Glimm's method to the green water problem on the bow deck. Using the relative wave motion input from model tests to determine the amount of water on the deck, he calculated the motion of the water as soon as it was on the deck. He did not take into account the ship motions yet. The main behaviour of the water flow on the deck was similar to the behaviour observed in his experiments. Mizoguchi used wave impact formulations coupled to his calculated water velocities to predict the impact loads.

In a detailed study into the green water problem, Vermeer (1980) developed a method for the prediction of the amount of green water on the deck. He coupled a strip theory approach for the calculation of the ship and relative wave motions to the flow of green water onto the deck based on the theoretical dam breaking problem, as proposed by Stoker (1957). The author concluded, however, that the developed model was not yet fully adequate to predict the behaviour as seen in his experiments.

Hamoudi and Varyani (1994) focussed on the prediction of the load of green water on deck-mounted equipment. They assumed that the combination of wave (phase) velocity and ship speed is the main parameter in this load and determined an impact type coefficient (dispersion factor) to account for unknown aspects in the loading process based on extensive experiments.

Numerical studies into the non-linear relative wave motions for slender vessels with (high) forward speed, were presented by Tagaki and Niimi (1990) based on 2D-self-similar flow and by Song and Maruo (1993) based on a 2D boundary element method.

1.3 Problem definition and objective of this study

From the problem description in Section 1.1 it can be concluded that green water is a significant problem for ship-type offshore structures. The historical overview in Section 1.2 presented the extensive research on naval and merchant vessels in the past, but also showed that:

- There is limited insight in the physics of the non-linear and strongly complex green water problem, which results in a wide range of assumptions in prediction methods. Lloyd (1983) concluded: "Current techniques for predicting deck wetness frequency on the basis of strip theory calculations of motions and allowances for bow wave and swell-up appear to be inadequate, especially when the wetness frequency is high. Further experiments to examine the wetness 'process' in detail will be required to resolve these problems".
- The existing research is focussing on slender hull forms with forward speed in sea states that can be qualified as moderate, because the ship speed enhances the problem significantly. The green water problem for floating ship-type offshore structures, however, focuses on:
 - more full (tanker-type) hull forms at zero or low current speeds. This makes 3-D wave reflection and its interaction with the incoming waves much more important.
 - extreme wave conditions ('100 year storms'), which increase the importance of the non-linear extremes in the wave statistics.
- There is very limited insight in the loading process on structures on the deck. Ship-type offshore structures, however, have much more sensitive equipment on their decks than merchant vessels and even naval vessels (their equipment is generally designed to withstand blast type loads). This requires detailed insight in the flow on the deck and the resulting loading, which is not found in existing studies.
- The important problem of green water loading from the side of the vessel has not been studied before.

- There are no practical tools for designers and operators to evaluate their ship-type offshore structures for the risks of green water loading.
- There is lack of detailed validation material for the numerical simulation methods under development.

Considering the problem description above, the main objective of this study is:

To develop methods for the evaluation of green water on ship-type offshore structures based on a clear description of the green water physics.

1.4 Outline of the thesis

To achieve this objective, the following structure was chosen for this thesis:

- Description of the physics of green water on the bow based on two series of initial model tests (Chapter 2).
- Definition of a semi-empirical design evaluation method, based on a systematic series of model tests (Chapter 3).
In the following chapters the different building blocks of the semi-empirical design evaluation method will be presented, based on the results of this systematic model test series:
 - Non-linear relative wave motions at the bow (Chapter 4)
 - Water flow onto and on the bow deck (Chapter 5)
 - Green water impact loading (Chapter 6)
 - Green water from the side and stern (Chapter 7)The development of the semi-empirical design evaluation method will be completed with a review, together with recommendations for its application in relation with metocean data and structural response analysis (Chapter 8).
- Finally the numerical prediction of green water loading will be discussed. A number of methods will be presented and evaluated based on the specific requirements related to the physics of green water loading (Chapter 9).
- The thesis is completed with conclusions and recommendations for further research (Chapter 10).

Various subjects in the present thesis have been discussed by the author in conference papers, see Buchner (1994-2002). The present thesis puts them in the perspective of the overall problem.

1.5 Model tests and their interpretation

As part of this study a number of model test series have been carried out:

- Test Series A: Pilot tests traditional full bow
- Test Series B: Comparative tests traditional full bow and alternative thin bow
- Test Series C: Systematic test series with different hull shapes and flare angles
- Test Series D: Pilot tests green water from the side

Furthermore, the results of a number of schematic dam breaking tests and 2-D wedge entry tests will be used. The results of these tests will be presented in this thesis at the appropriate places. Technical details are provided in Appendices A-D.

Throughout this thesis Froude scaling is applied to scale the model test results to full scale values. This is discussed in Appendix I. If not stated otherwise, full scale values will be used in this thesis.

In Appendix II it is shown that green water loading is not hydro-elastic, so that the hydrodynamic loading and structural response can be uncoupled. Therefore, the measurements of the green water impact loading were carried out with stiff force-measurement panels in stiff models.

2. THE PHYSICS OF GREEN WATER ON THE BOW

2.1 Introduction

The main objective of this study is to develop methods for the evaluation of green water on ship-type offshore structures based on a clear description of the green water physics.

As concluded in Chapter 1, there is limited insight in the physics of the non-linear and strongly complex green water problem, which resulted in a wide range of assumptions in prediction methods. Therefore, in this chapter these physics are studied for ship-type offshore structures.

Model tests were performed with a model representing a Floating Production Storage and Offloading (FPSO) unit. The weather-vaning character of FPSOs around their rotating turret exposes important equipment and superstructures on the bow to the most critical wave conditions.

Two series of initial model tests were performed:

- Pilot tests with a traditional full bow (Test Series A)
- Comparative tests with a traditional full bow and alternative thin bow (Test Series B)

To describe the main physics of the green water problem at the bow, in these initial model tests only head wave conditions were considered. In later test series also other wave directions are studied.

First the two test series will be described. Then the observations from the model tests will be presented. Finally the green water process will be discussed step by step:

1. Motions and relative wave motions
2. Water flow onto the deck
3. Water behaviour and loading on the deck
4. Green water impact on structures

2.2 Model tests

2.2.1 Test Series A: Pilot tests FPSO with traditional full bow

For the model tests a typical 160,000 DWT FPSO was used at scale 1:60. Its body plan is shown in Figure 2-1.

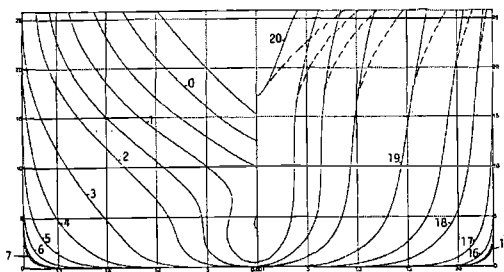


Figure 2-1
Body plan of the 160,000 DWT FPSO with and without bow flare
(flare indicated with dashed line)

The model was tested at its fully loaded draft without trim. It had a freeboard of 8.88 m. No deck camber and bulwark were applied to avoid added complication to the flow at this stage of the study. A drawing of the instrumented foredeck of the ship is shown in Figure 2-2. The main dimensions, weight data and stability parameters can be found in Appendix A, together with details about the measurements, basin set-up and environmental conditions.

As can be seen in the body plan in Figure 2-1, the original tanker had an almost vertical bow without much bow flare. To investigate the effect of flare on the relative wave motions and green water, an interchangeable bow part was made with a significant flare above the waterline. This is also shown in Figure 2-1 with the dashed line. The flare also has effect on the deck shape, as is shown by the dashed line in Figure 2-2. A comparison between the results with and without bow flare was presented in Buchner (1995a). The effect of bow flare will be discussed in more detail in later chapters.

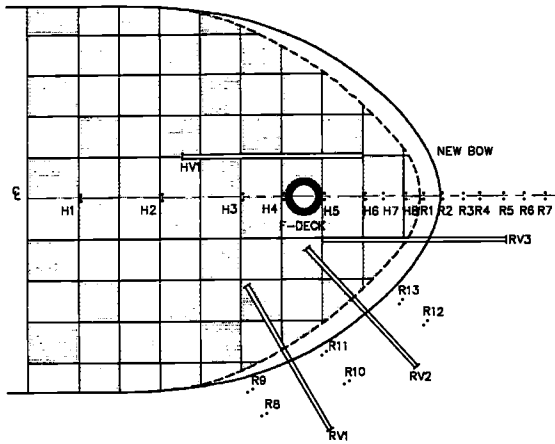


Figure 2-2
Instrumented foredeck of the FPSO
(the effect of flare on the deck area is indicated with dashed line)

To simulate a turret protection or superstructure, an instrumented vertical plate was designed for the present study. It had a height of 20 m and a width of 15 metres. It is shown in Figure 2-3.

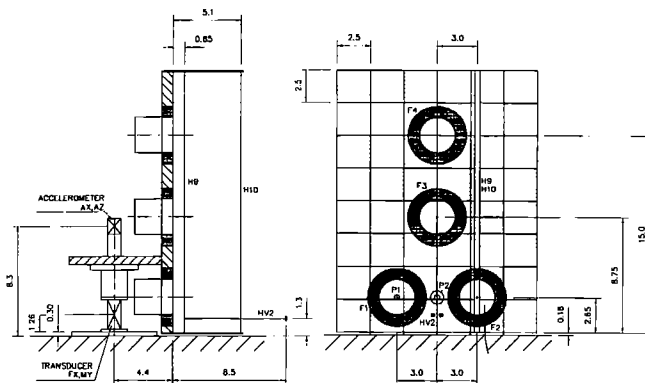


Figure 2-3
Instrumented vertical plate on the deck of the FPSO
(dimensions in metres full scale)

The initial tests were carried out in regular and irregular head waves, which are summarised in Appendix A. The following should be noted:

- Wind does not have influence on the solid green water, only on the light spray. Therefore, the wind was not simulated during the experiments.
- Most of the tests were carried out without current. However, the effect of current was investigated by towing the model with the carriage through the Seakeeping Basin, taking the moving carriage as the reference system.
- The water depth in the Seakeeping Basin amounted to 150 metres full scale.
- For practical purposes the surge motion was restricted in Test Series A. To achieve realistic wave and low frequency surge motions, in later test series the models were placed in a mooring system with a realistic horizontal stiffness.

Photo 2-1 shows the model in its set-up in the Seakeeping Basin.

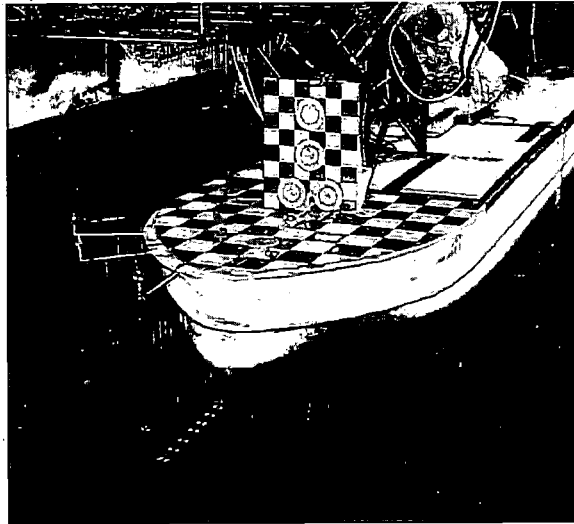


Photo 2-1
FPSO model in the Seakeeping Basin

2.2.2 Test Series B: Comparative tests traditional full bow and alternative thin bow

The purpose of this comparative test series was to study the sensitivity of the under water and above water bow shape of ship-type offshore structures for the green water problem. For this purpose model tests were carried out with three different bow shapes of an FPSO with the same main dimensions and stern shape. The first bow

shape is a traditional tanker hull with only a small flare in the bow region (the same model as in Series A). The first alternative bow has a triangular shape from ordinate 15 towards the forward perpendicular. This bow shape does not have any flare and has vertical sides from the bilges up to the main deck. The second alternative bow is equal to the first triangular alternative, but from the waterline it has a significant flare. The alternative bow shapes are shown in Figure 2-4.

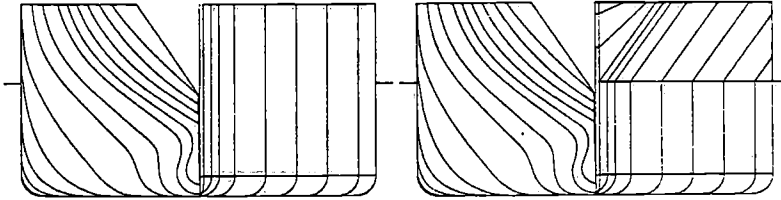


Figure 2-4
Body plans of the alternative bow shapes
without (left figure) and with (right figure) bow flare

The main dimensions, weight data and stability parameters of the three hulls can be found in Appendix B, together with details about the measurements, basin set-up and environmental conditions. These tests were carried out in the Seakeeping Basin at a scale of 1:60 and with a water depth of 150 m as well.

2.3 Observations

2.3.1 Visualisation techniques applied

To study the physics of green water, two types of visualisation techniques were used:

- Vessel-fixed photo and video cameras were used to study the flow during the normal measurements. Photo 2-2 shows the typical sequence during a green water event. The checkerboard pattern on the deck has blocks of 5*5 m, on the structure 2.5*2.5 m.
- In Test Series A a special series of observation tests was carried out with a thin plate placed at the centreline of the ship in front of the bow, see Figure 2-5. Due to its position at the centreline, the plate was not disturbing the waves and ship motions in head waves. Recordings were made with a vessel-fixed video camera. Using the grid on the plate with its 5*5 m blocks, it was possible to analyse the vessel-fixed relative wave contour as function of time.

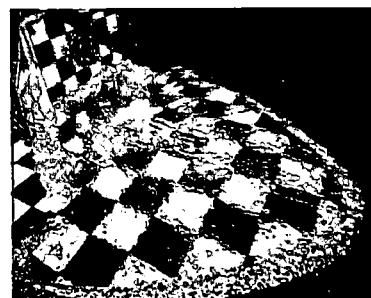
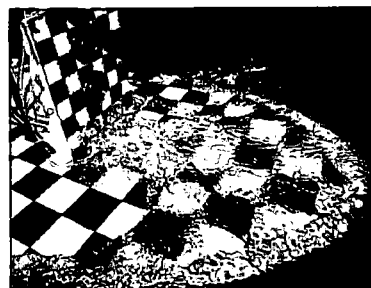
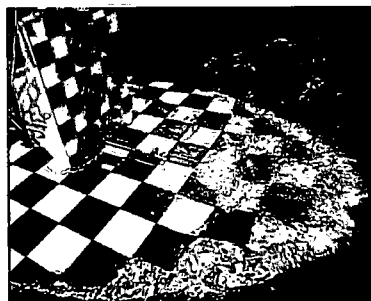
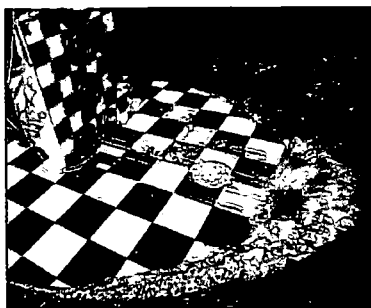


*Photo 2-2
Typical sequence during a green water event*

Figure 2-5 shows the results of an observation test with the plate for a regular wave with a height of 17.3 m and a period of 11.2 s. The water front contours are given for time steps of 0.25 s full scale.

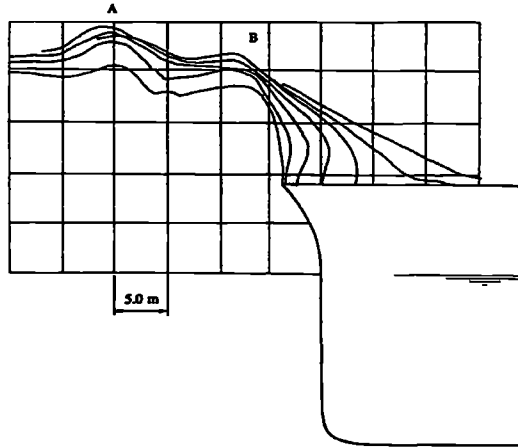


Figure 2-5

Vessel fixed contours of water flow onto the deck with time steps of 0.25 s for a wave height of 17.3 m and a period of 11.2 s

From the vessel-fixed camera during the normal tests, Figure 2-6 shows the typical contours of the water front on the deck in regular waves of 11.2 s (above) and 12.9 s (below). Again the water contours are given for time steps of 0.25 s full scale.

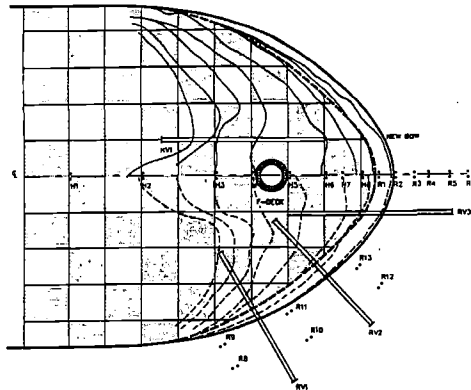


Figure 2-6

Contours of water flow on the deck with time steps of 0.25 s for wave periods 11.2 s (port) and 12.9 s (starboard)

Finally the green water impact on the vertical plate at the deck was studied. Figure 2-7 shows the typical front and side view water front contours against the structure. Now the contours are given for time steps of 0.15 s full scale.

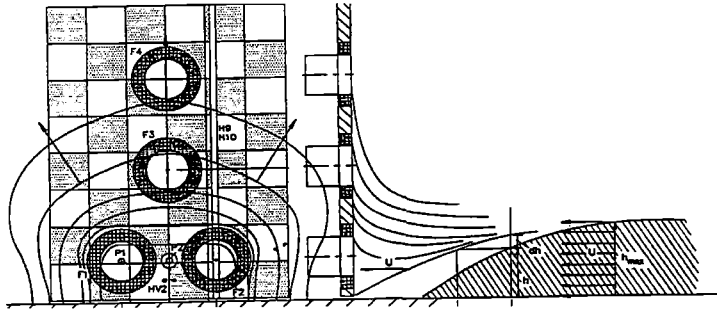


Figure 2-7
Front and side view contours of water flow against the vertical plate at the deck
with time steps of 0.15 s

2.3.2 Summary of observations

From Photo 2-2 and Figures 2-5 through 2-7, the following typical sequence of events can be observed during a green water event:

1. The relative wave motions exceed the freeboard level
2. The water flows onto the deck
3. The green water on the deck forms a high-velocity water jet
4. The green water impacts on a structure like an impinging jet

Studying Figure 2-5 in more detail, the following phases can be distinguished in the flow onto the deck:

Time t	Phase
0.0 s	First an almost vertical wall of water is observed around the bow. The horizontal velocity of this wall of water is almost zero. The pitch angle is at its maximum at this moment.
0-0.5 s	The vertical wall of water translates onto the deck and starts to be considerably curved. This gives the impression that it intends to break.
0.5-1.0 s	However, due to the high quasi-static pressure at deck level the water close to the deck starts to accelerate and prevents actual breaking.
1.0-1.5 s	Finally a high velocity jet shoots over the deck. During this process short (non-linear) reflecting and radiating waves slowly propagate away from the bow on top of the incoming waves, the first as a result of the re-entrance of the keel into the water (A) and the second of the bow flare (B).

Although the flow on the deck depends on the wave period, also in Figure 2-6 a typical sequence of phases can be observed:

Time t	Phase
0.0 s	The horizontal velocity of the water front (the position of the water wall on the deck) is almost zero.
0-0.75 s	The water front starts to translate onto the deck with a similar velocity from all sides, perpendicular to the local deck contour.
0.75-1.75 s	The water contours from the front and sides meet at the centreline of the ship and result in a high water 'jet', which flows with a high velocity aft along the middle of the deck. Typically water front velocities of 15-25 m/s are observed.

Finally the water front reaches the structure at the deck. In Figure 2-7 the following typical sequence can be identified:

Time t	Phase
0.0-0.15 s	The high velocity water front on deck reaches the structure. In general the water front can be seen as a jet with an increasing height rather than a solid 'block' of water flowing over the deck.
0.15-0.60 s	The direction of the green water flow (with its momentum) is changed 90 degrees (upwards and sideways) in a very short period of time, resulting in an impulsive load on the structure.
0.60-4.5 s	After that, the remainder of the green water on the deck builds up in front of the structure, resulting in quasi-static type loads against the structure and on the deck.

As will be seen later, the exact flow contours will depend on bow flare angle and shape of the deck, but the main trend in the flow is generally as described above. This shows that the flow onto the deck is a result of the large relative motion between incoming wave and downward moving bow, resulting in a 'wall' of water with almost zero forward velocity around the bow. The height, shape and behaviour of this 'wall' are significantly influenced by the bow flare. For one thing this implies that there is no simple relation between the orbital or phase velocities of the undisturbed waves and the flow of the water onto the deck, as was assumed by some authors, like Hamoudi and Varyani (1994).

It is also incorrect to assume that the flow of the water onto the deck can be seen as a breaking wave, as done by Takezawa, Hagino, Kobayashi and Sawada (1977). However, in some cases steep and energetic waves can result in special green water events. In these cases the loading is almost independent of the ship shape and a direct result of the wave crest overtopping the freeboard level and hitting the structure. This was observed for instance by Hellan, Hermunstad and Stansberg (2001) and will also be discussed in later chapters.

In the next sections the different phases in the green water problem are discussed based upon the Test Series A and B:

1. Motions and relative wave motions
2. Water flow onto the deck
3. Water behaviour and loading on the deck
4. Green water impact on structures.

This discussion will be the basis for further detailed investigations in later chapters.

2.4 Motions and relative wave motions

As observed in the previous section, the relative wave motions around the bow can be seen as the input to the green water problem. The relative wave motion (r) is defined as the difference between the local vertical vessel motion (z) and the local (disturbed) wave motions (ζ) according to:

$$r = \zeta - z \quad (2.1)$$

As soon as the relative wave motions exceed the freeboard level, as shown in Figure 2-8, there is a chance that green water will flow onto the deck. The freeboard exceedance (h) is defined as:

$$h = r - fb \quad (2.2)$$

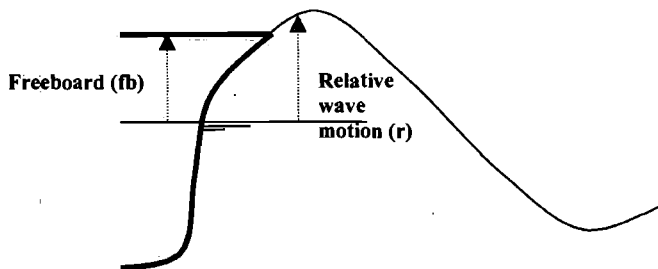


Figure 2-8
Definition of relative wave motion (r) and freeboard with respect to the waterline in calm water (fb)

The relative wave motions should, therefore, be predicted accurately to come to a reliable prediction of green water loading. As can be seen from Expression (2.1), the relative wave motions are a function of both the ship motions and (disturbed) wave motions, with all their non-linearities. Both will be discussed below.

2.4.1 Ship motions

2D linear (or non-linear) strip theories are the basis for most green water prediction methods for slender naval and merchant vessels. However, for full ship-type offshore structures the motions and relative wave motions are generally predicted with 3D linear diffraction analysis, see for instance Van Oortmerssen (1973). In linear diffraction analysis the wave exciting forces on the ship due to the undisturbed waves and waves reflected (diffracted) on the hull are determined. Furthermore, the added mass and damping due to the wave generation by the motions of the ship are calculated.

Figure 2-9 shows the element distributions for the diffraction analysis for the hull shapes of Test Series B.

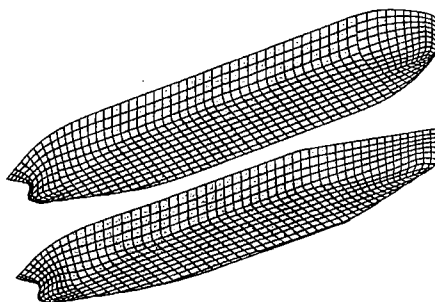


Figure 2-9
Element distributions for the traditional full bow and alternative thin bows

The following main assumptions apply for 3D linear diffraction theory:

- The fluid is assumed to be 'ideal' (viscosity is neglected).
- The waves are considered to be sinusoidal.
- The waves and vessel motions are assumed to be small.
- The interaction between the structure and the fluid is only taken into account up to the still waterline.

Based upon these assumptions it is possible to linearise the problem. Therefore the relation between the ship or relative wave motion amplitude and the incoming wave amplitude can for each frequency be expressed in the frequency domain as a linear Response Amplitude Operator $H(\omega)$. This RAO can also be determined experimentally from regular wave tests as the ratio between the output signal amplitude o_a and the input wave amplitude ζ_a , or from irregular wave tests as the square root of their spectral densities:

$$H(\omega) = \frac{o_a(\omega)}{\zeta_a(\omega)} = \sqrt{\frac{S_o(\omega)}{S_\zeta(\omega)}} \quad (2.3)$$

It is questionable whether the linear assumptions above hold for ship-type offshore structures in survival conditions. In Figure 2-10 the calculated and measured RAOs of the pitch motions are given for the three bow shapes in Test Series B.

From the model tests both the irregular wave test results (significant wave height 13.5 m) as well as the regular wave test results for three different heights per wave period are shown (100%, 75% and 25% of the maximum wave height, see Appendix B). The results for these different heights at the same wave frequency are connected in the figures to indicate the non-linearity in the results.

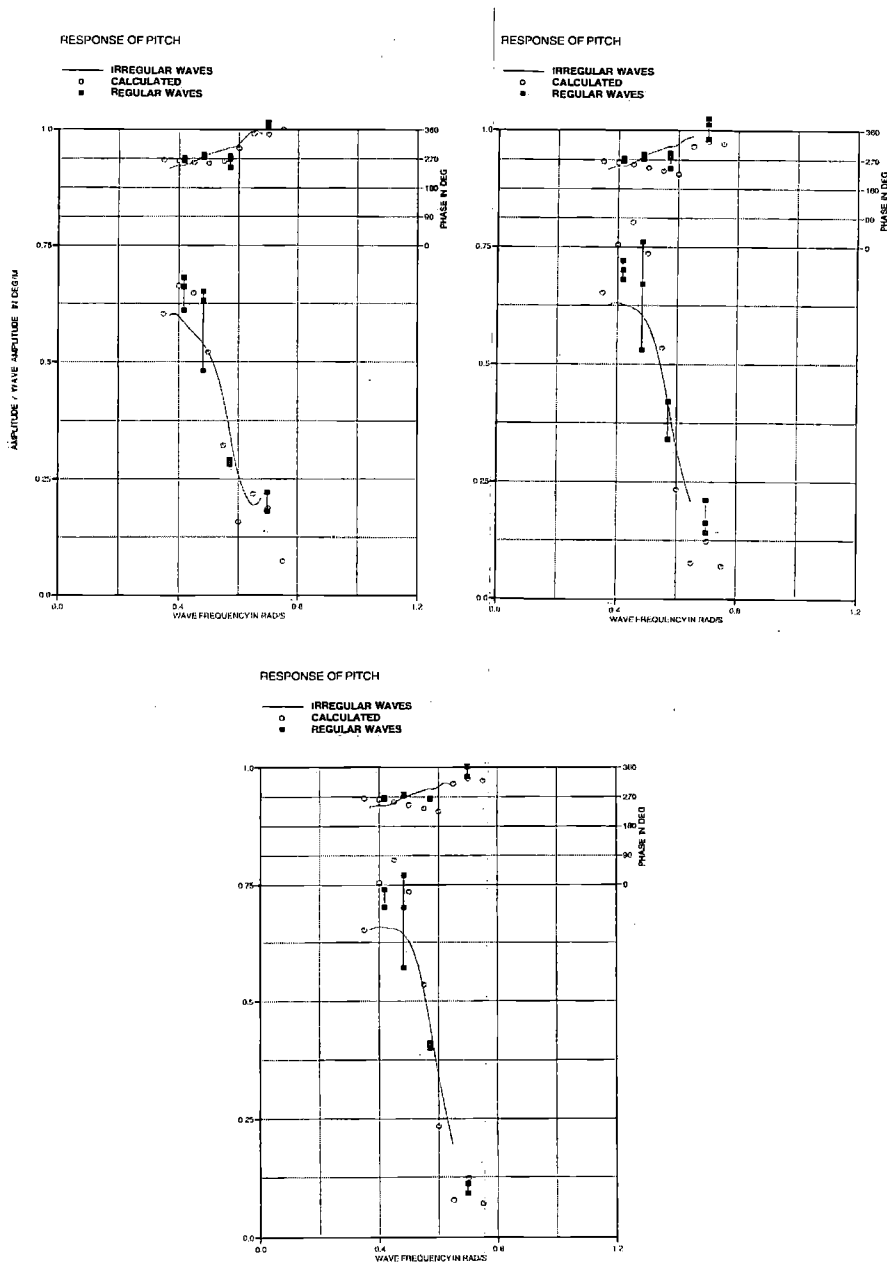


Figure 2-10
 Calculated and measured RAOs of the pitch motions for the three bow shapes in Test Series B: Traditional full bow (top left), Alternative thin bow with flare (top right) and Alternative bow without flare (bottom)

The following observations can be made from Figure 2-10:

- For the traditional bow shape the diffraction analysis results are in good agreement with the model test results in smaller regular wave amplitudes. If the wave height increases, as is the case in the irregular survival waves, the calculations seem to overpredict the motions. Especially around wave frequencies with a wave length approximately equal to the ship length (0.5 rad/s), a significant non-linearity is observed. From 25% to 100% of the wave amplitude the pitch motion RAO decreases by 25%. In shorter waves there is a tendency in the measurements towards somewhat larger pitch motions than calculated.
- For the alternative bows the measured RAOs are also closer to the calculated RAOs for the smaller wave heights. With the wave length equal to the ship length, the pitch decreases by 30% when the wave height increases. Although the bow flare of the alternative bow is not taken into account in the diffraction analysis, it is clear from the model tests that it affects the ship motions. For the alternative bow with flare the differences in the measured and calculated RAOs are larger than without flare. The motions and relative wave motions are smaller with the bow flare. This is due to the small buoyancy below the still waterline for this type of thin bow. The additional buoyancy of the bow flare, consequently, has a significant effect for larger pitch motions.
- For the alternative bows the difference in measured and calculated phase angles is much larger than for the traditional bow. For the wave frequency of 0.571 rad/s the difference in pitch phase angle with large waves is even 65 degrees. This can have a significant effect on the green water loading.

Investigating the differences between measured and calculated pitch motions, it was found that the large amounts of green water on the bow deck, with their large moment arm with respect to the centre of gravity, have a significant effect on the pitch motions. To investigate the sensitivity of the ship motions for the green water on the bow deck, the following study was carried out:

1. For the traditional full bow, the deck of the FPSO was divided into transverse strips at the longitudinal positions of water height probes H1-H8 with associated areas $ar_1 - ar_8$. The water height is assumed constant and equal to the water height at the position of the wave probe for all strips. The distances from the vessel COG to the positions of the probes were taken as the moment arms $l_1 - l_8$. The green water moment can now be estimated as:

$$M_g(t) = \sum_{i=1}^8 H_i(t) \cdot (g + \ddot{z}_1(t)) \cdot \rho \cdot ar_i \cdot l_i \quad (2.4)$$

g and \ddot{z} are the gravitational acceleration and vertical acceleration of the deck. Taking the time traces of the vessel motions and water heights on the deck from the tests in regular waves (wave amplitude 8.5 m), the time traces of the green water moment M_g were determined. This resulted in a peak moment M_g of $6.25 \cdot 10^6$ kNm for long waves (0.487 rad/s) and $6.50 \cdot 10^6$ kNm for short waves (0.56 rad/s).

2. As a next step the mass, added mass, damping, restoring coefficient and linear pitch moment M_θ (combined undisturbed wave and diffraction moment) were determined with linear diffraction analysis. This resulted in pitch moment amplitudes of $1.573 \cdot 10^7$ kNm (0.487 rad/s) and $4.412 \cdot 10^6$ kNm (0.56 rad/s) in waves of 8.5 m amplitude.
3. Finally, assuming linear wave exciting moments and neglecting memory effects in the reaction forces because the simulation is carried out in a regular wave, the pitch motion of the FPSO was simulated in the time domain according to the following uncoupled equation of motion:

$$(m + A)\ddot{\theta} + B\dot{\theta} + C\theta = M_\theta \sin \omega t + M_g(t) \tag{2.5}$$

In Figure 2-11 the resulting exciting moments and pitch motions are shown for the two wave lengths.

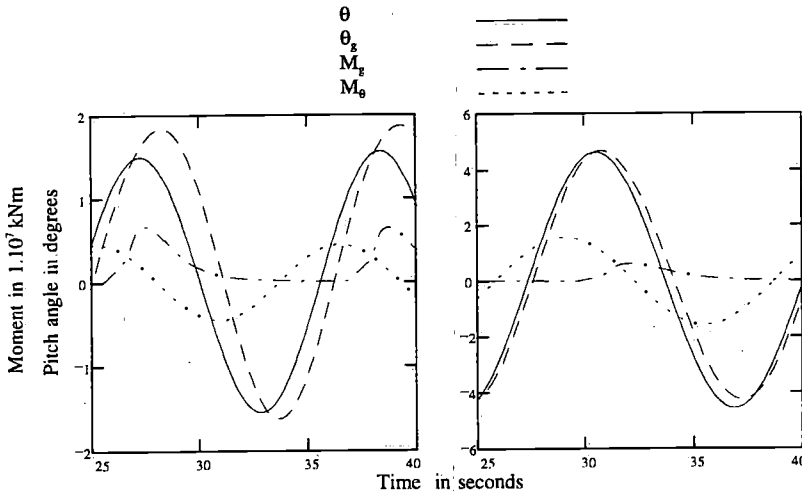


Figure 2-11

Wave exciting moment (M_θ), green water moment (M_g), and pitch motions simulated with (θ_g) and without (θ) green water moment for two regular wave lengths: shorter waves (0.56 rad/s) left and longer waves (0.487 rad/s) right

Figure 2-11 shows that the pitch motion and phase change significantly as a result of the green water in shorter waves (0.56 rad/s), whereas the effect in the longer waves (0.487 rad/s) is small. This is due to the ratio between the wave exciting moment M_θ and the moment due to the green water M_g . This ratio is large for the longer waves and small for the shorter waves.

2.1.2 Relative wave motions

As indicated in Expression (2.1), the other component in the relative wave motions is the local (disturbed) wave motion (ζ). According to linear diffraction theory the wave motions around the bow are due to the incoming undisturbed waves (ζ_0), radiating waves due to the ship motions in 6 degrees of freedom (ζ_i) and the reflected (diffracted) waves against the vessel hull (ζ_7). In linear theory it is assumed that all these components, including the vertical vessel motions (z), are linear dependent on the wave height. Consequently, they can be calculated separately and added later into a combined relative wave motion, all depending of the wave frequency ω :

$$r(\omega, x) = \left[\zeta_0(\omega, x) + \sum_{i=1}^6 \zeta_i(\omega, x) + \zeta_7(\omega, x) \right] - z(\omega, x) \quad (2.6)$$

In Figure 2-12 the calculated relative wave motion RAOs in front of the bow are presented for the traditional full and alternative thin bow from Test Series B. The figure shows the typical trends in relative wave motion RAOs as well as the differences between full and thin bows:

- In long waves the vessel follows the wave slope, which implies that the vertical motion of the bow completely follows the local wave motion. In long waves the wave reflection on the bow is also low due to the small orbital velocities in the waves. The relative wave motion is consequently zero.
- In short waves the vessel motions become very small whereas the incoming waves are still present. Additionally, the wave reflection reaches its maximum in short waves. Consequently, the relative wave motions are a result of the incoming wave (RAO value of 1.0), plus the effect of wave reflection (which can vary between 0.0 for very thin bows to 1.0 for very full bows with full reflection: standing waves in front of the bow).
- In the area in between, where the ship length is similar to the wave length, the relative wave motions are a result of the pitch motions that are out of phase with the wave motions, plus the effect of partial wave reflection.

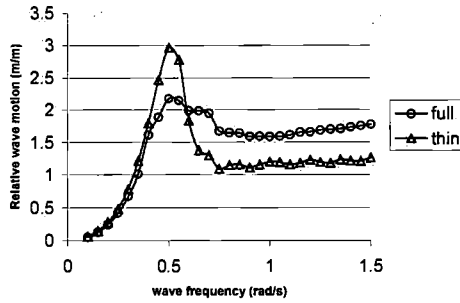


Figure 2-12

Calculated relative wave motion RAOs (in front of bow) for the traditional full and alternative thin bow from Test Series B

To get insight in the relative contributions of the relative wave motion components in Expression (2.6) for the traditional full and alternative thin bows from Test Series B, Table 2-1 presents them for $\omega=0.483$ and 0.571 rad/s.

Table 2-1

Relative wave motion components (in front of bow) for the traditional full and alternative thin bow

Relative motion component	Traditional full bow $\omega=0.483$ rad/s	Alternative thin bow $\omega=0.483$ rad/s	Traditional full bow $\omega=0.571$ rad/s	Alternative thin bow $\omega=0.571$ rad/s
Undisturbed wave (ζ_0)	32%	32%	32%	32%
Diffacted wave (ζ_7)	12%	5%	26%	4%
Result of ship motions (z)	46%	65%	23%	39%
Radiated wave ($\zeta_{s, 1-6}$)	10%	10%	7%	6%
TOTAL	100%	112%	88%	81%

A comparison of the two bow shapes shows the following:

- For the full traditional bow the diffracted wave is a significant part of the relative wave motions, especially in the shorter waves. The thin alternative bow is hardly reflecting the waves with its underwater shape, resulting in a negligible contribution in the relative wave motions.
- In the contribution of the ship motions there is a significant difference as well. For the alternative thin bow this is the dominant component in the relative wave motions, especially in the longer waves.

In Figure 2-13 the calculated and measured RAOs of the relative wave motions are now given for the three bow shapes in Test Series B, the pitch motions of which are given in Figure 2-10.

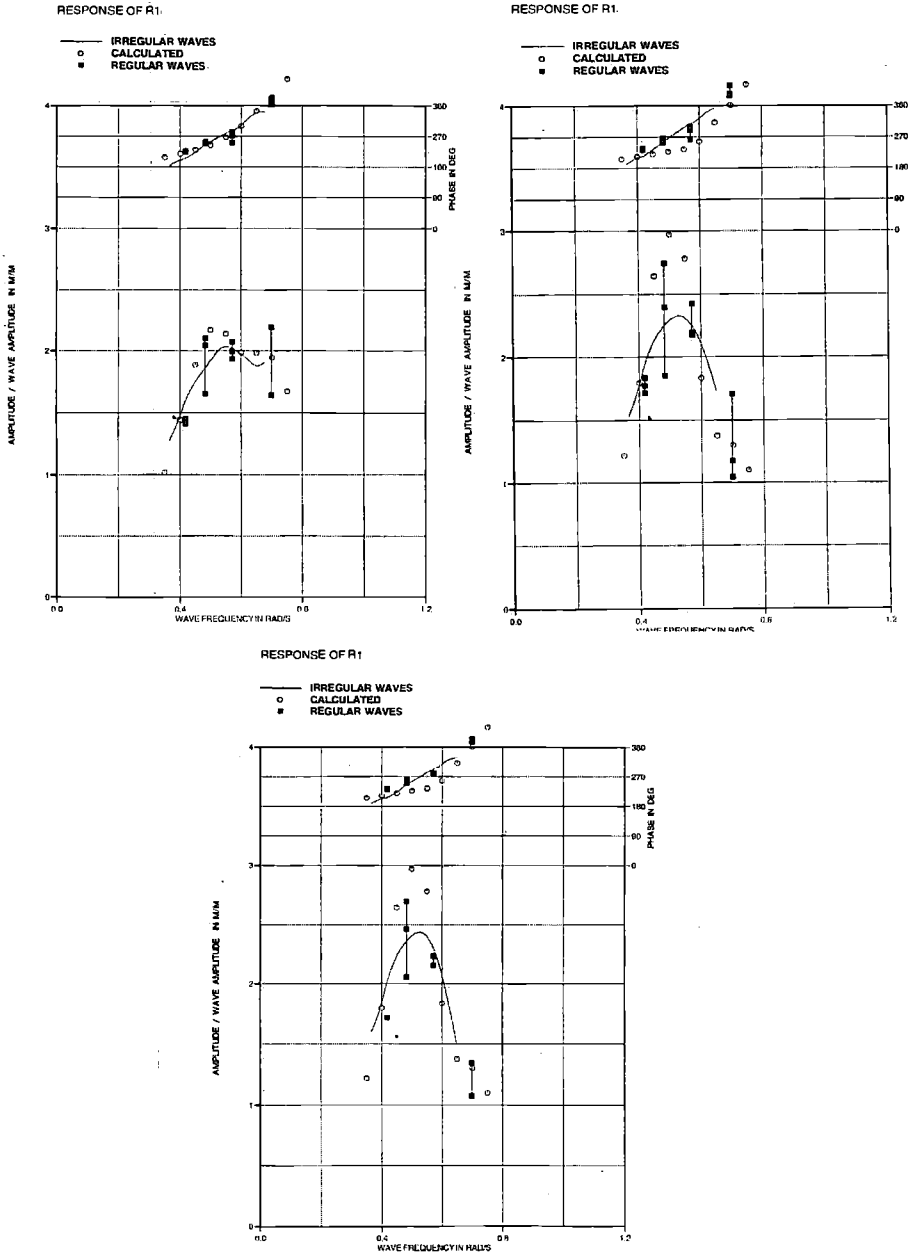


Figure 2-13

Calculated and measured RAOs of the relative wave motions for the three bow shapes in Test Series B: Traditional full bow (top left), Alternative thin bow with flare (top right) and Alternative bow without flare (bottom)

Based on these RAOs, similar conclusions can be drawn as for the pitch motions in Figure 2-10.

However, analysis of non-linearities in RAOs is not sufficient to determine the extreme relative wave motions that are the input to the most critical green water events. To determine these, the short-term statistics of the relative wave motions need to be considered.

Based on the assumption of a narrow banded linear motion response to Gaussian distributed waves, Ochi (1964) showed that the Rayleigh distribution applies to the probability of exceedance P of a certain value R of a peak or trough of the relative wave motions in an irregular sea state:

$$P(r > R) = \exp \left[-\frac{R^2}{2s^2} \right] \quad (2.7)$$

s is the standard deviation. Based on these assumptions the Most Probable Maximum (MPM) value of R can be determined. For this value R_{MPM} the following relation applies, with N as the number of maxima in the considered time period:

$$P(r > R_{\text{MPM}}) = \frac{1}{N} \quad (2.8)$$

Longuet-Higgins (1952) showed that the MPM value under these assumptions can be expressed as:

$$R_{\text{MPM}} = s \cdot \sqrt{2 \ln N} \quad (2.9)$$

However, as expected based on the RAOs, it was found that the statistics of the actual relative wave motions are non-linear. Figure 2-14 shows the measured probability of exceedance plots for the three bows in Test Series B for a JONSWAP spectrum of $H_s=13.2$ m and $T_p=12.9$ s ($\gamma=3.3$). A Rayleigh distribution (based on narrow banded linear response) would result in a straight line on this paper. The measured curves, on the other hand, are significantly curved.

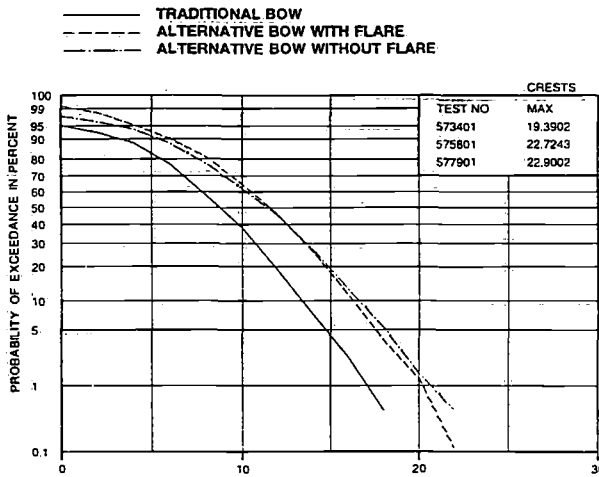


Figure 2-14
Measured probability of exceedance functions on Rayleigh distribution paper
for the bows in Test Series B

Taking into account the assumptions in linear diffraction theory, the observed non-linearities in the RAOs and probability of exceedance plots have the following backgrounds:

- The waves in survival conditions are not small and sinusoidal, see the wave crest statistics presented by Kriebel and Dawson (1993).
- The effect of above water hull shape on the motions and swell-up around the bow, which is neglected in linear diffraction theory because the interaction between the structure and the fluid is only taken into account up to the still waterline.
- The effect of the green water on deck on the ship motions.

All three points above will be investigated further in later chapters.

2.5 Water flow onto the deck

As was reported by Goda, Miyamoto and Yamamoto (1976) and Vermeer (1980), there is a clear resemblance between most cases of green water flow onto the deck and the theoretical dam breaking problem. In this theoretical problem, described extensively by Stoker (1957), it is assumed that at time $t=0$ there is a vertical wall of water of height h' on one side of a vertical dam. At that moment the dam is removed and the water flows into the empty region, see Figure 2-15.

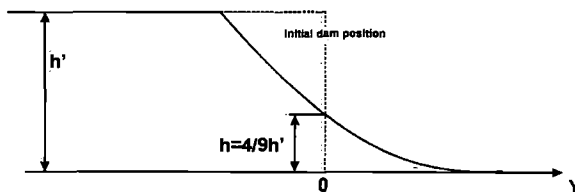


Figure 2-15

Theoretical dam breaking problem after some time t

The flow velocity into the empty region is proportional to the square root of the height of the water before the dam breaks (h'):

$$U = 2\sqrt{gh'} \quad (2.10)$$

Figure 2-16 shows an example of the water contour at different time steps according to the dam breaking problem. It should be noted that the freeboard exceedance (h) of 10 m is taken as $(4/9)h'$ (see for further details Chapter 7).

Goda, Miyamoto and Yamamoto (1976), Vermeer (1980), Dillingham (1981) and Mizoguchi (1988) applied the theoretical results of the dam breaking problem to the calculation of the flow of the water onto the deck.

Although the theoretical dam breaking does show clear resemblance with the typical green water flow onto the deck, it will be clear from a comparison between Figure 2-16 and Figure 2-5 that the actual flow is far more complex:

- The ship deck is moving.
- The height of the freeboard exceedance is varying in time.
- The initial velocity is not per definition zero and is influenced by wave kinematics and run up effects. This is especially of importance when steep and energetic waves reach the deck, as reported by Hellan, Hermunstad and Stansberg (2001).

Despite this, the dam breaking model can help to understand the green water physics better, as will be seen in later chapters of this thesis.

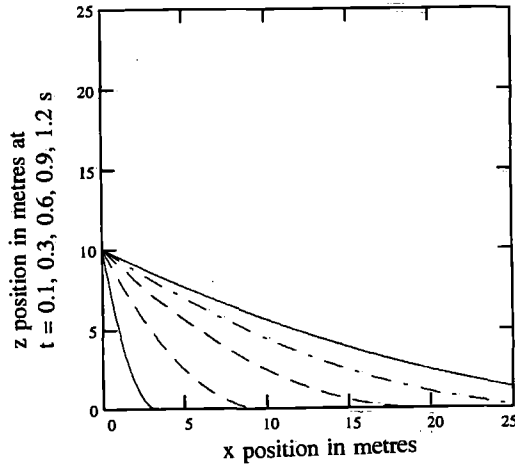


Figure 2-16

Water contour at different time steps according to the dam breaking problem

2.6 Effect of above water hull shape

The flow onto the deck is significantly influenced by the bow flare as well. As an example Table 2-2 shows test results for the two alternative thin bows from Test Series B with and without bow flare. For regular waves with a frequency of 0.571 rad/s, the exceedance of the freeboard at the bow centreline (h) is compared with the water height on the deck (H) 28.6 m from the fore perpendicular. Also the ratio between the two is given.

Table 2-2

Comparison of freeboard exceedances and water heights on deck for the alternative thin bow with and without flare

	Alternative thin bow with flare	Alternative thin bow without flare
Exceedance of freeboard h	9.74 m	9.94 m
Water height on deck H	3.62 m	5.23 m
Ratio H/h	0.37	0.53

It is observed again that the height of the water on the deck is not equal to the exceedance of the freeboard. But it is also found that the ratio between the water height on the deck and the exceedance of the freeboard is much lower when bow flare is applied above the waterline. This is due to the fact that the flare does not only push the water up, but also away from the bow. Consequently, a smaller part of the height of water exceeding the freeboard outside the deck region finally reaches the deck itself.

2.7 Water behaviour and loading on the deck

In Section 2.3 and Figure 2-6 the typical flow of water on the deck was presented, with its typical high velocity water jet at the centreline of the deck. As will be seen in later chapters, the exact pattern of this flow on the deck is a result of the:

- absolute height of the freeboard exceedance around the bow
- bow flare angle (which influences the inflow onto the deck)
- shape of the deck in plan view
- vessel motions
- wave period

Beside the velocities and pattern of the water on the deck, also the pressure on the deck of the vessel is of importance for the design. In Section 1.2 reference was made to the earlier work of Buchner (1994) on the prediction of these pressures for frigates with forward speed. Investigations showed that the large pressure peaks occurred at the moment that the water height on the deck at a certain position increased rapidly, see Figure 2-17. This indicated that the rate of change of water height on the deck has an important effect on the maximum deck pressures.

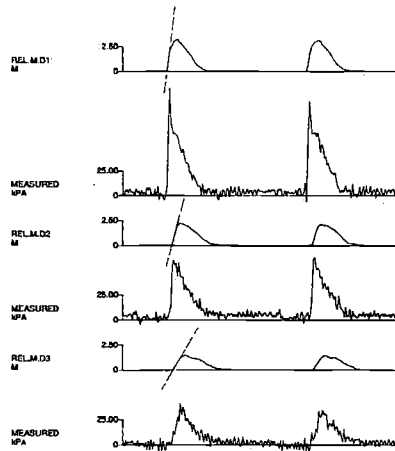


Figure 2-17

Time traces of water height and pressure on deck at 3 locations on the deck of a frigate (from Buchner, 1994)

To explain the peak pressures, the control volume above the force panel in the deck in Figure 2-18 should be considered. It has a vessel-fixed vertical velocity w .

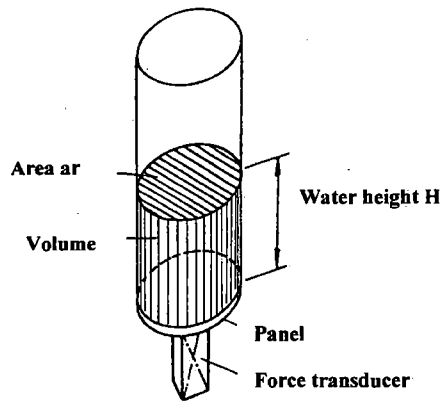


Figure 2-18

Definition of the control volume on the deck

For a control volume that makes vertical motions, the following relation applies according to Newton's law:

$$F = \frac{d(m \cdot w)}{dt} = \left(\frac{\partial m}{\partial t}\right)w + \left(\frac{\partial w}{\partial t}\right)m \quad (2.11)$$

The mass (m) in the control volume is equal to $\rho \cdot H \cdot ar$. Implementing this in Expression (2.11), dividing by the area (ar) and taking into account the acceleration of gravity with a pitch inclination angle (θ), results in the following expression for the pressure on the deck in head waves:

$$p = \rho \left(\frac{\partial H}{\partial t} \right) w + \rho (g \cos \theta + \frac{\partial w}{\partial t}) H \tag{2.12}$$

The importance of the first term, which concerns the rate of change of water height on the deck, will now be shown in Figure 2-19 based on a comparison of the measured and calculated pressures for a regular wave test with the frigate. For the calculation it is assumed that the water height (H) over the total control volume is equal to the height at the position of a wave probe in front of the panel. For the calculations the different components of the pressure are also plotted separately.

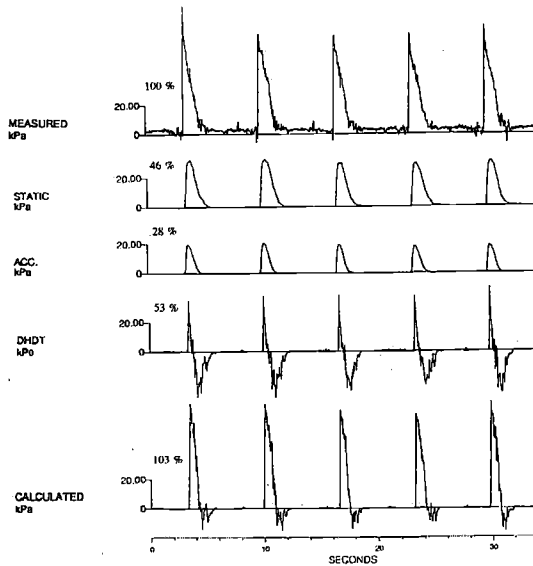


Figure 2-19

Measured pressure (top) versus the total calculated pressure (bottom) and its components for a frigate with forward speed (from Buchner, 1994): STATIC (static water head), ACC (pressure due to vertical deck acceleration) and DHDT (pressure due to rate of change of water height)

However, for a ship-type offshore structure the accelerations are generally at their maximum at the moment the water comes onto the deck. Consequently, the vertical velocity is close to zero. This results in a pressure at the deck that is dominated by the static pressure and the acceleration component, as can be seen in Figure 2-20. The figure shows the results for the traditional bow from Test Series B in regular waves with $T=11.2$ s and $H=17.3$ m.

On the other hand it should be noted that the largest water height on the deck occurs in front of structures, such as deckhouses. At the moment that the fluid flow is blocked by a structure, the water is running up in front of it. This can have a large effect on the maximum water pressure on the deck. Another important type of impact loads can come from water running up in front of a structure (such as the hatches of a ship) and falling back on its top, see for instance Dallinga and Gaillarde (2001).

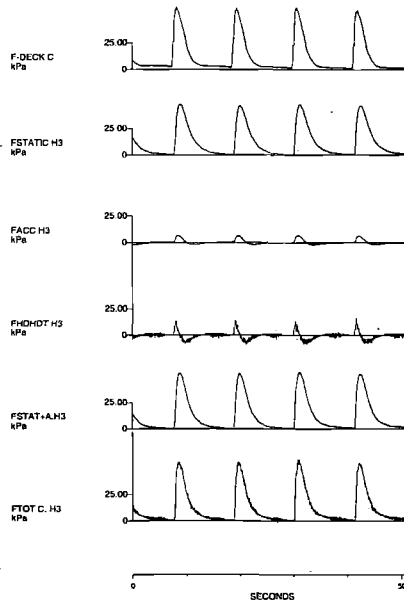


Figure 2-20

Pressure on the deck of an FPSO: measured pressure (F-DECK C) compared to the static water head (FSTATIC H), the component due to the vertical acceleration of the deck (FACC H), the additional component which depends on the vertical velocity and rate of change of water height (FHDHDT) and the total of the 3 calculated components (FTOT C. H)

2.8 Green water impact on structures

When the high velocity water front on the deck reaches a structure, this results in significant impact loading on the structure. The green water flow direction is changed as described in Section 2.3. After some time there is a significant amount of water built up in front of the structure, which falls back on the deck after some time.

In Figure 2-21 a typical time trace of the pressure on the structure is shown.

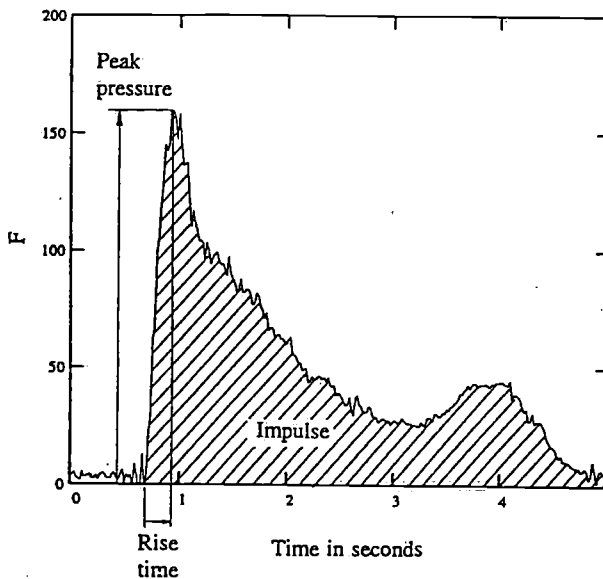


Figure 2-21

Typical time trace of a green water impact pressure (in kPa) on a structure on the deck

Three stages in the loading of the water on the structure are identified:

- The 'impact stage', resulting in the first and highest peak load (which has a typical rise time to maximum pressure between 0.10 and 0.35 s). This has the character of an impinging jet or wedge entry.
- The 'quasi-static load stage', which occurs as soon as most of the kinetic energy is out of the fluid and a large amount of water has been built up in front of the structure.
- The 'plunging water stage' when the water built up in front of the structure falls back onto the deck. This can result in a secondary maximum in the pressure.

Sometimes minor (short duration) peak loads are observed in the early stages of the impact. These are a result of fast thin water jets in front of the main amount of green water. However, the impulse of these initial load peaks is small.

The described main phenomena show considerable resemblance with a jet impinging perpendicularly at a plate. Based on experiments with such a set-up, Suhara, Hiyama and Koga (1973) found that the pressure peak is dependent on the square of the velocity according to:

$$p = C \rho u^2 \quad (2.13)$$

They propose an impact coefficient $C=1.4$ for bottom slamming situations based upon empirical relations.

During the analysis of Test Series A, the validity of this assumption for green water impacts was investigated. For this purpose the mean pressure over the force panel F2 was plotted in Figure 2-22 as function of the square of the water front velocity U (from time differentiation of horizontal wave probe HV1). The figure shows the results for a test in a JONSWAP spectrum of 13.5 m significant height and a current speed of 2.0 m/s.

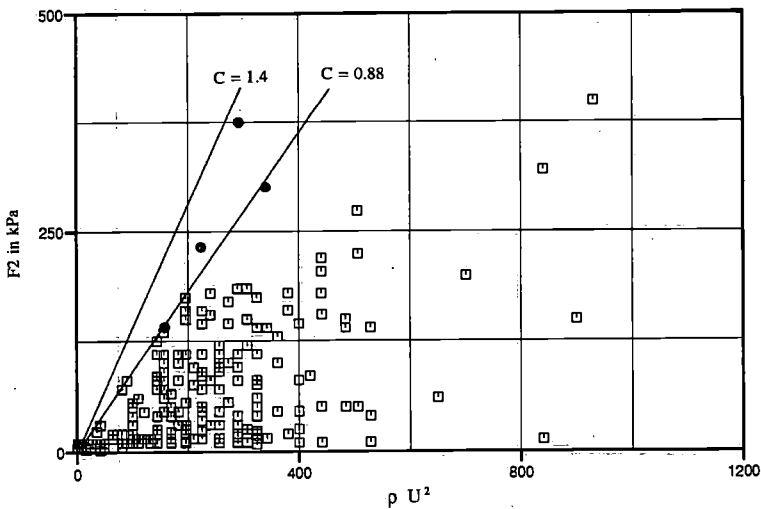


Figure 2-22

Mean pressure over force panel F2 as function of the square of the water front velocity U (from horizontal probe HV1) in an irregular wave test. Some local pressures (P_2) from regular wave tests are shown with circles

The figure shows the total number of green water events, a line according to Expression (2.13) for $C=1.4$ and a line with the maximum coefficient from the measurements with $C=0.88$. Some points with local pressures (from pressure transducer P2) from regular wave tests are presented as well. From this figure it will be clear that the factor $C=1.4$ is rather conservative for the mean (integrated) pressure over the panel. Only the local pressures come close to the line for $C=1.4$. However, the integrated pressures (over stiffened plate fields) will determine the design loads for this type of structures, rather than the (larger) local pressures. Taking this into account, and considering the large scatter in Figure 2-22, it was decided to study the occurring phenomena in more detail.

Considering the character of the green water impact flow carefully, it can be concluded that the load of the water on the structure is not due to a solid impact (as is the case for bottom slamming or in the experiments of Suhara, Hiyama and Koga). Green water impact loading is much more similar to the impacting of a jet with an increasing height, as shown schematically in Figure 2-23. This indicates that the time derivatives of the phenomena (dH/dt) will not be infinite, resulting in a wedge angle α significantly smaller than 90 degrees. Therefore, the load may be developed as a sequence of quasi-stationary loads due to the impinging jet of height H . This is a case of classical fluid dynamics.

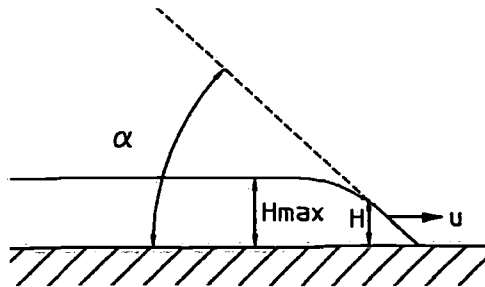


Figure 2-23
Schematic green water flow over the deck

For each time step dt in the initial stage of the impact the incoming momentum of the water flow is destroyed by the impulse of the structure on the fluid according to:

$$F dt = m dU = m (U - 0) = m U \quad (2.14)$$

Based upon the assumption of a constant velocity U of the incoming water flow in the initial stage of the impact and the shallow water assumption of a constant velocity over the full height H , the impulse will be linear with water height (characterising the mass) and the velocity at some distance from the structure (position H_3). This is confirmed by the results in Figure 2-24 in which the impulse at F2 (area under the time trace of the force) is given as function of the maximum water height H_3 multiplied by the velocity of the water front at 1 metre above the deck.

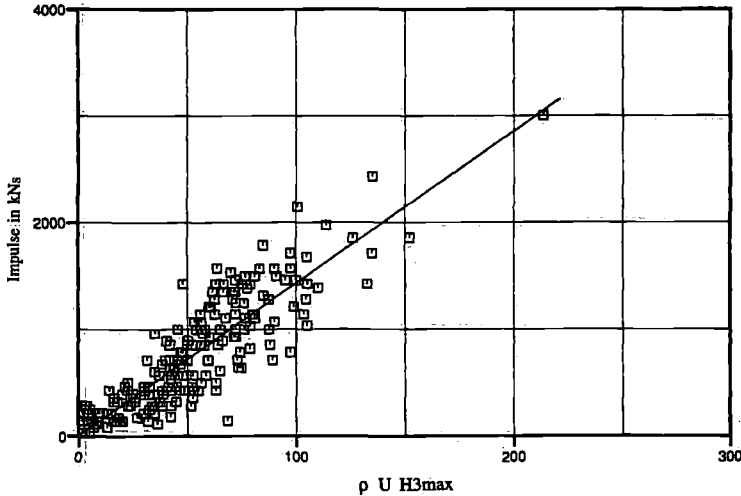


Figure 2-24

Impulse on force panel F2 as function of the maximum water height H_3 multiplied by the velocity of the water front at 1 metre above the deck

Based upon these considerations it is assumed that the peak force per metre breadth can now be expressed as the rate of change of linear momentum at the moment the maximum water height at the deck reaches the structure. This can be written as:

$$F_{\text{peak}} = \rho H_{\text{max}} U^2 \quad (2.15)$$

These values can be determined with a measurement of the water height and velocity in front of the structure, or calculated with numerical schemes. In Figure 2-25 the measured peak forces at panel F2 are shown as function of the applicable H_3 and square of the front velocity U .

Expression (2.15) and Figure 2-25 indicate that not only the water velocity is important for the structural loading per metre breadth, but that also the water height on the deck plays an important role. There is, however, no direct relation between Expression (2.15) and Figure 2-25.

The force at the circular panel F2 with a diameter of 2.70 m (5.725 m²) at a height of 2.65 m above the deck cannot be compared directly with the force in Expression (2.15) per metre breadth over the full height of the structure. The relation between the impact pressure and water height/water velocity will be studied further in later chapters.

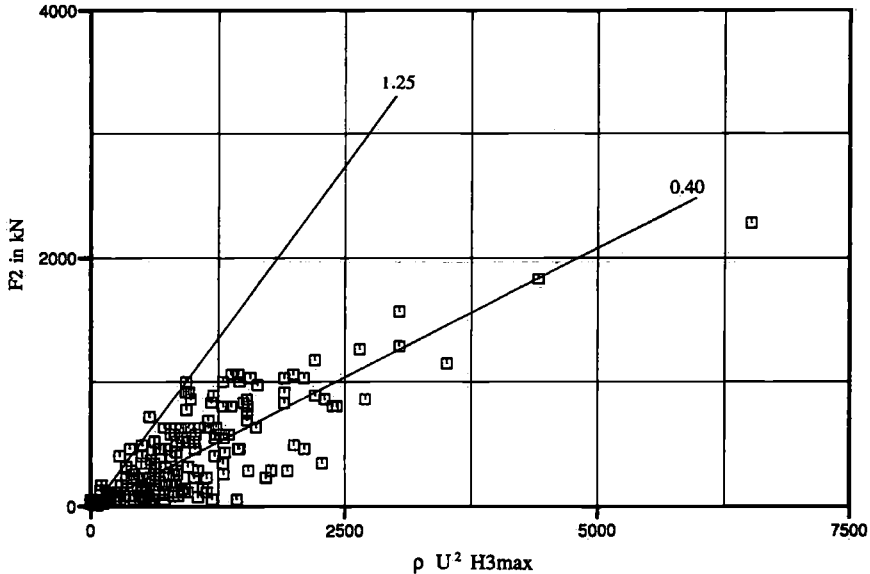


Figure 2-25

Peak force on panel F2 as function of the maximum water height H3 multiplied by the square of the velocity of the water front at 1 metre above the deck

2.9 Summary of the physics of green water on the bow

After studying the physics of green water on the bow based on these two initial series of model tests, the following can be concluded:

- A. The green water process shows the following typical sequence of events:
 - The relative wave motions exceed the freeboard level
 - The water flows onto the deck
 - The green water on the deck forms a high-velocity water jet
 - The green water impacts on a structure like an impinging jet
- B. The relative wave motions around the bow are complex and clearly non-linear.
- C. The green water on the deck has a significant effect on the ship motions, especially in shorter waves.

- D. Although the actual flow of green water onto the deck is more complex, the theoretical dam breaking theory can help to understand the green water physics better.
- E. The pressure on the deck is determined by the static water head, the vertical acceleration of the deck and an additional term related to the combination of vertical velocity of the deck and the rate of change of water height on the deck. This last term can result in peak loads in the pressure on deck of vessels. However, for a ship-type offshore structure with zero speed the accelerations are generally at their maximum at the moment the water comes onto the deck. Consequently, the vertical velocity is at its minimum. This results in a pressure on the deck that is dominated by the static pressure and the acceleration component.
- F. Green water impacts on structures typically occur in three stages: an 'impact stage', a 'quasi-static load stage' and a 'plunging water stage'.
- G. The peak load of green water on the structure is not due to a solid impact (as is the case for bottom slamming). Green water impact loading is more similar to an impinging jet with an increasing height.

These conclusions will be the basis for further detailed investigations in later chapters.

3. SYSTEMATIC MODEL TESTING

3.1 Introduction

Chapter 2 has given important insight in the physics of the green water problem in all its phases:

1. Relative wave motions
2. Water flow onto the deck
3. Water behaviour and loading on the deck
4. Green water impact on structures

In all phases of the problem non-linear and highly complex phenomena occurred. Consequently, the green water problem cannot be predicted with existing linear prediction methods. In Chapter 9 new numerical methods will be evaluated based on their ability to predict the phenomena observed in the different phases of the green water problem. However, they still need significant further development, integration and validation before they can be used to predict the green water as a whole within a reasonable timeframe.

Therefore, in this chapter the structure of a semi-empirical design evaluation method will be proposed, to predict the green water loading problem from the input (extreme relative wave motions) to the output (predicted load levels) based on a clear description of the green water physics. This semi-empirical model will be based on a systematic series of model tests. The test results will be used to:

- Further improve the understanding of the physics of the different phases in the green water problem.
- Derive empirical relations between the different parameters in the problem, based on this understanding.

These model tests can also be used for the validation of numerical prediction methods.

In this chapter first the structure of the method will be proposed. Then the systematic model test series will be presented.

3.2 Structure of the semi-empirical design evaluation method

Figure 3-1 presents the structure of the semi-empirical design evaluation method, as it will be developed in the present thesis. The figure:

- shows the building blocks with their mutual input and output relations;
- presents the design parameters the designer of ship-type offshore structures has in hand during the design process against green water (the dashed lines from the top);
- gives an overview of the required input from metocean specialists in this process (the dashed lines from the bottom).

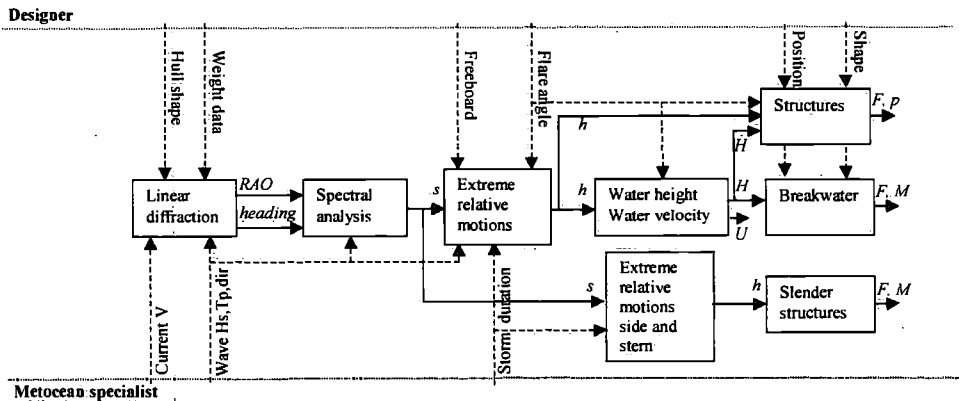


Figure 3-1
Structure of the proposed semi-empirical design evaluation method

The method will be semi-empirical because the basis for the evaluation of the green water problem is a linear diffraction calculation at zero speed. Therefore, it is possible to take into account the main characteristics of the vessel, such as its main dimensions, underwater hull shape and weight distribution. If necessary, this linear diffraction calculation can be corrected for the current speed.

After that the main (linear) vessel response in a specific sea state will be determined based on spectral analysis. Following that step, the empirical relations derived from the systematic model tests will be used to predict the non-linear green water process (from the exceedance of the freeboard by the relative wave motions to the actual loading on structures on the deck).

In the following chapters the different building blocks of the semi-empirical design evaluation method will be presented, based on the results from the systematic model test series:

- Non-linear relative wave motions at the bow (Chapter 4)
- Water flow onto and on the deck (Chapter 5)
- Green water impact loading (Chapter 6)
- Green water from the side and stern (Chapter 7)

3.3 Systematic model series

The present systematic series of model tests was carried out to understand the physics of green water on ship-type offshore structures and to derive the parameters in the semi-empirical design evaluation method for these structures. This also makes clear the focus of the study and tests:

- ship-type offshore structures: monohull structures, either being converted tanker-type hull shapes or new built barges with a certain slenderness (length over beam ratio, to be discussed further in Chapter 8).
- offshore structures: moored or dynamically positioned, with zero speed or in current.

To study the effect of the hull shape on the occurrence and loading of green water, model tests were performed with a variety of hull shapes. This variation considered the following aspects:

- For existing tankers converted to FPSOs, it is necessary to determine the probability of green water occurrence and the severity of the possible freeboard exceedances. Based on this knowledge the bow height can be modified or protecting structures can be designed.
- For new hulls it is possible to determine an optimum hull shape, which combines a minimum of green water with low wave drift forces.

The scale of all models was 1:60.

The present systematic test series was denoted Test Series C. The technical details of this test series can be found in Appendix C. Full data reports of all tests can be found in Buchner and Van Ballegoyen (1997).

3.3.1 Bow shape variations

Taking into account the aspects above, the following main bow variations were considered in this study, both with a variation of different flare angles:

- A thin triangular bow
- A full elliptical bow

The waterlines of both bows are given in the Figure 3-2. Their body plans (with bow flare of 30 degrees) are given in Figure 3-3.

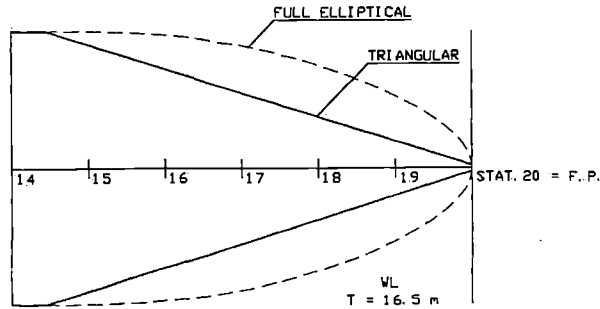


Figure 3-2
Waterlines of the thin triangular bow and full elliptical bow

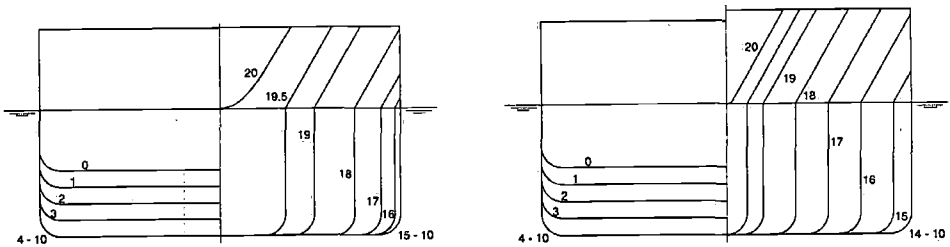


Figure 3-3
Body plans of the full elliptical bow (left) and thin triangular bow (right) with a bow flare of 30 degrees (and full stern)

The thin triangular bow represents typical new designs with sharp bows. It has been used in Test Series B as well. The full elliptical bow represents the base case for both new full bow designs as well as traditional tanker bows. A survey of typical tanker hulls showed that, with some simplifications, most of the existing tankers can be seen as a variation (in flare) of this base shape, see the examples in Figure 3-4.

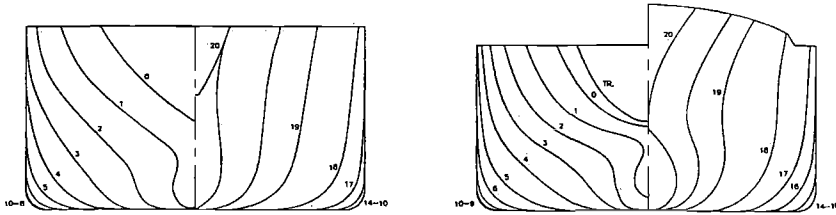


Figure 3-4
Body plans of typical existing tanker hulls

3.3.2 Bow flare variations

The bow flare angle in this Test Series C is defined as the angle of the ships side above the still waterline with the vertical, see Figure 3-5. For the thin triangular bow the bow flare angle was defined in the plane perpendicular to the ship axis, for the full elliptical bow the bow flare angle was defined in planes perpendicular to the full elliptical waterline. This implies that for the full elliptical bow the bow flare-angle is actually the rake angle in the forward section of the ship.

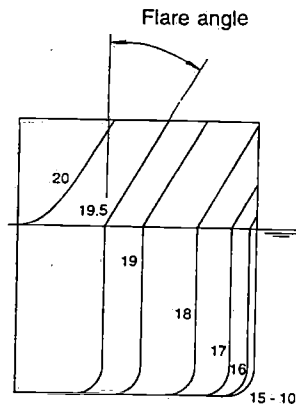


Figure 3-5
Definition of bow flare angle

The investigated hull shapes of traditional tankers had flare angles at the forward perpendicular between 10 and 50 degrees with the vertical, with a mean value of 35 degrees. This is also the typical range for new built barges. Therefore, flare angles of 10, 30 and 50 degrees were investigated for both bow shapes. In a later stage it was decided to test the full elliptical bow as well without any flare because this can be a realistic option for new barges. This model can also be used as a direct comparison with (linear) diffraction calculations, which neglect the above-water flare and assume wall-sided ships.

The main thin triangular and full elliptical bows were produced without any flare and thus with vertical sides. The flares of the hull were made as separate modules, which were fixed to the vertical sides of the main hulls above the still waterline. An example is given in Photo 3-1 for the full elliptical bow with 10, 30 and 50 degrees bow flare.

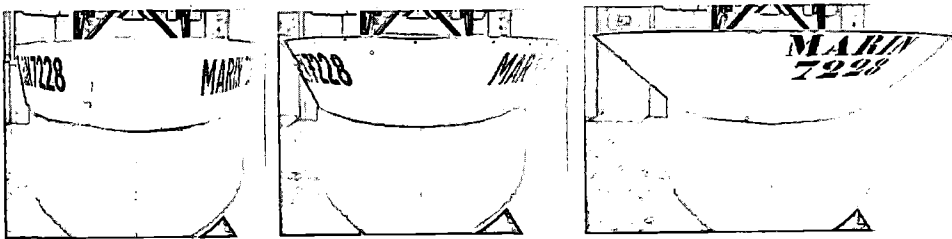


Photo 3-1

Full elliptical bow with bow flare modules of 10, 30 and 50 degrees

3.3.3 Stern shapes

It is assumed that the stern shape can have an effect on the ship motions and drift forces. For new built designs generally a flat stern is used with large buoyancy. Existing tankers are optimised on still water resistance and have thin stern shapes below the waterline.

Therefore, the (new) thin triangular bow was modelled with a flat stern. The full elliptical bow was generally used with a traditional tanker stern, but for one flare angle of the full elliptical bow also the flat stern was tested. The body plan of the full elliptical bow with traditional stern is presented in Figure 3-6.

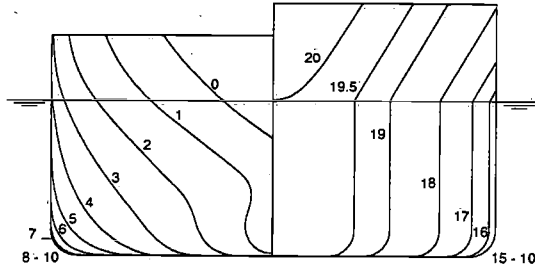


Figure 3-6
Body plan of the full elliptical bow with traditional type stern

3.3.4 Summary of basic hull models

In Table 3-1 an overview of the basic hull models is given.

Table 3-1
Overview of all the basic hull models tested

	Flare angle			
	No flare	10 degrees	30 degrees	50 degrees
Thin triangular bow, full stern	-	T10	T30	T50
Full elliptical bow, Traditional tanker stern	F0	F10	F30	F50
Full elliptical bow, full and flat stern	-	-	F30/flat	-

3.4 Structures at the bow

To investigate the sensitivity of the impact load on structures on the bow for the structural shape, a series of seven different structures was tested. The structures can represent a protection structure around the turret for bow turret systems, as well as an accommodation superstructure for heading controlled FPSOs with the turret further aft. The following structural shapes were investigated:

- Squared structure (Nos 1 and 2)
- Tilted structure under 30 degrees angle with vertical (No. 3)
- Triangular structure with 45 degrees semi-angle (No. 4)
- Triangular structure with 60 degrees semi-angle (No. 5)
- Cylindrical structure (No. 6)
- Squared structure with triangular support (No. 7)

As an example, Photo 3-2 shows the tilted structure (No. 3) and the triangular structure with 60 degrees semi-angle (No. 5), whereas Figure 3-7 shows the model and instrumentation of squared structure (No. 1). Further details about the structures and their instrumentation can be found in Appendix C.

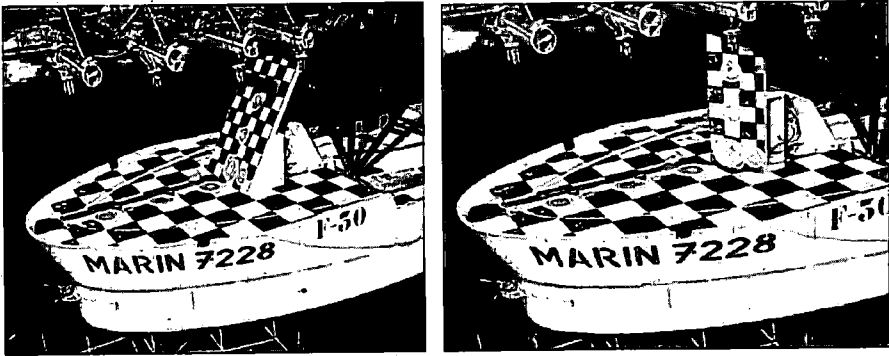


Photo 3-2

Tilted structure (No. 3) and triangular structure (No. 5, 60 degrees)

The position of the front of the structures was generally 30 m from the forward perpendicular. To check the sensitivity of the impact loads for the distance to the forward perpendicular, a limited number of tests has been carried out with Structure 2 at 10 and 20 m from the forward perpendicular.

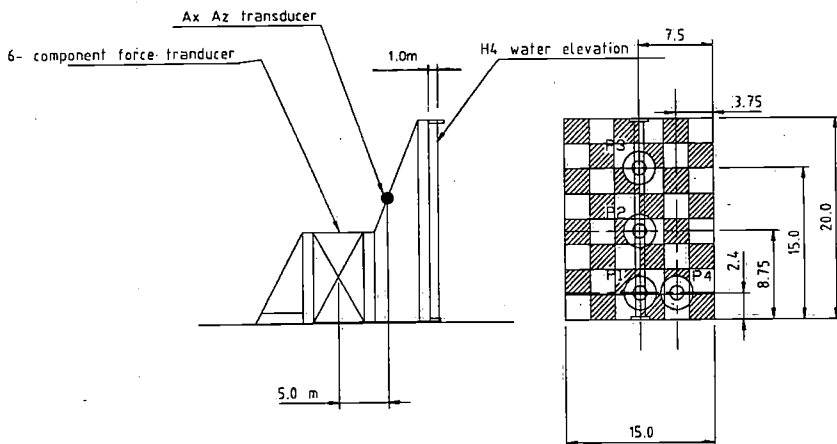


Figure 3-7

*Model and instrumentation of the squared structure: Structure 1
(dimensions in metres full scale)*

3.5 Protective breakwaters

If it is not necessary to keep an installation on the deck completely dry, it is possible to use a breakwater (water deflector) in front of it. Such a structure can also be used as a first barrier for a lighter protective structure or a superstructure. In this study three different types of breakwaters were evaluated:

1. Traditional V-type breakwater (No. 1)
2. Vertical wall breakwater with its upper side tilting forward (No. 2)
3. Vane type breakwater (No. 3)

The different breakwater shapes are shown in Photo 3-3.

All breakwaters had a height of 4.98 m from the deck level. The breakwaters were placed at a position of 16 m in front of Structure 2, which was placed 30 m from the fore perpendicular. More details can be found in Appendix C.

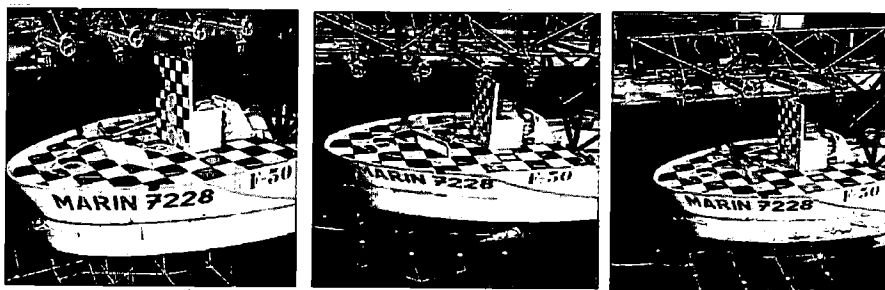


*Photo 3-3
The different breakwater types tested*

3.6 Set-up: soft spring mooring system

During all tests the model was moored in a system of 4 horizontal soft springs with a total stiffness in the x-direction corresponding to a typical medium depth mooring system (approximately 430 kN/m). In this way the first order motions are free and the low frequency motions are simulated as realistically as possible. The first order surge can be quite important for the phasing of the phenomena.

An overview of the model in the basin is given in Photo 3-4.

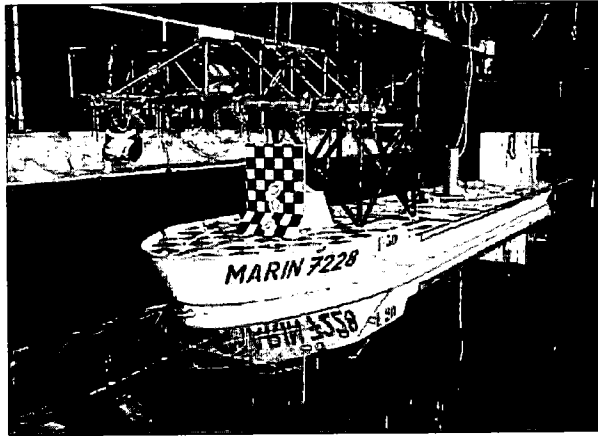


*Photo 3-4
Set-up of the model in the basin with Structure 7 on the deck*

3.7 Environmental conditions

The models were tested in a series of critical environmental conditions of regular and irregular waves. Both types of tests have their specific advantages:

- Regular wave tests can be used as a snapshot of a critical wave train in an irregular sea state. In this way the critical event is repeated and can be studied a number of times with controlled input waves, whereas in irregular waves it only occurs once or twice. The sensitivity for changes of parameters (wave height, wave period, etc.) and the effects of design variations (breakwater type, structural shape, etc.) can be studied accurately in this way. The tests also give important insight in the variability of the results with (nearly) constant input.
- Irregular wave tests can be used to determine the statistics in both the green water occurrence and loading. In irregular waves also wave phenomena can be simulated that do not occur in regular waves, such as steep and breaking wave effects.

An overview of the actual regular and irregular wave conditions used can be found in Appendix C. A range of wave heights and wave periods/lengths was used to determine the sensitivity of the results for these parameters. The main focus was on wave conditions where the wave length (λ) is similar to the ship length (L) because in this range the most critical relative wave motions occur ($0.75 < \lambda/L < 1.25$).

3.8 Analysis of combined extremes

The tests were subjected to a combined extreme analysis. In this analysis the relation was determined between the exceedance of the freeboard in front of the bow for each green water event (relative wave signal R2) and the subsequent events on the deck (water heights, water velocities, pressure on the deck, loads on the structure at the deck). Because these extremes do not occur at the same moment but sequentially, a special analysis routine was developed to couple the input (exceedance of the freeboard) to the output (water heights and impact loads) that occurs at a later stage. An example of the relation between an extreme relative motion and subsequent events on the deck in combined extreme analysis is shown in Figure 3-8.

These combined extremes over a complete test can be used to derive the relation between extreme relative wave motions (and the related freeboard exceedances) and subsequent events on the deck.

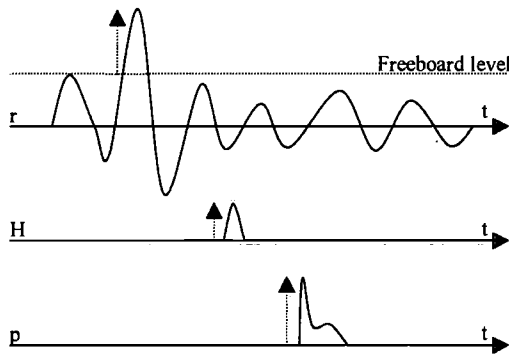


Figure 3-8

Example of the relation between an extreme relative motion and subsequent events on the deck in combined extreme analysis

4. NON-LINEAR RELATIVE WAVE MOTIONS AT THE BOW

4.1 Introduction

In this chapter the predictive model for the first step in the green water loading process will be presented: the extreme relative wave motions. Figure 4-1 shows (in grey) the exact blocks in the semi-empirical design evaluation method that are considered in this chapter.

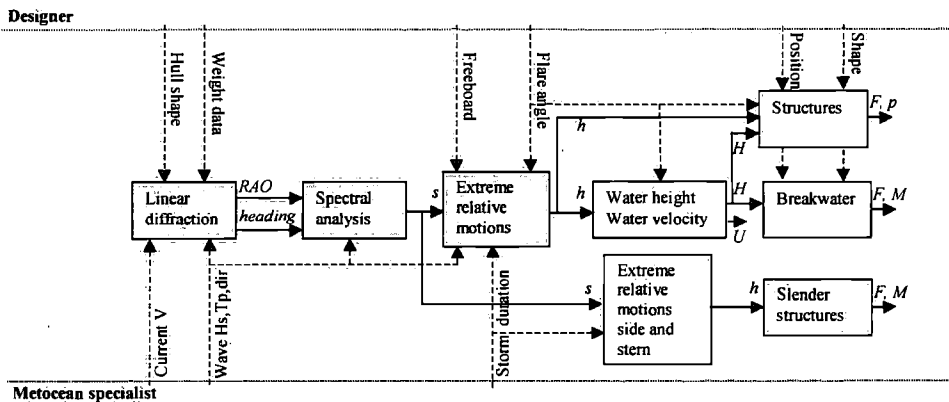


Figure 4-1

Part of the proposed semi-empirical design evaluation method considered in this chapter (in grey): prediction of extreme relative wave motions and related freeboard exceedance (h) at the bow

This part of the method has the following input:

- Hull shape
- Weight data
- Freeboard level
- Flare angle
- Significant wave height (H_s), peak period (T_p), spectral shape and wave direction
- Current speed
- Storm duration

The output is the prediction of the Most Probable Maximum (MPM) freeboard exceedance: h . This will be the input to the subsequent blocks in the design evaluation method.

4.2 Description of non-linearities

As was found in the initial model tests in Test Series A and B, the relative wave motions measured in the systematic Test Series C were significantly non-linear. Figure 4-2 shows the probability of exceedance of the relative wave motions in front of the bow for the full elliptical bow. The results are given for the different irregular waves with peak periods T_p of 12 s, 14 s and 16 s and a significant wave height H_s of 13.5 m. Both the measured probability of exceedance and the linear narrow-banded Rayleigh distribution based on the measured standard deviation (7.86 m, 7.40 m and 6.32 m respectively) are presented.

As can be seen from these figures, the measured distribution deviates significantly from the Rayleigh distribution. The Rayleigh distribution underpredicts the probability of exceedance of small crests, but overpredicts the probability of exceedance of the larger crests (above the freeboard level). The difference between the Rayleigh and measured distributions is dependent on the wave period. In shorter period waves the differences are much larger than in longer period waves.

Clearly a discontinuity of the distribution around the freeboard level (10.5 m) is observed. The effect of the water on deck on the ship motions and the effect of the above water hull shape on the dynamic swell up both show a discontinuity at this point.

Not only the relative wave motions are highly non-linear; also the pitch motions in survival waves with water on the deck deviate much from the predictions based on linear theory. In Figure 4-3 the measured probability of exceedance of pitch amplitudes is compared with the Rayleigh distribution for a T_p of 14.0 seconds.

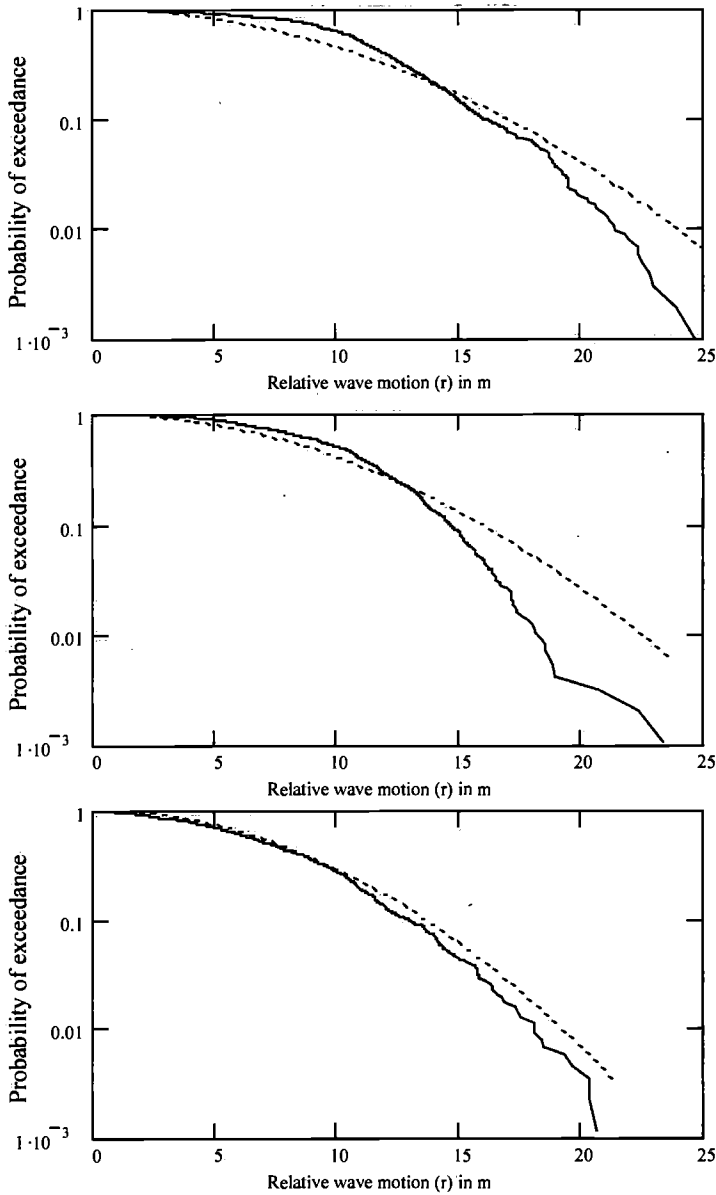


Figure 4-2

Probability of exceedance of the relative wave motions in front of the bow (position R2) for the full elliptical bow with a flare angle of 30 degrees for $T_p = 12$ s, 14 s and 16 s (from top to bottom). The solid line presents the measured probability of exceedance, the dotted line shows the Rayleigh distribution (based on the measured standard deviation)

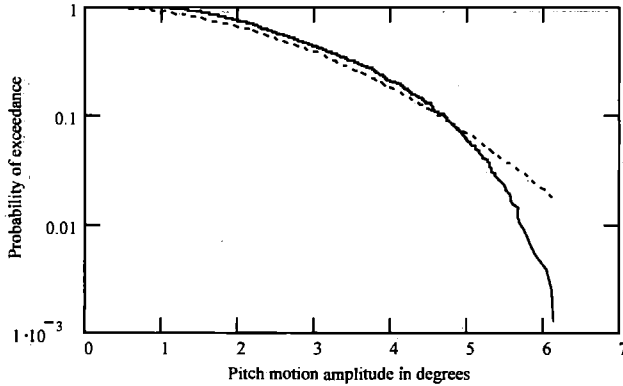


Figure 4-3

Probability of exceedance of the pitch motions for the full elliptical bow with a flare angle of 30 degrees for $T_p = 14$ s, the dotted line shows the Rayleigh distribution (based on the measured standard deviation)

Especially for large pitch angles the Rayleigh distribution predicts a much higher probability of exceedance. This is largely due to the effect of the water on the deck.

The observed non-linearities are not only present in irregular waves, but also in regular waves. Because a large number of wave heights were tested per wave length, this non-linearity could be quantified. Figure 4-4 shows the differences between linear predicted relative wave motion results and the actual measured results with the same regular wave heights. The straight line in the figures represents a perfect match between the measurements and calculations. If the points are above this line, the measurements are lower than the linear prediction. If they are below the line, the measurements are higher than the linear prediction. The results are shown for different ratios between the wave length (λ) and the ship length (L). Table 4-1 shows the values of the linear relative wave motion RAO $H(\omega)$ at the different wave lengths.

Table 4-1

Linear relative wave motion RAO for the different wave lengths (full elliptical bow with 30 degrees flare and traditional stern)

λ/L	ω	$H(\omega)$
1.25	0.435 rad/s	2.229 m/m
1.00	0.487 rad/s	2.824 m/m
0.75	0.563 rad/s	2.310 m/m

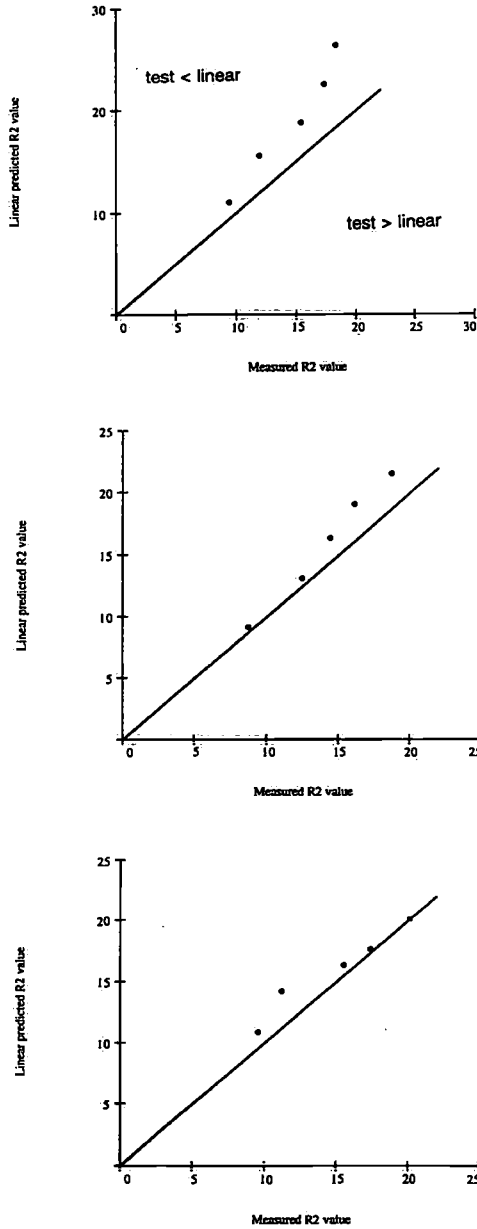


Figure 4-4
Measured versus calculated relative motion amplitudes for different ratios between regular wave length and ship length full elliptical bow with 30 degrees flare and traditional stern:
 $\lambda/L = 1.25$ (top), 1.0 (middle) and 1.75 (bottom)

For small wave heights the measurements are close to the theoretical results, which confirms the validity of linear theory for smaller wave heights. However, when the wave height increases, the differences in general seem to increase too. Especially for the long waves the measured results are lower than the linear prediction. In the short waves ($\lambda/L=0.75$) the results come close to the linear result at the largest wave amplitudes again, after a larger difference at smaller amplitudes.

This non-linearity is confirmed by the comparison between measured and calculated pitch and relative wave motion RAOs in Figures 4-5 and 4-6 for the full elliptical bow with 30 degrees flare angle and traditional tanker stern.

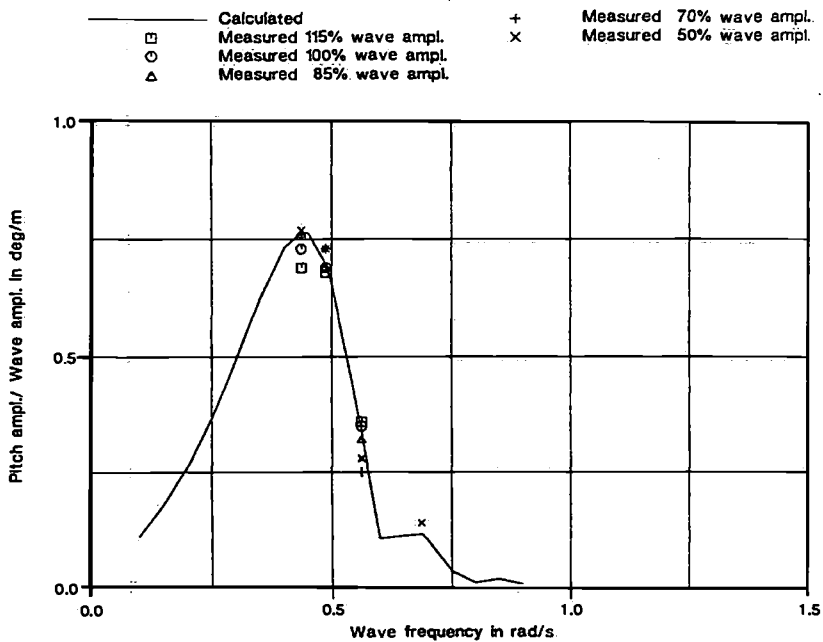
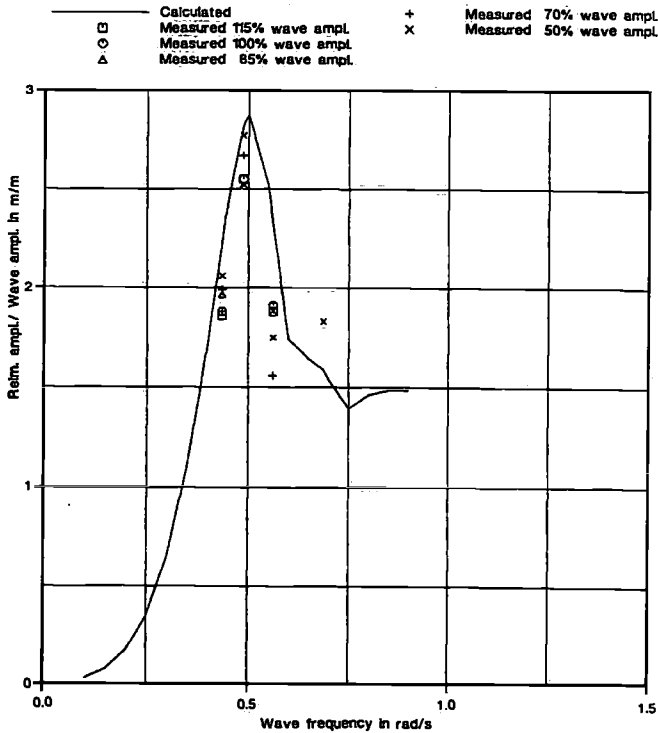


Figure 4-5

Calculated pitch motion RAO for the full elliptical bow with 30 degrees flare angle and traditional tanker stern compared to regular wave measurements for different wave amplitudes



*Figure 4-6
 Calculated relative wave motion RAO for the full elliptical bow with 30 degrees flare angle
 and traditional tanker stern compared to regular wave measurements
 for different wave amplitudes*

In general, the measurements approach the calculations when the wave amplitude decreases.

4.3 Physical background of non-linearities

The physical background of the observed non-linearities can be related to the following effects:

- The effect of the water on deck on the ship motions
- The effect of the above water hull shape at bow and stern
- The effect of the non-linearities in the waves

These effects will be discussed below.

4.3.1 The effect of the water on deck on the ship motions

As was discussed in Section 2.4.1, the green water on the deck has a large moment arm with respect to the centre of gravity of the ship. In this way the moment as a result of the green water (M_g) is relatively large with respect to the wave exciting moment (M_θ), especially in short waves.

For the full elliptical bow with a bow flare of 30 degrees the moment as a result of the green water on deck was estimated for the three different regular wave lengths tested. For this purpose the deck of the FPSO was divided into three strips around the water height probes H_1 , H_2 and H_3 with areas a_{r1} , a_{r2} and a_{r3} , see Figure 4-7. In accordance with Expression (2.4) the green water moments were calculated.

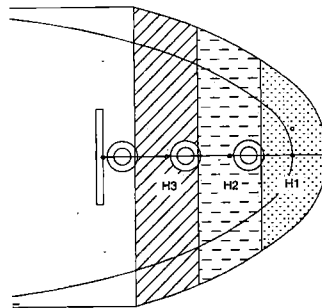


Figure 4-7

Transverse strips used to calculate the green water moment. The water height is assumed to be constant and equal to the water height at the related water height probe at the centreline

In Table 4-2 the maximum values of M_g are shown for the three different regular wave lengths at their maximum wave height of 115%. The linear wave moment M_θ is also shown for the same wave height.

Table 4-2

Maximum values of the green water moment M_g for the three different regular waves lengths at their maximum wave height of 115% and the linear pitch moment amplitude M_θ for the same wave height

Ratio wave length to ship length λ/L	Estimated maximum green water moment M_g in kNm	Linear wave moment amplitude M_θ in kNm
1.25	$7.13 \cdot 10^6$	$2.82 \cdot 10^7$
1.00	$6.44 \cdot 10^6$	$1.37 \cdot 10^7$
0.75	$4.82 \cdot 10^6$	$4.82 \cdot 10^6$

It will be clear from these numbers that the green water moment can have a large effect on the ship motions, especially in short waves. Its final effect is dependent on the phase of this moment compared to the ship motions and wave exciting moment.

4.3.2 The effect of the above water hull shape

Another important aspect in the non-linearity of the relative wave motions, is the effect of the hull shape above the still waterline in large waves. Based on the assumption that the waves are small, linear theory only considers the part of the ship which is submerged in calm water. Everything above the still waterline is neglected in this type of analysis.

However, if the waves and ship motions are large, the bow and stern of the vessel are pushed into the water and the effect of the above water shape cannot be neglected any more. The additional buoyancy and wave loading results in an effect on the ship motions, such as pitch. The above water bow flare also has a significant disturbance on the wave pattern around the bow. Figure 4-8 shows the wave contour in front of the full elliptical bow with a bow flare of 30 degrees, based on a similar plate at the centreline of the ship as was described in Section 2.3.1.

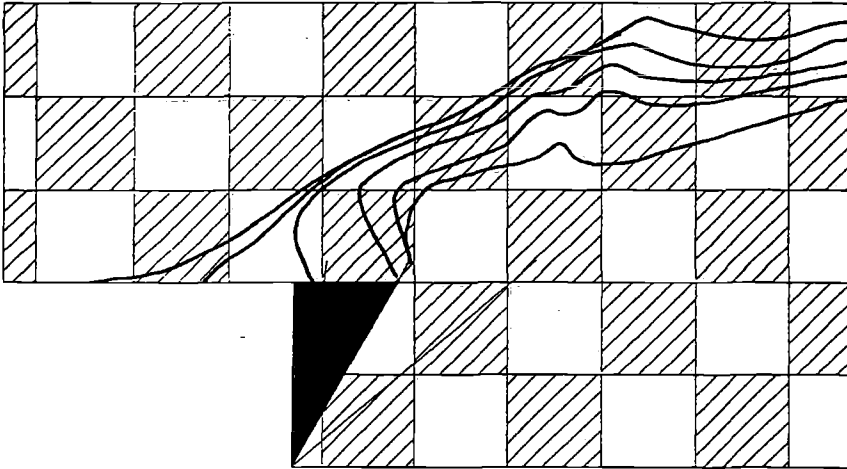


Figure 4-8

Wave contour in front of the full elliptical bow with a bow flare of 30 degrees with time steps of 0.31 s (regular wave of $\lambda/L=1.0$, $H=115\%$)

This figure clearly shows the disturbance of the wave in a ripple, which is progressing away from the bow. This ripple is caused by the above water hull shape and has its effect on the relative wave motions. The flared (3D) wedge, which is pushed in the water with a certain velocity, results in a swell-up around the bow.

In Figure 4-9 the time traces are shown of the relative wave motion at position R3 in regular wave tests on the full elliptical bow with flare angles of 10, 30 and 50 degrees. It is clear from these time traces that the ripple on the relative wave signal is increasing with the flare angle. With hardly any flare (10 degrees) the time traces are almost sinusoidal, but for 30 and 50 degrees the disturbance of the sinusoidal signal is significant.

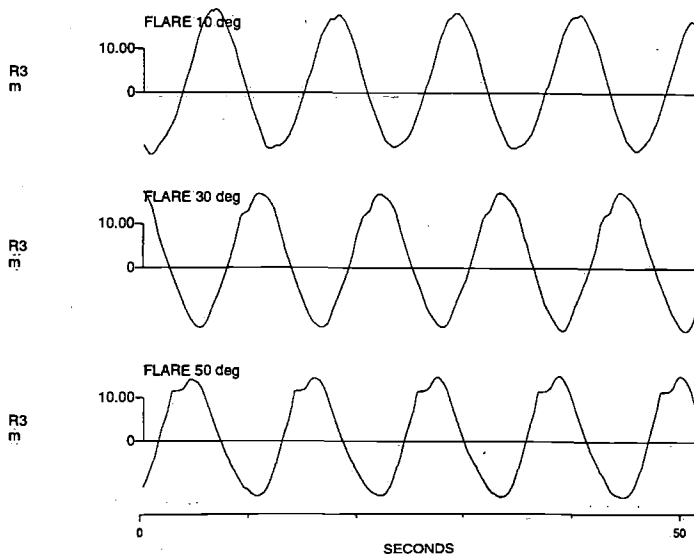


Figure 4-9

Time traces of relative wave motion probe R3 in front of the full elliptical bow with bow flare angles of 10, 30 and 50 degrees in a regular wave.

It should be noted that the disturbance of the bow flare stops when the relative wave motion comes above the deck edge. After such freeboard exceedance the ripple progresses away from the bow and does not affect the relative wave motions around the deck edge any more. Watanabe, Ueno and Sawada (1989) and Watanabe (1990) found something similar in their study on the effect of bow flare on relative wave motions and deck wetness for a container ship. They point to the complex deformation of the incoming wave profile by the bow flare and observed a concentration of amplitudes at approximately the freeboard height in irregular waves.

Considering the effect of this wave disturbance on the peaks in the relative wave motions now, it can be seen that the effect on the peak values for large freeboard exceedances is small. In this case the wave disturbance is already at a distance from the bow at the moment that the relative wave motion reaches its maximum, as can be seen in the wave contour in the Figure 4-8.

However, for smaller maxima in the relative wave motions, which do not come (high) above the deck edge, the effect of the bow flare is relatively large. This is shown in the time traces in Figure 4-10 for the relative wave motion R2 in front of the bow for three different regular wave heights (100, 85 and 70%).

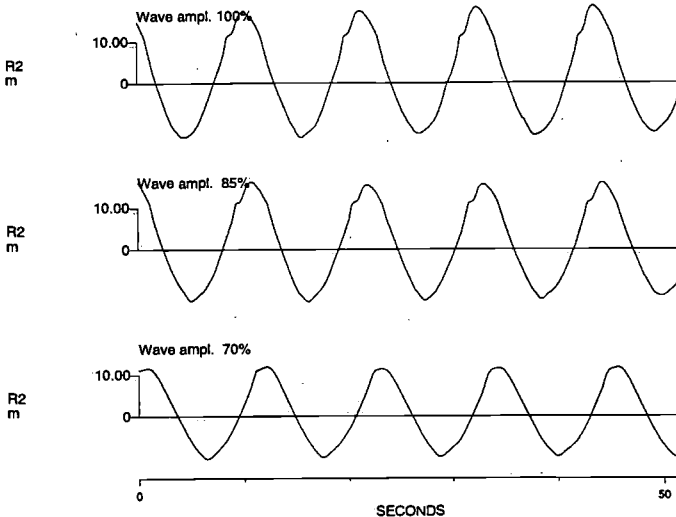


Figure 4-10

Time traces of relative wave motion probe R2 in front of the full elliptical bow with bow flare angle of 30 degrees in a regular wave of different wave heights (70, 85 and 100%)

For the largest wave amplitude (100%) the bow flare disturbance is a ripple on the time trace of the relative wave motions, without an effect on the maximum amplitude. However, for the smaller wave heights the disturbance really affects the maximum amplitudes (especially at 70% wave height). In irregular wave spectra something similar will happen, where the small maxima below the freeboard are increased by the above water flare angle, whereas the larger maxima are not affected.

This is confirmed by the probability of exceedance plots of the relative wave motions in Figure 4-2. The probability of exceedance of the small maxima was larger than predicted according to the Rayleigh curve, whereas the Rayleigh curve overpredicts the large maxima. This overprediction for the larger amplitudes is partially a result of the effect of the water on the deck on the ship motions, but it is also affected by the water that flows onto the deck. This decreases the water height in the area around the bow, as can be seen in the theoretical solution of the dam breaking problem. The effect of a breaking dam is not limited to the downstream (deck) side. It also lowers the water on the upstream (water) side, see Stoker (1957).

4.1.3 The effect of the non-linearity in the waves

As input to the green water problem the incoming waves can be an important source of non-linearities in the relative wave motion result. In Figure 4-11 the probability of exceedance of the wave crests is shown for the three applied survival spectra with peak periods of 12 s, 14 s and 16 s. The theoretical lines based on the Rayleigh distribution and the measured standard deviations (3.40 m, 3.42 m and 3.36 m respectively) are shown as well.

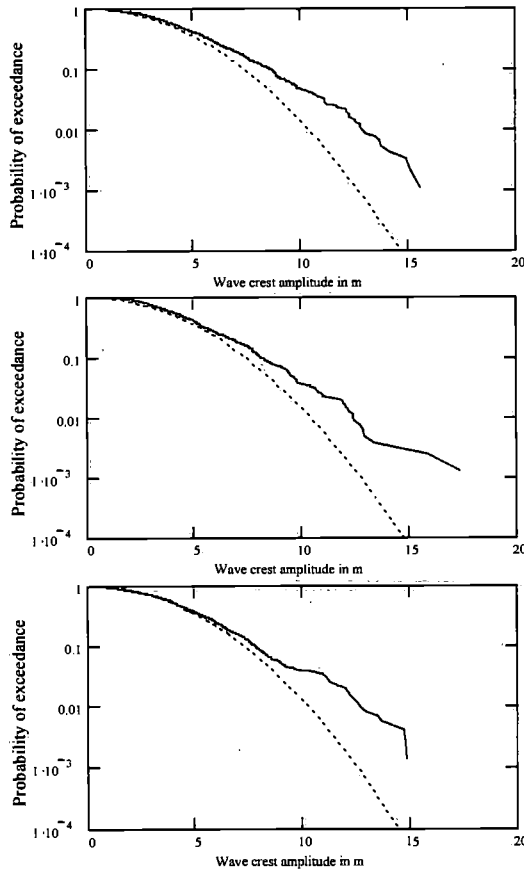


Figure 4-11

Measured probability of exceedance of wave crests for a significant wave height of 13.5 m and peak periods of 12 s, 14 s and 16 s (from top to bottom), compared to the linear narrow-banded Rayleigh distribution (dotted line)

This figure clearly shows that for this type of survival waves the wave crests do not follow the Rayleigh distribution. In fact, the Rayleigh distribution underestimates the probability of exceedance of extreme wave crests significantly.

Although this effect was expected (see Kriebel and Dawson, 1993), it is surprising that this does not lead to an underestimation of the relative wave motions by the Rayleigh distribution. This suggests that the effect of the water on deck and the effect of the above water hull shape decrease the relative wave motions in large waves, whereas the non-linearity in the waves has an opposite effect. This makes the description of the combined non-linearity even more complex.

A similar trend was found in the regular waves. In Figure 4-12 the non-linear wave crest and trough amplitudes of the regular waves are compared with the first harmonic wave amplitudes for the ratio $\lambda/L=0.75$.

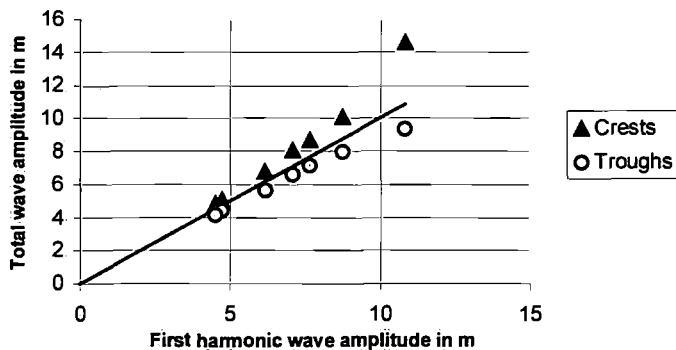


Figure 4-12

The non-linear total wave crest and trough amplitudes of the regular waves compared with the first harmonic wave amplitudes for the ratio $\lambda/L=0.75$

As expected, the figure shows that the wave crests, which are important for the green water problem, are higher than the first harmonic amplitude, whereas the troughs are smaller.

4.4 Review of existing descriptions of non-linearities

The observed non-linearities in the previous section show that the relative wave motions cannot be predicted reliably with the direct use of linear response functions, spectral analysis and a Rayleigh distribution. A number of methods was investigated for the description of these non-linearities. In this section first a number of possibilities are discussed, before the final method will be chosen in the next section.

The number of methods for the description of non-linear distributions of extremes is large. A number of them was investigated and evaluated on the applicability for the present green water problem.

Blok and Huisman (1984) evaluated the relative wave motions around a frigate bow. Based on earlier work by Tasai (1961), they presented a dynamic Swell-Up Coefficient (SUC) for the relative wave motions calculated with linear strip theory.

$$r_s = \text{SUC} \cdot r_0 \quad (4.1)$$

Although other definitions of the SUC are found as well, in this expression r_s is the relative wave motion including the swell-up and r_0 is the relative wave motion as a result of heave, pitch and the undisturbed incoming wave. In linear strip theory the reflected (diffracted) wave motions are not taken into account and are included in the Swell-Up Coefficient, together with the effect of the hull shape above the still waterline.

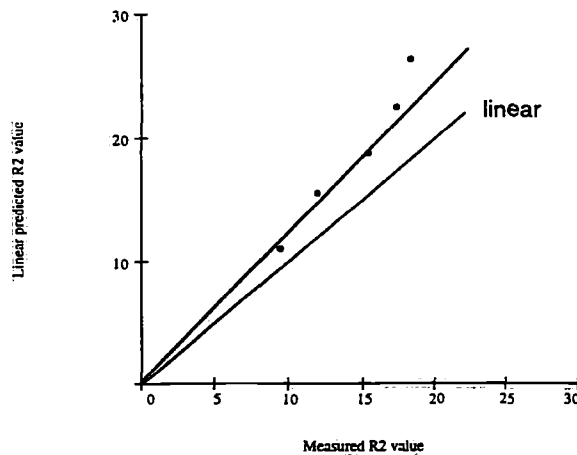


Figure 4-13

Measured versus calculated relative wave motion amplitude with a line based on a linear assumptions and a line applying a Swell-Up Coefficient (SUC) for $\lambda/L=1.25$

The problem with this type of approach is that the Swell-Up Coefficient is constant and, consequently, a linear - or linearised - correction. However, in the extreme cases considered in this study, the deviation from the linear prediction is strongly dependent on the wave height and thus non-linear. Therefore it cannot be expressed as a straight line in the regular wave results, as shown in Figure 4-13. In this case the SUC would even be smaller than 1.0.

The same applies to irregular waves. If the Rayleigh distribution is applied based on the standard deviation corrected with a SUC, the typical non-linear curvature observed in the measurements cannot be reproduced. Figure 4-14 shows, as example, the probability of exceedance for the relative wave motion R2 in the wave spectrum with a peak period of 14.0 s. The Rayleigh distribution is shown for a standard deviation of 7.4 m (from the linear diffraction calculation) and two lower values of 6.4 m and 5.4 m (assuming some SUC-value).

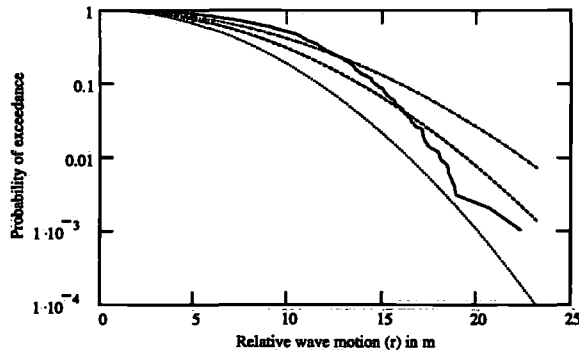


Figure 4-14

Measured probability of exceedance curve compared to the Rayleigh distribution curve for the standard deviation calculated with linear theory (7.4 m) and for SUC-corrected values (6.4 m and 5.4 m)

It will be clear that none of these curves result in a good fit with the measured results. Therefore, it can be concluded that methods using a Swell-Up Coefficient are not sufficient and do not significantly improve our capabilities to predict extreme values. This indicates that a modified distribution of extremes has to be developed.

Adegeest (1995) successfully applied a third order Volterra modelling to determine non-linear hull girder loads in irregular waves. He used the first, second and third order response functions from regular wave tests or time domain simulations of ship motions taking into account the Froude-Krylov forces on the above water hull shape. The applied method assumes that the non-linear response on a linear wave input can be described by a combination of a limited number of harmonics, which in Adegeest (1995) was limited to the first, second and third harmonics. It should be noted that this requires a smooth output signal. The presented simulations were carried out in relatively low waves that did not show much non-linearity. Freeboard exceedances were not studied. Taking into account the importance of the freeboard exceedances and the discontinuity in the relative wave motions at this point, this method cannot be used directly for the green water problem.

A lot of literature is also available on the non-linearity of ocean waves, see e.g. Longuet-Higgins, Kriebel and Dawson (1993), Arhan and Plaisted (1981) and Tayfun. Empirical, semi-empirical as well as theoretical expressions are proposed. Kriebel and Dawson for instance used Stokes second-order wave theory to come to a modified Rayleigh distribution for the prediction of the extreme wave crest heights.

Some authors working in the field of green water predictions, such as Drake (2000, 2001) and Stansberg and Karlsen (2001) take the non-linearity in the waves as the main component in the prediction of the extreme relative wave motions. Wang, Juncher Jensen and Xia (1998) use an instantaneous correction of relative wave motion depending on the submergence of the deck, in this way taking into account the discontinuity at the freeboard level. As will be the case for the method proposed in the present study, all approaches include empirical corrections based on model test results.

In the method proposed in the present study, the discontinuity in the relative wave motions at the freeboard level is accounted for as well. It is not based on time domain simulations, but on a probabilistic evaluation of the relative wave motions. A modified expression for the probability of exceedance is used to determine the Most Probable Maximum relative wave motions. This expression will be based on systematic Test Series C and is dependent on bow flare and wave period.

4.5 Proposed method for the prediction of relative wave motion extremes

4.5.1 Introduction

As indicated in Section 4.1, the output of this part of the design evaluation method should be the Most Probable Maximum freeboard exceedance h , as function of the following input:

- Hull shape
- Weight data
- Freeboard level
- Flare angle
- Significant wave height (H_s), peak period (T_p), spectral shape and wave direction
- Current speed
- Storm duration

It was finally decided to develop a modified Rayleigh distribution that accounts for the non-linearities and discontinuity observed, using the linear relative wave motion

response from diffraction theory and spectral analysis as input. This has the following background:

- a. The results of 3D linear diffraction analysis are taken as a starting point of the investigations because linear diffraction analysis is a reliable and validated method that is widely available in the offshore industry. It is fast because it can be used in the frequency domain. The results presented in this study show differences between measurements and diffraction calculations in large survival waves, but still it is clear that diffraction theory predicts the main trends correctly. In small waves the validity of the method is very good. The use of linear diffraction theory also makes it possible to apply the empirical results from the present systematic test series for other hull shapes than tested (see Chapter 8 for the range of applicability).
- b. The Rayleigh distribution, applicable for linear narrow-banded response to Gaussian distributed waves, is the other starting point of the development of the method. Considering again that in small wave amplitudes the relative wave motion response is rather linear, it was decided to use the existing Rayleigh distribution as basis and apply corrections for the discontinuity at the freeboard level and non-linearities for the larger extremes, rather than proposing a completely new distribution.
- c. The non-linearities in the relative wave motions are a result of different (but interacting) non-linear processes: the effect of the water on deck on the ship motions, the effect of the above water hull (bow flare and discontinuity at the deck edge) and the non-linearities in the waves. Non-linear time domain simulation methods presently under development cannot account for this combination yet. Because of the interaction between all non-linearities observed, they cannot be considered separately. Therefore, the non-linearities are considered together in their effect on the relative wave motions.
- d. The discontinuity in the relative wave motions at the freeboard level can be accounted for as well.

In the following sections the development of the method will be discussed. After that the method will be validated. In Chapter 8 important notes are finally made about its range of applicability.

4.5.2 Relative wave motions below the freeboard

Starting point is the linear diffraction calculation of the relative wave motions at the centreline of the ship directly in front of the bow (at waterline in calm water). This linear calculation includes the ship motions and the incoming undisturbed, reflected (diffracted) and radiated waves. Using the Response Amplitude Operators from the

diffraction calculations the relative wave motion response in the applicable wave spectrum can be determined, with its standard deviation and typical period.

Based on the observation that linear theory predicts the relative wave motion very well in small waves, it was decided to develop a modified Rayleigh distribution for the relative wave motions below the freeboard. A similar procedure will be followed as was used by Kriebel and Dawson (1993) for the description of non-linear wave crest statistics.

The start is the assumption that the deviation of the non-linear result r from the linear result r_1 can be expressed with the following second-order polynomial function:

$$r_1 = \alpha \cdot r + \beta \cdot r^2 \quad (4.2)$$

This expression is always going through zero, which implies that for small motions the linear result and non-linear result are approaching each other. An example is shown in Figure 4-15 for the regular wave tests with different wave heights for $\lambda/L=1.25$.

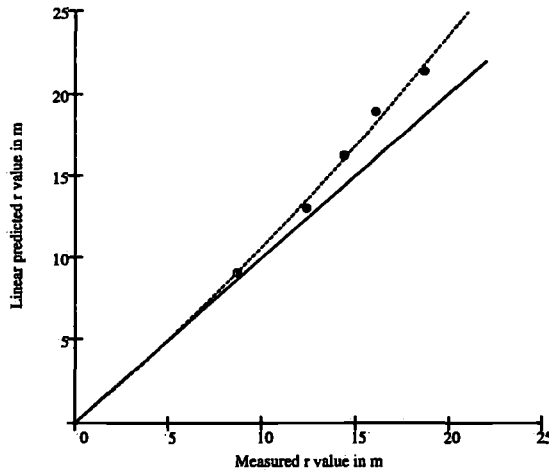


Figure 4-15

Measured versus calculated relative wave motion amplitudes (dots) with a line based on a linear assumption (solid line) and a second-order polynomial function (dashed line) for $\lambda/L=1.25$

For narrow band linear systems the probability of occurrence $p(\eta)$ can be expressed as:

$$p(\eta) = \frac{\eta}{s^2} \cdot \exp\left[-\frac{\eta^2}{2s^2}\right] \quad (4.3)$$

The probability of exceedance is equal to the Rayleigh distribution.

The probability of occurrence of the non-linear amplitude $p(r)$ can now be obtained from Expressions (4.2) and (4.3) by transformation of random variables, see for instance Kriebel and Dawson (1993) and Tayfun:

$$p(r) = p(\eta) \frac{d\eta}{dr} \quad (4.4)$$

Therefore:

$$\frac{d\eta}{dr} = \alpha + 2\beta \cdot r \quad (4.5)$$

This results in the following expression for the probability of occurrence of the non-linear relative motion r :

$$p(r) = \frac{\alpha \cdot r + \beta \cdot r^2}{s^2} \cdot \exp\left[-\frac{(\alpha \cdot r + \beta \cdot r^2)^2}{2s^2}\right] \cdot (\alpha + 2\beta \cdot r) \quad (4.6)$$

The probability of exceedance of a certain value R can now be expressed as:

$$P(r > R) = \int_R^{\infty} \frac{\alpha \cdot r + \beta \cdot r^2}{s^2} \cdot \exp\left[-\frac{(\alpha \cdot r + \beta \cdot r^2)^2}{2s^2}\right] \cdot (\alpha + 2\beta \cdot r) dr \quad (4.7)$$

To come to a closed form solution, this is converted according to:

$$P(r > R) = 1 - P(r < R) \quad (4.8)$$

$$P(r > R) = 1 - \int_0^R \frac{\alpha \cdot r + \beta \cdot r^2}{s^2} \cdot \exp\left[-\frac{(\alpha \cdot r + \beta \cdot r^2)^2}{2s^2}\right] \cdot (\alpha + 2\beta \cdot r) dr \quad (4.9)$$

Which is equal to:

$$P(r > R) = \exp \left[\left(-\frac{R^2}{2s^2} \right) \cdot (\alpha^2 + 2\alpha\beta.R + \beta^2.R^2) \right] \quad (4.10)$$

Simplifying the constants in the equation, this can be written as the following modified Rayleigh distribution for the relative wave motions below the freeboard:

$$P(r > R) = \exp \left[\left(-\frac{R^2}{2s^2} \right) \cdot (a + b.R + c.R^2) \right] \quad (4.11)$$

This is a second order correction of the original Rayleigh distribution. For $a=1$, $b=0$ and $c=0$ it reduces to the Rayleigh distribution itself. This expression was proposed in Buchner (1998), but based there on the incorrect assumption of a third order polynomial as a start. The related probability of occurrence $p(r)$ becomes:

$$p(r) = \left[\left(-\frac{r}{2s^2} \right) \cdot (2.a + 3.b.r + 4.c.r^2) \right] \exp \left[\left(-\frac{r^2}{2s^2} \right) \cdot (a + b.r + c.r^2) \right] \quad (4.12)$$

Using the measured probability of exceedance of the relative wave motions, it is now possible to determine the parameters a , b and c such that Expression (4.11) follows the measured distribution as good as possible. The assure realistic values for P and p (between 0 and 1), the coefficients a , b and c should fulfil the following conditions for a realistic range of r or R : $2.a + 3.b.r + 4.c.r^2 > 0$ and $a + b.R + c.R^2 > 0$. For the coefficients presented in Tables 4-3 and 4-4 this is the case for relative wave motions between 0 and 25 m.

This solution works for the distribution of the extremes below the freeboard. However, the discontinuity around the freeboard level has to be accounted for as well.

4.1.3 Relative wave motions above the freeboard

After an evaluation of the problem it was decided to develop an additional expression for extremes above the freeboard. Starting point is the probability of exceedance of the freeboard level (fb):

$$P(r > fb) = \exp \left[\left(-\frac{fb^2}{2s^2} \right) \cdot (a + b \cdot fb + c \cdot fb^2) \right] \quad (4.13)$$

For the probability of exceedance of relative wave motions above the freeboard the following expression was developed:

$$P(r > R) = \exp \left[\left(-\frac{fb^2}{2s^2} \right) \cdot (a + b \cdot fb + c \cdot fb^2) + \left[(R - fb) \cdot d + (R - fb)^2 \cdot e + (R - fb)^3 \cdot f \right] \right] \quad (4.14)$$

This expression guarantees a connection between the probability of exceedance curves above and below the freeboard and is similar to the assumed correction in the part below the freeboard. Using the expressions above (Expression 4.14) and below (Expression 4.11) the freeboard level, it is now possible to determine the parameters a to f for a fit on the measured distributions.

In Figures 4-16 and 4-17 the measured probability of exceedance is compared with the modified Rayleigh distribution for the full elliptical bow and traditional stern. Figure 4-16 shows the results for a bow flare of 30 degrees for different spectral peak periods of 12, 14 and 16 s. Figure 4-17 presents the results for a spectral peak period of 14 s, but now for different bow flare angles of 0, 10, 30 and 50 degrees.

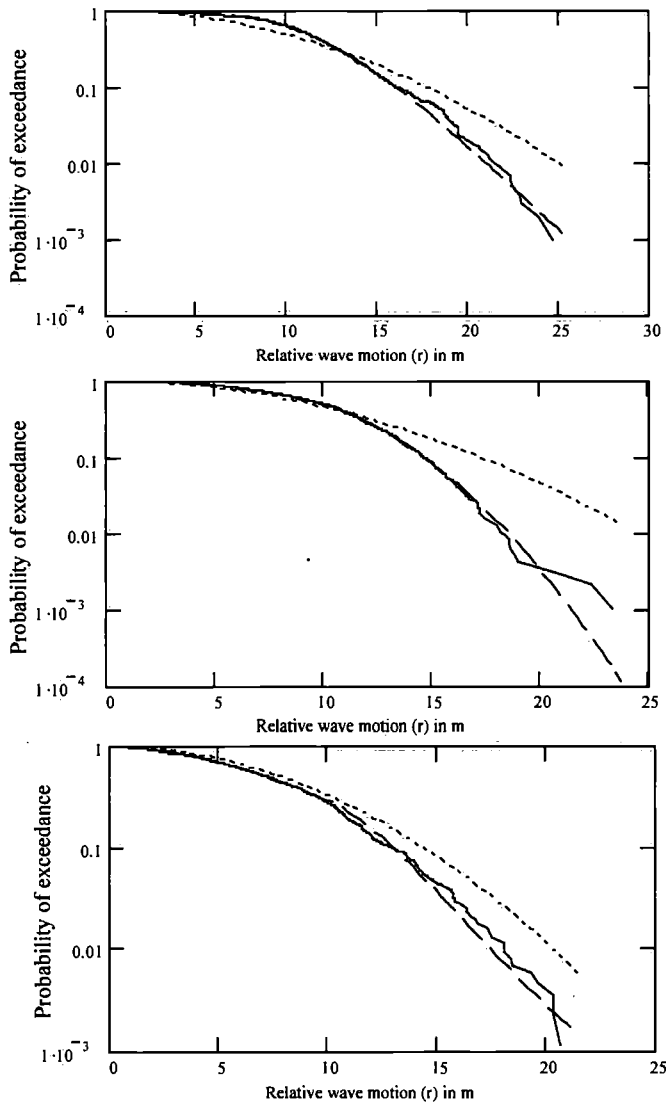


Figure 4-16

Measured probability of exceedance curves with the fitted modified Rayleigh distributions for the full elliptical bow with traditional stern, bow flare of 30 degrees and spectral peak periods of 12, 14 and 16 s (from top to bottom). The figure shows: the measurement (solid line), the Rayleigh distribution (dotted line) and the modified Rayleigh distribution (dashed line)

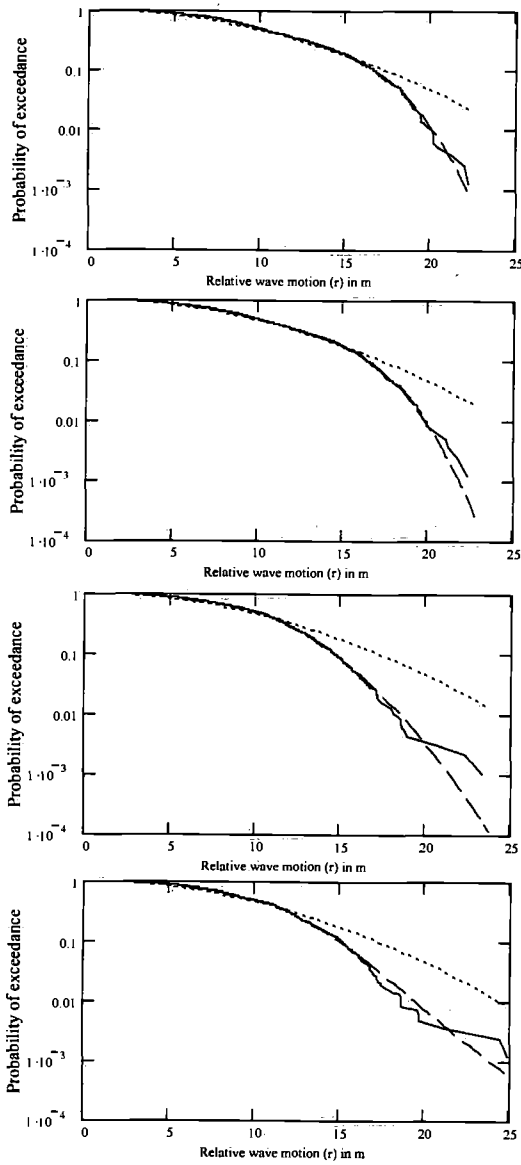


Figure 4-17

Measured probability of exceedance curves with the fitted modified Rayleigh distributions for the full elliptical bow with traditional stern, spectral peak period of 14 s and bow flare angles of 0, 10, 30 and 50 degrees (from top to bottom). The figure shows: the measurement (solid line), the Rayleigh distribution (dotted line) and the modified Rayleigh distribution (dashed line)

The following can be observed:

- For the longer periods the modified Rayleigh distribution is closer to the standard Rayleigh distribution with its linear and narrow banded assumptions, whereas in the short waves strong non-linearities are observed.
- The chosen expressions are able to describe the observed non-linear distributions with their different behaviour above and below the freeboard. The probability of exceedance shows the typical discontinuity at the freeboard level, but no unrealistic step. Finally it is continuously decreasing with increasing relative wave motion amplitude for the considered probability range.

In Tables 4-3 and 4-4 a complete overview of the parameters a-f is given for the full elliptical and thin triangular bows respectively. They will be used in the semi-empirical design evaluation method, but can also be used to validate future numerical prediction methods for a wide range of conditions. All relative wave motions (r) are for position R2 (1.2 m in front of the most forward part of the bow, including bow flare extensions). The related linear wave motion input (standard deviation s) was calculated at the fore perpendicular for all bow flare angles.

Table 4-3
Parameters of the modified Rayleigh distribution for the full elliptical bow

Freeboard = 10.5 m, bow flare 0 degrees							
Peak period	Linear standard deviation	Fitting parameters					
T_p in s	s in m	a	b	c	d	e	f
12	8.2152	0.61629	-0.04015	$2.76587 \cdot 10^{-3}$	-0.20033	$-5.6744 \cdot 10^{-3}$	$-1.33447 \cdot 10^{-3}$
14	8.0309	0.17968	0.09908	$-2.6478 \cdot 10^{-3}$	-0.18591	0.01027	$-3.35482 \cdot 10^{-3}$
16	6.6740	1.3853	-0.0406	$1.12433 \cdot 10^{-3}$	-0.2215	$-7.02728 \cdot 10^{-3}$	$-5.29345 \cdot 10^{-3}$

Freeboard = 10.5 m, bow flare 10 degrees							
Peak period	Linear standard deviation	Fitting parameters					
T_p in s	s in m	a	b	c	d	e	f
12	8.2152	0.07759	0.05252	$7.14157 \cdot 10^{-6}$	-0.14087	-0.01561	$-6.14256 \cdot 10^{-4}$
14	8.0309	0.32872	0.08247	$-2.18203 \cdot 10^{-3}$	-0.18244	0.0101	$-3.66455 \cdot 10^{-3}$
16	6.6740	1.66564	-0.07725	$2.31045 \cdot 10^{-3}$	-0.22693	$-6.12402 \cdot 10^{-3}$	$-5.27154 \cdot 10^{-3}$

Freeboard = 10.5 m, bow flare 30 degrees							
Peak period	Linear standard deviation	Fitting parameters					
T_p in s	s in m	a	b	c	d	e	f
12	8.2152	0.01081	0.03307	$3.16795 \cdot 10^{-3}$	-0.2069	-0.02348	$6.14791 \cdot 10^{-4}$
14	8.0309	0.38723	0.0644	$-1.33613 \cdot 10^{-3}$	-0.26589	-0.02458	$-2.25772 \cdot 10^{-3}$
16	6.6740	1.62113	-0.07868	$2.8344 \cdot 10^{-3}$	-0.30617	-0.03817	$2.10988 \cdot 10^{-3}$

Freeboard = 10.5 m, bow flare 50 degrees							
Peak period	Linear standard deviation	Fitting parameters					
T_p in s	s in m	A	b	c	d	e	f
12	8.2152	0.19828	0.03323	$6.30474 \cdot 10^{-4}$	-0.19686	-0.02862	$9.19671 \cdot 10^{-4}$
14	8.0309	0.1692	0.10502	$-2.87864 \cdot 10^{-3}$	-0.1895	-0.03861	$1.37299 \cdot 10^{-3}$
16	6.6740	1.41313	-0.04009	$1.0366 \cdot 10^{-3}$	-0.45522	0.04287	$-5.16766 \cdot 10^{-3}$

Table 4-4
Parameters of the modified Rayleigh distribution for the thin triangular bow

Freeboard = 11.9 m, bow flare 10 degrees							
Peak period	Linear standard deviation	Fitting parameters.					
T_p in s	s in m	a	b	c	d	e	f
12	8.4732	0.03202	0.06605	$2.1944 \cdot 10^{-4}$	-0.21079	-0.01961	$-8.88394 \cdot 10^{-4}$
14	8.3079	0.66341	0.06156	$-1.52883 \cdot 10^{-3}$	-0.16682	$-4.87203 \cdot 10^{-3}$	$-3.5727 \cdot 10^{-3}$
16	6.9477	1.83596	-0.07842	$2.34458 \cdot 10^{-3}$	-0.27151	$-1.32437 \cdot 10^{-3}$	$-1.07994 \cdot 10^{-3}$
Freeboard = 11.9 m, bow flare 30 degrees							
Peak period	Linear standard deviation	Fitting parameters					
T_p in s	s in m	a	b	c	d	e	f
12	8.4732	0.0304	0.0808	$-1.37582 \cdot 10^{-3}$	-0.16673	$-7.18623 \cdot 10^{-3}$	$-2.23666 \cdot 10^{-3}$
14	8.3079	0.86069	0.02381	$-6.67581 \cdot 10^{-4}$	-0.1802	$-9.57098 \cdot 10^{-3}$	$-2.32965 \cdot 10^{-3}$
16	6.9477	1.36718	-0.01883	$3.11103 \cdot 10^{-4}$	-0.25908	0.01443	$-3.58686 \cdot 10^{-3}$
Freeboard = 11.9 m, bow flare 50 degrees							
Peak period	Linear standard deviation	Fitting parameters					
T_p in s	s in m	a	b	c	d	e	f
12	8.4732	0.22708	0.06772	$-1.3893 \cdot 10^{-3}$	-0.19428	-0.02363	$8.49818 \cdot 10^{-4}$
14	8.3079	0.08322	0.11858	$-2.71136 \cdot 10^{-3}$	-0.21943	$-9.5613 \cdot 10^{-3}$	$-1.96608 \cdot 10^{-3}$
16	6.9477	1.26745	-0.03156	$1.71551 \cdot 10^{-3}$	-0.28543	-0.01223	$-3.9935 \cdot 10^{-4}$

An important possibility of the modified Rayleigh distribution is the discontinuity at the freeboard level, which allows an evaluation of the effect of the freeboard level on the extreme relative wave motions. To investigate whether the developed expression is able to predict variations of the freeboard level correctly, some tests were carried out with an increased freeboard height by 5.0 m to 15.5 m. The flare of the extension was equal to the 30 degrees bow flare, as shown in Figure 4-18.

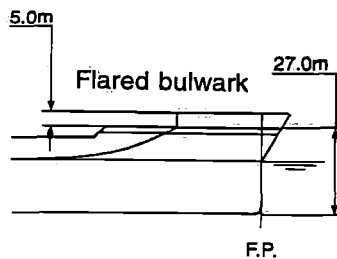


Figure 4-18
Increased freeboard height from 10.5 m to 15.5 m for the full elliptical bow with bow flare of 30 degrees

In Figure 4-19 the probability of exceedance is shown for the base case with a freeboard of 10.5 m and with the increased freeboard to 15.5 m. This figure confirms that the relative wave motions increase if the freeboard increases.

This is due to the fact that the water is not flowing onto the deck anymore (which reduced the relative wave motions for lower freeboard heights) and the reduced effect of green water on the pitch motions.

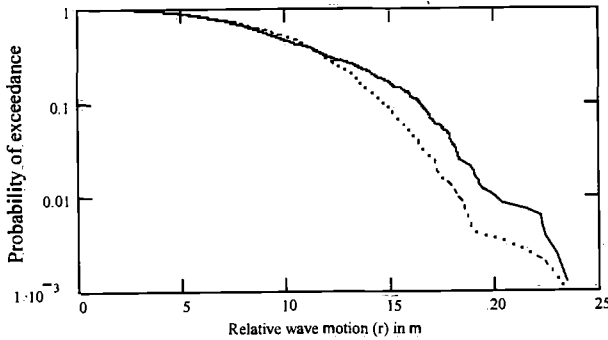


Figure 4-19

Measured probability of exceedance curve for the original freeboard height of 10.5 m (dotted line) and the increased freeboard height of 15.5 m (solid line)

In Figure 4-20 the modified Rayleigh distribution is applied to predict the effect of the higher freeboard height of 15.5 m. The prediction up to the freeboard level is good, which implies that the chosen method with a discontinuity at the freeboard level is working well. For the part of the distribution above the freeboard the predicted line is conservative with respect to the measurements, but still below the Rayleigh line.

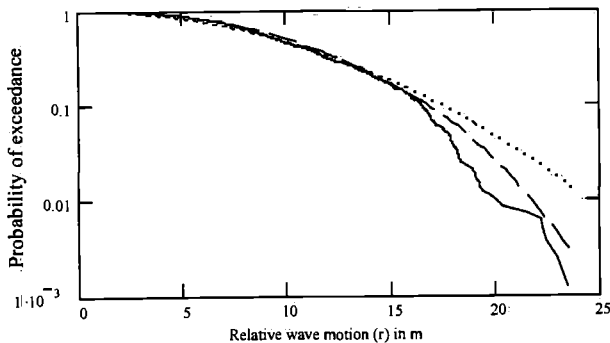


Figure 4-20

Measured probability of exceedance curve (solid line) compared to the initial prediction with the modified Rayleigh distribution for the increased freeboard height (dashed line). Also the linear Rayleigh distribution is shown (dotted line)

This difference is related to the fact that the distribution above the freeboard is dependent on the value of Expression (4.13): the probability of exceedance of the freeboard level. Because of the higher freeboard, this value is different for both situations. This effect can be understood if one considers that Expression (4.14) can be rewritten as:

$$P(r > R) = \exp \left[-\frac{fb^2}{2.s^2} \cdot (a + b.fb + c.fb^2) \right] \cdot \exp \left[(R - fb).d + (R - fb)^2.e + (R - fb)^3.f \right] \tag{4.15}$$

Several possibilities to account for this effect were investigated. Finally it was decided to include a factor τ in the expression above the freeboard level, which is dependent on the ratio between the standard deviation of the linear relative wave motion (s) and the freeboard height (fb):

$$P(r > R) = \exp \left[-\frac{fb^2}{2.s^2} \cdot (a + b.fb + c.fb^2) + \tau \left[(R - fb).d + (R - fb)^2.e + (R - fb)^3.f \right] \right] \tag{4.16}$$

τ is equal to 1.0 for $fb/s=1.3$ (the ratio for which the fitting parameters were determined) and 1.5 for $fb/s=1.9$. At present a linear relation is assumed between τ and fb/s , which can be expressed as:

$$\tau = 1.0 + 0.83 \cdot \left(\frac{fb}{s} - 1.3 \right) \tag{4.17}$$

In Figure 4-21 the results from the final Expression (4.16) are presented.

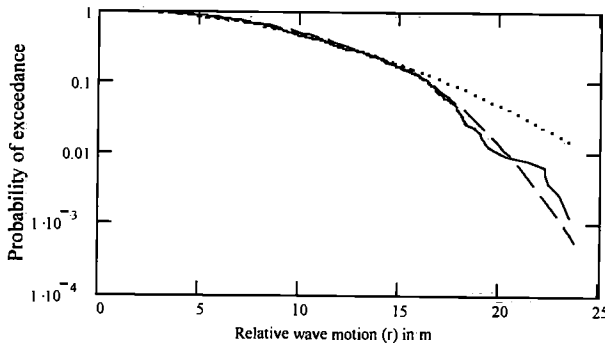


Figure 4-21

Measured probability of exceedance curve (solid line) compared to the final prediction with the modified Rayleigh distribution (dashed line) for the increased freeboard height. Also the linear Rayleigh distribution curve is shown (dotted line)

4.6 Validation of the developed expression

4.6.1 Variations available for validation

It should now be confirmed whether these relations can be used to predict the relative wave motions in other conditions than the condition for which the modified Rayleigh distribution was fitted. For this purpose two cases were used with the full elliptical bow and a bow flare of 30 degrees:

- A test with an angle of the ship with respect to the waves (210 degrees instead of 180 degrees)
- A test with a different stern, but with the same bow and bow flare angle (Full elliptical bow, full stern, flare angle 30 degrees)

For both cases the relative wave motions were calculated in the applied wave spectra with linear theory. The calculated linear standard deviations are shown in Table 4-5.

*Table 4-5
Calculated linear standard deviations for different conditions ($T_p=14$ s, $H_s=13.5$ m)*

Case	Condition	Linear standard deviation (s)
A	Full elliptical bow, traditional stern, 180 degrees heading (base case)	8.031 m
B	Full elliptical bow, traditional stern, 210 degrees heading	8.154 m
C	Full elliptical bow, full stern, 180 degrees heading	7.167 m

Using the same coefficients a to f as determined for the base case A, the relative wave motions will now be predicted for the cases B and C.

4.6.2 Validation results

For the 210 degrees heading (Case B, wave 30 degrees off the bow) the results are shown in Figure 4-22.

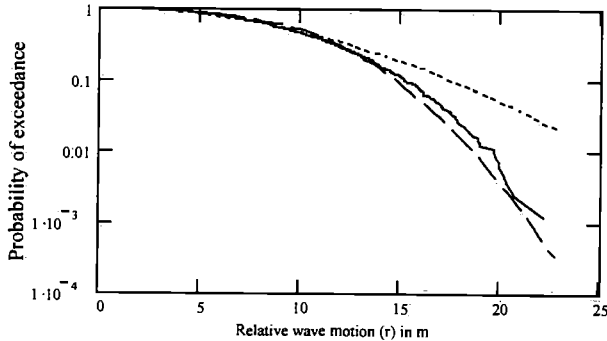


Figure 4-22

Comparison of the measured (solid line) and predicted (dashed line) probability of exceedance curves for the 210 degrees heading. The linear Rayleigh distribution curve is shown as well (dotted line)

In Figure 4-23 the predictions for the full stern (Case C) are shown.

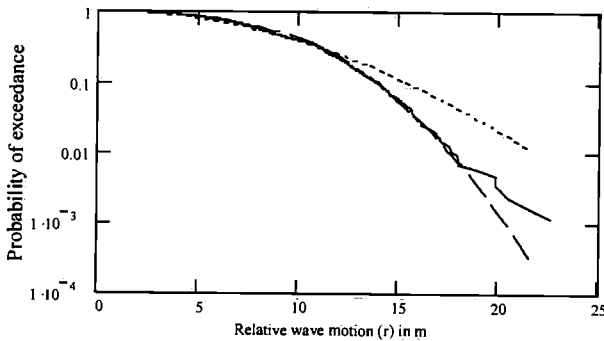


Figure 4-23

Comparison of the measured (solid line) and predicted (dashed line) probability of exceedance curves for the full stern. Also the linear Rayleigh distribution curve is shown (dotted line)

These figures confirm that the new modified Rayleigh distribution is able to predict the probability of exceedance for other conditions than used to determine the curve coefficients. Another check on the validity of the modified Rayleigh distribution for other conditions will be performed in the next section: the situation in current.

4.7 Effect of current

During most of the extreme environmental conditions, the tidal current and storm surge current play an important role. Therefore, the effect of current on green water loading was investigated.

In Figure 4-24 the effect of the current on the measured (linearised) RAO for the relative wave motions in irregular survival waves is shown for 0, 1.0 and 2.0 m/s current speed (current component in the direction of the waves). It is clear that the relative wave motion response is increased significantly with current.

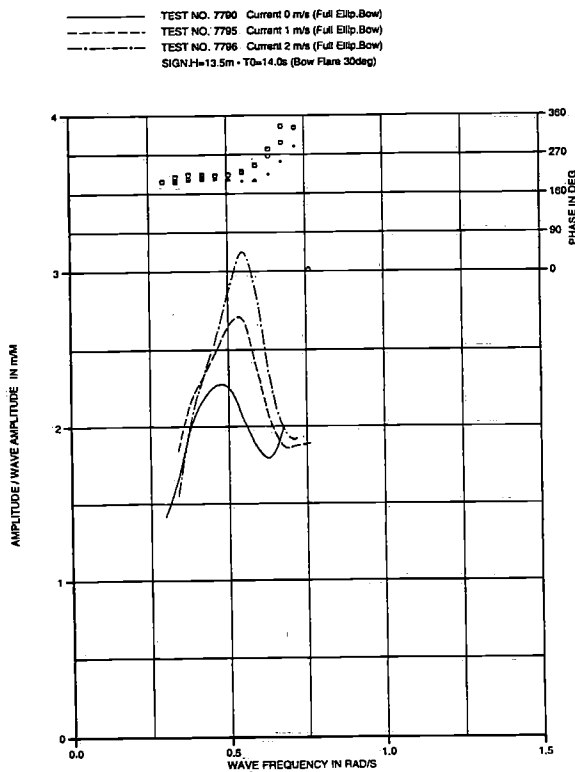


Figure 4-24

Measured effect of the current on the (linearised) RAO for the relative motions for 0, 1.0 and 2.0 m/s current speed for the full elliptical bow (30 degrees bow flare)

This effect is mainly due to the increased pitch motions in current. These are a result of the increased wave length with the same earth fixed wave frequency. This dependency of the wave length λ on the current speed (U) is:

$$\lambda = \frac{4\pi U^2}{g - \sqrt{g^2 + 4Ug\omega} + 2U\omega} \quad (4.18)$$

In Figure 4-25 it is shown that the wave length increases significantly with the current speed in the direction of the waves (depending on the wave period). The deep water wave length is shown for wave periods of 11.2 s (λ_1) and 12.9 s (λ_2).

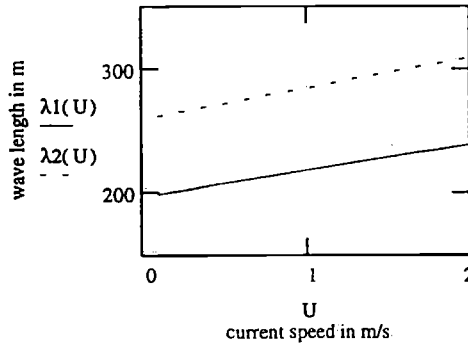


Figure 4-25

Calculated effect of the current speed on the wave length shown for wave periods of 11.2 s (λ_1) and 12.9 s (λ_2)

Due to this increase in wave length, the wave exciting forces on the tanker increase, whereas the wave period remains close to the pitch natural period of the FPSO. This effect, taking into account the influence of the current on added mass and damping, results in the increase of vessel motions.

These effects can be calculated with linear theory using the zero speed diffraction analysis results, based on the encounter frequency of the waves on current and making a velocity-correction on the added mass and damping. Details of this method can be found in Huijsmans and Dallinga (1983) and Beck and Loken (1989). The effect of the disturbance of the velocity field by the vessel is neglected in this analysis. In Figure 4-26 the calculated relative wave motions are shown.

The calculation shows the same increasing trend with current as the measured linearised RAO in large waves. Based on the calculated relative wave motion RAOs, the standard deviation of the relative motions can now be calculated in the applicable wave spectrum with $T_p=14.0$ s. These standard deviations can be included in Expressions (4.11) and (4.16) for the probability of exceedance of the relative wave motions.

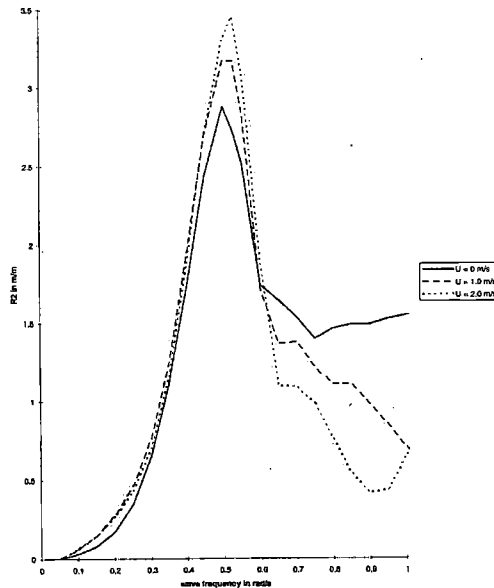


Figure 4-26

Calculated effect of the current on the calculated RAO for the relative wave motions for 0, 1.0 and 2.0 m/s current speed for the full elliptical bow (traditional stern)

Based on Expression (4.17) the applicable value for τ is determined based on the ratio between the freeboard and standard deviation. This results in the overview in Table 4-6.

Table 4-6

Standard deviation s and parameter τ for the situation with and without current for $T_p=14.0$ s and $H_s=13.5$ m

Current speed in m/s	s in m	fb/s	τ
0	8.031	1.3	1.0
1.0	9.450	1.11	0.843
2.0	10.57	0.99	0.745

In Figure 4-27 the comparison is made between the measured and predicted probability of exceedance for a current speed of 1.0 m/s (~2 knots). The predicted probability of exceedance shows a very good agreement with the measurement.

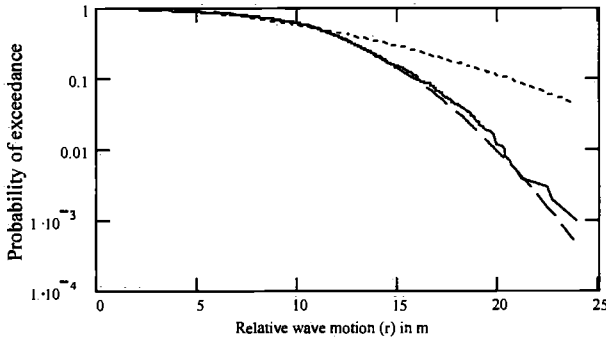


Figure 4-27

Comparison of the measured (solid line) and predicted (dashed line) probability of exceedance curves for a current speed of 1.0 m/s. Also the linear Rayleigh distribution curve is shown (dotted line)

The same comparison is made in Figure 4-28 for a current speed of 2.0 m/s (~4 knots).

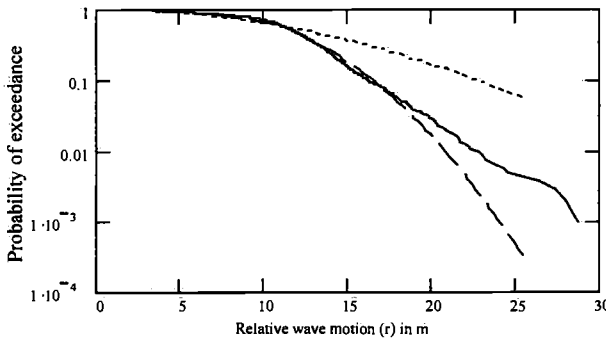


Figure 4-28

Comparison of the measured (solid line) and predicted (dashed line) probability of exceedance curves for a current speed of 2.0 m/s. Also the linear Rayleigh distribution curve is shown (dotted line)

The comparison between the measured and predicted distribution is still good for the lower values of the relative wave motions. The large values are underpredicted.

These results indicate that the chosen method works well for the prediction of relative wave motions and freeboard exceedances up to moderate current speeds.

4.8 Summary of the development of the modified Rayleigh distribution

The parameters for the proposed modified Rayleigh distribution were determined for the full elliptical and thin triangular bows based on a systematic test series for spectral peak periods 12 s, 14 s and 16 s and bow flare angles of (0), 10, 30 and 50 degrees. In all these cases the new expressions were able to describe the measured phenomena. In this way they can be used to validate future numerical simulation results in a wide range of extreme conditions.

They also give interesting insight in the complex effect of the bow flare angle on the extreme relative wave motions, as was identified as well by Watanabe, Ueno and Sawada (1989). Figure 4-29 shows the probability of exceedance for the full elliptical bow with a freeboard of 10.5 m (wave spectrum $T_p=14$ s and $H_s=13.5$ m) for the four bow flare angles tested: 0, 10, 30 and 50 degrees.

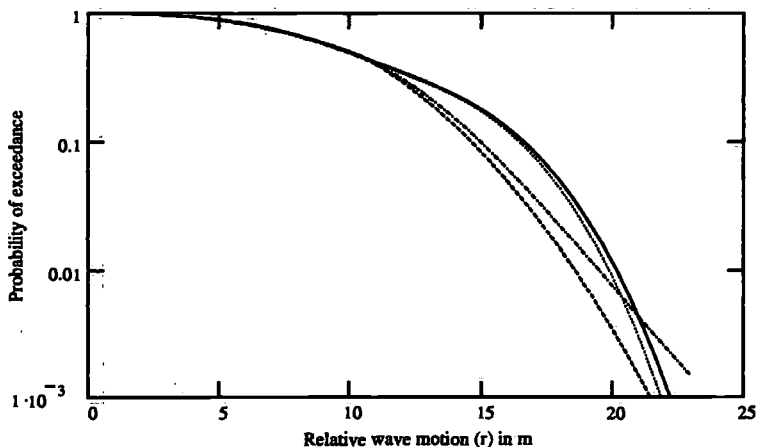


Figure 4-29

Example of probability of exceedance for the full elliptical bow with a freeboard of 10.5 m (Wave spectrum $T_p=14$ s and $H_s=13.5$ m) for the four bow flare angles tested: 0 (solid line), 10 (dotted line), 30 (dashed line) and 50 (dash-dot line) degrees

For this particular condition the 30 degrees bow flare angle results in the lowest freeboard exceedances, but the actual difference also depends on the probability level. It will be clear from the results presented in this chapter that the freeboard level and wave period will play a role in this as well.

Finally it should be noted that insight in the extreme freeboard exceedances is not enough to determine whether a certain ship is susceptible for the green water problem. To determine this, the water heights and loading on structures on the deck need to be determined. As will be shown in the following chapters, these will be influenced by the bow flare angle as well.

The application of these fitted parameters for the prediction of the extreme relative wave motions for other conditions was checked for:

- the increase of the freeboard height
- a different main hull shape
- a different wave heading
- the application of current speed

In all these cases a good agreement between prediction and measurement was found. However, due to the non-linearities involved, the results of predictions with the method should always be evaluated with care. Important notes on the range of applicability are given in Chapter 8.

5. WATER FLOW ONTO AND ON THE BOW DECK

5.1 Introduction

With the modified Rayleigh distribution presented in Chapter 4, the extreme relative wave motions around the bow and related freeboard exceedance (h) can be predicted. This extreme freeboard exceedance (h) is the input to the prediction to the flow onto the deck, which will be discussed in this chapter. Based on the systematic Test Series C, the relation between the extreme freeboard exceedance (h) and the water height (H) and velocity (U) on the deck is determined, see Figure 5-1.

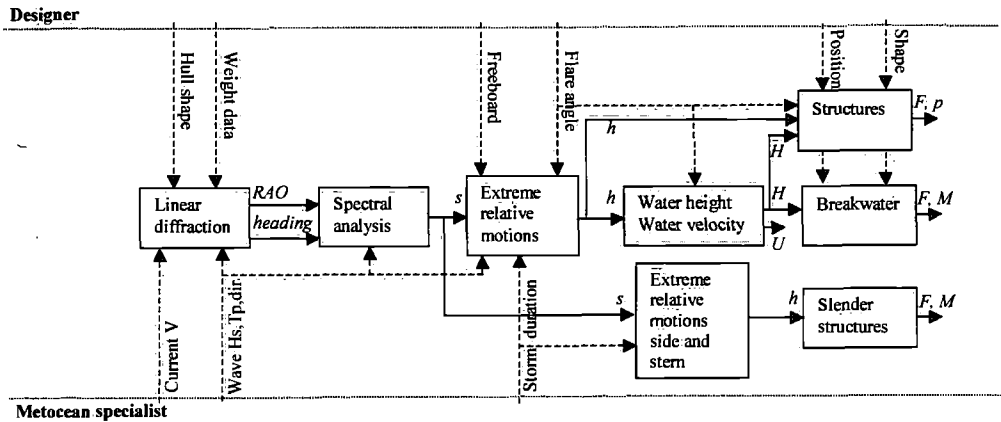


Figure 5-1

Part of the proposed semi-empirical design evaluation method considered in this chapter (in grey): prediction of water height (H) and velocity on deck (U)

5.2 Observation of the flow onto the deck for different flare angles

As was done in Test Series A, in the systematic Test Series C the wave contour in front of the full elliptical bow was determined with a thin plate at the centreline of the ship. To study the effect of the bow flare on this behaviour, this was done for the full elliptical bow with flare angles of 10, 30 and 50 degrees, see Figure 5-2.

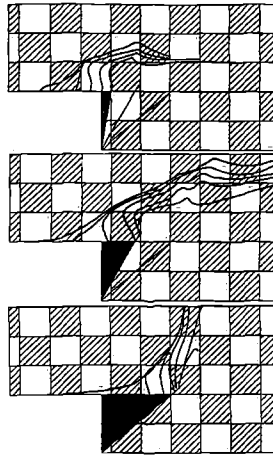


Figure 5-2

Wave contour in front of the full elliptical bow with a bow flare of 10, 30 and 50 degrees (from top to bottom) with time steps of 0.31 s (regular wave of $H=115\%$)

As was observed in Section 2.3, these figures show a clear resemblance with the theoretical dam breaking problem as described by Stoker (1957). However, there is also a significant effect of the bow flare on the flow onto the deck:

- The non-linear run-up in front of the bow increases with the bow flare angle, as discussed in the previous chapter.
- With a small flare angle the vertical wall of water translates gradually and with an almost constant speed onto the deck in the early stages. When more bow flare is applied, the flow is pushed away from the deck by the bow flare in this initial stage. The initial horizontal translation of the water front is almost zero in these cases.
- Surprisingly, the situation changes after this initial stage. With large bow flare angles the water flow at the deck level accelerates faster than with little bow flare and reaches high velocities. However, the thickness of the water layer on the deck is smaller. Because the final impact on structures is both a function of water height and water velocity, the effect of the bow flare is of influence on the impact loading.

5.3 Relation between relative motions and water height on the deck

Now the relation between a freeboard exceedance and the water height on deck will be considered in a quantitative way. In Figure 5-3 this relation is presented for the full elliptical bow with 30 degrees flare angle for positions at the centreline of the deck 0 m, 10 m and 20 m from the fore perpendicular. The analysis of combined extremes presented in Section 3.9 is used. This gives insight in the variation of the water height with the distance from the fore perpendicular. In addition, Figure 5-4 shows the water height 0 m from the fore perpendicular as function of the bow flare angle (0, 10, 30 and 50 degrees). All figures show the combined regular wave test results for all tested wave heights and periods.

The figures show that there is an almost linear relation between the freeboard exceedance (h) and the water height on deck (H). This can be explained considering the theoretical expression for the water height (H) on a certain position x from a breaking dam with an initial height h' at time t :

$$H = \left(-\frac{x}{3\sqrt{g}t} + \frac{2}{3}\sqrt{h'} \right)^2 \quad (5.1)$$

Keeping the position x fixed, the expression makes clear that the water height is dependent on h' and $\sqrt{h'}$. For large (but limited) values of t the $\sqrt{h'}$ dependency can be neglected. It should be noted that the freeboard exceedance in the green water problem (h) is taken as $h = (4/9)h'$, see for further details on the theoretical dambreaking problem Chapter 7.

Although the water height h is constant for the dam breaking problem, whereas the freeboard exceedance is not constant, the linear dependency on h is taken as a starting point for the description of the relation between the freeboard exceedance and water height on the deck:

$$H = a_H \cdot h \quad (5.2)$$

The coefficient a_H was determined with a least square fit through the measurement points in regular waves. This analysis was carried out for both bow shapes and all flare angles. The parameter a_H is independent on the underwater hull shape.

To check this assumption of a linear relation between the freeboard exceedance and water height on deck the standard error was determined, defined (with n as the number of measurement points) as:

$$\text{standard error} = \sqrt{\frac{1}{n-2} \cdot \sum_i^n (H_{i,\text{measured}} - H_{i,\text{least square}})^2} \quad (5.3)$$

Table 5-1 shows the standard error for the full elliptical bow with flare angle of 30 degrees, for the assumed linear relation as well as for water height on deck (H) being proportional to the square root, square or cube of the freeboard exceedance (h).

*Table 5-1
Standard error for different least square fit curves for the full elliptical bow with bow flare of 30 degrees (0 m from fore perpendicular)*

Assumed relation	Standard error
$H = a_H \cdot \sqrt{h}$	1.81
$H = a_H \cdot h$	1.07
$H = a_H \cdot h^2$	1.56
$H = a_H \cdot h^3$	2.46

Table 5-1 clearly confirms the assumed linear relation. For other bow flare angles the standard error based on this linear relation ranged from 0.69-0.90. In Table 5-2 an overview of the parameter a_H is given for all bow flare angles and positions from the fore perpendicular.

*Table 5-2
Coefficient a_H as function of bow flare angle (γ) and position from the fore perpendicular*

	Distance from the fore perpendicular		
	0 m	10 m	20 m
$\gamma = 0$ degrees	0.88499	0.60117	0.62701
$\gamma = 10$ degrees	0.83387	0.58068	0.58776
$\gamma = 30$ degrees	0.74172	0.58961	0.55541
$\gamma = 50$ degrees	0.62279	0.50507	0.34959

In Figure 5-5 the trendline from the regular wave tests is plotted in the results for the irregular wave tests for the 30 degrees bow flare angle on the full elliptical bow.

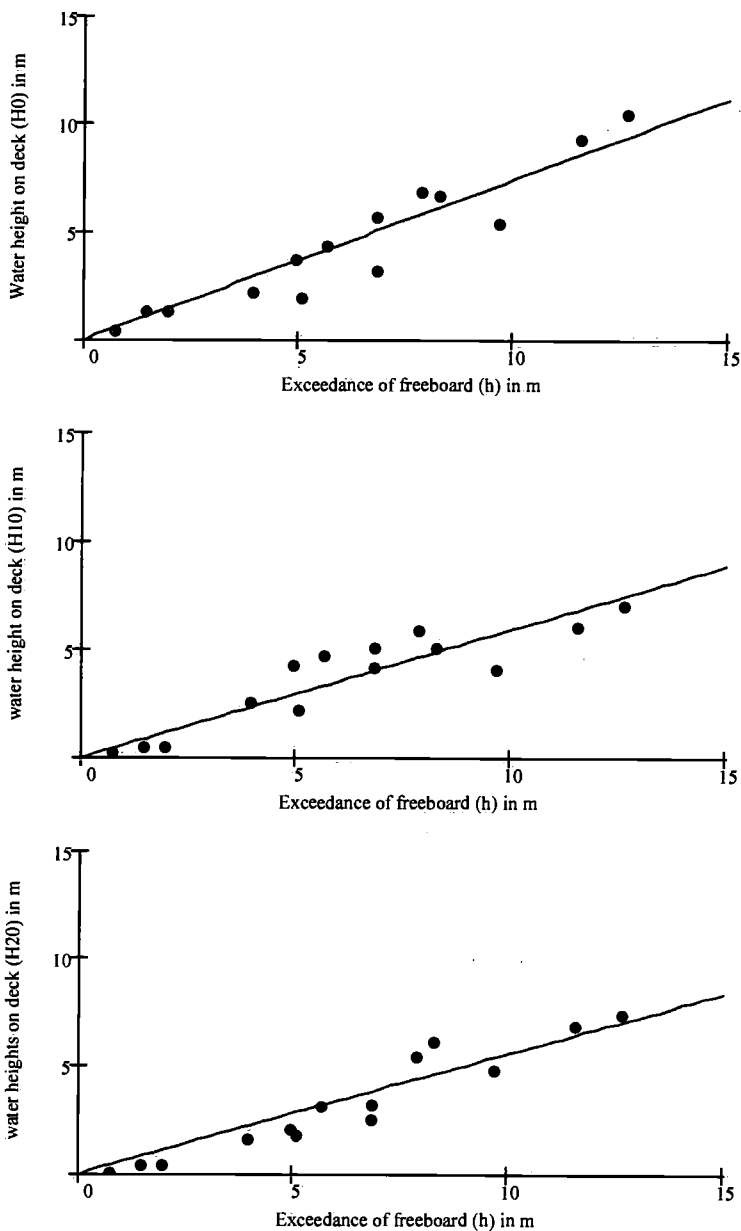


Figure 5-3

Relation between freeboard exceedance at bow centreline and the water height on the deck for the full elliptical bow with a bow flare angle 30 degrees, for positions 0, 10 and 20 m from fore perpendicular (from top to bottom)

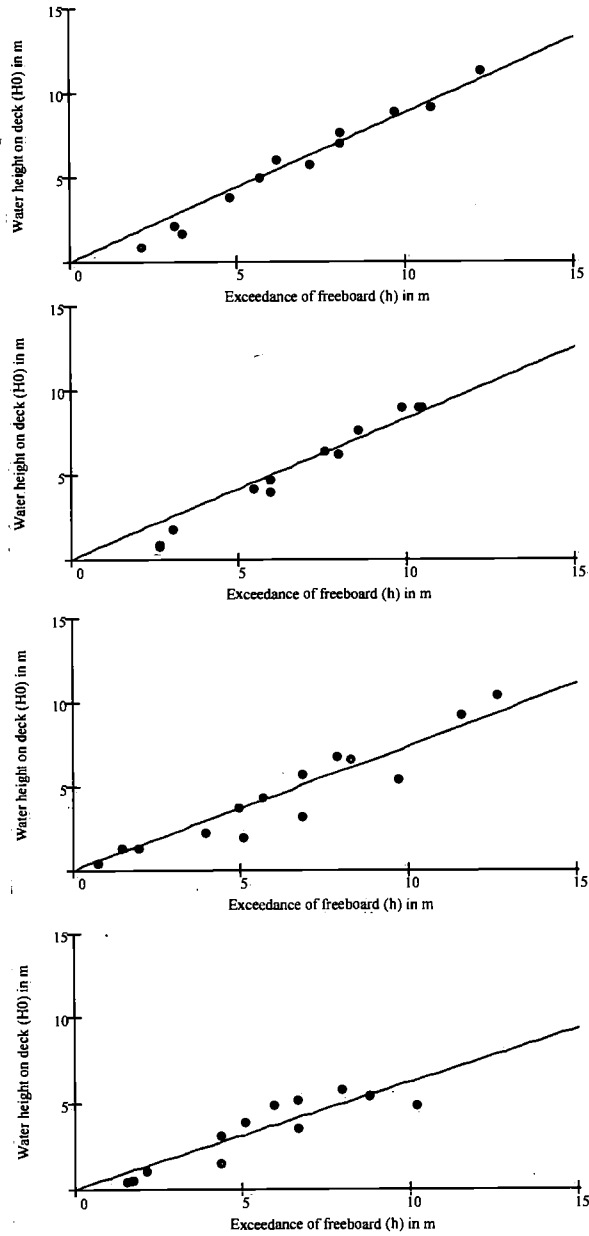


Figure 5-4

Relation between freeboard exceedance at bow centreline and the water height on the deck for the full elliptical bow at the fore perpendicular, for bow flare angles 0, 10, 30 and 50 degrees (from top to bottom)

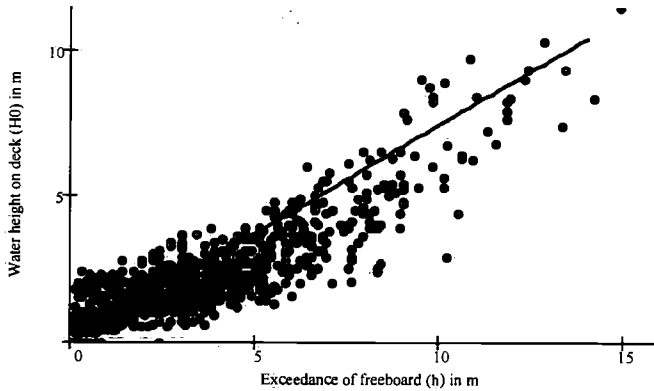


Figure 5-5

Relation between freeboard exceedance and the water height on deck at the fore perpendicular: the trendline from the regular wave tests is shown combined with the results in irregular waves (full elliptical bow with 30 degrees bow flare)

The figure shows a reasonable comparison, except for some effect of waves reflecting on the structure back to the wave probes after a large wave. In the analysis of combined extremes (as described in Section 3.9) the reflections are counted as the water heights related to a much lower next freeboard exceedances. A typical reflection is shown on Photo 5-1.

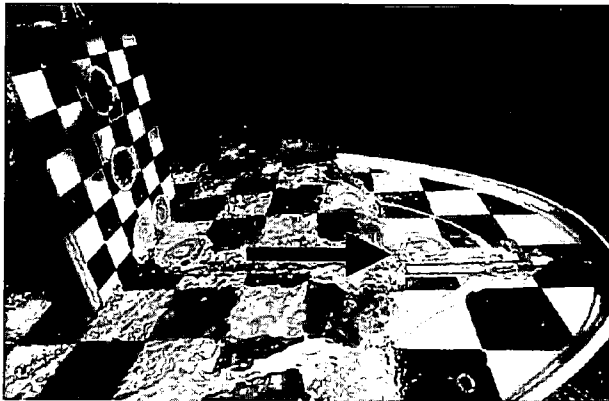


Photo 5-1

Reflection of green water back onto the deck, resulting in water on deck measurements with no or small freeboard exceedance

The standard error between the curve predicted based on the regular waves and the irregular wave test results is 0.98, close to the standard error for the regular waves themselves.

The current speed (0 to 2.0 m/s) and wave direction (180 to 150 degrees) have no significant effect on the relation between the freeboard exceedance and water height on deck. This is shown in Figures 5-6 and 5-7, where this relation is presented for a wave heading of 210 degrees and a current speed of 2.0 m/s in head waves (the trendlines from the regular waves with 180 degrees heading and zero current speed are used). The trendlines are very close to the measurements with another heading or with current speed. The standard error between the curve predicted based on the regular waves and the irregular wave tests with current or with another wave heading is again small (0.81 and 0.85 respectively).

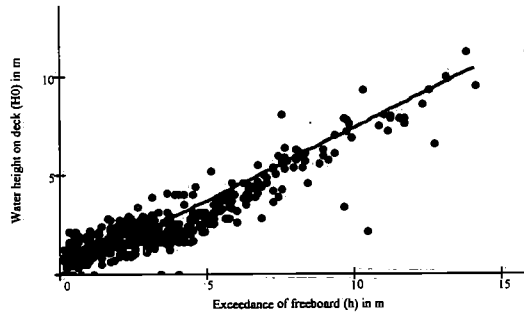


Figure 5-6

Relation between freeboard exceedance and the water height on deck at the fore perpendicular: the trendline from the regular wave tests is shown combined with the results in irregular waves with 2.0 m/s current speed (full elliptical bow with 30 degrees bow flare)

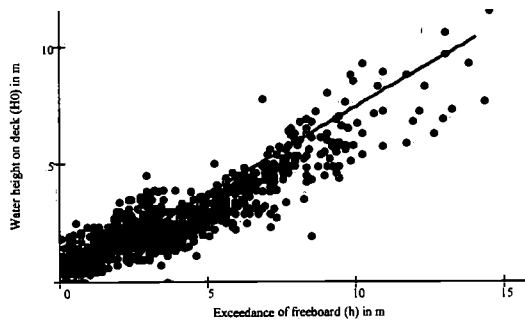


Figure 5-7

Relation between freeboard exceedance and the water height on deck at the fore perpendicular: the trendline from the regular wave tests is shown combined with the results in irregular waves with 210 degrees heading (full elliptical bow with 30 degrees bow flare)

The differences in the parameter a_H as presented in Table 5-2 and Figure 5-8 give insight in the effect of the bow flare angle on the water height on the deck, as well as in the water height variation with the distance from the fore perpendicular:

- A larger bow flare reduces the water height on the deck (assuming the same freeboard exceedance)
- In general there is a significant reduction of water height between the 0m and 10m from the fore perpendicular, but after that the water height remains constant (except for the 50 degrees bow flare) or becomes even higher due to the focussing of the water jet at the centreline
- With larger bow flare a smaller part of the freeboard exceedance is finally resulting in water height on the deck because the bow flare pushes the water away from the bow deck.

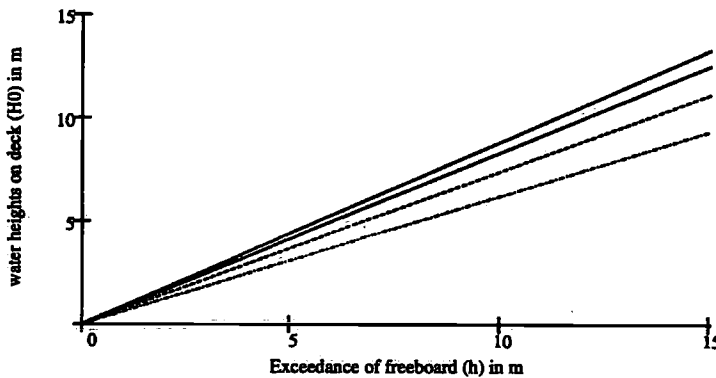


Figure 5-8

Relation between freeboard exceedance and the water height on the deck at the fore perpendicular for bow flare angles of 0, 10, 30 and 50 degrees

5.4 Flow patterns and velocities over the deck

The combined flow onto the deck from the stem and the sides results in a typical water pattern on the deck: the two water fronts from the sides meet at the centreline, resulting in a high and fast water jet over the centreline of the deck.

This pattern is very much dependent on the bow shape, where it should be noted that a different bow flare angle also results in a different shape of the deck in plan view. The final flow pattern is a result of the flow onto the deck (which is influenced by the bow flare) and the interaction of the flow from the different sides on the deck (which is influenced by the plan view shape).

Figures 5-9 and 5-10 show the flow patterns for the thin triangular bow and full elliptical bow respectively with 10, 30 and 50 degrees bow flare angle for a wave length which is equal to the ship length ($\lambda/L=1.0$).

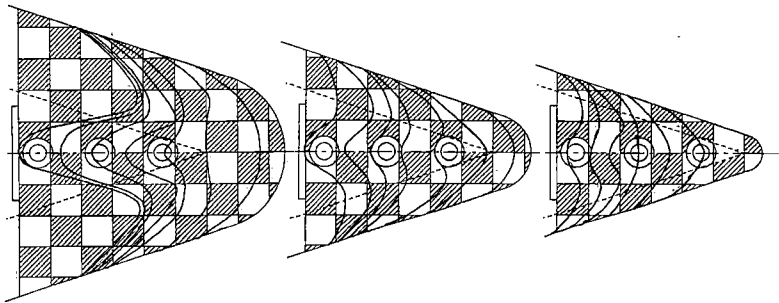


Figure 5-9

Flow pattern for the thin triangular bow in regular waves of $\lambda/L=1.0$ ($H=115\%$) for 50, 30 and 10 degrees (left to right) bow flare with time steps of 0.31 s

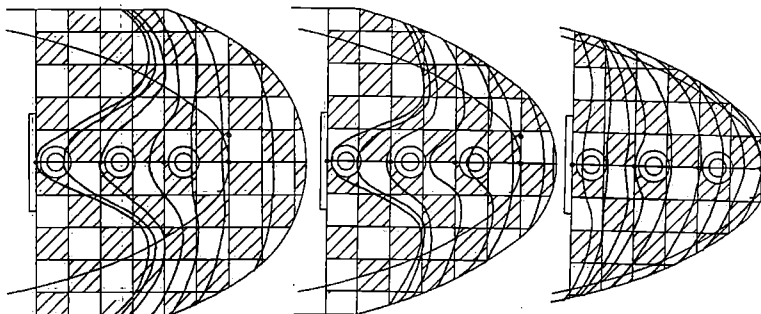
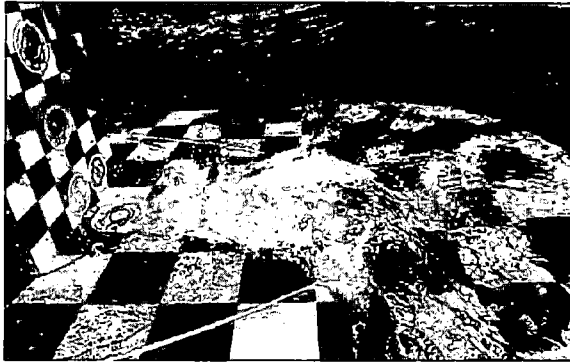


Figure 5-10

Flow pattern for the full elliptical bow in regular waves of $\lambda/L=1.0$ ($H=115\%$) for 50, 30 and 10 degrees (left to right) bow flare with time steps of 0.31 s

In most cases there is a high velocity water jet in the middle of the deck, see also Photo 5-2. However, for the bow flare angle of 10 degrees the water front is almost parallel over the width of the deck because there are no strong water flows from the sides meeting at the centreline in this case.



*Photo 5-2
High velocity water jet over the centreline of the ship*

The complexity of the flow makes it very time and space dependent. Beside the technical difficulty of a water velocity measurement, this complexity makes it difficult to quantify the water velocity and relate it to (for instance) the freeboard exceedance.

Taking into account these limitations, the following attempts were made as part of this study:

- The water front position was measured with the horizontal wave probe HV1 parallel with -but 2.7 m from- the centreline. It was positioned 1.2 m above the deck. It should be noted that this is a correct position measurement of the water front only as long as the back end of the wave probe is submerged, see Figure 5-11.

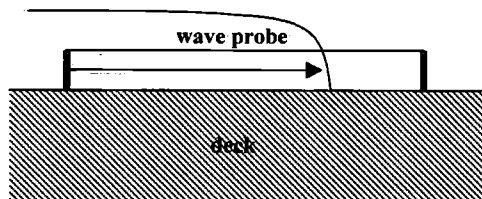


*Figure 5-11
Measurement of the water front position with horizontal wave probe HV1
(valid as long as the back end of the wave probe is submerged)*

- The water front position was now differentiated to estimate the water front velocity (U). The maximum value in these time traces was used as an estimate of the maximum water front velocity.

Figure 5-12 shows the maximum velocities of the water front as function of the freeboard exceedance in regular waves for the full elliptical bow with a bow flare angle of 30 degrees.

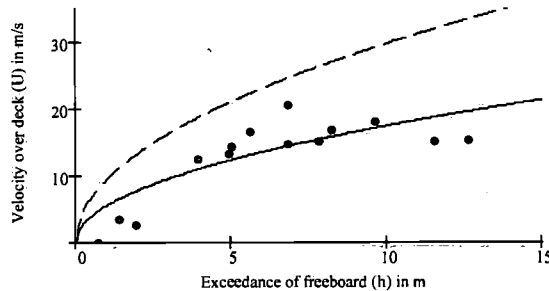


Figure 5-12

Relation between freeboard exceedance and the maximum water front velocity over the deck for the full elliptical bow with a bow flare angle of 30 degrees in regular waves. The line based on the theoretical dambreaking problem (dashed line) and the least square fit (solid line) based on Expression (5.5) are shown as well

In the figure also the dashed line according to the theoretical dam breaking problem is shown. According to this formulation the water front velocity into the empty region is proportional with the square root of the original height of the dam (h'):

$$U = 2\sqrt{g h'} \quad (5.4)$$

It should be noted that the freeboard exceedance (h) should be taken as $(4/9)h'$ (see for further details Chapter 7). In analogy with this expression, the figure also shows a line fitted through the measurements according to the following expression:

$$U = a\sqrt{h} \quad (5.5)$$

A reasonable fit is found for the full elliptical bow in Figure 5-12, but for the triangular bow the scatter was larger. Alternatively, the relation between the square-root of the velocity over deck and the water height on the deck at the fore perpendicular H_0 (instead of the freeboard exceedance) was determined, as indicated in Expression (5.6):

$$U = a_u\sqrt{H_0} \quad (5.6)$$

Figures 5-13 and 5-14 show this relation for the full elliptical and thin triangular bows.

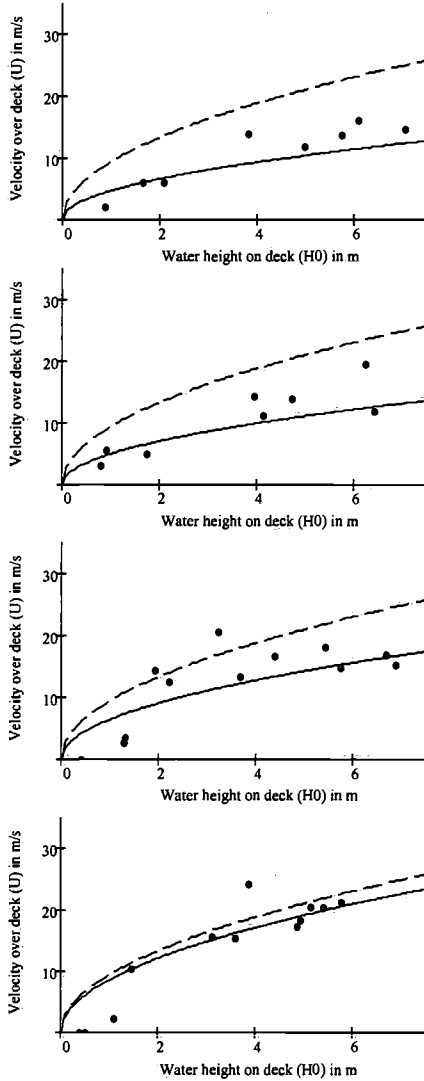


Figure 5-13

Relation between the water height at the fore perpendicular (H_0) and the maximum water front velocity over the deck for the full elliptical bow with bow flare angles of 0, 10, 30 and 50 degrees (from top to bottom) in regular waves. The line based on the theoretical dambreaking problem (dashed line) and the least square fit (solid line) based on Expression (5.6) are shown as well

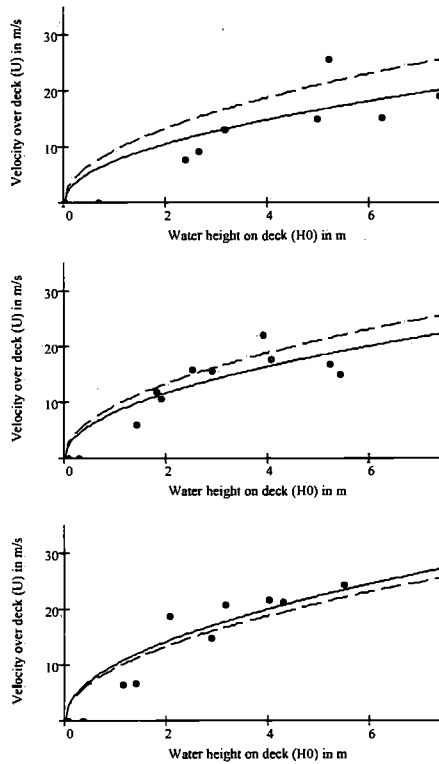


Figure 5-14

Relation between the water height at the fore perpendicular (H_0) and the maximum water front velocity over the deck for the thin triangular bow with bow flare angles of 10, 30 and 50 degrees (from top to bottom) in regular waves. The line based on the theoretical dambreaking problem (dashed line) and the least square fit (solid line) based on Expression (5.6) are shown as well

Table 5-3 shows the related parameter a_0 .

From these figures and table it can be observed that:

- In general the maximum water front velocity increases with the square root of the freeboard exceedance (or related water height at the fore perpendicular).
- The velocity curves from the theoretical dambreaking problem typically seem an upper limit for the velocities. This is surprising because there are two clear differences between the flow of green water onto the deck and the dambreaking problem: in the first place the initial flow velocity is influenced by the waves and run up in reality and in the second place the focussing water fronts result in the observed high velocity water jet.

- Although the water height on the deck reduces with bow flare angle (see Section 5.3), the related water front velocity is higher. This is important because the resulting impact loading is a function of both water heights and water velocity, see Expression (2.15).
- The thin triangular bow results in higher velocities than the full elliptical bow. This is probably related to the fact that the water from the side of the bow comes onto the deck in two almost parallel fronts in this case, resulting in a strong jet effect.

Table 5-3

Parameter a_u for the full elliptical and thin triangular bows as function of bow flare angle

	Full elliptical	Thin triangular
$\gamma = 0$ degrees	4.63376	-
$\gamma = 10$ degrees	4.94792	7.39312
$\gamma = 30$ degrees	6.34439	8.16391
$\gamma = 50$ degrees	8.52956	9.97322

6. GREEN WATER IMPACT LOADING

6.1 Introduction

In Chapter 5 the water heights and water velocities after an exceedance of the freeboard have been discussed. Taking into account the results presented there, this chapter focuses on the resulting green water loading on structures and breakwaters on the deck (see Figure 6-1). The tests and measurements in the systematic Test Series C will be used to determine prediction methods for the:

- Impact loading on structures on the deck
- Horizontal and vertical load profiles
- Effect of the structural shape on the impact loading
- Effect of the position of the structures on the deck
- Efficiency of (and loading on) protecting breakwaters

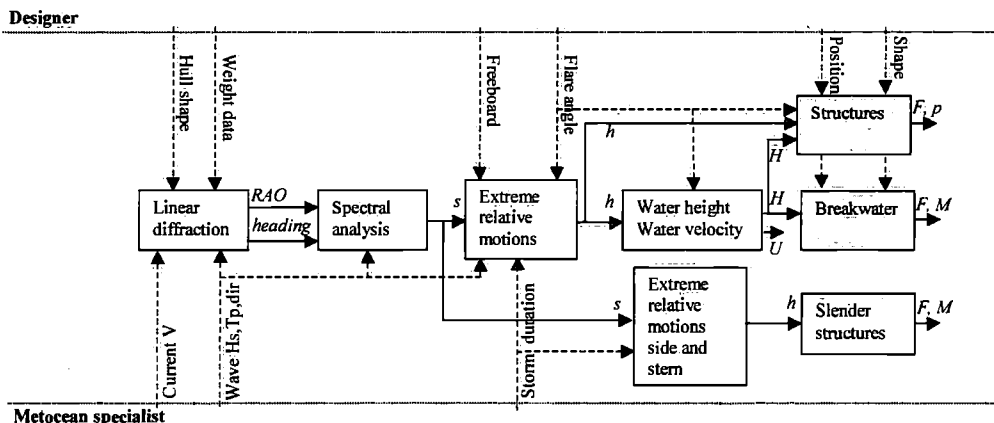


Figure 6-1

Part of the proposed semi-empirical design evaluation method considered in this chapter (in grey): prediction of impact loading on structures and breakwaters

6.2 Relation freeboard exceedance and impact loading

In Section 2.8 it was shown that the peak impact loads on structures are proportional to the maximum water height on the deck and the square of the velocity of the water front over the deck:

$$F_{\text{peak}} = \rho H_{\text{max}} U^2 \quad (6.1)$$

In the previous chapter it was found that the relation between water height and water velocity over the deck is dependent on the bow shape and bow flare angle. Therefore, it was decided to define the relation between the freeboard exceedance and the impact loading, dependent on the bow shape and flare. To describe this new relation, the nearly linear relation between the water height on the deck (H) and the freeboard exceedance (h) was taken as starting point (see Section 5.3):

$$H_{\text{max}} = a_H \cdot h \quad (6.2)$$

The velocity of the water front over the deck (U) is was found to be proportional to the square root of the freeboard exceedance (or the resulting water height at the fore perpendicular, see Section 5.4):

$$U = a \cdot \sqrt{h} \quad (6.3)$$

Combination of Expression (6.1) with Expressions (6.2) and (6.3) shows that the impact loading will typically be proportional to the square of the freeboard exceedance.

Consequently the following general expression was used for the pressure on the squared reference structure:

$$p = a_p \cdot h^2 \quad (6.4)$$

A similar expression applies to the global horizontal FX-load on the squared structure:

$$FX = a_F \cdot h^2 \quad (6.5)$$

a_p and a_F are dependent on the bow shape (full or thin) and bow flare angle (0, 10, 30 and 50 degrees).

In Figures 6-2 and 6-3 this relation is determined based on a least square fit through the measurement points of the impact load at panel (P1) and the horizontal FX-load at the structure. The analysis of combined extremes as described in Section 3.9 is used.

The results for all different regular wave periods were combined because the relation between impact loading and freeboard exceedance is only slightly dependent on the wave length.

To check the assumption of a quadratic relation between the freeboard exceedance and the loads on structures on deck, the standard error was determined, defined (with n as the number of measurement points) as:

$$\text{standard error} = \sqrt{\frac{1}{n-2} \cdot \sum_i^n (P_{i,\text{measured}} - P_{i,\text{least square}})^2} \quad (6.6)$$

Table 6-1 shows the standard error for the full elliptical bow with flare angles of 0, 10, 30 and 50 degrees, for the assumed quadratic relation, as well as for the pressure being proportional to the square or cube of the freeboard exceedance.

Table 6-1
Standard error for different least square fit curves for the full elliptical bow
with bow flare of 0, 10, 30 and 50 degrees

Assumed relation	Standard error 0 degrees	Standard error 10 degrees	Standard error 30 degrees	Standard error 50 degrees
$p = a_p \cdot h$	71	61	43	71
$p = a_p \cdot h^2$	42	34	25	23
$p = a_p \cdot h^3$	52	28	47	29

This result justifies the chosen quadratic relation (although the standard error for the cubed relation is acceptable in general as well). Table 6-2 shows the final values for a_p and a_f for the regular wave tests.

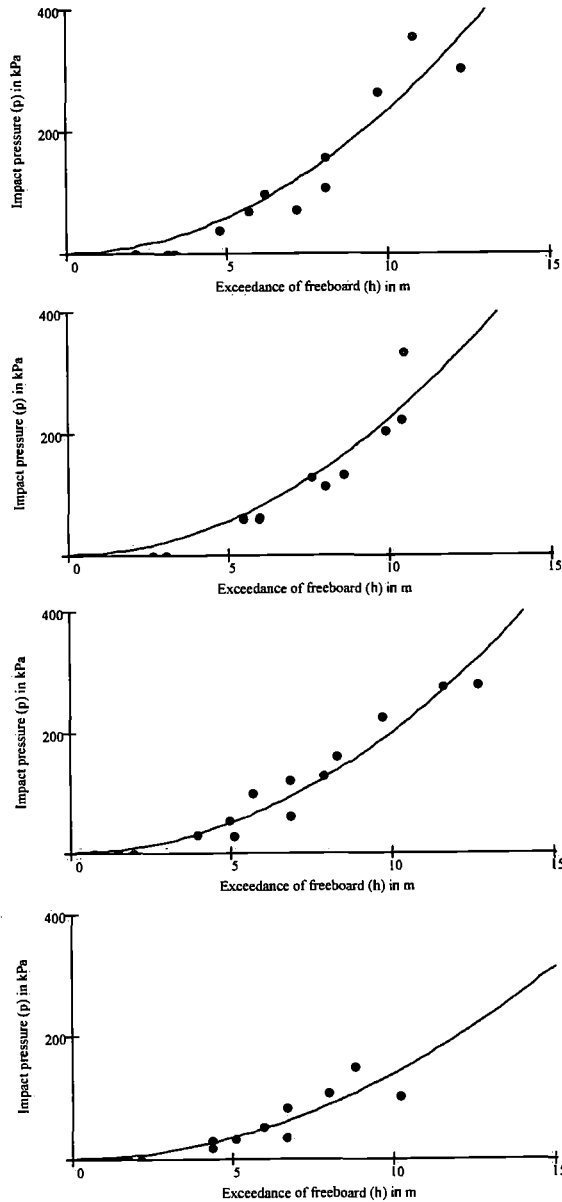


Figure 6-2

Relation between freeboard exceedance and the maximum impact pressure (p) on panel PSTRUC1 on the squared structure (Structure 1) for the full elliptical bow with bow flare angles 0, 10, 30 and 50 degrees (from top to bottom). Regular wave test results for all periods and heights and the least square fit are presented

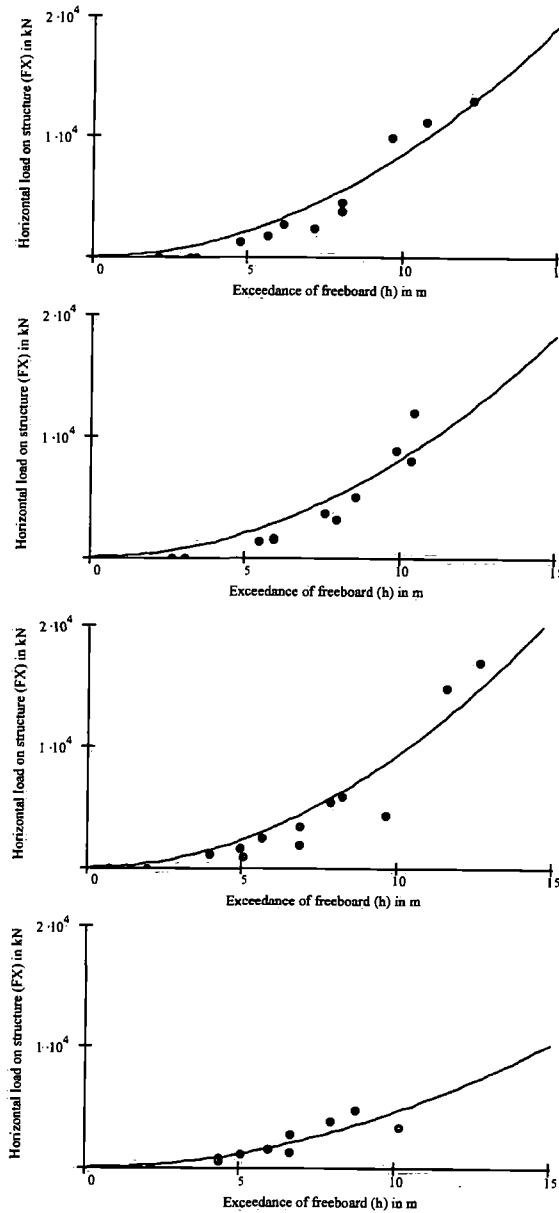


Figure 6-3

Relation between freeboard exceedance and the maximum total FX-load on the squared structure (Structure 1) for the full elliptical bow with bow flare angles 0, 10, 30 and 50 degrees (from top to bottom). Regular wave test results for all periods and heights and the least square fit are presented

*Table 6-2
Parameters a_p and a_F for the regular wave test results of the full elliptical
and thin triangular bows*

Full elliptical bow	Factor a_p	Factor a_F
$\gamma = 0$ degrees	2.37	85.4
$\gamma = 10$ degrees	2.27	81.7
$\gamma = 30$ degrees	2.02	93.4
$\gamma = 50$ degrees	1.39	45.3

Thin triangular bow	Factor a_p	Factor a_F
$\gamma = 10$ degrees	2.01	47.2
$\gamma = 30$ degrees	1.19	25.2
$\gamma = 50$ degrees	0.79	17.7

On the other hand it will be clear from these figures that there is also a significant scatter in the results. This is related to the fact that the final impact loading itself is very sensitive to small variations in the input. A slightly different water height, water front speed and shape of the water front just before the impact can result in large variations in the actual loading. The local impact pressure (P_1) is the most sensitive for this type of variations. This is shown in Table 6-3, which presents a further analysis of a number of regular wave tests.

The trend lines for the regular wave tests were determined based on the mean of all peak values during the regular wave tests (MEAN+). Typically 20-30 peaks were used to determine such mean value. However, also in the regular wave tests with an almost constant wave input the variation in loads was considerable. In Table 6-3 the relation is given between the maximum and mean of all maxima in regular waves for the tests with the full elliptical bow and 30 degrees bow flare angle. The results for the water height on deck at the fore perpendicular (H_0), the impact pressure (p) and the global load on the structure (FX) are given.

These tables make clear that the variation is significantly larger for the impact loads than for the water heights on deck. The global load on the structure is less sensitive to this type of variations as well.

As expected, based on the above, the irregular wave test results show an even larger variation in the loads with the same freeboard exceedance. Figure 6-4 shows the results in all (combined) irregular waves for the full elliptical bow with a bow flare angle of 30 degrees for the local pressure.

Table 6-3

Maximum values and mean of all peaks in regular waves for the tests with the full elliptical bow and 30 degrees bow flare angle for the water height on deck at the fore perpendicular (H_0), the impact pressure (p) and the global load on the structure (FX)

H_0 MEAN+	H_0 MAX	MAX/MEAN
2.20	2.49	1.13
4.37	5.16	1.18
6.64	7.53	1.13
9.26	9.61	1.04
10.4	11.5	1.11

p MEAN+	p MAX	MAX/MEAN
29.7	56.1	1.89
97.7	175	1.79
160	210	1.31
276	378	1.37
277	344	1.24

FX MEAN+	FX MAX	MAX/MEAN
1100	1310	1.19
2480	3170	1.28
5910	8350	1.41
14800	19900	1.35
17000	21600	1.27

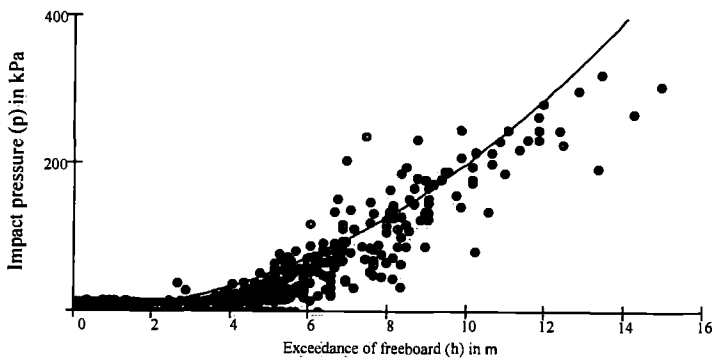


Figure 6-4

Relation between freeboard exceedance and the maximum impact pressure (p) on panel PSTRUC1 on the squared structure (Structure 1) for the full elliptical bow with a bow flare angle of 30 degrees. Irregular wave test results for all peak periods are presented. The solid line gives the trendline from the corresponding regular wave test results

There is a clear relation between the results in regular and irregular waves, but the scatter in the results in irregular waves is clear. This larger scatter in irregular waves can be explained if we consider that there are basically two types of green water events:

1. Green water as a result of the pitch motion being out of phase with the waves.
2. Green water due to single extreme (steep/energetic/breaking) wave events.

The physics of both types of events are given below:

1. In regular waves and most of the irregular wave events the green water occurs when the bow is pitching downwards at the moment the wave rises at this point. This results in large relative wave motions and exceedances of the freeboard. An example of such an event is shown in the time traces in Figure 6-5.
2. However, green water can also occur as a result of extremely steep and energetic wave events, see also Hellan, Hermunstad and Stansberg (2001). These events can occur even after a period of reasonably low waves. In this type of events the freeboard exceedance is caused by a (very local) steep wave and can occur with low pitch motions. An example is shown in Figure 6-6. For this irregular wave there is hardly any pitch motion and the freeboard exceedance is almost purely due to the incoming steep wave crest.

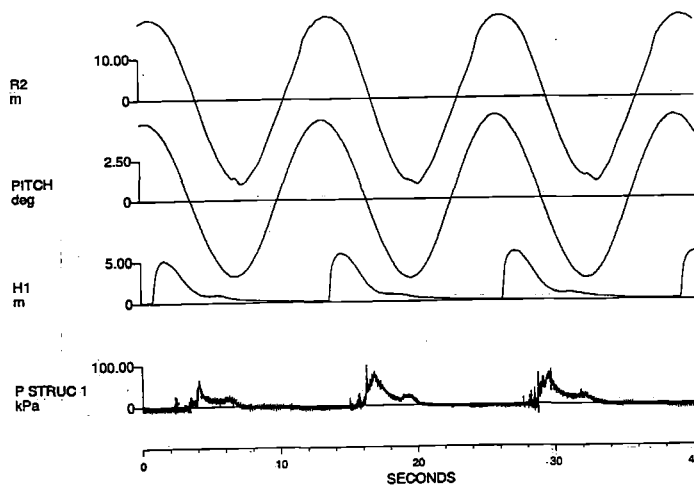


Figure 6-5

Time traces of relative wave motion at bow centreline (R2), pitch angle, water height at the fore perpendicular (H1) and impact pressure (PSTRUC1) in a regular wave

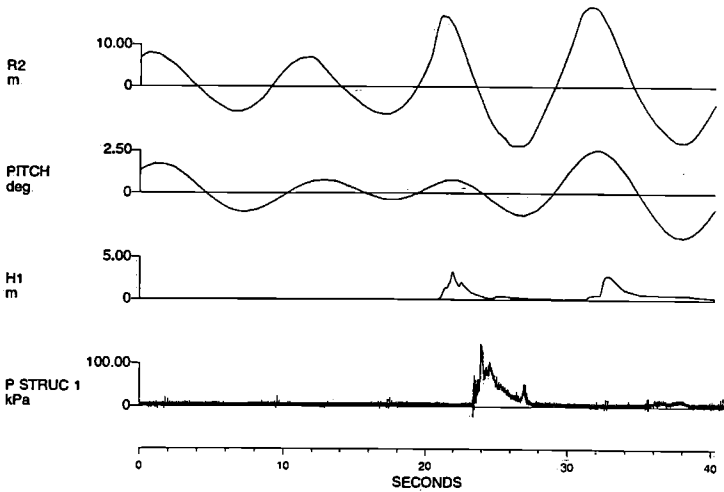


Figure 6-6

Time traces of relative wave motion at bow centreline ($R2$), pitch angle, water height at the fore perpendicular ($H1$) and impact pressure ($PSTRUC1$) in an extreme (steep) wave event

The resulting water flow onto the deck, the velocity of the water over the deck and the impact loading can be significantly different from the green water occurrences caused by the out-of-phase pitch motions. Although there are fewer of this type of special events, they are critical because they result in large impact pressures with relatively low freeboard exceedances, as shown in Figure 6-7. They are also more difficult to predict.

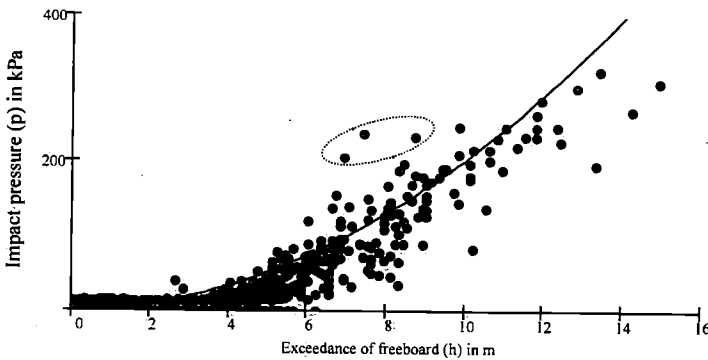


Figure 6-7

Identified green water events due to extreme (steep/breaking) waves in circle

These effects are the main background of the additional scatter in irregular waves. Therefore, it is not possible to use the expressions from the regular wave tests directly for the impact loading in irregular waves. A slightly different approach was chosen to find valid expressions in irregular waves. Starting point was again the assumption that the impact is proportional to the square of the freeboard exceedance, see Expressions (6.4) and (6.5). This implicates that the factor 'a' had to be determined for each bow shape and flare angle. Because of the significant variation in the loads, in this study two different approaches are used:

1. The factor 'a' is determined based on the condition that 95 percent of the impacts are below the line for p or FX. In this way it represents a reliability line, which predicts the maximum impact loads with a high probability.
2. The factor 'a' is determined based on a least square fit through the measurements in irregular waves. In this way it gives a good description of the trend in the loads.

The least square fit gives a reliable fit through the measurements, but it should be noted that the maximum loads can be significantly higher. The 95% exceedance level line directly gives an indication of the extreme loads that can be expected. Examples are shown in Figure 6-8 for the impact pressures on structures on the full elliptical bow. Figure 6-9 shows the lines for horizontal FX-load.

Low values of the impacts in the measurements (<35 kPa) were not taken into account in the curves because they are mainly caused by noise in the signals (which were not filtered to prevent loss of impact information). Table 6-4 shows the final numbers for a_p and a_f for the 95% reliability line and the least square fit for the irregular waves.

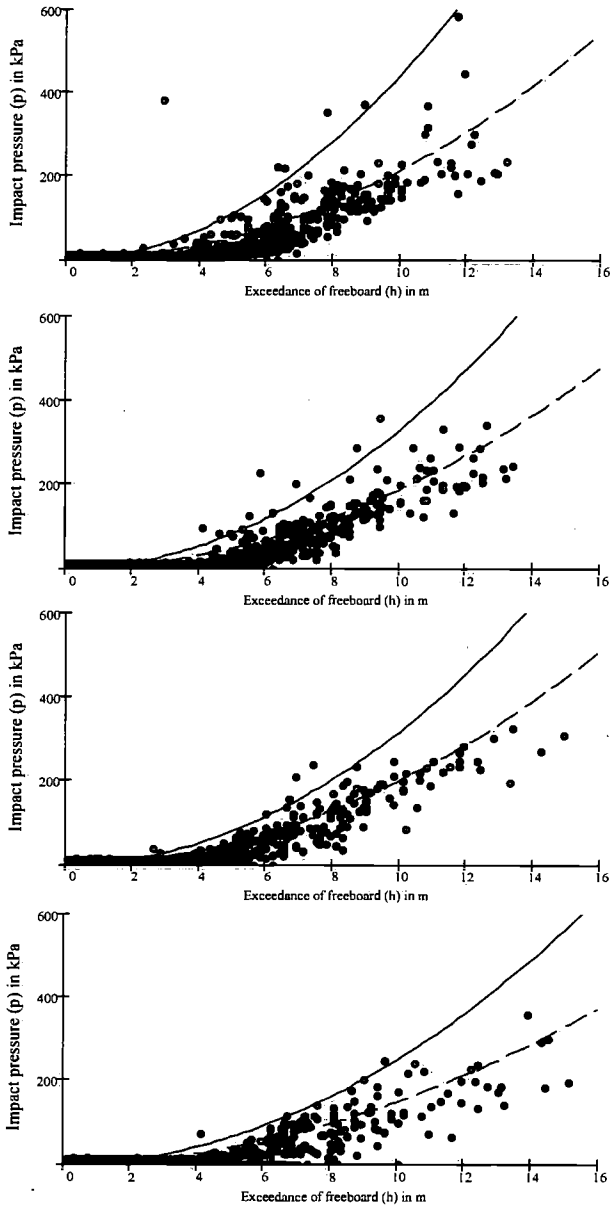


Figure 6-8

Relation between freeboard exceedance and the maximum impact pressure on panel PSTRUC1 on the squared structure (Structure 1) for the full elliptical bow with bow flare angles of 0, 10, 30 and 50 degrees (from top to bottom). The least square fit (dotted line) as well as the 95% reliability line (solid line) are indicated

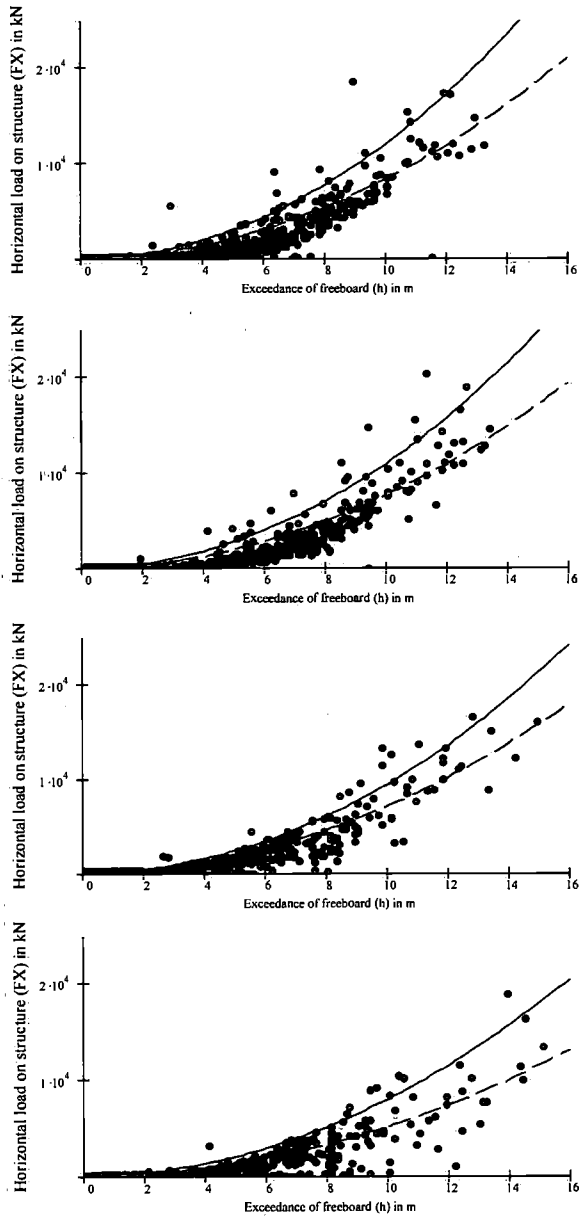


Figure 6-9

Relation between freeboard exceedance at bow centreline and the maximum the global load on the structure FXCOR on the squared structure (Structure 1) for the full elliptical bow with bow flare angles of 0, 10, 30 and 50 degrees (from top to bottom). The least square fit (dotted line) as well as the 95% reliability line (solid line) are indicated

Table 6-4
Parameters a_p and a_F for the 95% reliability line and the least square fit
for the irregular waves

95% reliability line

Full elliptical bow	Factor a_p (95% reliability)	Factor a_F (95% reliability)
$\gamma = 0$ degrees	4.41	120
$\gamma = 10$ degrees	3.28	110
$\gamma = 30$ degrees	3.16	95
$\gamma = 50$ degrees	2.49	80

Thin triangular bow	Factor a_p (95% reliability)	Factor a_F (95% reliability)
$\gamma = 10$ degrees	7.2	125
$\gamma = 30$ degrees	5	100
$\gamma = 50$ degrees	5.6	125

Least square fit line

Full elliptical bow	Factor a_p (least square fit)	Factor a_F (least square fit)
$\gamma = 0$ degrees	2.12	82.6
$\gamma = 10$ degrees	1.86	76.4
$\gamma = 30$ degrees	1.99	70.9
$\gamma = 50$ degrees	1.46	51.0

Thin triangular bow	Factor a_p (least square fit)	Factor a_F (least square fit)
$\gamma = 10$ degrees	3.15	72.0
$\gamma = 30$ degrees	2.23	54.7
$\gamma = 50$ degrees	2.18	42.0

With Expressions (6.4) and (6.5) and the parameters in Table 6-4 the pressure and global horizontal loads on the squared reference squared can be determined based on the freeboard exceedance (h).

The pressure p is based on a circular panel with a diameter of 1.35 m (area 1.43 m²) with its centre 2.4 m above the deck level, see Figure 6.10 (left). The global load is the load F_X in the x -direction on the total squared structure.

For the full elliptical bow the impact pressures and global loads decrease clearly with an increasing bow flare angle: the impact pressure with an angle of 50 degrees is only 56% of the impact with 0 degrees flare (95% reliability).

The thin triangular bow results in significantly larger local impact pressures than the full elliptical bow. Surprisingly, the horizontal FX-load is in the same range as for the full elliptical bow. The larger local pressures are most likely due to the different flow patterns and higher velocity of the water jet over the deck.

6.3 Vertical and horizontal load profiles

6.3.1 Vertical load profile

The horizontal and vertical load profiles of the impact pressure on structures on the deck are important design aspects.

In this section first the vertical load profile will be discussed for the squared Structures 1 and 2. The two structures are identical, except for the size and position of the force panel transducers, see Figure 6-10 with Structures 1 and 2.

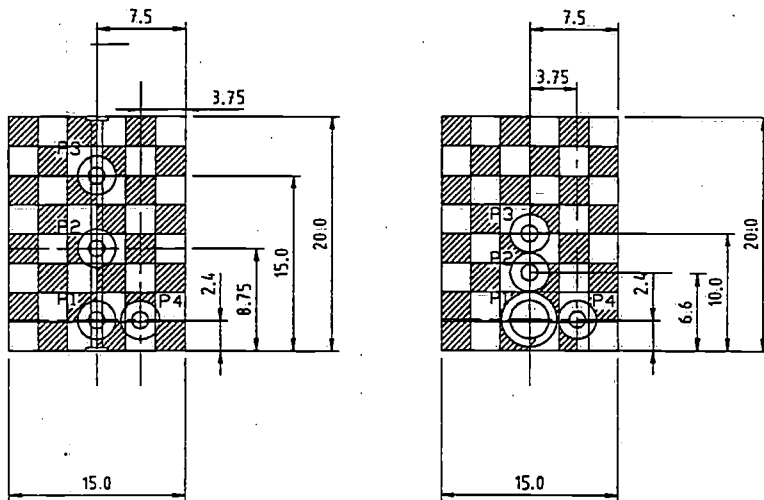


Figure 6-10
Squared Structures 1 (left) and 2 (right) with different instrumentation
(dimensions in metres full scale)

Using the small transducers with a diameter of 1.35 m as reference, a wide range of heights above the deck level could be investigated, combining the test results for the two structures in the same waves. An overview is given in Table 6-5.

Table 6-5
Height of the centres of the transducers above the deck

Transducer	Height of centre above deck in m
P1 of Structure 1	2.4
P2 of Structure 2	6.6
P2 of Structure 1	8.75
P3 of Structure 2	10.0
P3 of Structure 1	15.0

For Structures 1 and 2 a number of regular wave tests was available with the same height and wave length, given in Table 6-6. Figure 6-11 shows the load profiles: the maximum pressure occurring at a certain height (not per definition at the same moment in time).

Table 6-6
Regular wave tests available for both Structures 1 and 2

Wave height	Wave length to ship length	Water height on deck H_{10}
140%	$\lambda/L=1.0$	7.19 m
115%	$\lambda/L=1.0$	6.16 m
100%	$\lambda/L=1.0$	4.78 m
115%	$\lambda/L=0.75$	4.96 m
100%	$\lambda/L=0.75$	2.49 m

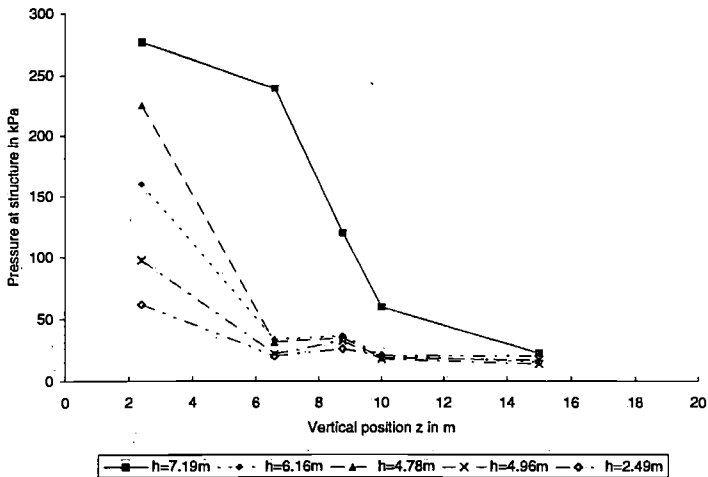


Figure 6-11
Pressure profiles for 5 different water heights on deck 10 m in front of the structure
(from 2.49 m to 7.19 m)

The vertical position z was now normalised with the input water height 10 metres in front of the structure (H_{20}). The impact pressures were normalised with the reference value of transducer P1 (PSTRUC1). This resulted in Figure 6-12.

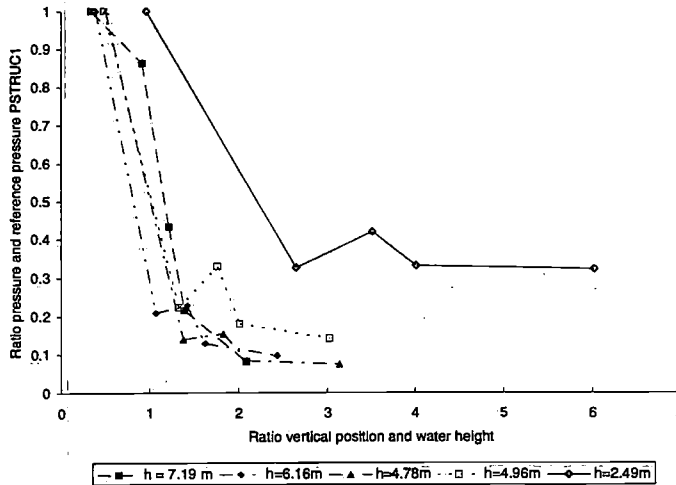


Figure 6-12

Pressure profiles for different regular wave heights with the vertical position z normalised with the input water height 10 m from the structure and the impact pressures normalised with the reference value of transducer P1 (PSTRUC1)

This figure makes clear that for large water heights the normalised water profile is constant. For smaller water heights the loads are relatively high at the higher positions. This is related to the fact that the absolute pressure at the higher level at the structure was found to be almost independent on the incoming water height.

This can be understood if the pressure profile is split up in the contribution of the two first stages of the green water impact (see Section 2.8):

1. The 'impact stage': at the moment that the water layer (jet) on the deck reaches a structure, the momentum in the fluid is transferred into an impact load on the structure. This load is concentrated around the height of the incoming water layer. In Figure 6-13 the typical side profile of the flow of the green water over the deck is shown. The front of the flow, which hits the structure first, can be seen as a triangular wedge.

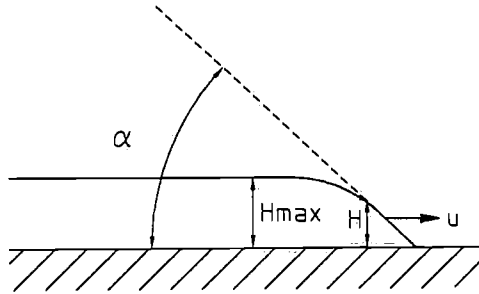


Figure 6-13
Typical side profile of green water on the deck

The wedge angle α can be estimated from the velocity of the water front over the deck (U) and the rate of increase of the water height (H) according to:

$$\alpha = \arctan\left(\frac{dH/dt}{U}\right) \quad (6.7)$$

In Table 6-7 the results of such an evaluation are shown for a number of regular waves. The angle α varies between 20 and 56 degrees:

Table 6-7
Wedge entry angle α found in the regular wave tests

λ/L	H	α
1.0	100%	20 degrees
1.0	115%	27 degrees
1.0	140%	56 degrees
0.75	100%	40 degrees
0.75	115%	30 degrees

The impact of a water wedge on a wall was studied theoretically by Cumberbatch (1960) based on similarity flow assumptions (neglect of gravity, two-dimensional flow, infinite wedge). He calculated the free surface shapes for wedge angles of 22.2 and 45 degrees, see Figure 6-14. He also determined the pressure distribution on the wall, which is shown in Figure 6-15. More recent and advanced applications of similarity flow for the prediction of impact pressures can be found by Greco, Faltinsen and Landrini (2000, 2001) and Stansberg, Hellan, Hoff and Moe (2002).

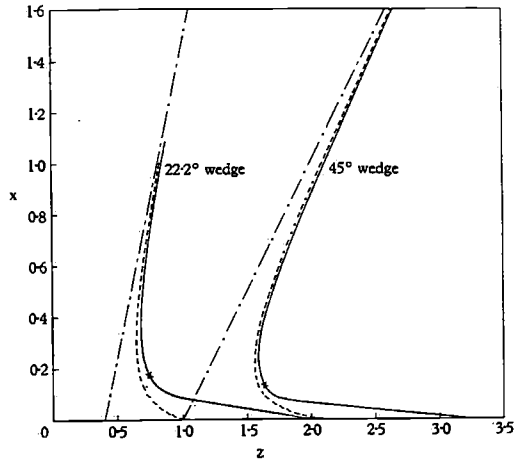


Figure 6-14
Free surface shapes for wedge angles of 22.2 and 45 degrees,
from Cumberbatch (1960)

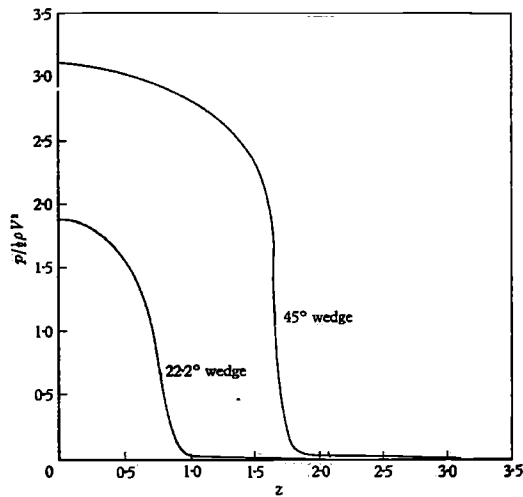


Figure 6-15
Pressure distribution over the wall for wedge angles of 22.2 and 45 degrees,
from Cumberbatch (1960)

If the two figures are combined it can be found that the pressure is concentrated in an area of $1.7H$ for the 45 degrees angle and $2.3H$ for the 22.2 degrees angle. In the green water case the maximum load seems to be limited to $1.5H$, which is very close to the pressure distribution for the 45 degrees angle.

2. The 'quasi-static load stage': as soon as the water reaches a structure, it runs up high in front of it (height H). The resulting vertical 'sheet' of water will induce a (quasi) static pressure on the structure, which is (almost) independent of the thickness of the sheet:

$$p_q = \rho (g + \ddot{z}) H \quad (6.8)$$

\ddot{z} represents the vertical acceleration of the deck. Because the pressure component in Expression (6.8) is independent of the thickness of the sheet of water in front of the structure, it has a relatively large effect on the normalised pressure profile for small incoming water heights on the deck which still run up in front of the structure.

Based on the considerations above, it was decided to formulate a schematic vertical pressure distribution which takes into account both the impact and quasi-static pressure contributions. For this purpose the pressure distribution was divided into three vertical regions: $0 < z < H$, $H < z < 1.5H$ and $1.5H < z < 20$.

1. The effect of the momentum impact is limited to the lowest two regions. The first region is from the deck level up to the maximum height of the incoming water front H . Based on the theoretical and measured pressure distributions a linear pressure variation is assumed, where the reference pressure p_{ref} (on P1) is applicable at $z=0.5H$ and a variation of $0.2 p_{ref}$ of this reference pressure is assumed over the height H . Therefore, for $0 < z < H$ the following relation applies:

$$p(z) = 1.1 p_{ref} - 0.2 \frac{z}{H} p_{ref} \quad (6.9)$$

2. For the region where $H < z < 1.5H$ the effect of the momentum impact is described as:

$$p(z) = 0.9 p_{ref} - 1.8 p_{ref} \frac{(z - H)}{H} \quad (6.10)$$

3. For the quasi-static pressure on the squared structures the following distribution was determined based on the absolute pressure as function of the height at the structure:

$$p(z) = k - j \cdot z \quad (6.11)$$

For the squared structure $k=42$ and $j=2.1$.

The quasi-static part applies to the region where $1.5H < z < 20$, but also in the area $H < z < 1.5H$ when it is larger than the contribution of the momentum impact.

In Figure 6-16 the resulting pressure distribution is shown. It should be noted that this is the peak pressure that occurs over the height of the structure. Due to the progressive nature of the green water loading on the structure, this peak pressure does not occur at the same time over the complete height of the structure. The quasi-static component occurs a significant time after the initial peak load. Very similar pressure distributions were found in the results of numerical simulations presented in Fekken, Veldman and Buchner (1999), see also Chapter 9.

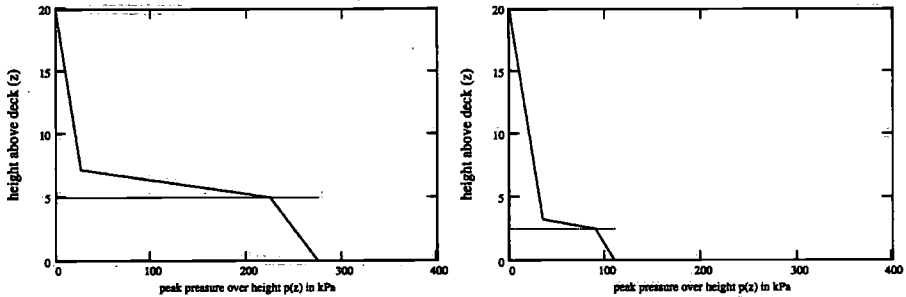


Figure 6-16
Assumed basic pressure distribution for a large (left) and small (right)
water height on the deck

This pressure distribution suggests that the moment on the structure will be relatively large with respect to the horizontal FX-force for low water heights on deck. This variation of the moment arm (maximum moment divided by maximum horizontal FX-force) with the water height on the deck is confirmed in Figure 6-17.

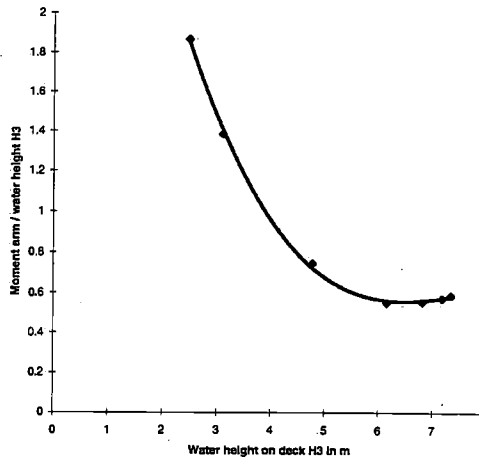


Figure 6-17
Moment arm normalised by the water height on the deck 10 m in front of the structure (H_{20})

It is clear from Figure 6-17 that the ratio between moment arm and water height increases rapidly with decreasing water height. With the larger water heights the ratio converges to a value around 0.6. The moment is then governed by the momentum impact.

6.3.2 Horizontal load profile

For the estimation of the horizontal profile of the impact pressure over the width of the structure, only two transducers were available: P1 (centre) and P4 (3.75 m to the side). For Structure 1 both transducers had the same diameter and were directly comparable. To indicate the horizontal pressure profile and the effect of the panel size, Table 6-8 shows the results for similar tests on Structures 1 and 2.

*Table 6-8
Comparison between the loads on Structures 1 and 2 for similar wave conditions*

Wave	P1 large (area 5.725 m ²) in kPa	P1 small (area 1.43 m ²) in kPa	P4 small (area 1.43 m ²) in kPa
140%	241	277	297
115%, $\lambda/L=0.75$	148	225	115
115%, $\lambda/L=1.00$	130	160	148

From this table it can be concluded that:

- The small area panel is conservative with respect to the large panel as expected. The differences vary between 15 and 52 percent.
- The differences between the small panels P1 and P4 are dependent on the wave length and in this way on the flow pattern on the deck. In general the load in the middle of the structure is higher, but for the largest wave height the load on P4 is slightly (7 percent) higher. Therefore, it is suggested to assume a constant horizontal profile of the pressure over the width of the structure until numerical methods give more insight in this pressure distribution.

6.4 Effect of structural shape on impact loading

6.4.1 Method

As described in Section 3.4, in Test Series C a systematic series of tests was carried out with different structures on the deck. Six different structural shapes were investigated, with the same height and width. Their fronts were all placed at the same position, 30 m from the fore perpendicular. The following structural shapes were investigated:

- Squared structure (Nos 1 and 2)
- Tilted structure under 30 degrees angle with vertical (No. 3)
- Triangular structure with 45 degrees semi-angle (No. 4)
- Triangular structure with 60 degrees semi-angle (No. 5)
- Cylindrical structure (No. 6)
- Squared structure with triangular support (No. 7)

The tests that were used to determine the effect of the different hull shapes and bow flare angles, were all with Squared Structure 1 at 30 m from the fore perpendicular of the full elliptical bow with a bow flare of 30 degrees. The load on this structure, and especially the load on P1 and the horizontal load FX, are used as a reference for the analysis of the loads on other structural shapes. All structural shapes were tested in regular waves of various lengths ($\lambda/L=1.0$ and 0.75) and heights ($H=100\%$ and 115%) to make a direct comparison between the different structures possible.

In Figure 6-18 the pressure profile against vertical position is shown for all these structures.

For these structures the following relations were determined:

- The ratio between the pressure on this structure and the pressure on the squared reference structure ($p_{ref,s}$).
- The ratio between the horizontal FX-load on this structure and the FX-load on the squared reference structure (FX_s).

These ratios are a function of the water height on the deck (H) at a position 10 m in front of the structure.

In this way the reference pressure ($p_{ref,s}$) and horizontal FX-load (FX_s) on the different structural shapes can be determined from the loads on the squared reference structure at the same distance (x) from the fore perpendicular ($p(x)$ and $F(x)$) according to:

$$p_{ref,s} = (a_s \cdot H + b_s) \cdot p(x) \quad (6.12)$$

$$FX_s = (c_s \cdot H + d_s) \cdot F(x) \quad (6.13)$$

p_{ref} is again related to a panel area of 1.43 m² positioned 2.4 m above the deck level, but now for a different structural shape.

For the triangular structure with 45 degrees angle these relations are presented as example in Figures 6-19 and 6-20.

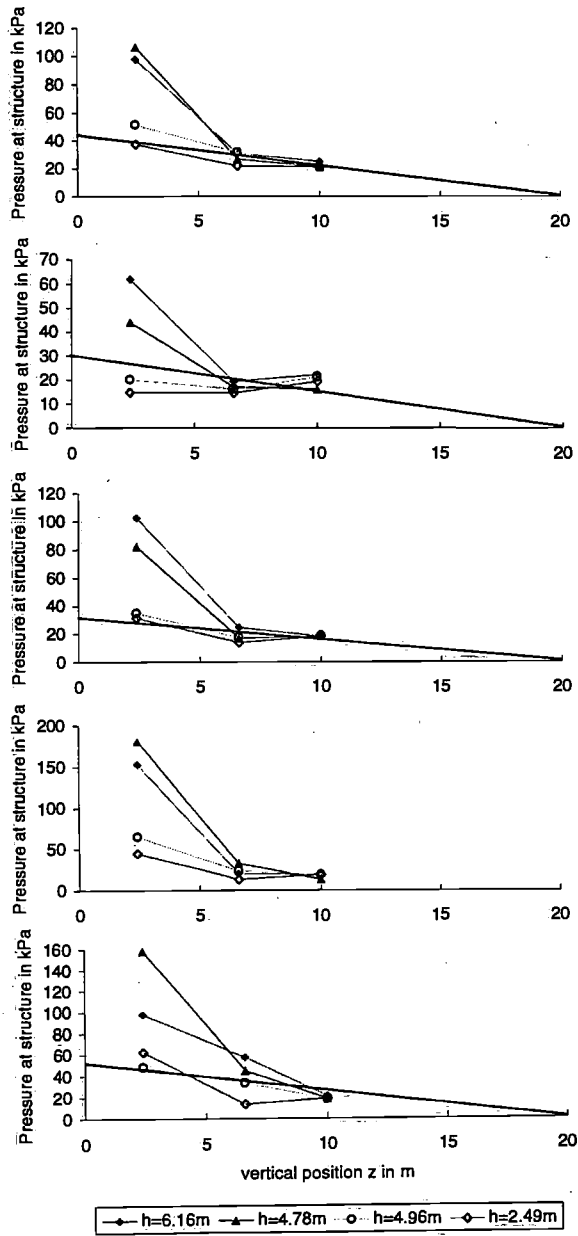


Figure 6-18

Pressure against vertical position for the structure under 30 degrees angle with vertical, the triangular structures with 45 and 60 degrees semi-angles, the cylindrical structure and the squared structure with triangular support (from top to bottom)

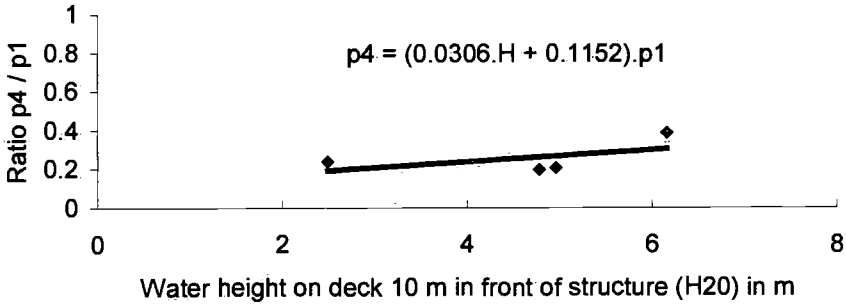


Figure 6-19

Ratio between the pressure on the triangular structure (45 degrees) and the reference pressure on squared structure 1 as function of water height on deck 10 m in front of the structure

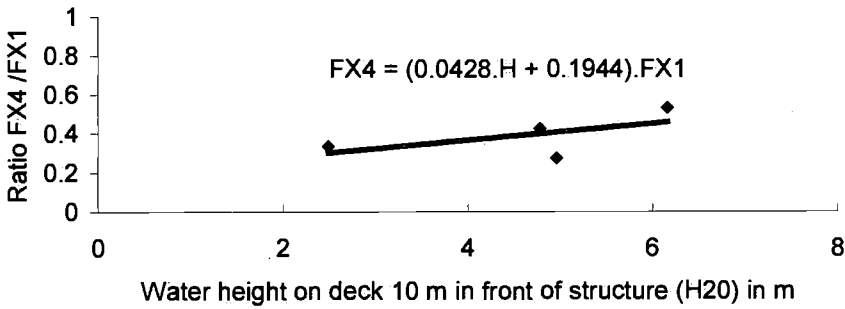


Figure 6-20

Ratio between the horizontal FX-load on the triangular structure (45 degrees) and the reference FX-load on squared structure 1 as function of water height on deck 10 m in front of the structure

The values for a_s to d_s for all structures are summarised in Table 6-9.

Table 6-9
Values a_s to d_s for all different structures

	a_s	b_s
30 degrees with vertical	-0.007	0.5851
Triangular 45 degrees	-0.0306	0.1152
Triangular 60 degrees	0.0177	0.3854
Cylindrical	0.0488	0.5631
Triangular support	-0.1233	1.27

	c_s	d_s
30 degrees with vertical	0.0067	0.5848
Triangular 45 degrees	0.0428	0.1944
Triangular 60 degrees	0.0145	0.5389
Cylindrical	0.0234	0.4067
Triangular support	-0.0354	1.0311

Based on Figure 6-18 a similar pressure distribution is assumed as for the Squared Structures 1 and 2 according to Expressions (6.9)-(6.11). Expression (6.12) and Table 6-9 can be used to determine the reference pressure (p_{ref}). In Table 6-10 the applicable values for k and j of the quasi-static pressure component are shown.

Table 6-10
Values k and j for all different structures

Structure		k	j
30 degrees with vertical	No. 3	42	2.1
Triangular 45 degrees	No. 4	30	1.5
Triangular 60 degrees	No. 5	33	1.65
Cylindrical	No. 6	40	2.0
Triangular support	No. 7	52	2.6

To calculate the global moment M on the structure with respect to the deck level, the moment arm l should be determined. This moment arm was found to be very dependent on the water height on the deck 10 m in front of the structure.

Done similarly as in Figure 6-17, the moment was determined as function of the water height on the deck for all structures according to the following formula:

$$M_s = (a_M \cdot H^2 + b_M \cdot H + c_M) \cdot H \cdot F_s \quad (6.14)$$

The values for a_M , b_M and c_M can be found in Table 6-11:

Table 6-11
Values a_M , b_M and c_M for all different structures

	a_M	b_M	c_M
Squared	0.0907	-1.0494	3.4984
30 degrees with vertical	0.0392	-0.5686	2.1714
Triangular 45 degrees	0.0968	-1.3251	4.9902
Triangular 60 degrees	0.1214	-1.8359	7.2326
Cylindrical	0.0949	-1.2862	4.8759
Triangular support	0.1985	-2.5598	8.8008

6.1.2 Direct comparison between the different structural shapes

With the expressions found in the previous section, it is now possible to make a direct comparison between the loading on the different structural shapes with the same amount of green water on the deck. In Table 6-12 the ratio is presented between the load on a particular structure and the loads on Squared Structure 1. Both the reference pressure p_{ref} and the horizontal FX-load are compared. A water height on the deck of 5 m is assumed.

Table 6-12
Ratio between the reference pressure and global load on the different structures with the values for the squared reference structures (Structures 1 and 2)

Structure	Ratio for p_{ref}	Ratio for FX
No. 3: 30 degrees with vertical	0.55	0.62
No. 4: Triangular 45 degrees	0.27	0.41
No. 5: Triangular 60 degrees	0.47	0.61
No. 6: Cylindrical	0.81	0.52
No. 7: Triangular support	0.65	0.85

The loads on these structures are all significantly lower than on the squared structure. These differences are a result of the fact that the momentum in the x-direction is not deflected completely (and over a longer period of time) for these structures.

6.5 Effect of distance from the forward perpendicular

Most of the tests in Test Series C were carried out with the squared structure at a distance of 30 metres from the fore perpendicular. To study the effect of the distance of the structure from the fore perpendicular, the position of Structure 2 was varied in some regular wave tests to 20 and 30 metres. These tests were carried out with the full elliptical bow with a 30 degrees bow flare angle. In Figure 6-21 an overview is given of the results in comparable waves with the different distances from the fore perpendicular.

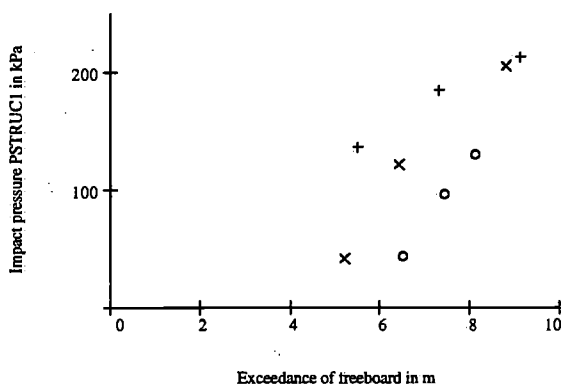


Figure 6-21

Effect of the distance from the fore perpendicular on the impact pressure on a squared structure. The results for 30 m distance are given with circles, for 20 m with crosses and for 10 m with plus-signs

Comparing the results in Figure 6-21, the impact pressures generally increase when the distance from the forward perpendicular decreases. This is due to the larger water height on the deck and differences in velocity of the water over the deck.

However, due to the limited amount of data it is not possible to define a reliable relation between the distance from the fore perpendicular and impact loading. At present the following heuristic approach is chosen: if one considers that the impact pressure is quadratic with the freeboard exceedance (Expression 6.4) and that the water height on the deck is linear with the freeboard exceedance (Expression 5.2), it is possible to assume that there is a quadratic relation between the impact pressure and water height on the deck as well. Based on this assumption the pressure on a structure at a certain position can be estimated from the reference pressure at 30 m from the fore perpendicular $p(30)$ and the water height 10 m in front of the structure as:

$$p(30) = a h^2 \quad (6.15)$$

$$p(20) = \left(\frac{H_{10}}{H_{20}} \right)^2 a h^2 \quad (6.16)$$

$$p(10) = \left(\frac{H_0}{H_{20}} \right)^2 a h^2 \quad (6.17)$$

The ratios $(H_{10}/H_{20})^2$ and $(H_0/H_{20})^2$ are dependent of the bow shape and can be found based on the results from the expressions in Section 5.3. They are summarised in Table 6-13. For the horizontal FX-load the same method can be applied.

The method, however, neglects the complex variation of the water velocity over the length of the deck due to focussing effects. This requires further research in the future, using numerical simulation models.

*Table 6-13
The ratios $(H_{10}/H_{20})^2$ and $(H_0/H_{20})^2$ for different bow flare angles*

	$(H_{10}/H_{20})^2$	$(H_0/H_{20})^2$
$\gamma = 0$ degrees	0.919	1.992
$\gamma = 10$ degrees	0.976	2.013
$\gamma = 30$ degrees	1.127	1.783
$\gamma = 50$ degrees	2.087	3.174

6.6 Summary of load prediction procedure for structures on the deck

To determine the loading on structures on the deck based on the material presented in this chapter, the following steps need to be followed:

- Step a: Determination of pressure and global load on a squared reference structure
- Step b: Correction for distance from the fore perpendicular
- Step c: Conversion to different structural shapes
- Step d: Determination of load profile and moment

6.7 Efficiency of protecting breakwaters

6.7.1 Design considerations

Breakwaters can be used to protect structures on the deck. For the design of this type of breakwaters, it is important to keep their purpose in mind: breaking or deflecting the green water that flows with a certain height at high velocity over the deck, to minimise the impact on the critical structure. This results in the following requirements:

- The breakwater should be higher than the water height on the deck.
- The breakwater has to deflect or break the green water flow efficiently, so that the amount of water that finally reaches the critical structure will be minimised in amount and/or velocity.
- The breakwater and the underlying support structure should be strong enough to deal with the dynamic load due to the water impact on the breakwater itself.

In this study three different types of breakwaters were evaluated:

1. Traditional V-type breakwater (No. 1)
2. Vertical wall breakwater with its upper side tilting forward (No. 2)
3. Vane type breakwater (No. 3)

More information can be found in Chapter 3 and Appendix C.

6.7.2 Observations

In front of closed breakwaters, such as the traditional V-type breakwater and vertical wall breakwater, the green water tends to run-up vertically as soon as the water front hits the breakwater. This fills the complete area in front of the breakwater, which results in the rest of the water flowing over the breakwater. This reduces the effective height of the breakwater, see Photo 6-1.

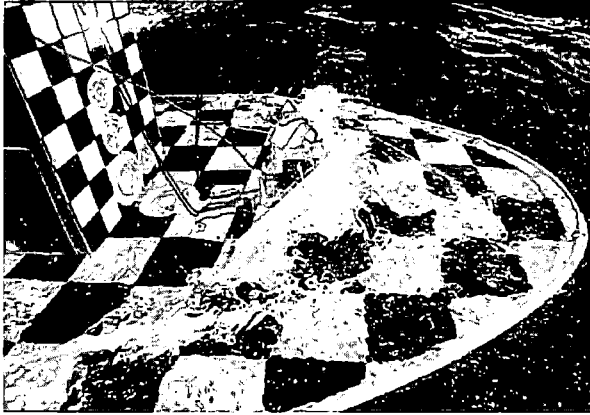


*Photo 6-1
Run-up of green water in front of the traditional breakwater*

To prevent this run-up as much as possible, the vane type breakwater is a good alternative (Beynet, 1994). This open breakwater with vertical vanes under an angle of 45 degrees, deflects the water away from critical structures, but does not completely block the fluid flow. This reduces the run-up in front of the breakwater as well as the impact loading on the breakwater itself. This will be quantified below.

6.7.3 Quantification of breakwater efficiency

Because the breakwaters were placed between water height probes H2 and H3, the mean value of these two water heights without the breakwater is taken as the input water height. The breakwater has to deal with this input water height. It is summarised for the different regular waves in Table 6-14.

*Table 6-14
Wave lengths, wave heights and input water heights in front of the breakwaters*

λ/L	Wave height	Input water height (H)
1.0	85%	2.04 m
1.0	100%	4.80 m
1.0	115%	5.64 m
0.75	100 %	3.33 m
0.75	115%	4.31 m

In the present study it was assumed that a breakwater height is effective at the moment that the water in front of the breakwater as a result of run-up is not coming above the height of the breakwater. The run-up is measured with water height probe H2.

In Figure 6-22 the efficiency of the three different breakwaters can be studied. Horizontally the input water height is shown and vertically the ratio between the run-up water height in front of the breakwater and the height of the breakwater. The horizontal line in the figure refers to a situation where the breakwater height is equal to the water height in front of the breakwater, including run-up. Due to this run-up the breakwaters should be higher than the water height on the deck.

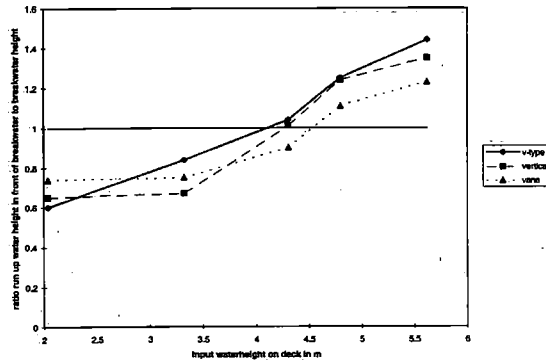


Figure 6-22

The input water height versus the ratio between the run-up water height in front of the breakwater and the height of the breakwater for the three breakwater types

In Table 6-15, the safe water height on deck is given, which can be dealt with efficiently by the three different breakwaters. Taking into account their height of 4.98 m, this safe water height can be used to define a safety factor for the required breakwater height. The water height on the deck has to be multiplied by this factor to find the required breakwater height.

Table 6-15

Safe water height for the three breakwater types and the resulting required safety factor for the water heights on the deck at the position of the breakwater

Breakwater	Safe water height	Safety factor
Traditional V	4.10 m	1.21
Vertical wall	4.27 m	1.17
Vane	4.54 m	1.10

The results confirm that the vane type breakwater is the most effective in the prevention of run-up. The remaining water height behind the breakwater and the loading on the structure behind the breakwater (which is partially due to the flow from the sides behind the breakwater) are almost equal for all three breakwater types.

6.7.4 Loading on the breakwater

Another point of concern is the peak load on the breakwater itself at the moment of impact. This impact load is due to the momentum in the green water, which is deflected by the breakwater.

During the present model tests the horizontal FX-load, the local FX-load on the centre part of the breakwater and the moment with respect to the deck level were measured. In Figures 6-23 and 6-24 the local and global loads are shown as function of the water height on deck.

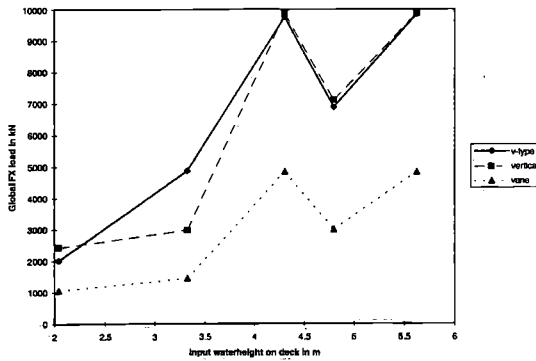


Figure 6-23

Horizontal FX-load on the three breakwater types as function of input water height on the deck

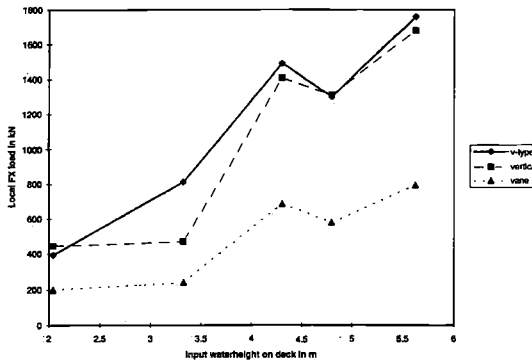


Figure 6-24

Local FX-load on the centre of the three breakwater types as function of input water height on the deck

From these figures the following becomes clear:

- The load levels on the vane type breakwater are much lower than for the closed V-type and vertical breakwaters. This is a result of the fact that the fluid flow is not completely blocked by the vane type breakwater. Not all the momentum of the green water is transferred into load on the breakwater.
- The loads on the breakwater increase with water height as expected, until the water flows over the top of the breakwater. At that moment the load on the breakwater shows a clear dip. This can be related to the flow of the water over the top and the resulting loading from the back of the breakwater. For large water heights the impact load is increasing again. But in this case a large amount of water will flow over the breakwater, which limits the increase in the loads.

Based on the fact that breakwaters are used to prevent water flow over their tops, it is assumed that the maximum load for water heights which can be dealt with by the breakwater, should be used as the design load for the breakwater. Table 6-16, therefore, gives the estimated maximum loads and moments for the present breakwaters with a height of 4.98 m.

Table 6-16

Estimated maximum loads and moments for the present breakwaters with a height of 4.98 m

Breakwater	Horizontal FX-load	Local FX-load	Moment with respect to deck
Traditional V	9760 kN	1490 kN	27900 kNm
Vertical wall	9870 kN	1410 kN	27400 kNm
Vane	4840 kN	687 kN	13200 kNm

For other breakwater heights it is proposed to scale the loads according to Froude scaling laws, based on the actual height of the breakwater hb' and the reference height hb (= 4.98 m).

$$F'' = F \cdot \left(\frac{hb'}{hb} \right)^3 \quad (6.18)$$

$$M'' = M \cdot \left(\frac{hb'}{hb} \right)^4 \quad (6.19)$$

In this scaling it is assumed of course that also the transverse dimensions vary according to the ratio hb'/hb .

7. GREEN WATER FROM THE SIDE AND STERN

7.1 Introduction

So far this thesis focussed on green water loading on the bow. However, in non-collinear directions of wind, waves and current a weather-vaning FPSO does not always encounter head waves. Wave headings of typically 15 to 30 degrees from head waves can occur. In this type of conditions, green water on the deck is not only a problem in the bow area of the FPSO, but it can also come onto the deck from the side of the ship. Green water from the side already caused damage on several FPSOs, typically at midships and further aft.

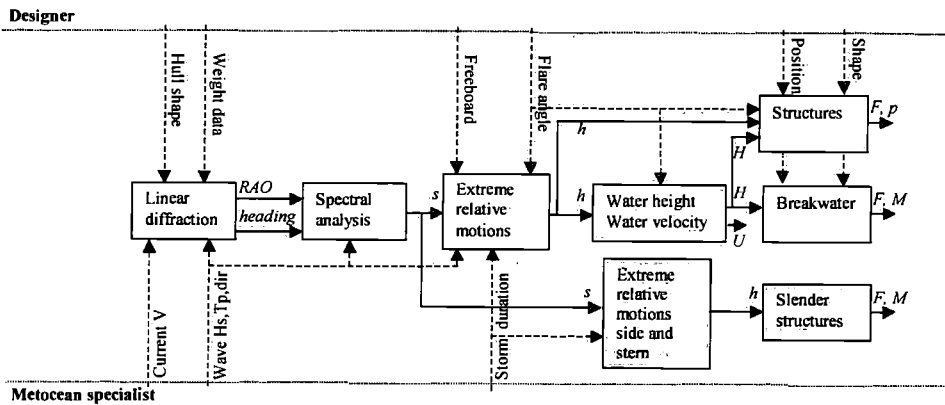


Figure 7-1

Part of the proposed semi-empirical design evaluation method considered in this chapter (in grey): prediction of green water from the side and stern

Although the damage generally concerns smaller structures (handrails, piping, cable trays, staircases, etc.), this damage can still result in safety problems on board. It is also a serious problem for people working on the deck, especially because it can happen unexpectedly in lower sea states.

Green water was also observed in some cases at the stern of FPSOs. Especially in longer waves the relative wave motions in the stern can also be large. For traditional tankers converted to FPSOs, this can result in freeboard exceedances because they have a relatively low freeboard aft.

In this chapter the extreme relative wave motions at the side and stern will be discussed, as well as some simplified prediction models for loads on slender structures (see Figure 7-1).

7.2 Model tests

In the Test Series D pilot tests were carried out with an angle between the ship heading and wave heading of 195 and 210 degrees. The full elliptical model (30 degrees bow flare) from Test Series C was used.

Additionally the relative wave motions along the side were measured at four positions, as well as water heights on the deck at the same longitudinal positions, see Figure 7-2. Tests were carried out in regular waves as well as in irregular wave spectra ($H_s=13.5$ m, $T_p=12, 14$ and 16 s).

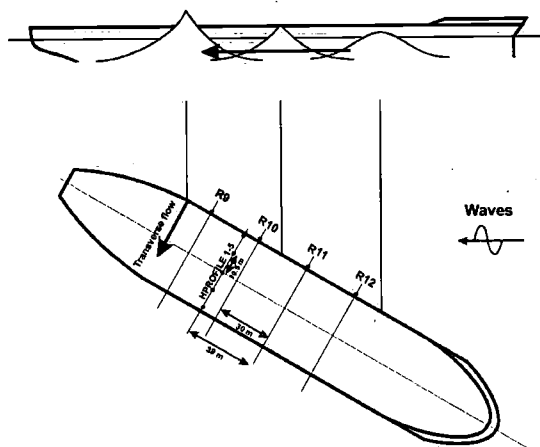


Figure 7-2

Overview of the measurement set-up with a sketch of the observed phenomena

7.3 Observations of relative wave motions along the side

From a detailed study of the behaviour of the (relative) waves along the side of the ship from video recordings, it became clear that the (relative) wave crests tend to be more and more peaked when the wave crests travel aft along the side, as shown schematically in Figure 7-2. This seems a result of the fact that the higher harmonic components in the wave become more important after reflection of the wave on the hull. At the moment the wave crest reaches midships, the vessel is pitching with the stern downwards as well. Typically at midships (of slightly further aft) the relative wave motion peaks become so high that they exceed the freeboard level. The roll motions of the vessel are still very moderate in this condition.

At the moment when the relative wave motions exceed the freeboard, a surprisingly fast transverse flow occurs over the deck. The main flow of water on the deck is not parallel with the side of the vessel, but has a dominant component perpendicular to the length of the ship. This transverse flow results in the main loading from green water from the side. The transverse flow onto the deck shows much resemblance with the theoretical dambreaking problem again, as will be discussed later in more detail.

7.4 Relative wave motions along the side of a hull

7.4.1 Calculated linear relative wave motions

The relative wave motions along the side of ship are generally calculated with linear (3D) diffraction analysis. In Figure 7-3 a comparison is made between the calculated and measured relative wave motion RAO at position R11 at the side of the ship in a limited number of regular waves. This comparison is reasonably good. It should be noted, however, that it is based on the first harmonic amplitudes of the input wave and relative wave motions. In reality the input and output signals also contained significant higher harmonics.

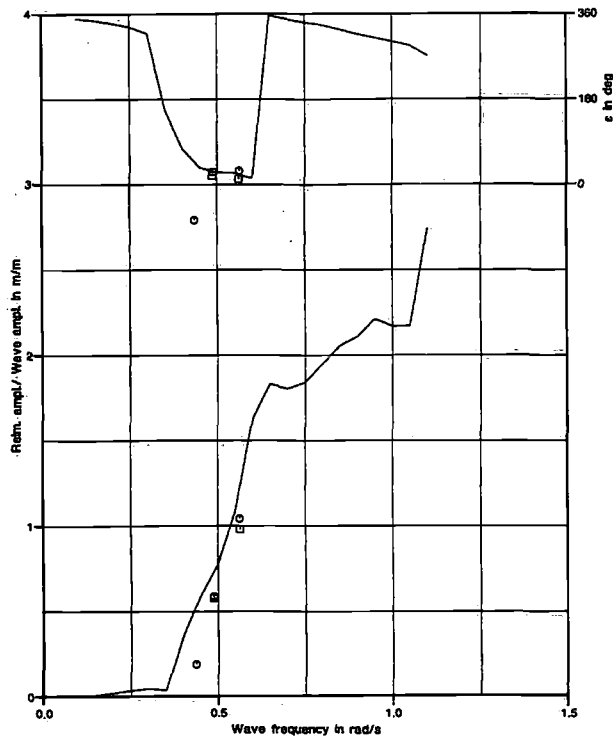


Figure 7-3

RAO and phase of relative wave motion at position R11 with 210 degrees wave heading (calculations as solid line, regular wave tests as points)

7.4.2 Measured non-linear relative motions along the side

It was found in the model tests that the relative wave motions are in reality significantly non-linear. In Figure 7-4 the probability of exceedance of the relative motions at point R11 is shown in the wave spectrum of $H_s=13.5$ m and $T_p=14.0$ s (wave heading 210 degrees). The figure shows both the linear narrow banded Rayleigh distribution and the measured probability of exceedance curve. It will be clear that the Rayleigh distribution underestimates the extreme relative wave motions significantly.

The measured number of extremes was much larger than predicted based on the total test duration and the mean calculated relative wave motion period in the spectrum. In Table 7-1 a comparison is made between the calculated and measured numbers of extremes for the 210 degrees heading.

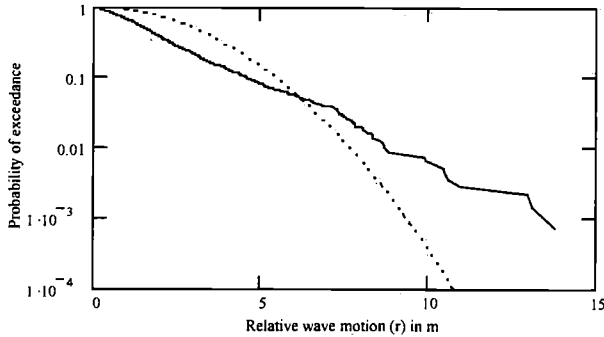


Figure 7-4

Comparison of linear (narrow banded) Rayleigh distribution (dotted line) with measured probability of exceedance (solid line) for R11 in a wave spectrum of $H_s=13.5$ m and $T_p=14.0$ s (wave heading 210 degrees)

Table 7-1

Calculated (linear) and measured number of extremes in a 3 hours storm

	$T_p = 12$ s		$T_p = 14$ s		$T_p = 16$ s	
	Linear	Measured	Linear	Measured	Linear	Measured
R9	1074	1279	973	1444	983	1419
R10	1034	1231	929	1377	935	1410
R11	1038	1214	913	1437	909	1367
R12	1072	1333	923	1622	900	1568

The number of measured extremes is much larger than the calculated number, especially for the longer waves. Together with the measured shape of the probability of exceedance, this points to a strong non-linearity in the results and the existence of higher order (such as double frequency) effects.

7.5 Physical background of observed behaviour

The strong non-linearity in the relative wave motions is confirmed by the time traces of the regular wave tests. The time traces in Figure 7-5 show the relative wave motions at positions R10, R11 and R12 together with the wave input signal for a wave period of 14.44 s ($\lambda/L=1.25$). It should be noted that the wave signal is measured during the test and contains reflections from the model.

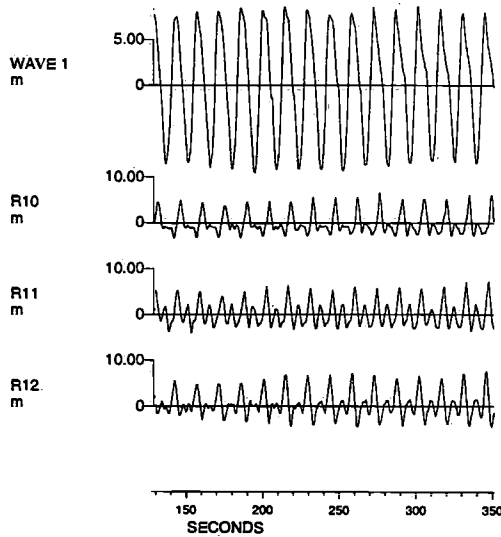


Figure 7-5

Time traces of incoming wave (WAVE 1) and R10-R12 for a regular wave period of 14.44 s, clearly showing higher harmonic responses. The WAVE1 signal is disturbed by the presence of the model in the basin

The time traces show significant double frequency effects compared to the input wave frequency. This is confirmed by the harmonic analysis of the signals, as summarised in Table 7-2. The second harmonics with their double frequency are of similar magnitude as the first harmonics.

Table 7-2

Harmonic analysis of wave input and output signals in a regular wave test

Signal	First harmonic amplitude in m ($T = 14.44$ s)	Second harmonic amplitude in m ($T = 7.22$ s)	Third harmonic amplitude in m ($T = 4.81$ s)
Wave input	11.45	0.89	0.71
R10	2.12	1.73	0.62
R11	1.75	2.37	0.81
R12	1.81	2.04	0.76

The background of these effects lies in the higher harmonics in the input wave, which are bound to the first order wave. They result themselves already in higher wave crests than troughs, as described by Kriebel and Dawson (1993).

However, in the presently studied conditions with waves slightly off the bow, they reflect on the side of the ship and are amplified significantly compared to the longer first harmonic amplitudes of the input wave and relative wave motion.

In the typical relative wave motion RAO in Figure 7-3, it was found that for higher frequencies the response (amplitude amplification) is around two, whereas at the longer wave frequencies the response is very small. If, in a heuristic approach, it is assumed that the response of the different harmonics can be dealt with separately, this implies that higher harmonic frequencies in the input (wave) signal become much more important in the output (relative wave motion) signal.

As an example the response at the first and second harmonic frequencies at position R10 is shown in Table 7-3 for the first harmonic wave frequency of 0.435 rad/s ($T=14.44$ s).

*Table 7-3
Response at position R10 of first, second and third harmonics with the linear RAO*

Harmonic	ω_n in rad/s	ζ_n^a in m	$H(\omega_n)$	Response
First	0.435	11.45	0.25	2.86
Second	0.87	0.89	2.0	1.78
Third	1.305	0.71	>2.0	>1.42

The table shows a reasonable agreement with the measured responses for the first and second harmonics, whereas the response at the third harmonic is overestimated.

Although this effect requires further study, it is presently assumed that this is the reason for the importance of the higher harmonics in the longer waves. For the shorter waves this effect is less important because of the higher linear response.

7.6 Description of non-linear relative wave motions

In the previous section the background of the strong non-linearities in the relative wave motions was investigated. Based on the limited series of tests in pilot Test Series D, in this section a first attempt is made to come to a prediction method for the relative wave motions along the side.

An approach similar to the method presented for the relative wave motions at the bow was chosen. To describe the non-linear distribution of extremes for the relative wave motions in the side, a modified Rayleigh distribution is defined, using the standard deviation from the linear diffraction calculation as starting point.

$$P(r > R) = \exp \left[-\frac{R^2}{2s^2} \cdot (a + b \cdot R + c \cdot R^2) \right] \quad (7.1)$$

This expression is now fitted onto the measured distribution. This fitting was carried out for both wave directions of 195 and 210 degrees and for all spectral peak periods of 12, 14 and 16 seconds. In Figures 7-6 and 7-7 the measurements and fits are shown for position R11 and wave directions of 195 and 210 degrees respectively. The standard deviation (s) is based on the linear diffraction analysis and spectral analysis.

The related parameters a, b and c are shown in Table 7-4:

Table 7-4
Parameters of modified Rayleigh distribution fits for R11 in spectral peak periods of 12, 14 and 16 s (from top to bottom) for wave angles of 195 and 210 degrees

Wave direction	Spectral peak period T_p	Linear standard deviation s in m	a	b	c
195 degrees	12 s	2.813	2.55292	-0.39872	0.02044
195 degrees	14 s	2.294	2.00121	-0.24894	0.01025
195 degrees	16 s	1.889	2.53706	-0.46767	0.02642
210 degrees	12 s	3.553	1.20543	-0.04767	0.00095
210 degrees	14 s	2.512	1.39521	-0.08988	0.00173
210 degrees	16 s	2.047	2.77046	-0.5076	0.02874

With the expressions for the probability of exceedance, design values for the maximum relative wave motions can be determined, such as the Most Probable Maximum (MPM) value. It should be noted that the number of oscillations N cannot be determined simply from the mean period to determine the most probable maximum relative wave motion. A correction should be applied to take into account the higher harmonic response. At present the following correction is proposed based on the results in Table 7-1:

$$N_n = \eta N_1 \quad (7.2)$$

N_1 is the number of extremes based on the mean period of the linear motion response, N_n is the actual number of extremes in the non-linear situation. In Table 7-5 an approximation of the factor η is proposed based on the mean values of the calculated and measured values of N.

Table 7-5
 Non-linearity correction factor η for the number of extremes

Peak period	Factor η
12 s	1.27
14 s	1.65
16 s	1.60

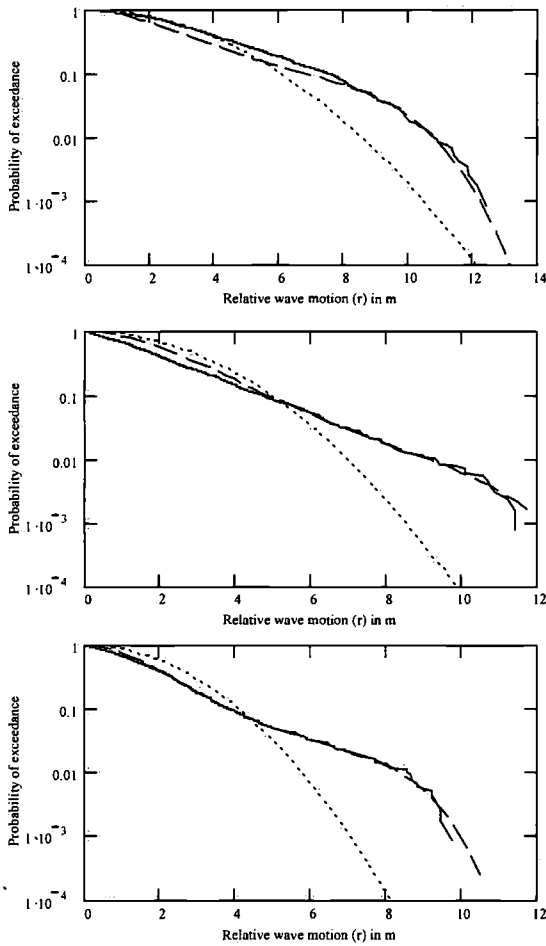


Figure 7-6

Modified Rayleigh distribution fits (dashed line) for R11 in spectral peak periods of 12, 14 and 16 s (from top to bottom) for a wave angle of 195 degrees. The solid line represents the measurement, the dotted line the linear Rayleigh distribution

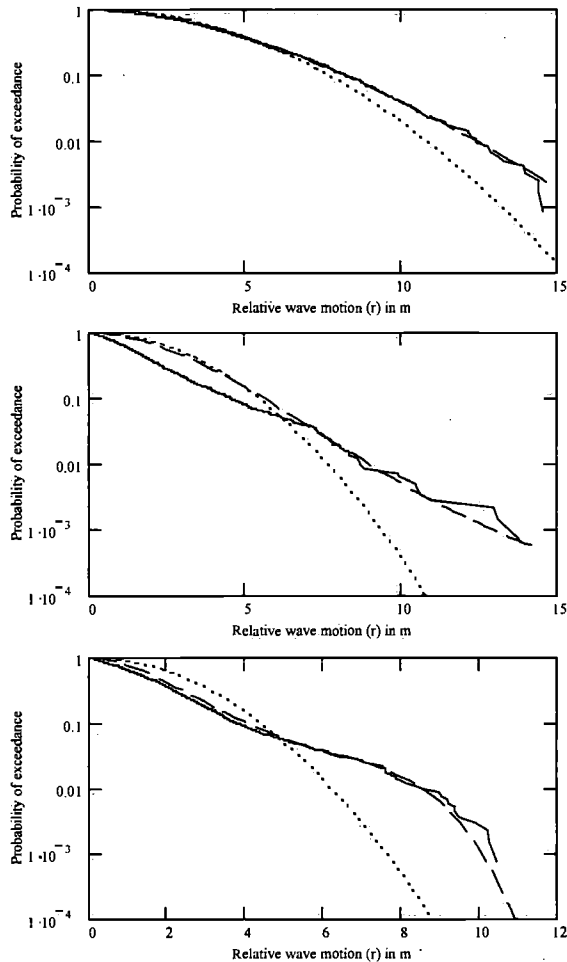


Figure 7-7

Modified Rayleigh distribution fits for R11 in spectral peak periods of 12, 14 and 16 s (from top to bottom) for a wave angle of 210 degrees. The solid line represents the measurement, the dotted line the linear Rayleigh distribution

In most cases a reasonable fit was achieved in Figures 7-6 and 7-7. However, it is clear that also differences are found, with the fitted curve following only a part of the measured curve. This indicates that the subject of relative wave motions along the side requires further study. With higher order diffraction theory it will be possible to predict the first and higher order response of the relative wave motions along the side theoretically, Vestbøstad (1999). Using higher order Volterra type modelling methods similar to those used by Adegeest (1995), it will then be possible to describe the non-linear distribution of the extremes, although his method assumes a linear wave input.

7.7 Green water flow and loading from the side

7.7.1 Transverse water flow onto the deck

The flow of green water from the side is a complex process. During the observations described earlier, it was found that a surprisingly fast transverse flow over the deck occurs when the relative wave motions exceed the freeboard. The water on the deck does not travel mainly with the velocity of the (orbital) motion of the wave crest along the side, but has a dominant component perpendicular to the length of the ship.

During the model tests, measurements were carried out with an empty deck and five water height probes (HPROFILE 1-5) at equidistant positions over the beam of the vessel (see Figure 7-2). In Figure 7-8 an example of the time traces of these measurements is given for one green water event from the side. From these time traces the (parabolic) decrease in maximum water height from the side can be determined, as well as the transverse velocity of the water front over the deck (by dividing the distance between the probes by the time necessary for the water front to travel from one to another). In this case the transverse velocity of the water front U is 16.8 m/s for a water height on the side h (approximately equal to the exceedance of the freeboard) of 3.4 m.

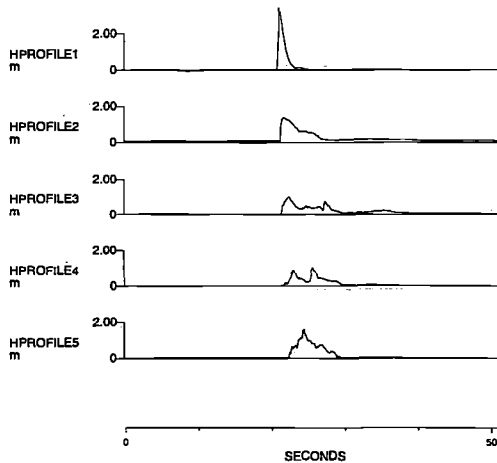


Figure 7-8

Time traces of the water height on the deck at equidistant positions (HPROFILE1-5) over the beam of the FPSO

From the tests in irregular waves, the transverse water height profile was now determined. For this purpose the time traces of the largest six green water events (including the one in Figure 7-8) were analysed.

In Figure 7-9 the transverse water height profile is shown for these largest six green water events. The figure presents the ratio of the water height at a certain transverse position (y) with the water height at deck edge. This figure shows that the water height decreases (parabolically) with the distance from the deck edge. However, at the lee side of the deck sometimes green water came on the deck too, which resulted in an increase of the water height again at a large distance from the wave side of the ship.

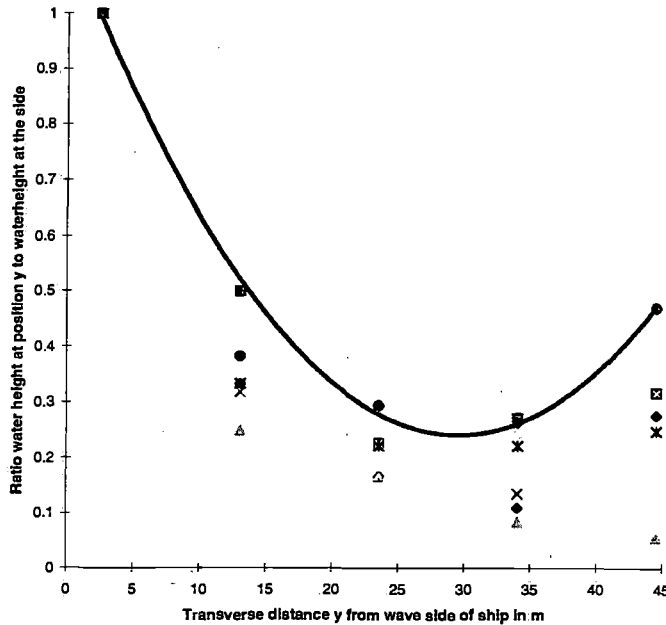


Figure 7-9
Ratio between the water height at a certain transverse position y and the water height at the deck edge

In Figure 7-9 an upper limit line for the present measurements is presented, which can be used as an estimate of the transverse water height profile as soon as the exceedance of the freeboard (h) is known. The transverse water height profile as function of y can be expressed (for $y > 2.5$ m) as:

$$H = (0.001y^2 - 0.0608y + 1.1399)h \quad (7.3)$$

7.7.2 Hydraulic models for green water flow from the side

The knowledge about the complex physics of green water flow from the sides onto the deck is limited. However, from the observations it became clear that the flow onto the deck shows much resemblance with the water behaviour in the theoretical dam breaking problem.

The theoretical dam breaking problem is described extensively by Stoker (1957), using shallow water wave assumptions. In the theoretical dam breaking problem there is a vertical wall of water of height h' at $t=0$, see Figure 7-10.

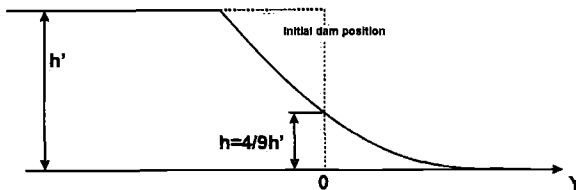


Figure 7-10
Theoretical dam breaking problem

At that moment the imaginary dam is taken away and the water flows into the dry area. Based on shallow water flow assumptions, Stoker determined the following expression for the water height $H(y,t)$ at time t and position y from the initial dam position with an initial height h' (not valid for $t=0$):

$$H(y,t) = \left(-\frac{y}{3\sqrt{g}t} + \frac{2}{3}\sqrt{h'} \right)^2 \quad (7.4)$$

In Figure 7-11 an example water contour (at a certain time) is shown of the water flow onto the deck of the FPSO. The input parameter is the exceedance of the freeboard h . However, this h is not equal to the initial dam height h' in Expression (7.4). The latter value is equal to $h=(4/9)h'$ and can be explained from Figure 7-10: after the breaking of the dam a depression travels into the water area. The water contours rotate around the point of the initial dam position at a height that is $4/9$ of the original water height h' of the dam. To apply the dam breaking theory to the green water problem from the side, the value h' in Expression (7.4) should not be taken as the freeboard exceedance (h), but as:

$$h' = \frac{9}{4}h \quad (7.5)$$

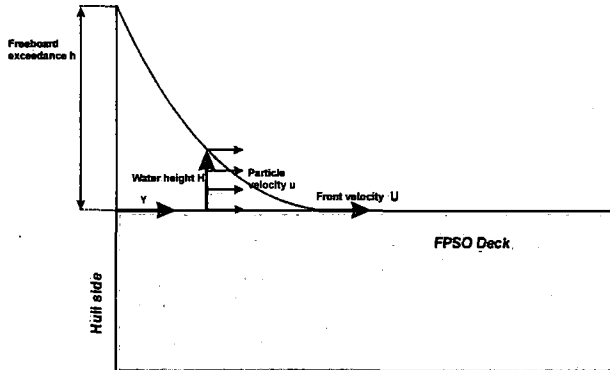


Figure 7-11

Application of dam breaking problem to green water flow from the side onto the deck

Finally it should be noted that Expression (7.4) is based on the assumption that the amount of water on the water side is infinite and without initial velocity. In the green water case the fluid flow in the (relative) waves is fully dynamic and only occurs for a short duration of time.

Taking into account these assumptions, it is clear that the theoretical dam breaking problem still provides a good simplified model of the flow of the green water onto the deck. It allows us to understand the typical flow behaviour and to estimate load levels. This is confirmed by the comparison of the velocities of the green water flow from the side in Figure 7-8 ($U=16.8$ m/s for an approximate freeboard exceedance of $h=3.4$ m), with the theoretical velocity of the water front U at the deck level. Based on the dam breaking problem this can be expressed as:

$$U = 2\sqrt{gh'} \quad (7.6)$$

This results (taking into account Expression (7.5)) in a theoretical front velocity U of 17.3 m/s, which is very close to the measured velocity.

With the dam breaking model as basis, it is now possible to study the typical flow behaviour on the deck as a result of green water from the side. Figure 7-12 can then be considered as the transverse flow onto the deck of an FPSO after the exceedance of the freeboard level by 3.4 m. The horizontal axis is the deck level and the vertical axis is the position of the original dam, as shown in Figure 7-11. The contours show the water profile on the deck at different time steps ($t=0.09, 0.11, 0.13$ s,...).

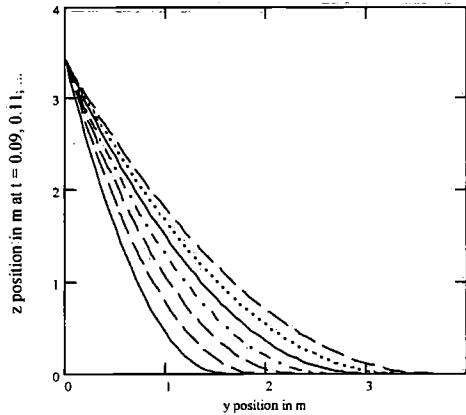


Figure 7-12

Water contours at time steps $t=0.09$ s, 0.11 s, 0.13 s, ... for a freeboard exceedance of 3.4 m

The velocity of the water particles (u) in the flow (different from the front velocity U) can be expressed as (Stoker, 1957):

$$u = \frac{2}{3} \left(\frac{y}{t} + \sqrt{g \cdot h'} \right) \quad (7.7)$$

It is important to note that dam breaking flow (and green water flow) can be seen as a shallow water wave. This implies that the velocity distribution over the height of the flow at one point is considered to be constant, as indicated in Figure 7-11. Consequently, Expression (7.7) gives the horizontal velocity of the flow at time t and position y over the complete height of the flow H .

For the estimation of the maximum green water load on slender structures in the next section, it is convenient to determine the velocity as function of the water height on the deck H and independent of time. To achieve this, it should be noted that Expression (7.4) can be modified to:

$$\frac{y}{t} = -3\sqrt{g \cdot H} + 2\sqrt{g \cdot h'} \quad (7.8)$$

Which results in a horizontal particle velocity as function of water height on the deck:

$$u(H) = 2 \left(\sqrt{g \cdot h'} - \sqrt{g \cdot H} \right) \quad (7.9)$$

It will be clear from this expression that the flow velocity with a certain water height H on the deck is significantly lower than the initial (water front) velocity, see Figure 7-13.

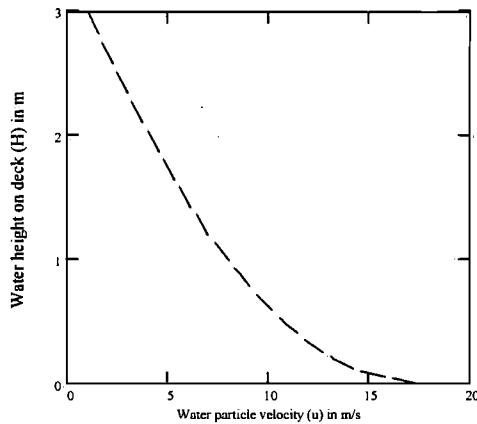


Figure 7-13
Water particle velocity as function of water height on the deck
(freeboard exceedance 3.4 m)

This has an effect on the loading on structures on the deck, which will be discussed in the next section.

7.7.3 Green water loading from the side on slender structures on the deck

Along the side of an FPSO a lot of slender structures are present, such as pipe and support structures. Therefore, in this section an analytical expression for the estimation of the green water loads on a vertical slender structure will be presented.

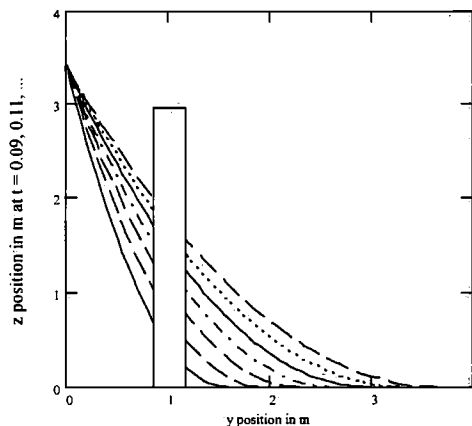


Figure 7-14
Example of a vertical pipe 1 m from the side

Figure 7-14 shows an example of such a structure: a vertical pipe at 1.0 m from the side of the ship.

If one assumes that the loading of green water on slender structures is dominated by the drag load, the load f on a slender structure can be expressed per metre length as:

$$f = \frac{1}{2} C_d \rho D u^2 \quad (7.10)$$

Typical C_d values for different structural shapes can be found in standard textbooks ($C_d=1.1$ for a circular pipe).

Using this equation and the considerations on the dam breaking flow above, the total sideways load F on a vertical pipe close to the deck edge can be estimated. First we consider that the (drag) load on the pipe due to the green water is constant over the total height of the green water layer with height H . This is due to the fact that the water particle velocity is constant over this height. The total load on the pipe therefore can be written as:

$$F = \frac{1}{2} C_d \rho D u^2 H \quad (7.11)$$

Including now the velocities from Expression (7.9), the total load on the pipe as function of the water height at the position of the pipe can be expressed as:

$$F(H) = 2C_d \rho g D (h' - 2\sqrt{h'H} + H)H \quad (7.12)$$

Taking half the local water height H as the moment arm with respect to the deck level (valid based on the shallow water assumptions) the moment on the pipe becomes:

$$M(H) = C_d \rho g D (h' - 2\sqrt{h'H} + H)H^2 \quad (7.13)$$

In Figures 7-15 and 7-16 these expressions are now plotted as function of the water height on the deck. From these figures it becomes clear that both the water height H and the water velocity play a role in the loading on the pipe. With a thin layer of water on the deck the water velocity is high (see Expression 7.9), but it is only integrated over a very small height H . With higher water heights, the water velocity is reduced such that the total load is decreasing again. In the presented case ($h'=3.4$ m, $D=0.3$ m, $y=1.0$ m, $C_d=1.1$) the maximum loading occurs at the moment that the water height H is 1.91 m, whereas the moment is the highest when the water height is 3.4 m. Stress analysis in the pipe will have to show which combination of load and moment is the most critical for the pipe.

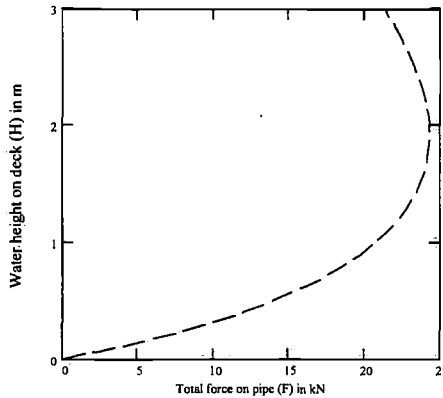


Figure 7-15

Load on a vertical pipe ($D=0.3$ m) as function of water height H due to transverse flow

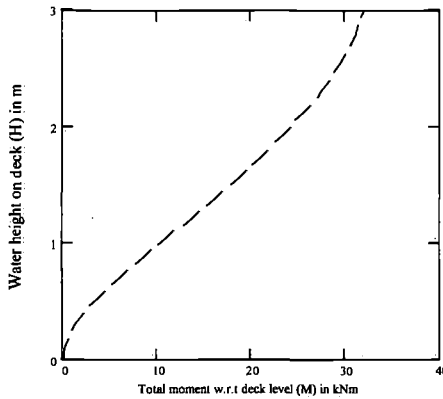


Figure 7-16

Moment on a vertical pipe ($D=0.3$ m) as function of water height H due to transverse flow

By differentiation of Expressions (7.12) and (7.13) with respect to the water height on the deck H and determining the maxima, the water height on the deck H at which the highest total load and moment occur can be found:

$$H_{F \max} = \frac{1}{4} h' \quad (7.14)$$

$$H_{M \max} = \frac{4}{9} h' \quad (7.15)$$

This, combined with Expression (7.5), finally allows us to define the estimated maximum load and moment on the pipe as function of freeboard exceedance h only:

$$F_{\max} = \frac{81}{128} C_d \rho g D h^2 \quad (7.16)$$

$$M_{\max} = \frac{1}{4} C_d \rho g D h^3 \quad (7.17)$$

In these expressions the effect of the longitudinal flow velocity as a result of the orbital motions in the wave crest, is still neglected. This longitudinal flow was observed during model tests and results in an additional load component.

If this additional longitudinal flow velocity (v) is also taken into account, the resulting total velocity is not perpendicular to the length of the ship anymore, but under an angle. The total resulting velocity V can simply be found by:

$$V = \sqrt{u^2 + v^2} \quad (7.18)$$

Taking into account that the load process (Expression 7.10) in the direction of the flow is quadratic with the resulting speed V , it is found that the load contributions of the transverse flow velocity (u) and longitudinal flow velocity (v) can be determined separately and added afterwards (assuming a constant C_d in all directions). The effect of the transverse flow component u was determined in Expressions (7.16) and (7.17). Now the additional terms as a result of the longitudinal flow component v are derived.

First the particle velocity in the wave is estimated. Because no water can flow through the hull of the vessel, the particle velocity in the waves along the hull will be along the length of the ship, even with wave headings slightly off the bow. The amplitude of the relative wave is equal to the freeboard (fb) plus the exceedance of the freeboard (h). Neglecting the effect of the ship motions on the relative wave motions, based on linear theory, the horizontal velocity in the wave crest can now be estimated as function of the wave period T :

$$v = \frac{2\pi \cdot (h + fb)}{T} \quad (7.19)$$

With Expression (7.10) and taking the moment arm $0.5H$ again, the load components due to the longitudinal velocity component can now be determined (for $h > 0$):

$$F' = 2 C_d \rho D \frac{\pi^2}{T^2} (h + fb)^2 H \quad (7.20)$$

$$M' = C_d \rho D \frac{\pi^2}{T^2} (h + fb)^2 H^2 \quad (7.21)$$

To determine the additional effect of the longitudinal flow component on the maximum force and moment on the slender vertical structure, Expressions (7.6), (7.14) and (7.15) are now included in the expressions above:

$$F_{\max}' = \frac{9}{8} C_d \rho D \frac{\pi^2}{T^2} (h + fb)^2 h \quad (7.22)$$

$$M_{\max}' = C_d \rho D \frac{\pi^2}{T^2} (h + fb)^2 h^2 \quad (7.23)$$

These expressions for the longitudinal flow component contribution should be added to Expressions (7.16) and (7.17) for the transverse flow component contribution to find the total loads on the slender vertical structures.

The example of the load process as discussed in this chapter, can also be used for other types of vertical slender structures, using their specific C_d values.

7.8 Green water in stern area

To investigate the green water sometimes observed at the stern of FPSOs, two types of sterns were investigated:

- A traditional tanker stern with a relatively low freeboard
- A new design full and flat stern with a high freeboard

Photo 7-1 shows a green water event with a traditional tanker stern.

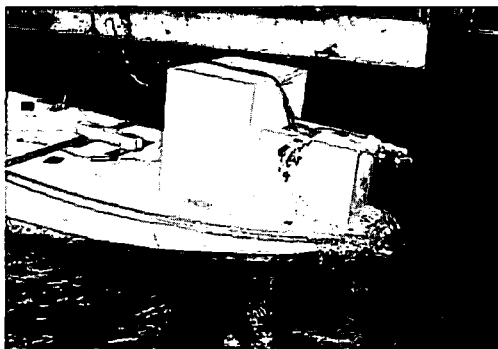


Photo 7-1

A green water event with a traditional tanker stern without poop deck

More details are given in Chapter 3 and Appendix C. In Figure 7-17 the probability of exceedance is shown for the traditional tanker stern in waves with a T_p of 12, 14 and 16 s. From this figure it is concluded that the modified Rayleigh distribution developed for the relative wave motions at the bow in Chapter 4 can also be used for the relative wave motions at stern. In the section below the results are discussed for the two stern types.

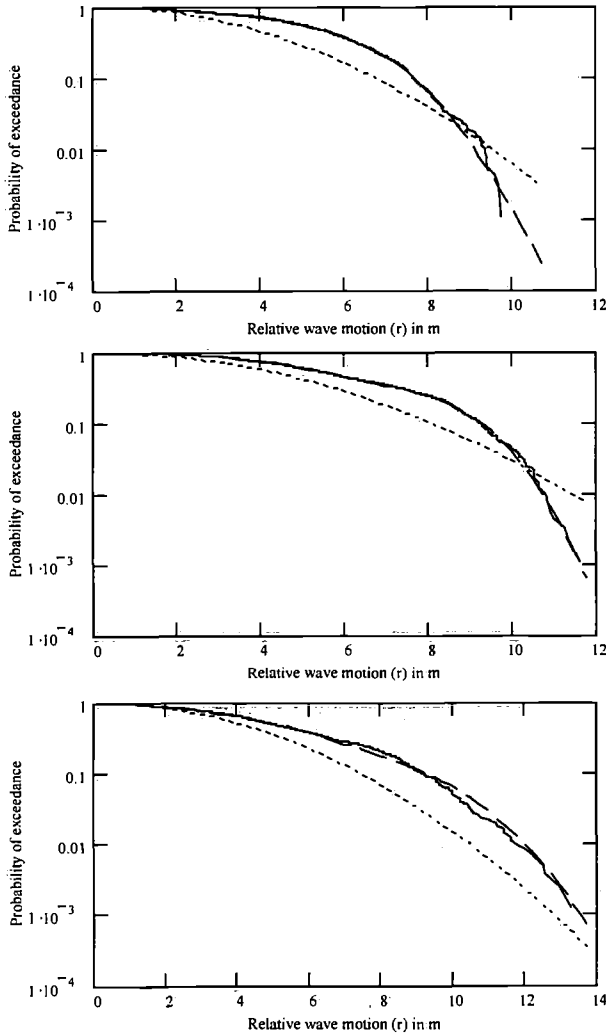


Figure 7-17
Probability of exceedance for the traditional tanker stern in waves with a T_p of 12, 14 and 16 s

7.8.1 Traditional tanker sterns with a relatively low freeboard

For the traditional tanker stern the non-linear probability of exceedance includes the discontinuity at the freeboard level, so that the probability of exceedance should be split up in a part below and above the freeboard level:

For extremes below the freeboard level:

$$P(r > R) = \exp \left[\left(-\frac{R^2}{2s^2} \right) \cdot (a + b \cdot R + c \cdot R^2) \right] \quad (7.24)$$

For extremes above the freeboard level:

$$P(r > R) = \exp \left[\left(-\frac{fb^2}{2s^2} \right) \cdot (a + b \cdot fb + c \cdot fb^2) + (R - fb) \cdot d + (R - fb)^2 \cdot e + (R - fb)^3 \cdot f \right] \quad (7.25)$$

The parameters a to f are shown in Table 7-6.

*Table 7-6
Parameters a to e for the traditional tanker stern*

Spectral peak period T_p	A	b	c
12 s	0.81570	-0.19153	0.02438
14 s	0.21302	0.11539	-0.00791
16 s	1.07953	-0.1500	0.01286
Spectral peak period T_p	D	e	f
12 s	-0.70897	-0.38024	0.02418
14 s	-0.27431	-0.03175	-0.03971
16 s	-0.34047	-0.01615	-0.00947

7.8.2 New design full and flat sterns with a high freeboard

For new design full and flat sterns with a high freeboard, which are designed to prevent water from coming onto the deck, the non-linear probability of exceedance does not include a discontinuity at the freeboard level. It can be expressed as:

$$P(r > R) = \exp \left[\left(-\frac{R^2}{2s^2} \right) \cdot (a + b \cdot R + c \cdot R^2) \right] \quad (7.26)$$

The parameters a, b and c are shown Table 7-7:

*Table 7-7
Parameters a to c for the new design full and flat stern*

Spectral peak period T_p	A	b	c
12 s	0.42791	-0.01012	0.00902
14 s	0.66215	0.00351	0.00412
16 s	0.0593	0.16464	-0.00727

As was the case with the green water from the side, the most probable maximum relative wave motion cannot simply be determined based on the number of oscillations based on the mean period T_1 . Table 7-8 shows the proposed correction that should be applied in Expression (7.2) to take into account the higher harmonics in the response.

*Table 7-8
The non-linearity correction factor η for the number of extremes for the relative motions at the stern*

Peak period	Factor η
12 s	1.36
14 s	1.90
16 s	1.95

8. REVIEW AND APPLICATION OF THE METHOD

8.1 Introduction

In Chapter 3 the structure of the semi-empirical design evaluation method was proposed. After that, Chapters 4 through 7 presented the details of its building blocks. The complete method, presented in Figure 8-1 and incorporated in the GreenLab program, allows the fast and practical evaluation of the green water problem by designers and operators of ship-type offshore structures.

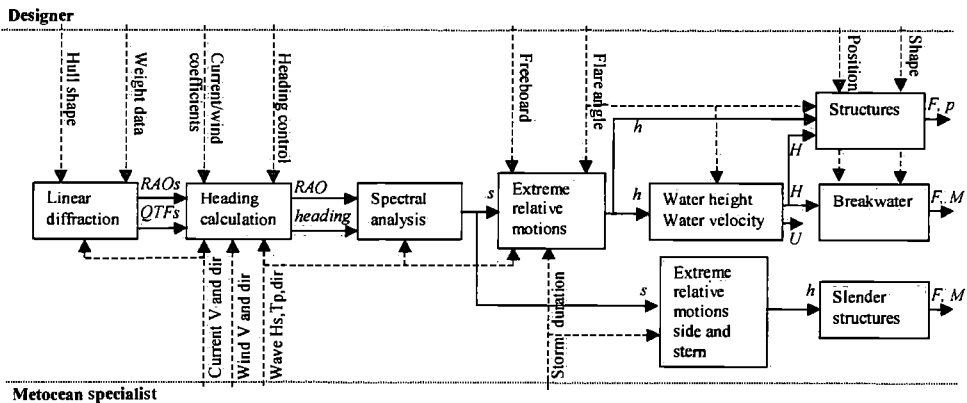


Figure 8-1

Outline of the semi-empirical design evaluation method

The method gives the designer the possibility to evaluate the relation between the available design parameters (dashed lines from the top) and the resulting green water effects. This allows the evaluation of the different options to solve the green water problem for a specific ship-type offshore structure:

- a. Design the vessel and structures on the deck against the predicted green water impact load levels.
- b. Optimise the bow shape (underwater shape and above water bow flare).
- c. Increase the freeboard height such that green water is prevented completely.
- d. Increase the freeboard height such that the green water loads are reduced to acceptable levels and design for these load levels.
- e. Optimise the structures on the deck to minimise the green water impact loads.
- f. Use protecting breakwaters in front of critical structures on the deck.

In Buchner, Voogt, Duggal and Heyl (2002) such evaluation is carried out for an FPSO in the Gulf of Mexico (GoM). In Table 8-1 an overview is given of the different design options, using the following expressions presented in this study :

- Freeboard exceedance (h): Expressions (4.11) and (4.16)
- Water height on deck 10 m in front of the structure (H): Expression (5.2)
- Pressure on structure on the deck (p): Expressions (6.4) and (6.12)
- Horizontal load on structure on the deck (FX): Expressions (6.5) and (6.13)
- Breakwater height: Table 6-15
- Horizontal load on breakwater (F^W): Expression (6.18)

The base case is a full elliptical bow with 30 degrees bow flare, a freeboard of 15.3 m and a squared structure 30 m from the fore perpendicular.

Table 8-1
Overview of design options for a GoM FPSO,
using the results of the semi-empirical design evaluation method

Design option	Freeboard exceedance (h)	Water height (H)	Pressure (p)	Load (FX or F ^W)
Design for load: fb=15.3m	5 m	2.78 m	79 kPa	2375 kN
Change flare angle: Bow flare 10 degrees, fb=15.3m	6.4 m	3.76 m	134 kPa	4506 kN
Change flare angle: Bow flare 50 degrees, fb=15.3m	4.9 m	1.71 m	60 kPa	1921 kN
Prevent fb exceedance: fb=22m	0 m	0 m	0 kPa	0 kN
Reduce fb exceedance: fb=18.7m	2.5m	1.39 m	19.8 kPa	594 kN
Optimise structure: triangular 45 degrees	5 m	2.78 m	16 kPa	744 kN
Optimise structure: tilted 30 degrees	5 m	2.78 m	45 kPa	1433 kN
Breakwater: Traditional, height 3.36 m	5 m	2.78 m	-	2998 kN (on bw)
Breakwater: vane, height 3.06 m	5 m	2.78 m	-	1123 kN (on bw)

Based on an evaluation as shown in Table 8-1, a designer can determine the most efficient design, also taking into account the cost levels of the different options. The table gives interesting insight in the effect of the bow flare angle for these specific design and conditions. The bow flare is reducing the amount of the green water coming onto the deck and the impact loading on structures on the deck. Because extreme bow flare angles will result in other problems such as bow flare slamming, the 30 degrees angle seems a good optimum.

In Morris, Millar and Buchner (2000) the methodology was used to evaluate the susceptibility levels of all North Sea FPSO/FSUs for the green water problem. They were rated as low (freeboard exceedance 0-3 m), medium (freeboard exceedance 3-6 m) or high (freeboard exceedance > 6 m). These results were compared with the 24 recorded damages on board these installations from 1995 to 2000. It was concluded that the analysis correctly predicted green water on the deck for all 24 of the recorded damage areas. 18 of the 24 damages (75%) show agreement with the predicted maximum susceptibility levels (high, medium or low). The remainder was underpredicted by one susceptibility category. This effectively gave confidence in the method to predict levels of potential freeboard exceedance and the areas susceptible to green water damage.

In this chapter a review will be given of the proposed method and the possibilities for its application. First the range of its applicability will be discussed. Second the coupling with specific metocean data will be considered. Finally the structural response to green water loading will be discussed briefly.

8.2 Range of applicability of the method

Because of the semi-empirical nature of the developed method (based on an extensive series of systematic model tests) and validation steps carried out already, there is no direct need for additional validation of the method. However, this semi-empirical nature requires a clear definition of the range of its applicability. Therefore, it is important to define within which (parameter) ranges the semi-empirical relations were determined. Based on that it is possible to evaluate where extrapolations are allowed and where they should only be applied with care.

Below an overview is given of important aspects:

- a. The parameters for the proposed modified Rayleigh distribution were determined for the full elliptical and thin triangular bows based on a systematic test series for spectral peak periods 12 s, 14 s, 16 s and bow flare angles of (0), 10, 30 and 50 degrees. In all these cases the new expressions were able to describe the measured phenomena. In this way they can be used to validate

future numerical simulation results in a wide range of extreme conditions. The application of these fitted parameters for the prediction of the extreme relative wave motions for other conditions was checked for:

- the increase of the freeboard height
- a different main hull shape
- a different wave heading
- the application of current speed

In all these cases a good agreement between prediction and measurement was found. However, due to the non-linearities involved, the results of predictions with the method should always be evaluated with care. In the points below the range of validity will be discussed.

- b. The systematic model tests were performed with ship-type (monohull) structures. This implies that the vessel should be a monohull and reasonably slender. Otherwise the motions and relative wave motions will be dominated by other phenomena than observed in the present model tests. For less slender structures the ratio between wave reflection effects and wave radiation effects for instance can be completely different from the one for the vessels considered.

The length (L) over beam (B) ratio for most tests was $L/B=5.5$. It is recommended to keep a lower limit of $L/B=4$ for the application of the present method. Of course the main (relative wave) motion behaviour should be determined carefully with linear diffraction analysis for each L/B ratio applied.

- c. With respect to the absolute size of the vessel, it is important to take into account two aspects:
- the ratio between the wave length (λ) and ship length (L)
 - the ratio between standard deviation of the relative wave motions (s) and the freeboard height (fb)

The λ/L ratio used in the tests ranged from 0.75 to 1.25 for the regular waves and from 0.85 to 1.5 for the irregular waves (based on peak periods). Especially in the shorter wave length range this is an important factor and it is recommended to use the method in this range with care.

The fb/s ratio tested was between 1.3 and 1.9 approximately. For larger values of this ratio the method can be used (relatively high freeboard levels) as long as extreme relative wave motions stay below 25 m (the range for which Expressions (4.11) and (4.12) have been checked).

For smaller values this should be done with care, because extremely large freeboard exceedances can occur relative to the freeboard height, which can introduce additional non-linearities. The chosen method does not guarantee that the expression for the probability of exceedance is per definition monotonically decreasing with the relative wave motion outside the range for which it was determined.

- d. The model tests were carried out with full (elliptical waterline) and thin (triangular waterline) bows. It is possible to use the method for cylindrical bows, but it is not recommended to use it directly for squared type bows (such as on some barges) because the extreme wave reflection can result in additional non-linearities.
- e. Bow flare angles between 0 and 50 degrees were applied, which cover the realistic range of bow flare angles.
- f. The method was developed and validated for zero speed and moderate current speeds. For the higher current speed of 2.0 m/s the predicted extreme relative wave motions start to deviate already from the measurements, so it is recommended to use this as a real upper limit.
- g. The model tests were carried out in regular waves of different heights and periods and irregular waves with a significant wave height H_s of 13.5 m. Spectral peak periods of $T_p=12$ s, 14 s and 16 s were used with a JONSWAP spectral shape ($\gamma=3.3$). Several considerations play a role with respect to these aspects:
 - For significant wave heights lower than 13.5 m, the results of the method will be applicable, because of the chosen methodology with its modified Rayleigh distribution.
 - For significant wave heights significantly larger than this 13.5 m, it is possible that the non-linear effects in the waves (crest heights, breaking waves) increase significantly, which can affect the results. Also the fb/s ratio (see point c) should be taken into account here.
 - The present tests were carried out in a water depth of 150 m, which can be considered as deep water. In shallow water the non-linear effects in the waves can be more pronounced.
- h. The present results are focussed on Most Probable Maximum (MPM) relative wave motion extremes in 3 hour storm durations (probability of exceedance $P\sim 1/1000$). The following should be noted:
 - Extrapolation to lower probabilities of exceedance (say in 6-12 hour storms) should only be done with care. The chosen method does not guarantee that the expression for the probability of exceedance is per definition monotonically

decreasing with the relative wave motion, outside the range for which it was determined.

- At present no information is available about the distribution of the extremes in a storm of N hours. Most Probable Maximum values are used now, but future research should provide more insight in this distribution (also taking into account the bandwidth of the wave spectrum).
- i. For green water from the side only wave headings 15 and 30 degrees from head waves were considered. Considering the rapid increase of the problem from 15 to 30 degrees observed, it is recommended not to use the results for larger heading angles. Further research should be carried out to investigate these more extreme heading angles.

The developed semi-empirical design evaluation method is a valid tool for the evaluation of the green water problem for ship-type offshore structures in the specific metocean conditions. However, the non-linear and highly complex character of the green water problem makes it sensitive to small changes in the input. Furthermore, the configurations of superstructures and equipment on the deck of these structures will be different and more complex than the configurations tested. This can, for instance, result in complex focussing or shielding of the green water flow. If an evaluation using the semi-empirical evaluation method shows that the green water problem is critical for (parts) of the structure, dedicated model tests are recommended.

8.3 Coupling with specific metocean data

8.3.1 Use of the contour of joint probabilities of wave height and period

Having the semi-empirical design evaluation method for green water loading available, it is very important that it is used for the specific environmental (metocean) data of a field location in a correct way.

In the past a lot of studies for specific fields focussed mainly on the wave period for which the highest significant wave height occurred, see Figure 8-2. This wave was generally referred to as the '100-year wave' and has typically a peak period above 15 seconds.

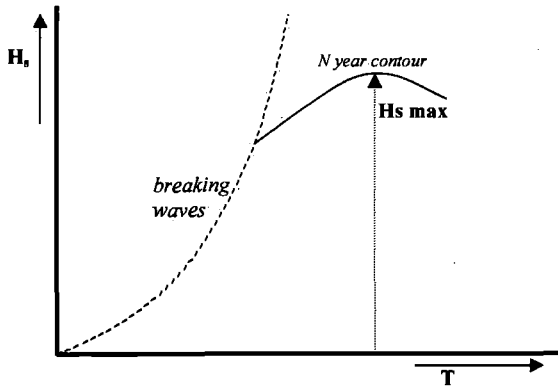


Figure 8-2

Typical contour of the N year joint probability of significant wave heights and wave periods in a harsh environment

However, when this type of floating offshore structures were investigated in more detail, it was found that this type of wave conditions do not generally result in the most critical green water events at the bow. In waves with a lower significant wave height, but shorter wave period typically more critical green water events can occur, see for instance Morris, Millar and Buchner (2000).

To understand this, it is important to consider the typical character of the relative wave motions Response Amplitude Operator (RAO) as presented in Figure 8-3, which peaks at the period where the ship length is equal to the wave length.

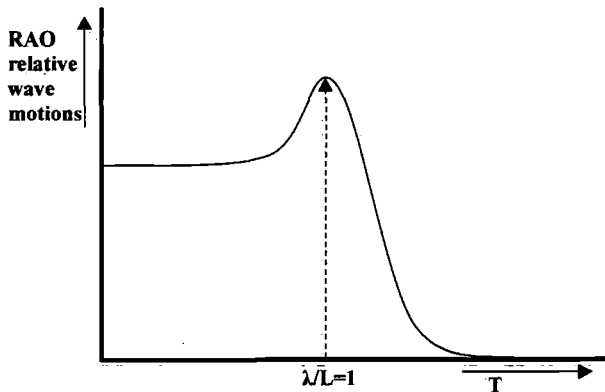


Figure 8-3

Typical character of the relative wave motions Response Amplitude Operator (RAO)

For typical lengths of ship-type offshore structures (200-300 m), this peak is around 12 seconds.

Combining the information in Figure 8-3 with the typical contour of joint probabilities of significant wave height and period in Figure 8-2, makes clear that the green water problem at the bow should be evaluated in detail along this contour. A focus on the highest significant wave height will result in an underestimation of the green water problem, with the resulting problems during the operation of the vessel.

8.3.2 Determination of the extreme heading angle with respect to the waves

As already mentioned in Section 7.1, the heading of the vessel with respect to the waves is of vital importance for the green water from the side. Application of the results from Chapter 7 makes clear that the relative wave motions along the side increase significantly with the heading angle, even for the small increase of the wave heading from 15 to 30 degrees off the bow.

It is important therefore not only to consider the joint probability contour of significant wave heights and wave periods as proposed in the previous section. In addition it is important to consider the joint probability of the waves, wind and current and their relative directions. These need to be used to determine the heading angles for which certain wave height-wave period combinations can be expected.

Therefore, Figure 8-1 shows one additional block in the method: the calculation of the heading of the vessel with respect to the wave direction due to the combined wind, wave drift and current forces on one hand and possible heading control measures on the other. In Buchner, Voogt, Duggal and Heyl (2002) such response based design method is presented for an FPSO in the Gulf of Mexico.

8.4 Dynamic structural response

The present thesis is focussed on the green water impact loading. However, for the evaluation of ship-type offshore structures, the structural response under this impact loading determines whether a structure is able to survive a certain event.

For the interpretation of the impact pressure and load results, it is important to note that:

- The impact pressures are based on measurements on a force panel with an area of 1.43 m². These pressures are representative for the impact loads encountered by plates at the lower level on structures on the deck.

- The vertical pressure profiles and global loads on the structures are also presented in Chapter 6. It should be noted that the vertical pressure profile presented does not occur at the same time over the complete height, but represents the maximum pressure occurring over a period of time.
- In Appendix II it is concluded that the structural elasticity is an important aspect in the structural response to green water loading, but that hydro-elastic aspects can be neglected.

This last point implies that in the structural evaluation of green water loading there are two areas of interest with respect to the typical rise time of green water loading (0.10-0.35 seconds):

- The area where the natural period (T_n) of the structural response, including added mass, is much shorter than the typical rise time of green water loading (T_r). In this case the green water peak load can be considered statically.
- The area where the natural period (T_n) of the structural response, including added mass, is approximately equal or longer than the typical rise time of green water loading (T_r). In this case the green water peak load should be considered including the dynamic response of the structure.

In Figure 8-4 the initial stage of a typical green water impact time trace is described with a simplified triangular shape time trace.

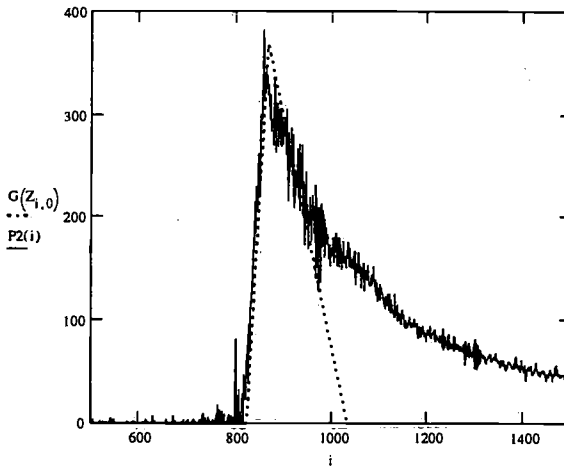


Figure 8-4

The initial stage of a typical green water impact time trace as approximated by a simplified triangular shape time trace

The dynamic response can now be determined for structures with natural periods T_n which are small, equal or larger than the rise time T_r .

As discussed in Appendix II, the dynamic response of the applied linear elastic force panels to green water loading can be described by the behaviour of a single degree of freedom mass spring system:

$$(m + a) \ddot{x} + b \dot{x} + c x = F(t, x) \quad (8.1)$$

In the case of static loading the velocity and acceleration forces are negligible and the green water force is independent on time and place. If dynamic response is observed without hydro-elastic effects, the structural response can be described with the equation of motion above when a constant damping and (added) mass are assumed. The quasi-static green water impact loading is only dependent on the time and independent of position.

In Figure 8-5 examples are shown for the ratios $T_n/T_r = 0.5, 1.0, 1.4$ and 2.0 . A damping of 8% of the critical damping is applied, with the critical damping defined as:

$$B_c = 2 \sqrt{(M + A)} \cdot C \quad (8.2)$$

This value is valid for the set-up of the model tests. For real steel structures the damping value will typically be lower.

It will be clear from this figure that the structural response is very much dependent on the ratio T_n/T_r . When this ratio is close to (or larger than) 1.0, dynamic amplification should be accounted for. In this case the green water impact load should be applied dynamically to the structure with a range of typical rise times (0.10-0.35 full scale).

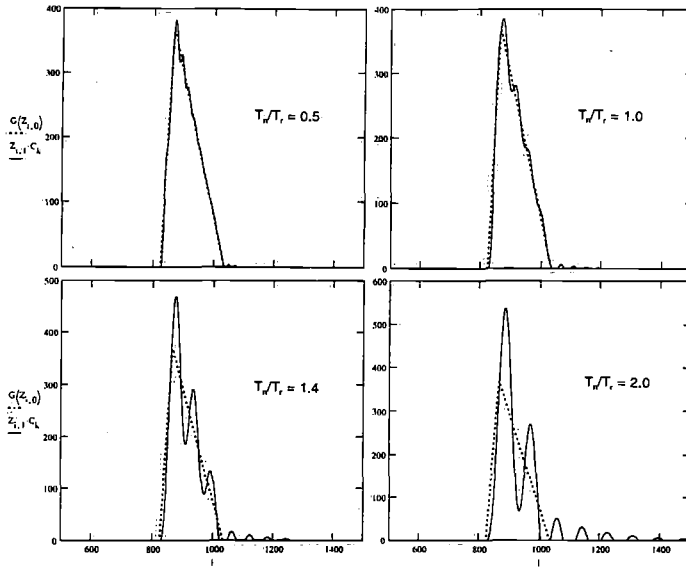


Figure 8-5

Examples of dynamic response to green water loading for different ratios between natural period (T_n) and rise time (T_r), $T_n/T_r = 0.5, 1.0, 1.4$ and 2.0 . The dotted line shows the load, the solid line the dynamic response (displacement multiplied by stiffness)

9. NUMERICAL PREDICTION OF GREEN WATER

9.1 Introduction

The model test results presented in this thesis have given insight in the complex and non-linear nature of green water loading. This complex nature cannot be predicted with existing linear (and slightly non-linear) prediction methods. Therefore, in previous chapters a semi-empirical design evaluation method for green water loading on ship-type offshore structures has been presented based on a systematic series of model tests.

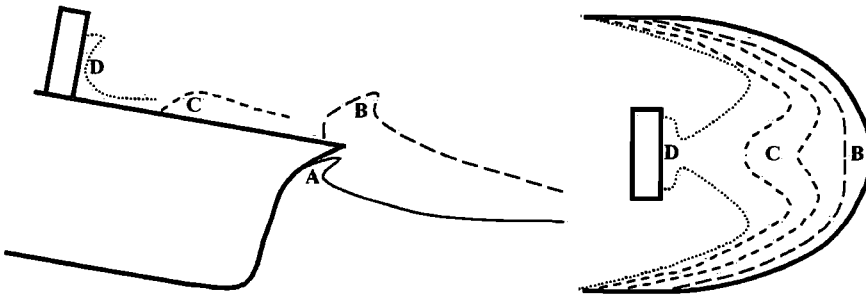


Figure 9-1

The main phases of the green water problem schematically in side view (left) and top view (right): from the non-linear relative wave motions in front of the bow, via the complex flow onto and on the deck to the impact on deck structures

In recent years the development of numerical simulation methods for complex free surface flows has made significant progress. In this chapter some of these methods will be evaluated based on their ability to predict the green water physics. The following steps will be followed:

- The requirements for numerical prediction methods for the prediction of (parts of) the green water loading will be determined, based on the different phases in the green water physics (see Figure 9-1).
- Two existing numerical methods will be discussed and evaluated briefly.
- A summary of the mathematical and numerical model of a modified-VOF method will be presented.
- The results of two case studies with the modified-VOF method will be discussed.
- Finally some conclusions will be drawn with respect to the future use of these numerical methods in the prediction of green water loading.

9.2 Requirements for numerical methods

To determine the requirements for numerical prediction methods for the prediction of green water loading, it is important to understand the main physics of the problem. Figure 9-1 summarises the main phases schematically:

- A. Non-linear swell-up around the bow
- B. 'Dam breaking'-type flow onto the deck
- C. 'Hydraulic jump'-type shallow water flow on the moving deck, focussing into a high velocity water 'jet' when the water fronts from the sides meet
- D. Water impact and water run-up in front of the structure, eventually turning over

To be able to describe these phenomena, the numerical method should be able to deal with complex non-linear flows. If the focus of the investigation is limited to the local flow around the bow, specifically it should be able to handle:

1. Water entry of a flared bow structure
2. Complex flow onto the deck, including the discontinuity at the deck edge
3. 'Hydraulic jump'-type shallow water flow on a moving ship deck
4. Meeting water flows on the deck
5. Short duration water impact on a structure
6. Overturning flow after run-up of the water in front of the structure

Based on these requirements three numerical methods have been evaluated on their ability to predict the green water phenomena.

It is not meant to present and evaluate the numerical details of the methods, but to discuss their general approach. For details reference is made to relevant publications.

9.3 Evaluation of existing numerical methods

9.3.1 General

The field of numerical prediction methods for the prediction of free surface flow is extremely wide. Therefore, the present evaluation does not claim to be complete. It focuses on a number of methods that are applied in ship hydrodynamics or closely related fields.

In analogy with what has been presented by Hirt and Nichols (1981), it is possible to divide the investigated methods by the way they describe the free surface. This is possible using:

- Height functions
- Line segments
- Fluid regions

9.3.2 Method using height functions: Glimm's method

Glimm's method (1965) can be used to solve the shallow water wave equations of water on a moving deck. The deck area is divided into a two-dimensional grid and in time domain the water flow between the grid points can now be calculated. Dillingham (1981) used Glimm's method to study the flow of the water on deck of small fishing vessels numerically. Later he was followed by others, such as Pantazopoulos (1988) and Huang and Hsiung (1996). Mizoguchi (1988, 1989) successfully applied the method to the green water problem on the bow deck. Using the relative wave motion input from model tests to determine the amount of water on the deck, he calculated the motion of the water as soon as it was on a fixed deck. Zhou, De Kat and Buchner (1999) used the method to study green water on a moving deck. The method is also used by Stansberg, Hellan, Hoff and Moe (2002) in their green water prediction method for FPSOs.

Summary of the method

In this method the flow on the deck is formulated as a non-linear hyperbolic system of equations using the shallow water theory. This assumes that the water height on the deck (λ) is small compared to the radius of curvature of the water surface. As a consequence of the shallow water assumptions, the water velocity (u, v) is constant over the height of the water on the deck.

By satisfying the conditions of conservation of mass and momentum and the boundary conditions on the free surface and the bottom, the governing equations for water on a moving deck can be written as:

$$\frac{\partial u}{\partial t} + u \frac{\partial u}{\partial x} + v \frac{\partial u}{\partial y} = -a_{(z)} \frac{\partial \lambda}{\partial x} + f_1(x) \quad (9.1)$$

$$\frac{\partial v}{\partial t} + u \frac{\partial v}{\partial x} + v \frac{\partial v}{\partial y} = -a_{(z)} \frac{\partial \lambda}{\partial y} + f_2(y) \quad (9.2)$$

$$\frac{\partial \lambda}{\partial t} + u \frac{\partial \lambda}{\partial x} + v \frac{\partial \lambda}{\partial y} + \lambda \frac{\partial u}{\partial x} + \lambda \frac{\partial v}{\partial y} = 0 \quad (9.3)$$

$f_1(x)$ and $f_2(y)$ represent the various body force contributions acting on the fluid in local x and y direction in the ship fixed co-ordinate system. $a_{(z)}$ represents the total acceleration acting on the fluid in vertical direction in the moving co-ordinate system.

The water height on the deck $\lambda(x,y)$ is a typical example of a height function. It is defined as function of the x - and y -positions on the moving vessel deck, as shown in Figure 9-2.

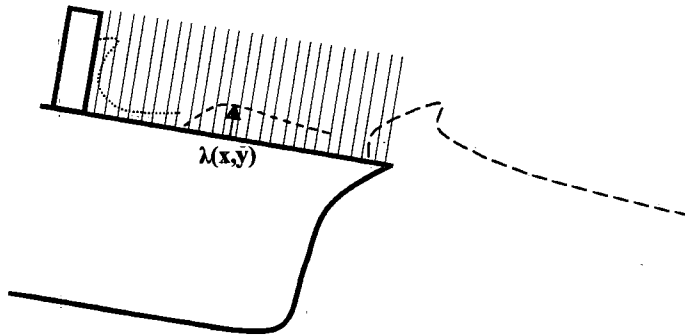


Figure 9-2
Definition of the (water) height function $\lambda(x,y)$ in the cells,
applied to the green water problem phases

The main difficulty of finding the solution for Expressions (9.1) - (9.3) is dealing with the hydraulic jumps that almost inevitably appear. Dillingham (1981) was the first to solve this by applying Glimm's method (Glimm, 1965). This method consists of two steps:

- First the analytical solutions of a local Riemann problem (the dam breaking problem) in each time interval are obtained by solving the initial value problem using the solution of the previous time step.
- Then the solution in the whole spatial domain is constructed as piecewise-constant solutions, by using a random sampling procedure to sample a series of obtained explicit solutions of the local Riemann problem.

By using Glimm's method, the solution of the water elevation λ and the velocities u and v with respect to the x - and y -direction at each grid point are obtained at each time step. The resulting estimates of elevation and velocity, which are random over short time spans, converge to the exact solution of Equations (9.1) - (9.3), as the number of time steps becomes large. More details can be found in Pantazopoulos (1988) and Zhou, De Kat and Buchner (1999).

Figure 9-3 shows a result of the method compared to regular wave results from Test Series A. As boundary conditions the relative wave motions around the bow and the measured motions of the deck were used. The figure shows the water height on the deck at position H4.

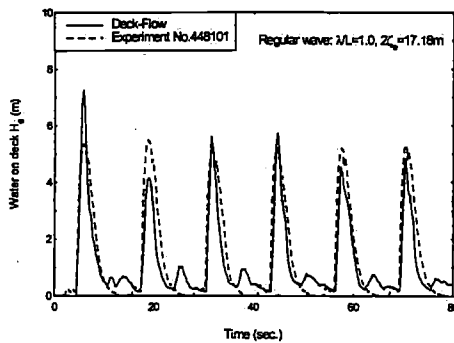


Figure 9-3

Calculated and measured water height on the deck at position H4 (from Test Series A), using the measured relative wave motions around the bow and the motions of the deck as boundary conditions

Evaluation of the method

Based on the requirements identified in Section 9.2, the application of Glimm's method will now be evaluated on its ability to predict the green water phenomena:

- Considering requirements 1 and 2, it will be clear directly that the application of Glimm's method cannot be used on its own, if one wants to consider the relative wave motions around the bow and the flow onto the bow as well. Its shallow water assumptions limit the applicability of the method to the flow on the deck itself. Therefore, the application of this method is generally limited to studies into the effect of green water on the ship motions. In that case the boundary conditions around the bow need to be defined with other methods, which are able to account for the strong non-linear swell-up around the bow and the sharp deck edge with its discontinuity in the flow.
- With respect to requirements 3 and 4, Glimm's method is attractive because it deals with relatively complex flows with multiple hydraulic jumps without any

special treatment of the discontinuities, as well as the case where the deck becomes partially dry. Mizoguchi (1988, 1989) therefore was able to predict the high-velocity water jet at the centreline of the deck with the method.

- If one considers requirements 1 and 2, it will be clear that the use of the water height function $\lambda(x,y)$ and the shallow water assumption of constant water velocity over the cell height, limits the possibility to predict green water impact loads on vertical structures (with its related strong change of water velocities over the height of the structure). The definition of the free surface with the height function also prevents the description of curved (overtopping) free surfaces, such as in phase B and D in Figure 9-1.

Taking into account the considerations above, it is concluded that the application of the fast Glimm's method has strong points, such as its ability to deal with multiple hydraulic jumps and its speed (it is limited to two dimensions only). The method can play an important role in the study of the effect of green water on the ship motions and on the global hull girder bending. However, for a detailed study of the green water problem other methods are necessary.

9.3.3 Method using line segments: non-linear boundary integral method

To investigate its ability to generate inflow conditions for the application of Glimm's method as described in the previous section, Buchner and Cozijn (1997) evaluated the 2D non-linear boundary integral method developed by Romate (1989) and Van Daalen (1993). A similar method was used by Greco, Faltinsen and Landrini (2000, 2001) and in 3D by Maskew, Wang and Troesch (1994, 1996).

Summary of the method

The method is based on the general assumptions of potential flow. The boundary conditions can be non-linear and time dependent. The boundary value problem is transformed into a boundary integral equation in terms of a source and a dipole distribution over the boundary $\partial\Omega$. A source represents a Neumann boundary condition, while a dipole represents a Dirichlet boundary condition. In Expression (9.4) a boundary integral equation for the potential on the boundary of the fluid domain Ω is presented.

$$\frac{1}{2}\Phi(\bar{x}) = \iint_{\partial\Omega} \left[\frac{\partial\Phi}{\partial n_{\xi}}(\bar{\xi}) \cdot G(\bar{\xi}, \bar{x}) - \Phi(\bar{\xi}) \cdot \frac{\partial G}{\partial n_{\xi}}(\bar{\xi}, \bar{x}) \right] \cdot dS_{\xi} \quad (9.4)$$

In the equation above, G and $\partial G/\partial n$ are the so-called influence functions. If on every point of the boundary either a source or a dipole strength is prescribed, the velocity potential Φ is known and unique.

The equation above is now solved numerically with a panel method. At time level t_n the boundary $\partial\Omega$ is divided into N smooth panels. Each of these panels has a length ΔL_j and a collocation point x_i in the centre of the panel. The boundary conditions are forced upon the collocation points. The boundary integral equation is now rewritten as follows.

$$\frac{1}{2}\Phi(\bar{x}_i) = \sum_{j=1}^N \int_{\Delta L_j} \left[G(\bar{\xi}, \bar{x}_i) \frac{\partial\Phi}{\partial n_{\xi}}(\bar{\xi}) - \Phi(\bar{\xi}) \frac{\partial G}{\partial n_{\xi}}(\bar{\xi}, \bar{x}_i) \right] dL_{\xi} \quad (9.5)$$

The original boundary integral is thus transformed into a summation of a series of integrals. Apart from collocation points, also grid points and intersection points are defined on the boundary. This is shown in Figure 9-4. Grid points define the edges of a panel and are used only as boundaries for integration of the singularity distributions for integration of the singularity distributions over a panel. They have no influence on the geometry of the panels. The point where two adjacent networks intersect is called an intersection point. An intersection point is a special case of a grid point, since an intersection point also defines the edge of the first or last panel in a network.

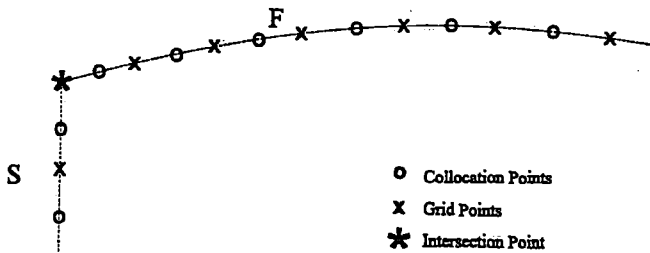


Figure 9-4

Collocation points, grid points and intersection points at the fluid domain boundary

When on time step t_n the boundary integral equation for the potential Φ is solved and the velocities $\nabla\Phi$ on the boundary have been determined, the boundary conditions on the free surface have to be updated for the next time step $t_{n+1} = t_n + \Delta t$.

The position of the collocation points and the value for the potential in the collocation points are integrated in time, see Figure 9-5. After that a new intersection point with the boundary has to be determined.

The results of simulations have shown that the method has significant problems with this situation, see Buchner and Cozijn (1997). Figure 9-6 shows a water surface moving upwards with high velocity combined with a sharp discontinuity of the boundary and a horizontal plane behind it. The intersection points with the boundary need to be determined with a one-sided differential scheme. This will be difficult in the second time step, resulting in an unrealistically large displacement of the intersection point over the deck. With the status of the method at that moment, a realistic flow on the deck could only be achieved with rounded corners at the deck edge.

Similar problems were encountered by Greco, Falinsen and Landrini (2000, 2001). To prevent them, they adopted a 'Kutta' type condition, enforcing the flow to leave the bow tangentially when the water reaches the freeboard level. Once the freeboard is exceeded, the fluid velocity relative to the ship determines whether the water will flow onto the deck or not. With this modification they were able to get a very good agreement with the 2D experiments of Cozijn (1995) and a good similarity with the 3D results of a moving bow from Buchner (1995). They also presented interesting 2D sensitivity studies and wave plunging simulations.

Evaluation of the method

As indicated, this method using the line segments was investigated as option to generate inflow conditions for Glimm's method. Based on the summary above, the following is concluded with respect to the requirements defined in Section 9.2:

- The basic method has difficulty with complex free surface flow close to discontinuities in the boundaries. Special measures are necessary to prevent unrealistic flow behaviour. However, with these measures applied, a very good agreement with 2D experiments was found. Further research will be needed to confirm whether the method is also able to simulate the water entry of a flared bow structure and the complex flow onto the deck in 3D (requirements 1 and 2).
- Because the method is based on a description of its boundary using line segments (panels), the method is unable to simulate meeting water flows. Therefore, it does not fulfil the requirements for meeting water flows on the deck (requirement 3), after wave breaking (requirement 1) or after overturning flow after run-up (requirement 6). Consequently, it needs to be combined with other types of methods.

9.3.4 Method using fluid regions: VOF

Based on the considerations presented in the previous two sections, it was concluded that a free surface description using a height function or line segments will have a limited applicability for the green water problem. Therefore, other methods describing time dependent free surface flows had to be considered. Generally this type of methods can be divided into finite-element methods (using a basis function over all elements), finite-difference methods (using finite-difference approximations) or finite-volume methods. The method investigated in the rest of this chapter is part of the last class of methods.

The Volume of Fluid (VOF) algorithm as developed by Hirt and Nichols (1981) is used as basis. The method solves the incompressible Navier-Stokes equations with a free-surface condition on the free boundary. In the VOF method a VOF function F (with values between 0 and 1) is used, indicating what part of the cells is filled with fluid. The VOF method reconstructs the free surface in each computational cell. This makes it suitable for the prediction of all phases of the local green water problem, as shown in Figure 9-7. A similar method was used by Orloff and Krafft (1997) in a numerical study into green water loading on FPSOs.

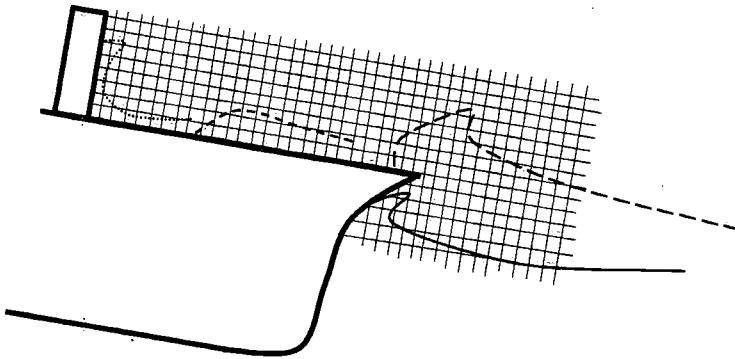


Figure 9-7

The cell grid in the VOF method related to the phases of the local green water problem

9.3.5 Evaluation of a modified-VOF method

In the following sections a modified-VOF method will be evaluated based on its applicability to the green water problem. The method is developed at the University of Groningen (RuG) as an improvement of the original VOF method. It was chosen because it is seen as particularly suitable for the study of free surface flows and has shown its capabilities even in micro-gravity environments, see Gerrits (1996, 2001).

First the mathematical and numerical model will be summarised. This will be limited to the main aspects, because the detailed numerical aspects are outside the scope of the present thesis. Excellent overviews of the numerical details of the method can be found in Gerrits (1996, 2001), Loots (1998) and Fekken (1998). To distinguish between the original VOF method of Hirt and Nichols (1981) and the present method with its extensive number of modifications, the name Modified-VOF method will be used in the rest of this chapter.

First the mathematical and numerical model will be summarised. After that, two case studies will be presented and discussed:

Case study 1: Flow onto a (fixed) deck with impact on different structural shapes

To verify requirements 3 to 6:

3. 'Hydraulic jump'-type shallow water flow on a moving ship deck
4. Meeting water flows on the deck
5. Short duration water impact on a structure
6. Overturning flow after run-up of the water in front of the structure

Case study 2: Water entry of a 2D wedge

To verify requirements 1 and 2:

1. Water entry of a flared bow structure
2. Complex flow onto the deck, including the discontinuity at the deck edge

Based on these case studies the present possibilities and limitations of the method will be identified and areas for further improvement will be defined.

9.4 Mathematical and numerical model of the modified-VOF method

9.4.1 Mathematical model

The incompressible Navier-Stokes equations describe the motions of a fluid in general terms. They are based on conservation of mass (Expression 9.6) and momentum (Expressions 9.7 - 9.9).

$$\frac{\partial u}{\partial x} + \frac{\partial v}{\partial y} + \frac{\partial w}{\partial z} = 0 \quad (9.6)$$

$$\frac{\partial u}{\partial t} + u \frac{\partial u}{\partial x} + v \frac{\partial u}{\partial y} + w \frac{\partial u}{\partial z} = -\frac{1}{\rho} \frac{\partial p}{\partial x} + \nu \left(\frac{\partial^2 u}{\partial x^2} + \frac{\partial^2 u}{\partial y^2} + \frac{\partial^2 u}{\partial z^2} \right) + F_x \quad (9.7)$$

$$\frac{\partial v}{\partial t} + u \frac{\partial v}{\partial x} + v \frac{\partial v}{\partial y} + w \frac{\partial v}{\partial z} = -\frac{1}{\rho} \frac{\partial p}{\partial y} + \nu \left(\frac{\partial^2 v}{\partial x^2} + \frac{\partial^2 v}{\partial y^2} + \frac{\partial^2 v}{\partial z^2} \right) + F_y \quad (9.8)$$

$$\frac{\partial w}{\partial t} + u \frac{\partial w}{\partial x} + v \frac{\partial w}{\partial y} + w \frac{\partial w}{\partial z} = -\frac{1}{\rho} \frac{\partial p}{\partial z} + \nu \left(\frac{\partial^2 w}{\partial x^2} + \frac{\partial^2 w}{\partial y^2} + \frac{\partial^2 w}{\partial z^2} \right) + F_z \quad (9.9)$$

$\bar{F} = (F_x, F_y, F_z)$ is an external body force, such as gravity.

The Navier-Stokes equations can also be written in a shorter notation as:

$$\nabla \cdot \bar{u} = 0 \quad (9.10)$$

$$\frac{\partial \bar{u}}{\partial t} + \nabla p = \bar{R} \quad (9.11)$$

\bar{R} now contains all convective, diffusive and body forces.

9.4.2 Numerical model: geometry and free surface description

Cartesian grid

For the discretisation of a computational domain in numerical simulations a large number of different methods is available. Basically, they can be divided into:

- structured and unstructured grids
- boundary fitted and non-boundary fitted grids

In the Modified-VOF method a structured (Cartesian) non-boundary fitted grid is chosen (not necessarily equidistant). This has the following advantages related to the use of the method for the prediction of the green water loading:

- easy generation of the grid around complex structures
- a lot of research on surface tracking on orthogonal grids is available
- moving objects in the fluid can be dealt with in a similar way as fixed boundaries, without re-gridding

The main disadvantage of this discretisation method is the fact that the boundary and free surface are generally not aligned with the gridlines. This requires special attention in the solution method, as will be shown below.

Apertures

An indicator function is used in the form of volume and edge apertures to track the amount of flow in a cell and through a cell face:

- Volume aperture: the geometry aperture F_b indicates which fraction of a cell is allowed to contain fluid ($0 \leq F_b \leq 1$). For bodies moving through the fluid, the geometry aperture may vary in time. The time-dependent fluid aperture F_s indicates which fraction of a cell is actually occupied by fluid and satisfies the relation $0 \leq F_s \leq F_b$.
- Edge aperture: the edge apertures A_x , A_y , and A_z define the fraction of a cell surface through which fluid may flow in the x, y and z direction respectively. Obviously, these apertures are between zero and one.

Figure 9-8 shows a two-dimensional example with $F_b=0.8$ and $F_s=0.3$.

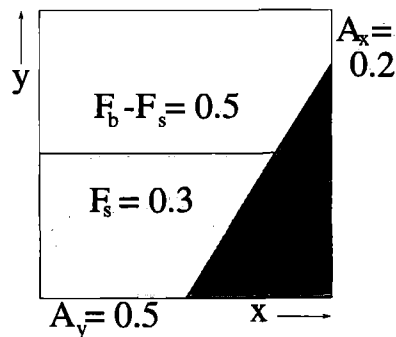


Figure 9-8

Two-dimensional example of a grid cell using apertures

Labelling

After the apertures have been assigned to the grid cells and the cell edges, every cell is given a label to distinguish between boundary, air and fluid. Two classes of labelling exist: Geometry cell labels and fluid cell labels. The geometry labelling at each time step divides the cells into three classes:

- F**(low)-cells : All cells with $F_b \geq 0$
B(oundary)-cells : All cells adjacent to a **F**-cell
(e)X(ternal)-cells : All remaining cells

The free-surface cell labelling is a subdivision of the **F**-cells. The subdivision consists of 3 subclasses:

- E**(mpty) cells : All cells with $F_s=0$
S(urface) cells : All cells adjacent to an **E**-cell
F'(luid)-cells : All remaining **F**-cells

Figure 9-9 shows an example of geometry cell labelling and free-surface cell labelling for a wedge entering a fluid.

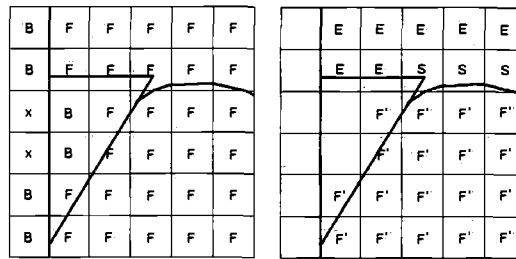


Figure 9-9
Geometry cell labelling (left) and free-surface cell labelling (right)
for a wedge entering a fluid

9.4.3 Discretisation of the Navier-Stokes equations

The discretisation is done on a staggered grid, which means that the pressure will be set in the cell centres and the velocity components in the middle of the cell faces between two cells. This is shown in 2D in Figure 9-10.

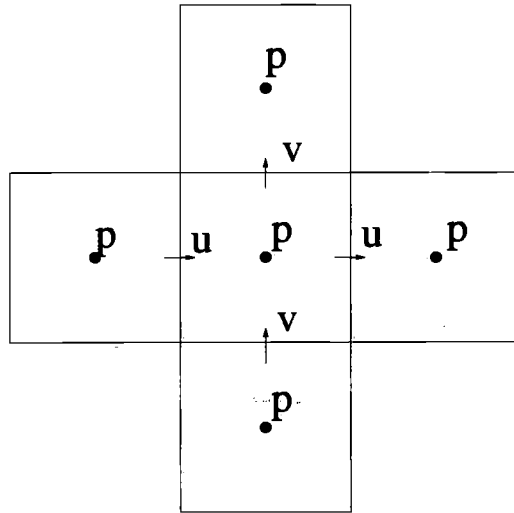


Figure 9-10
Location of the pressure and velocity components in the staggered grid

Discretisation in time

The Navier-Stokes equations are discretised in time according to the explicit first order Forward Euler method as follows:

$$\nabla \cdot \bar{u}^{n+1} = 0 \tag{9.12}$$

$$\frac{\bar{u}^{n+1} - \bar{u}^n}{\Delta t} + \nabla p^{n+1} = \bar{R}^n \tag{9.13}$$

Δt is the time step and $n+1$ and n denote the new and old time level. The conservation of mass in Expression (9.12) and the pressure in Expression (9.13) are treated on the new time level $n+1$ to assure that the new \bar{u} is divergence free (no loss of fluid).

Discretisation in space

The spatial discretisation will now be explained using the computational cell shown in Figure 9-11.

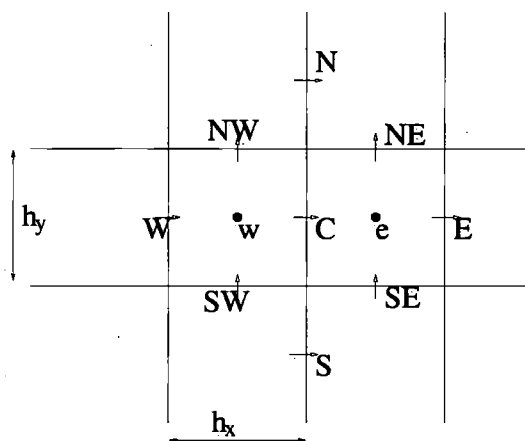


Figure 9-11

Spatial discretisation cell, using compass indication for cell phases

Expression (9.12) is applied in the centres of the cells and a central discretisation is used. In the cell with centre w the discretised equation becomes:

$$\frac{u_C^{n+1} - u_W^{n+1}}{h_x} + \frac{v_{NW}^{n+1} - v_{SW}^{n+1}}{h_y} = 0 \quad (9.14)$$

The momentum Expression (9.13) is applied in the centres of the cell faces, thus the discretisation in point C becomes:

$$\frac{u_C^{n+1} - u_C^n}{\Delta t} + \frac{p_e^{n+1} - p_w^{n+1}}{h_x} = R_C^n \quad (9.15)$$

9.4.4 Other aspects in the numerical model

In the detailed work of Gerrits (1996, 2001), Loots (1998) and Fekken (1998) other aspects of the numerical method are described in detail, such as:

- Discretisation of R_c^n
- Discretisation near the free surface
- In- and outflow discretisation
- Pressure Poisson equation
- Free surface reconstruction and displacement
- Use of the Courant-Friedrichs-Levy (CFL) number
- Calculation of forces

9.5 Case study 1: Flow onto a deck with impact on different structural shapes

9.5.1 General

To verify the ability of the Modified-VOF method to simulate the complex (meeting) shallow water flows on the deck and impacts on structures; simulations were carried out of the green water flow on a (fixed) deck. As boundary condition a wall of water around the bow was used. Although these are significant simplifications with respect to the real situation of a moving deck and complex inflow conditions, the simulations will show whether the Modified-VOF method is essentially able to fulfil requirements 3 to 6 as defined in Section 9.2. Details of this case study can be found in Fekken (1998) and Fekken, Veldman and Buchner (1999).

9.5.2 Computational domain and initial conditions

As basis for the present simulations the model tests in Test Series A were used. The deck was approximated by a parabola, as shown in Figure 9-12. This figure also shows the rest of the computational domain.

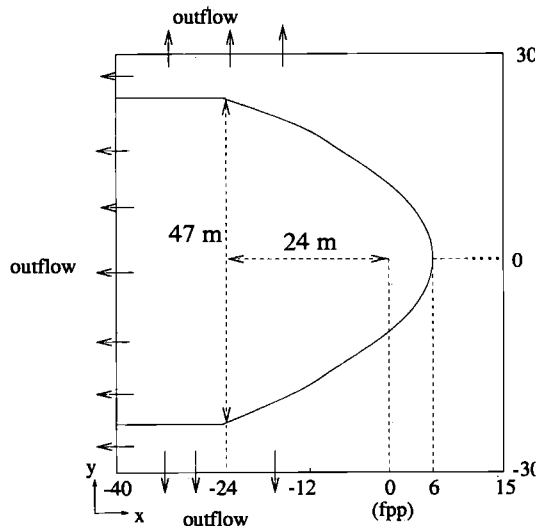


Figure 9-12
Initial situation in the xy -plane

First the relative wave motions around the bow in a regular wave test with wave amplitude of 8.65 m and ratio wave length/ship length = 0.75 were determined.

Taking into account the resemblance with the dam breaking problem, these relative wave motions were translated into a boundary condition of a wall of water around the bow. At the start of the simulation it was 13 m high at the most forward point of the bow, linearly decreasing to 5 m below the deck level 25 m behind this point (see Figure 9-13).

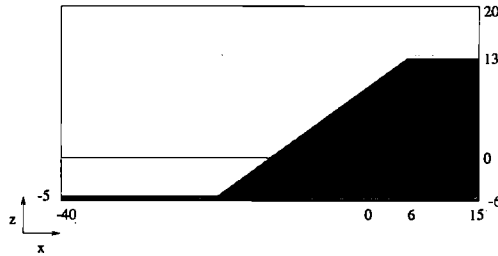


Figure 9-13
Initial situation in the xz -plane

The simulation used a uniform grid of $72 \times 72 \times 32$ cells in the x , y and z -direction respectively.

The heights of the water on the deck were measured and calculated at three different points at the axis of the deck, see Figure 9-14. At one position the pressure at the deck was measured and calculated.

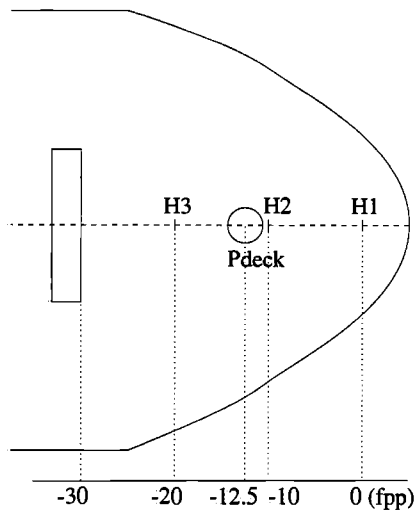


Figure 9-14
Positions of water heights, pressure and vertical structures

Squared, triangular (60 degrees front angle) and cylindrical structures were placed with their fronts at 30 m from the fore perpendicular (fpp), see for details Chapter 2 and Appendix A (a slightly different designation of the measurement/simulation signals is used). The area of their pressure panels was 5.73 m².

9.5.3 Results

The results of the simulations were analysed both visually and graphically. Figure 9-15 shows the visualisation of simulated flow on the deck. It shows a strong resemblance with the sequence in Photo 2-2 of the model tests:

- A wall of water around the bow, flowing on the bow as after the breaking of a dam.
- The shallow water flow on the deck, focussing in a high velocity water jet.
- The impinging jet type impact of the flow on the structure on the deck, with a strong run-up in front of the structure afterwards.

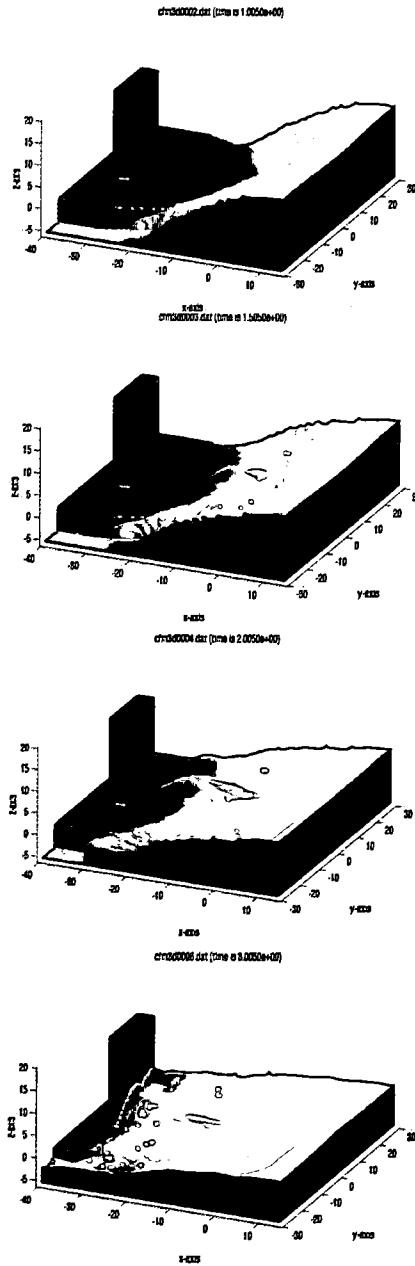


Figure 9-15
Visualisation of simulated flow on the deck

This good resemblance is confirmed if we study the results graphically in Figure 9-16. This figure shows the calculated and measured water heights on the deck on positions H1, H2 and H3 (0, 10 and 20 m from the fore perpendicular respectively). Even with the simplified boundary conditions the character of the time traces is very similar. The water heights are close and also the behaviour time is reproduced well: the initial increase of the water height as well as the secondary maximum caused by the water which is 'reflected' on the structure.

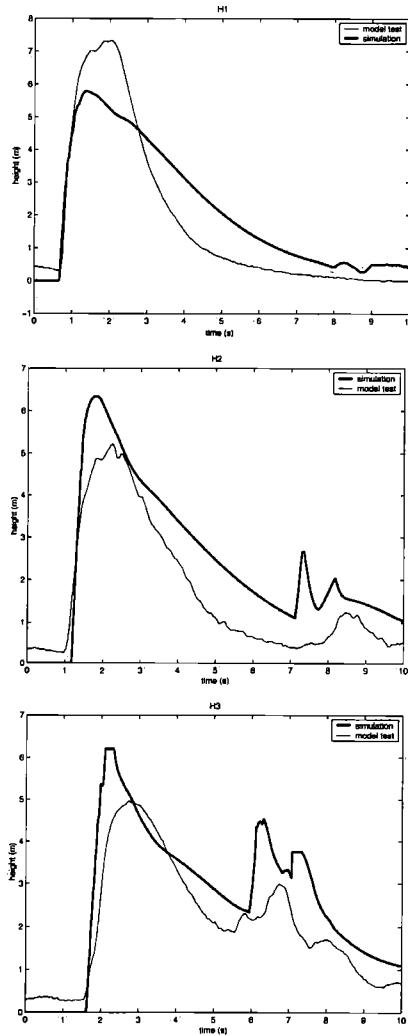


Figure 9-16
 Calculated and measured water heights on the deck

The pressure on the deck, shown in Figure 9-17, is also similar to the measured deck pressure. Although the calculated water height at this position (H2) is higher than measured, the pressure is equal. This is due to the fact that in the simulation the motions of the deck are neglected.

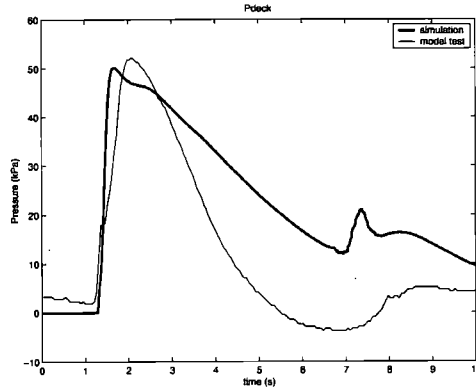


Figure 9-17
Calculated and measured water pressure on the deck

Figures 9-18 through 9-20 show the calculated and measured pressures and global FX-loads on the squared, triangular and cylindrical structures respectively.

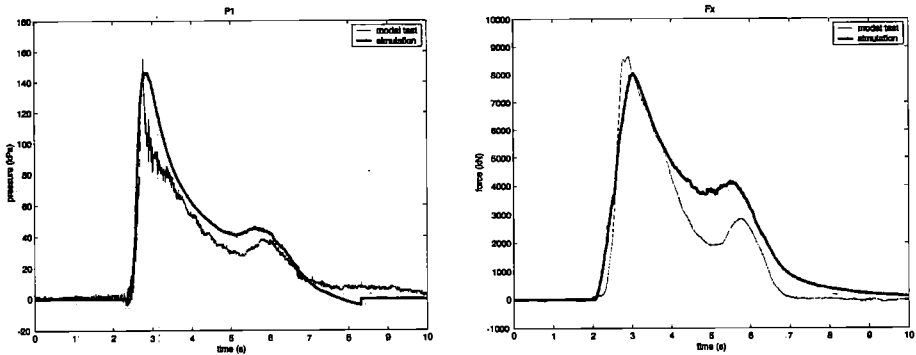


Figure 9-18
Calculated and measured pressure and global FX-load on the squared structure

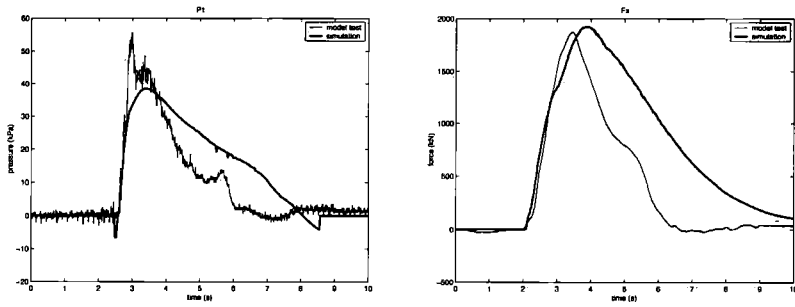


Figure 9-19
 Calculated and measured pressure and global FX-load on the triangular structure

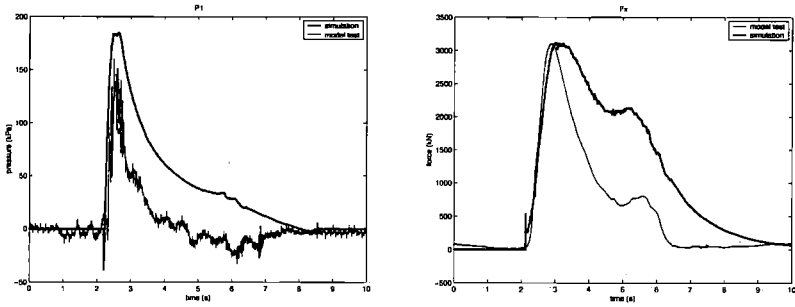


Figure 9-20
 Calculated and measured pressure and global FX-load on the cylindrical structure

Studying these results, the following can be observed:

- The load levels and their time character are very similar to the measured pressures and global loads, especially for the squared structure. For this structure both the initial and secondary peaks are simulated well.
- For the triangular and cylindrical structures the comparison is also good, but clearer differences are observed in the load levels and their character. It should on one hand be noted that the starting conditions in the simulations are schematic and that only one realisation of the measured pressure is shown, whereas in the tests also a significant variation in loads was observed. On the other hand this type of structures is more difficult to simulate because they involve the use of partial cells and boundaries cutting diagonally through the Cartesian grid.

- In the simulations negative pressure peaks are observed at the beginning (and end) of the impact. These can be understood based on Figure 9-21, which shows the flow of a water contour along a boundary. In the modified-VOF method the pressure in the Surface (S) cells p_S is determined based on a linear interpolation or extrapolation of the pressure in the Fluid (F) cell p_F and the pressure at the free surface p_{fs} , see e.g. Fekken (1998). In the situation in Figure 9-21 this results in a negative pressure until the water contour has passed the centre of the free surface cell. This example makes clear that the method is sensitive to details of the numerical model close to the free surface.

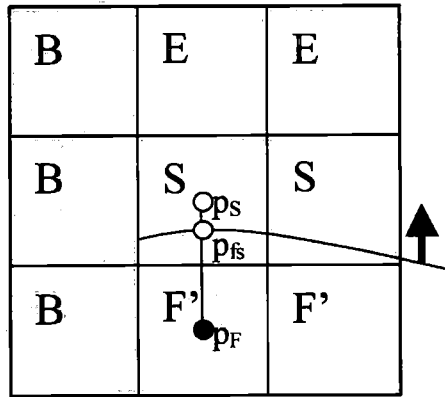


Figure 9-21

Linear extrapolation of the pressure in the Fluid cell (F) and at the free surface (FS) to the pressure in the centre of the free surface cell

9.6 Case study 2: Water entry of a 2D wedge

9.6.1 General

To verify the ability of the Modified-VOF method to simulate the strong non-linear swell-up around a flared bow structure (requirements 1 and 2), schematised 2D model tests and simulations were carried out. For this purpose, the Modified-VOF method was extended with the simulation of moving bodies in the fluid domain. The details of this extension are the subject of a separate PhD study by Fekken (to be published).

A wedge with a flare angle of 30 degrees was pushed into the water surface, as shown in Figure 9-22. The pressure on the wedge and the wave run-up in front of the wedge were measured and calculated.

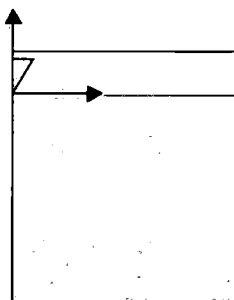


Figure 9-22

Fluid domain with wedge with flare angle of 30 degrees on the free surface

Details of this case study can be found in Buchner, Bunnik, Fekken and Veldman (2001).

9.6.2 Model tests

Figure 9-23 shows the test set-up for the wedge with a flare angle of 30 degrees (width 10.1 cm and height 17.5 cm). On the edge of the wedge, a pressure transducer has been placed that measures the pressure impact of the wedge when it penetrates into the water. The relative wave height is measured 20 cm in front of the wedge.

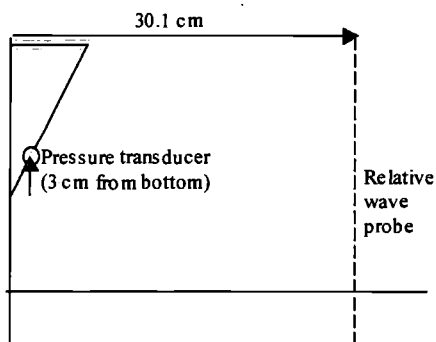


Figure 9-23

Set-up and instrumentation of the model tests

Two model test cases were investigated:

- Case A: a wedge with 30 degrees flare angle, starting 20 cm above the water surface, which is entirely submerged and not lifted out of the water. The mean velocity of the wedge is 1.43 m/s.

- Case B: a wedge with 30 degrees flare angle, starting on the water surface, which is not entirely submerged and lifted out of the water. The mean velocity is 0.54 m/s.

During the tests, the position of the wedge was measured. This position and the corresponding velocity of the wedge served as input for the simulation with the Modified-VOF method. The wave height can be obtained by subtracting the motion from the relative wave height. In all figures that show the relative wave height, the motion is, therefore, shown as well.

Because the measured position contains high-frequency noise, it was first filtered to enable accurate numerical differentiation. This results in the curves in Figures 9-24 and 9-25:

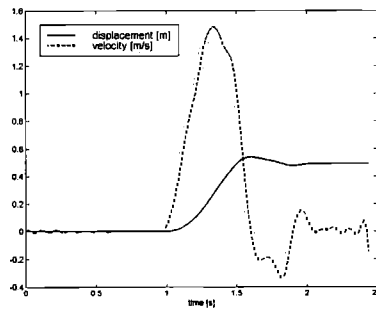


Figure 9-24
Vertical displacement and velocity of the wedge in Case A

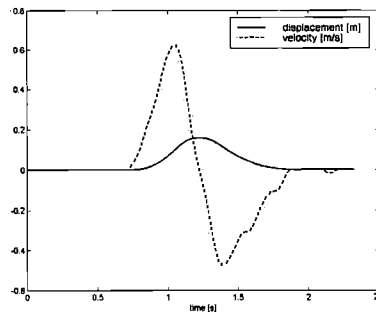


Figure 9-25
Vertical displacement and velocity of the wedge in Case B

9.6.3 Modified-VOF simulation model

To simulate the wedge entry, the method was modified to be able to move the wedge relative to the grid with any prescribed motion.

The vertical and horizontal sizes of the computational domain were limited to 1.0 m to keep the number of grid cells and computational time acceptable. A total number of 50 cells was used in the vertical and horizontal directions.

9.6.4 Results

In Figure 9-26 the typical simulated water contours are shown during the wedge entry.

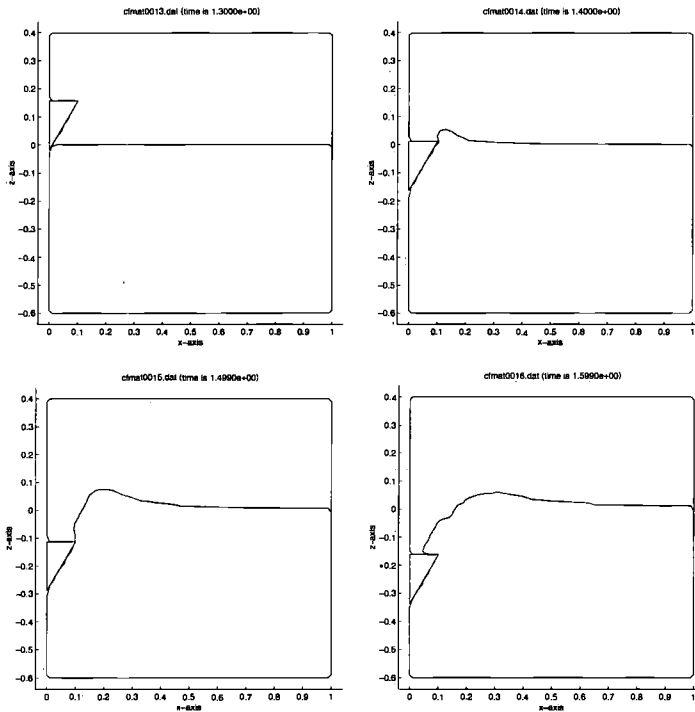


Figure 9-26
 Simulated water contours are shown during the wedge entry

The pressure results of the simulations show that the pressure contains spikes of one time step, especially directly after the high-velocity water entry. This behaviour is shown in Figure 9-27, where the measured pressure is compared with the computed pressure as it comes out of the simulation with the Modified-VOF method.

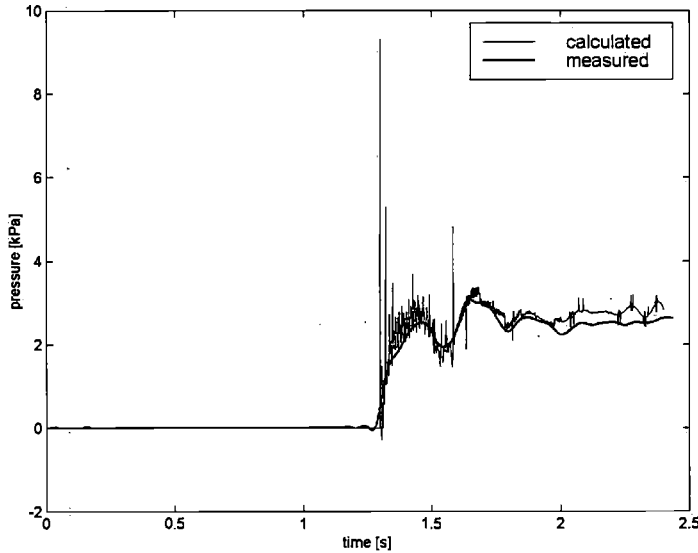


Figure 9-27

Measured and unfiltered calculated pressure for test case A

These pressure peaks are a result of the fact that the method is sensitive to details of the numerical model close to the free surface and geometry boundary, as was also found in Case study 1. These details have become even more complex after the extension of the Modified-VOF method with the simulation of moving bodies in the fluid domain: not only the fluid labels are changing, but also the geometry labels due to the motion of the body in the Cartesian grid. This requires special care with respect to small cells that are formed, changes in cell labelling, conservation of mass and momentum and flow along boundaries that cut diagonally through the Cartesian grid. These aspects are part of the special PhD study by Fekken (to be published) and will not be studied in detail here.

When the computed signal is filtered and the high-frequency oscillations are removed, the agreement between measurement and calculation is good. This is shown in Figure 9-28. Therefore, in the remainder of this chapter, only the filtered signals are shown.

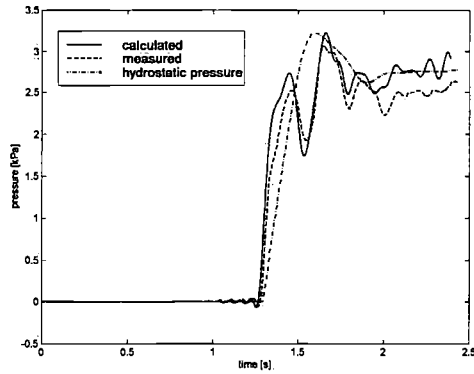


Figure 9-28
 Measured and filtered calculated pressure for Case A

The calculated and measured relative wave heights in front of the wedge shows the same behaviour, see Figure 9-29. However, the initial high-velocity run-up is underestimated. This is likely to be related to the same problems as for the pressure impact.

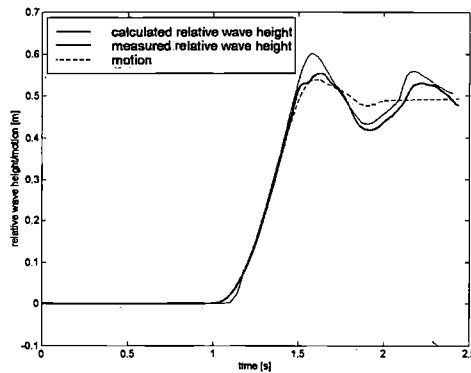


Figure 9-29
 Measured and calculated relative wave height for Case A

In Case B, the entrance velocity of the wedge is smaller and the water reaction less violent. Therefore, the pressures are more in line with the hydrostatic pressure. The peak pressure is less than for the previous simulation because the wedge is not entirely submerged.

The relative wave elevation in front of the wedge is better predicted than in the previous simulation. The initial wave elevation is predicted correctly now. The remainder of the wave signal looks very similar to the test results although there is a small shift in the wave pattern after 1.5 seconds. The results are shown in Figures 9-30 and 9-31.

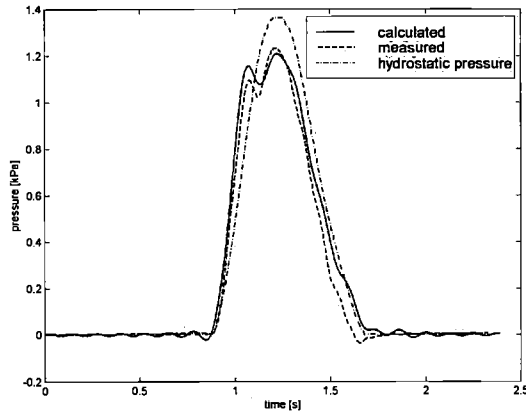


Figure 9-30
Measured and filtered calculated pressure for Case B

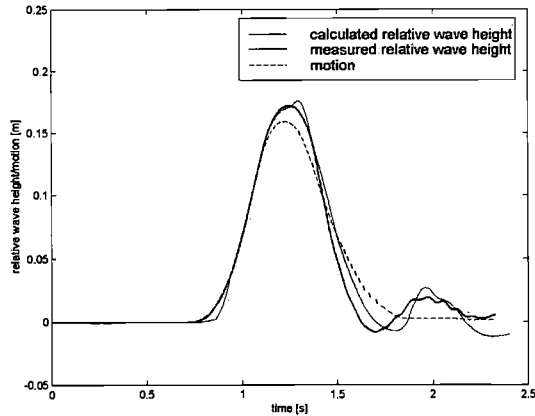


Figure 9-31
Measured and calculated relative wave height for Case B

9.7 Evaluation of the Modified-VOF method related to the green water problem

The case studies performed were carried out to evaluate the Modified-VOF method on its ability to simulate the complex green water problem. Although a number of numerical problems still need to be resolved, the results of the case studies have shown that the method is in principle able to fulfil the requirements as formulated in Section 9.2:

- Simulation of water entry of a flared bow structure and the complex flow onto the deck are possible and no problems are foreseen for the discontinuity at the deck edge (requirements 1 and 2).
- Prediction of the shallow water flow on the deck is possible without loosing the 'hydraulic jump'-type behaviour (no smearing of this discontinuity in time). A moving deck was not applied in the present case study, but the ability of the method to simulate this type of flow within moving boundaries was already extensively shown by Gerrits (2001). This satisfies requirement 3.
- Simulated meeting water flows on the deck shows a similar behaviour as the model tests: a high velocity water jet (requirement 4).
- Although the pressure spikes and actual pressure levels require further detailed study, the rise times and time characteristics of the pressures and global loads is very similar to the test results. This shows that the method is able to fulfil requirements 5 and 6.

This confirms that the Modified-VOF method can play an important role in the prediction of green water. To achieve this, the following needs at least detailed attention in future research:

- The details of the numerical model, including the simulation of moving bodies in the fluid domain (in 3D): the small cells that are formed during the body motions through the Cartesian grid, changes of cell labelling, conservation of mass and momentum and flow along boundaries that cut diagonally through the Cartesian grid.
- It is assumed that the small computational cell size required and consequential large computation times of the Modified-VOF method will focus its use initially on the direct vicinity of the vessel. This requires special attention to the creation of the correct interaction at the boundaries of the computational domain with other methods (such as potential flow codes) that will be used to determine the global wave field and vessel motions.

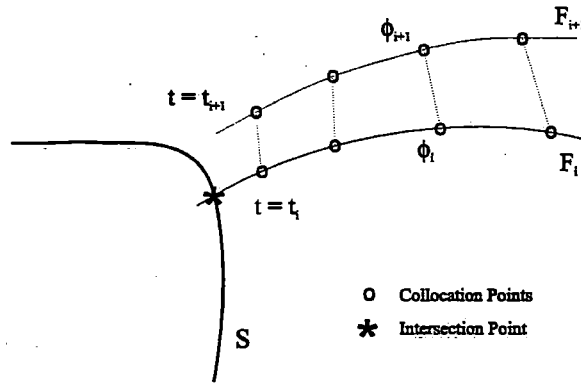


Figure 9-5

Time integration of the boundary conditions on the free surface F

In Buchner and Cozijn (1997) this method was applied to the problem of green water and more specifically to the non-linear relative wave motions around the bow. Purpose of this study was to determine whether this method could be used to define boundary conditions for the application of Glimm's method on the deck. In Figure 9-6 this is presented schematically, showing clearly that this method is based on a definition of the free surface using line segments (or panels in 3D). Instead of using a moving vessel, a 2D fixed deck and bow contour was used in the method and in a series of model tests in the basin of Delft University of Technology (Cozijn, 1995).

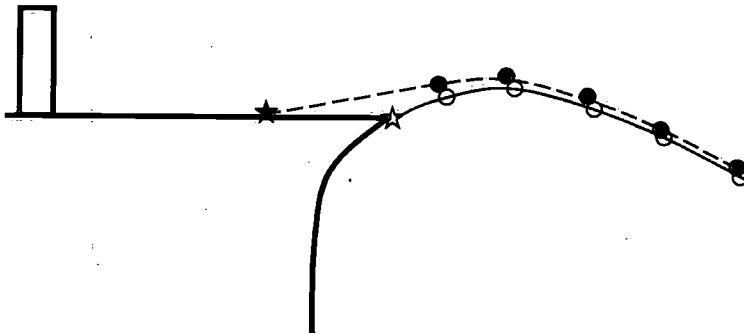


Figure 9-6

Simulation of flow onto a fixed deck for two time steps (solid line time step 1 and dashed line time step 2, at which the horizontal free surface exceeds the deck level)

9.8 Possibilities for the present application of the Modified-VOF method

At the moment it is already possible to use the method to simulate parts of the green water problem, using the results of the present semi-empirical model or direct model tests as input. The numerical method has the advantage that, when properly validated, it generally gives detailed insight in velocity fields and pressure distributions. In this section a number of examples will be given.

Figure 9-32 shows an interesting result from the numerical simulation: the pressure distribution over the structure on the deck in time. This can be used for further dynamic structural (FE) analysis of the structure. The figure clearly shows the initial impact of the high-velocity water jet at the centre, followed by a more quasi-static pressure over the complete structure.

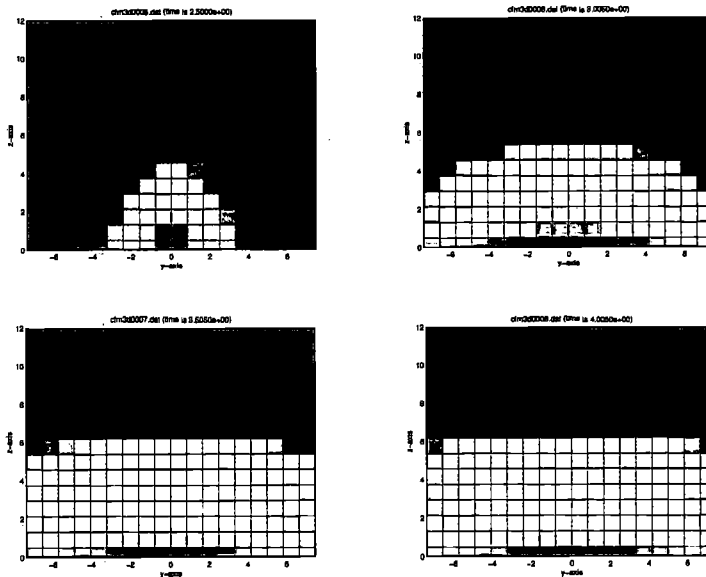


Figure 9-32

Calculated pressure distribution on the squared structure for different moments in time (front view: pressure in kPa, positions in m)

From this pressure distribution also the vertical pressure profile can be derived. Figure 9-33 shows this for the squared structure for different moments in time. This distribution shows strong resemblance with the pressure distribution proposed in the empirical method presented in this thesis (Section 6.3).

It clearly has two different stages as well: a momentum impact focussed on the lower part of the structure and lower quasi-static pressure over the complete height.

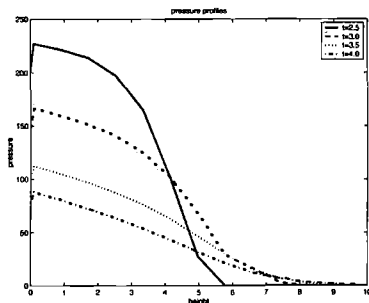


Figure 9-33

Calculated vertical pressure profile on the squared structure for different moments in time (pressure in kPa, height in m)

Figure 9-34 finally shows an example of how the method can be used to check different options in a design, after the initial model tests have been performed. Taking the results for the squared structure of 15 m wide (Figure 9-18) as reference, the figure shows the global FX-loads for widths of 5, 10, 15 and 20 m.

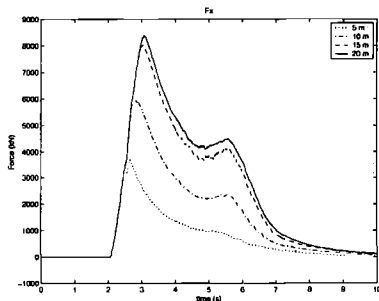


Figure 9-34

Global FX-loads on a squared structure for widths of 5, 10, 15 and 20 m (20 m high)

The figure shows at least two interesting effects:

- The load is not linear with the width of the structure, because the main loading is concentrated at the centre of the structure as a result of the high velocity water ‘jet’ over the deck.
- The run-up in front of the structure is significantly less when the flow is not completely blocked by the width of a structure.

10. CONCLUSIONS AND RECOMMENDATIONS

10.1 Summary of objective

The main objective of this study was:

To develop methods for the evaluation of green water on ship-type offshore structures based on a clear description of the green water physics.

10.2 Conclusions

Based on the research presented in this thesis, the following conclusions seem to be justified:

Chapter 2: The physics of green water at the bow

- A. The green water process shows the following typical sequence of events:
 - The relative wave motions exceed the freeboard level
 - The water flows onto the deck
 - The green water on the deck forms a high-velocity water jet
 - The green water impacts on a structure like an impinging jet
- B. The relative wave motions around the bow are complex and clearly non-linear.
- C. The green water on the deck has a significant effect on the ship motions, especially in shorter waves.
- D. Although the actual flow of green water onto the deck is more complex, the theoretical dam breaking theory can help to understand the green water physics better.
- E. The pressure on the deck is determined by the static water head, the vertical acceleration of the deck and an additional term related to the combination of vertical velocity of the deck and the rate of change of water height on the deck. This last term can result in peak loads in the pressure on deck of vessels. However, for a ship-type offshore structure with zero speed the accelerations are generally at their maximum at the moment the water comes onto the deck.

Consequently, the vertical velocity is at its minimum. This results in a pressure on the deck that is dominated by the static pressure and the acceleration component.

- F. Green water impacts on structures typically occur in three stages: an 'impact stage', a 'quasi-static load stage' and a 'plunging water stage'.
- G. The peak load of green water on the structure is not due to a solid impact (as is the case for bottom slamming). Green water impact loading is more similar to an impinging jet with an increasing height.

Chapter 3: Proposed semi-empirical design evaluation method

- A. It was concluded that in all phases of the green water problem non-linear and highly complex phenomena occur. Consequently, the green water problem cannot be predicted directly with linear prediction methods.
- B. New numerical methods still need significant further developing, integration and validation before they can be used to predict the green water as a whole within a reasonable timeframe. Therefore, a semi-empirical design evaluation method was proposed, to predict the green water loading problem from the input (extreme relative wave motions) to the output (predicted load levels) based on a clear description of the green water physics.

Chapter 4: Non-linear relative wave motions at the bow

- A. To describe the non-linear relative wave motions, a modified Rayleigh distribution was developed. It describes the probability of exceedance and can be used to determine the Most Probable Maximum relative wave motions.
- B. The parameters for the proposed modified Rayleigh distribution were determined for the full elliptical and thin triangular bows based on a systematic test series for spectral peak periods 12 s, 14 s, 16 s and bow flare angles of (0), 10, 30 and 50 degrees. In all these cases the new expressions were able to describe the measured phenomena. In this way they can be used to validate future numerical simulation results in a wide range of extreme conditions.
- C. The application of these fitted parameters for the prediction of the extreme relative wave motions for other conditions was checked for the increase of the freeboard height, a different main hull shape, a different wave heading and the application of current speed. In all these cases a good agreement between prediction and measurement was found.
- D. Due to the observed non-linearities in the relative wave motions, the results of predictions with the method should always be evaluated with care.

Chapter 5: Water flow onto and on the deck

- A. Based on the measurements and physical considerations, in the semi-empirical design evaluation method a linear relation is identified between the freeboard exceedance and water height on the deck. This relation is dependent on the bow flare angle, but independent of the wave period in the range tested.
- B. A strong high-velocity water jet occurs at the centreline of the deck due to meeting water flows. This jet is mainly dependent on the shape of the deck in plan view and, consequently, on the bow flare angle.
- C. The water front velocity over the deck appears to be proportional to the square root of the water height on the deck at the fore perpendicular.

Chapter 6: Green water impact loading

- A. Based on the measurements and physical considerations, in the semi-empirical design evaluation method a quadratic relation is identified between the freeboard exceedance and impacts loads on structures on the deck. This relation is dependent on the bow flare angle, but independent of the wave period in the range tested. Exceptions to this quadratic relation are single extreme (steep/energetic/breaking) wave events.
- B. The pressure distribution over the height of the structure (and in time) is a result of a short duration momentum impact at the lower part of the structure and a longer duration quasi-static water pressure over the full height occurring later.
- C. The loads on structures depend on their shape. For structures which deflect the green water momentum not completely (or more gradually), the resulting momentum impact is significantly lower than for squared structures.
- D. The shape of protecting breakwaters has a large effect on their ability to deflect the green water flow efficiently, so that the amount of water that finally reaches the critical structure will be minimised in amount and velocity. The breakwater and the underlying support structure should be strong enough to deal with the dynamic load due to the water impact on itself.

Chapter 7: Green water from the side and stern

- A. For waves under an angle with the vessel heading, green water on the deck is not only a problem in the bow area of the FPSO, but it can also come onto the deck from the side of the ship.
- B. Linear theory strongly underpredicts the relative wave motions along the side, especially in longer waves. This non-linearity is a result of the non-linearities in the incoming waves and the reflection of these waves against the side of the vessel.
- C. Green water loading on slender members along the side of the vessel is a result of a dam breaking type transverse flow, combined with the effects of wave crest kinematics along the side of the vessel.

Chapter 8: Review and application of the method

- A. A semi-empirical method requires a clear definition of the range of its applicability. Important aspects are the slenderness of the vessel, its absolute size and its bow shape on one hand and the wave characteristics, storm duration and wave heading on the other.
- B. The developed semi-empirical design evaluation method is a valid tool for the evaluation of the green water problem for ship-type offshore structures in the specific metocean conditions. However, the non-linear and highly complex character of the green water problem makes the problem sensitive to small changes in the input. Furthermore, the configurations of superstructures and equipment on the deck of these structures will be different and more complex than the configurations tested. This can, for instance, result in complex focussing or shielding of the green water flow. If an evaluation using the semi-empirical method shows the importance of the green water problem for (parts) of the structure, dedicated model tests are recommended.
- C. The green water problem at the bow should be evaluated in detail along the contour of joint probabilities of significant wave height and period. A focus on the highest significant wave height ('100-year wave') will result in an underestimation of the green water problem.
- D. The structural elasticity is an important aspect in the structural response to green water loading, but hydro-elastic aspects can be neglected. The structural response is very much dependent on the ratio between the natural period and rise time (T_n/T_r). When this ratio is close to (or larger than) 1.0, dynamic amplification should be accounted for. In this case the green water impact load should be applied dynamically on the structure with a range of typical rise times (0.10-0.35 full scale).

Chapter 9: Numerical prediction of green water

- A. To be able to predict the green water problem, a numerical method should be able to deal with complex non-linear flows. If the focus of the investigation is limited to the local flow around the bow, it specifically should be able to deal with:
 - 1. Water entry of a flared bow structure
 - 2. Complex flow onto the deck, including the discontinuity at the deck edge
 - 3. 'Hydraulic jump'-type shallow water flow on a moving ship deck
 - 4. Meeting water flows on the deck
 - 5. Short duration water impact on a structure
 - 6. Overturning flow after run-up of the water in front of the structure
- B. The evaluation of the Modified-VOF method based on these requirements has shown its ability to simulate the complex green water problem.

- C. A number of aspects in the numerical model, including the simulation of moving bodies in the fluid domain (in 3D), need further detailed study. Examples are: the small cells that are formed during the body motions through the Cartesian grid, changes of cell labelling, conservation of mass and momentum and flow along boundaries that cut diagonally through the Cartesian grid.
- D. At the moment it is already possible to use the method to simulate parts of the green water problem, using the results of the present semi-empirical model or direct model tests as input. The numerical method has the advantage that, when properly validated, it generally gives detailed insight in velocity fields and pressure distributions.

10.3 Recommendations for further research

The semi-empirical design evaluation method presented in the thesis allows the practical and fast evaluation of the green water problem for a wide range of ship-type offshore structures.

For further research on the subject of green water on ship-type offshore structures, it is recommended to focus on the further development and validation of numerical simulation methods. The correct description of the green water physics should be the guideline in this development. The systematic test series and resulting semi-empirical model presented in this thesis can be used as validation material.

In this development the following steps are foreseen:

1. Domain decomposition: simulation of the different parts of the green water process with methods that are optimised for the simulation of these specific processes. Examples are the developments presented in Greco, Faltinsen and Landrini (2000, 2001), Stansberg, Hellan, Hoff, and Moe (2002) and in Chapter 9 of this thesis. In general the output of one method is input to the other method.
2. Coupling of these methods/domains: coupling the different simulation methods to account for their interaction. Ship and wave motions simulated with potential theory can be coupled to accurate local flow simulation with (for instance) the modified-VOF method presented in Chapter 9. In this way the fluid domain of the modified-VOF method is kept as small as possible to reduce calculation times. This might be combined with the work on conditional wave testing and simulation as presented by Pastoor (2002) to further reduce the calculation time. The numerical simulation of non-linear waves by Westhuis (2001) can be used to simulate accurate input waves. However, the coupling between the different fluid domains and methods is very challenging. Some interesting first steps are presented in Meskers (2002).

3. Fully integrated numerical simulation methods: the simulation of the complete green water process from the beginning (the incoming non-linear waves) to the final green water impact with one consistent method, including all interactions.

Parallel to this the details of the numerical model need to be developed and validated further.

Besides this numerical method development, the following subjects are recommended for further study:

- A. Green water loading in the case of extreme wave events, such as breaking waves and steep fronted waves.
- B. The distribution of the extremes in a storm of N hours. Presently Most Probable Maximum values are used, but future research should provide more insight in this distribution of the extremes, to define an n% non-exceedance level.
- C. The physics behind the non-linear relative wave motions along the side.
- D. Green water from the side for wave headings more than 30 degrees from head waves, because the problem increases rapidly with the angle between the ship heading and the waves.
- E. Green water on the bow and from the side in short-crested waves.
- F. Validation of the method for the prediction of loading on slender members due to green water from the side.

APPENDIX I: SCALING OF GREEN WATER PHYSICS

I.1 Introduction

Model tests for seakeeping problems are generally scaled according to Froude scaling. In this Appendix the applicability of Froude scaling for model tests results into green water effects will be discussed based on a literature review.

It is generally agreed that seakeeping problems are dominated by the ratio between inertia and gravity forces. Consequently they can be scaled according to Froude scaling. The relative wave motions around the bow and the flow onto the deck are clearly dominated by this ratio between inertia and gravity forces. The problem occurs at the moment that the shallow water flow over the deck reaches a structure, resulting in an impact pressure. To confirm the applicability of Froude scaling for green water impact loading, a literature review was carried out.

I.2 Literature review

In slamming literature the problem of scaling has been studied extensively. A good overview has been given by SNAME panel HS2 (1993). The following observations are presented in this reference:

- Drop tests of wedges and flat bottoms at different scales have confirmed that slamming pressures are proportional to the square of the impact velocity for all scales:

$$p = C_i \rho V^2 \quad (I.1)$$

C_i is a constant that depends on the cross sectional shape. If compressibility of the water played an important role, the pressures would have been proportional to the impact velocity instead of the square of the impact velocity.

- According to Froude scaling the relation between full scale pressure p_f and model scale pressure p_m is:

$$p_f = \mu p_m \quad (I.2)$$

μ is the linear scale between model and prototype.

For the velocity the relation between full scale value V_f and full scale value V_m is:

$$V_f = \sqrt{\mu} V_m \quad (I.3)$$

If this scaling method is applied to scale the model scale pressures to the full scale pressures, we get:

$$\eta p_f = C\rho(\sqrt{\eta} V_f)^2 \quad (I.4)$$

This reduces to the formula for the impact pressures at model scale, Expression (I.1). This implies that Expression (I.1) applies to both model and ship, regardless of the scaling ratio.

Another field with similar problems, is the field of sloshing in tanks. An overview of research on scaling in this field can be found in the SNAME HS1 Technical and Research Bulletin (1975) and the ISSC Committee I13 report (1979). This overview resulted in the following conclusions:

- Fluid properties such as viscosity, compressibility and surface tension do not affect the magnitude of impact pressures significantly for large amplitude sloshing.
- Effects of air entrapment and the interaction between the structure and the fluid (hydro-elasticity) are identified as effects in which scale effects can occur. However, this depends on the amount of air that can be entrapped and the actual stiffness of the structure.

Finally a similar problem occurs in the field of civil engineering, when peak pressures occur on breakwaters due to breaking waves. Also in this field generally Froude scaling is applied, whereas a lot of attention is paid to the typical air entrapment problems related to breaking waves. Most of the recent research is referring to the older work of Bagnold (1939) and Nagai (1960).

In Chapter 2 it is shown that the typical flow of the water onto the deck of an FPSO shows considerable resemblance with the breaking of a dam. This results in a relatively thin, but fast, jet on the deck of the ship. Impact loading occurs when this jet reaches a structure on the deck. This impact shows considerable resemblance with a jet impinging perpendicularly at a plate. The load of the water on the structure is not due to a solid impact, but due to a jet with an increasing height. The load may therefore be developed as a sequence of quasi-stationary loads due to an impinging jet of an increasing height H . The peak force F' per metre breadth is expressed as function of maximum water height on the deck H_{\max} and the water front velocity over the deck U as:

$$F' = \rho H_{\max} U^2 \quad (1.5)$$

If this expression is converted to a pressure, it will be clear that a similar expression as Expression (1.1) is found. This implies that most of the conclusions with respect to the scaling of impact pressures in slamming, sloshing and breaking wave research are also valid for the impact of green water on structures. Viscosity, compressibility and surface tension can be neglected. Only air entrapment and the effect of the structural elasticity can be the cause of possible remaining scale effects.

In comparison with the breaking (overtopping) wave problem, the air entrapment seems to be less onerous for the green water problem. This is due to the fact that no overtopping is observed in the green water problem, so that no real air pockets can be trapped between the structure and the water.

However, during the process of water flowing onto the deck, air may come into the fluid. During the final impact this air in the fluid can result in some cushioning. Going from model scale to full scale a scale effect in this type of phenomena can occur.

If a wall is reasonably elastic, the response of the water and the wall during the impact load at the wall can become coupled, which can result in an effect on the pressures. This is an effect additional to the dynamic response of the structure on a peak load, where interactions are neglected. This is discussed in Appendix II.

I.3 Conclusion on scaling of green water loading

Based on this literature review it is concluded that Froude scaling of the green water impact pressures can be used to scale model pressures to full scale pressures. The effect of structural elasticity will be discussed in Appendix II.

All tests presented in the thesis are carried out to a linear scale of 1:60. In Table I-1 the Froude scaling factors as applied are shown.

*Table I-1
Froude scaling applied for scale 1:60*

Quantity	Scaling factor	Model	Prototype	
Linear dimensions	60	1 m	60.0	m
Area	60^2	1 m ²	3,600	m ²
Volume	60^3	1 m ³	216,000	m ³
Time	$\sqrt{60}$	1 s	7.746	s
Velocity	$\sqrt{60}$	1 m/s	7.746	m/s
Angle	-	1 degree	1	degree
Forces	$1.025 \cdot 60^3$	1 N	221.4	kN
Moments	$1.025 \cdot 60^4$	1 Nm	13284.0	kNm
Pressures	$1.025 \cdot 60$	1 Pa (N/m ²)	0.0615	kPa (kN/m ²)

1.025 represents the ratio between the specific mass of seawater and the fresh water in the basin.

APPENDIX II: EFFECT OF STRUCTURAL ELASTICITY

I.0 Introduction

Green water loading is a typical impact loading with a small rise time (T_r) from the beginning of the impact to the peak load as shown in Figure II-1.

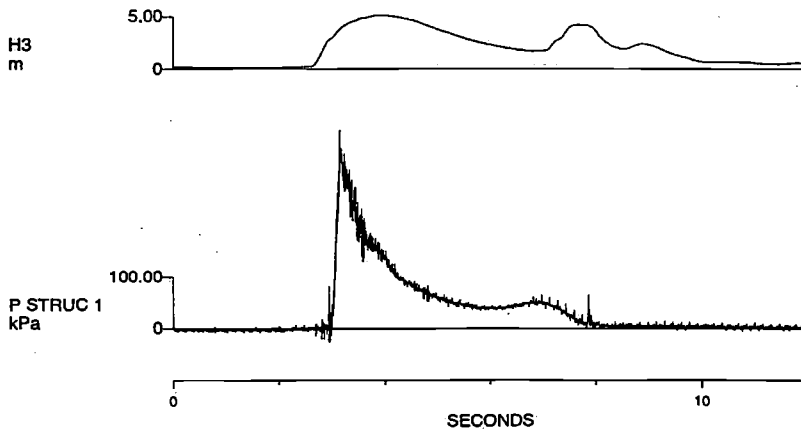


Figure II-1
Time traces of water height on deck (H3) and impact pressure (PSTRUC1)
for a typical green water impact

The green water impact rise time is typically between 0.10 and 0.35 seconds prototype time (0.15 s in the above time trace). Although this should be considered as an impact, the duration of the impact is significantly longer than in the case of bottom slamming. For slamming the structural response to the impact and the possible interaction with the hydrodynamic loading (hydro-elasticity) is an important aspect. It is the question whether this is also the case for green water loading.

Therefore the effect of structural elasticity on green water impact loading was investigated. The objective of this investigation was to determine how the green water impact load should be taken into account in the design:

- a. As a static load, where the peak load measured with a stiff force impact panel is applied on the structure statically.
- a. As a quasi-static load, where the dynamically measured load with a stiff force impact panel is applied on the structure dynamically with its typical behaviour in time.
- a. As a hydro-elastic problem, where the structural elasticity of the structural panel should be modelled during the model test to include the interaction between structural response and hydrodynamic loading.

II.1 Model tests

II.1.1 Model and set-up

To determine possible hydro-elastic effects in green water loading, the impact loads on a rigid type transducer should be compared with the load (and response) of a transducer that has a realistic structural elasticity.

Because transducers with a realistic structural elasticity show a dynamic response after impact, the internal friction of the force transducer should be minimised as much as possible. During Test Series A it was experienced that it is very difficult to design such a force transducer at scale 1:60. Consequently, this aspect was investigated in a schematised set-up at a large scale, as is shown in Figure II-2.

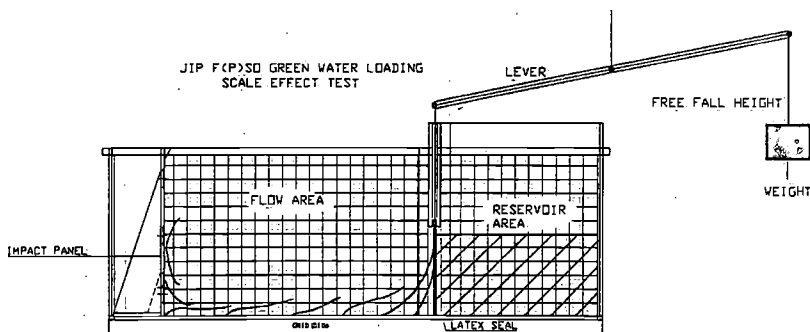


Figure II-2

Set-up simulating green water impact flow as a breaking of a dam

This set-up was designed initially for experiments into possible scale effects in green water loading. Therefore, a copy of the model was also made at a factor 4 smaller. However, technical problems with the smaller scale model prevented the use of the results for this purpose. The large model proved to be very useful as part of the investigations into the effect of structural elasticity. The set-up and instrumentation are shown in Figures II-3 and II-4.

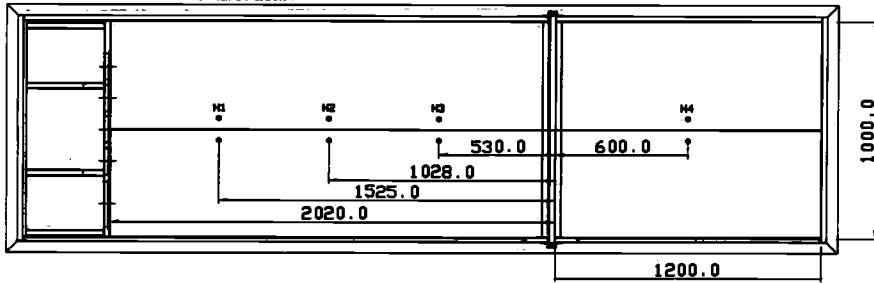


Figure II-3
Set-up and instrumentation in top view (dimensions in mm)

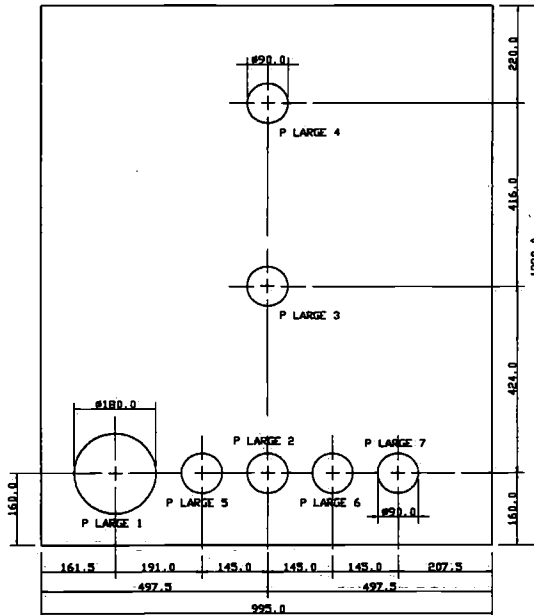


Figure II-4
Set-up and instrumentation of the impact panel (dimensions in mm)

The tests were carried out with this set-up as follows, see Figure II-2 and Photo II-1:

- In the beginning of a test the water was in the reservoir area on the right hand side of the flap.
- The weight was lifted to a certain height and than released in a free fall.
- At the moment the wire between the weight and the lever was tightened, the flap was lifted vertically with a large vertical velocity.
- The vertical wall of water in the reservoir area flows into the flow area as after the breaking of a dam at the flap position.
- The water flow reaches the impact panel and results in impact loading on the structure and force panel transducers.

The flow of the water into the flow area and the impact at the panel shows significant resemblance with the flow of the water onto the deck in the case of a freeboard exceedance (dam breaking problem) and the impact on a structure at the deck.

In Figure II-5 a typical example is shown of the time traces of the tests, including water heights and impact loads on rigid force panels (scale 1:1).

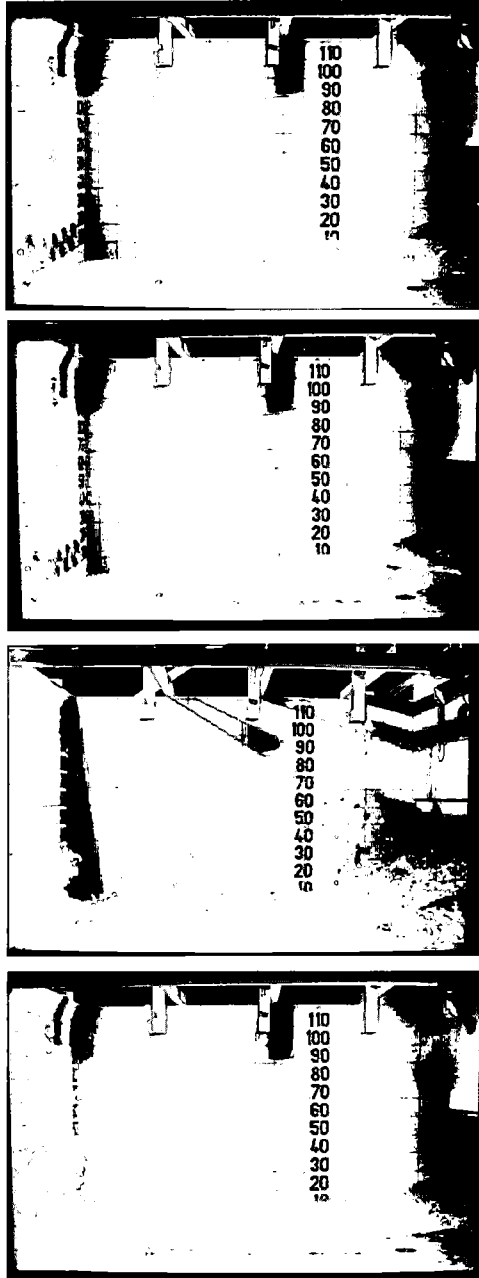


Photo II-1
Typical sequence of effects

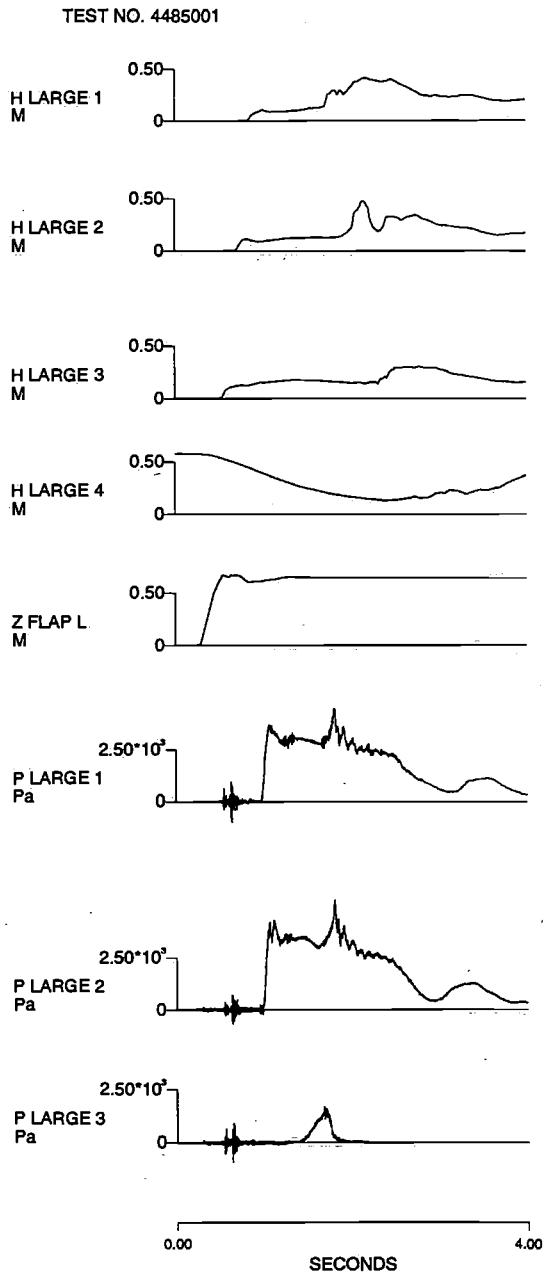


Figure II-5
Typical example the time traces of the tests, including water heights and impact loads
on rigid force panels

II.1.1 Force transducers with axial elasticity

To study the effect of structural elasticity, three additional force panel transducers were designed, which had the following features:

- A linear spring between the panel and the axial strain gauge force transducer.
- A roller bearing set-up to guide the panel in the axial direction with minimum friction to prevent rotations and sideways deflections.
- Openings at the back of the panel to prevent pressure build up behind the panel with a moving panel (to achieve constant atmospheric pressure).

The transducer is shown in Figure II-6. The panels can be seen at the bottom row in Figure II-3 and Photo II-1.

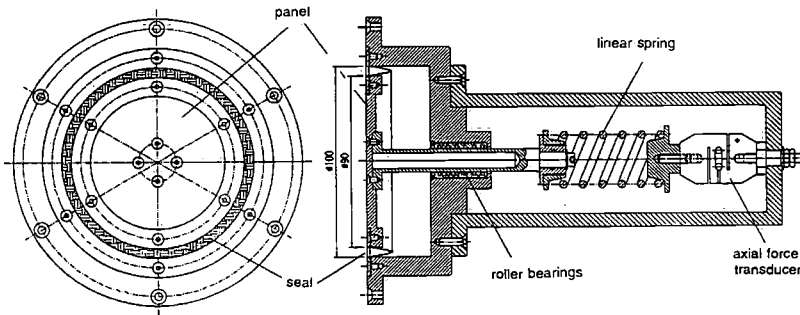


Figure II-6

Front and side view of the transducer with axial elasticity of a linear spring

Three different axial stiffnesses were investigated, which can represent the stiffness of a similar size panel (plate including local stiffeners) at full scale. In Table II-1 the model scale stiffnesses are given, as well as the corresponding full scale stiffnesses. Assuming that the large model is a 1:15 scale model of reality, a scaling factor of 15^2 is used for the stiffness. Besides the stiffness, also the mass of the moving part of the transducer is of importance for the structural response. Therefore also the weights of the separate parts of the transducers are given in Table II-1. It should be noted that the panel (every part in front of the spring) is moving with the maximum amplitude, whereas the mass of the linear spring is moving from a zero amplitude (at the front of the force transducer) to a maximum amplitude (at side of the panel).

Table II-1
Characteristics of the elastic forces panels

Panel number	Stiffness at model scale (large model)	Stiffness at ship scale (1:15)	Mass of spring at model scale	Mass of panel at model scale
5	22.07 N/mm	4966 N/mm	126.8 g	179.1 g
6	44.1 N/mm	9923 N/mm	180.0 g	179.1 g
7	109.9 N/mm	24727 N/mm	300.8 g	179.1 g

The three elastic panels were placed in a row on the impact panel of the large scale effect model. In the same row a stiff panel (P2) was placed with the same size of panel. The load on this panel was used as the reference load. Repeat tests were performed to determine the typical variability of the results

II.1 Results of model tests

From the time traces of the tests it was found that there are sometimes differences between the measurements with the stiff and elastic panels. However, the differences are not extreme. Also a significant variation was observed between the different tests. Both aspects are confirmed if the time traces are investigated in detail, as is done in Figure II-7 for two tests: 4485 and 4657. In the figures the reference pressure P2 and the load on the elastic panels P5, P6 and P7 is shown.

The rise time T_r of the reference load P2 is 0.05 seconds, which relates to a rise time of 0.19 seconds at ship scale (1:15). This rise time is in the typical range for green water impacts.

The results make clear that the load on the stiff panel P7 is almost equal to the load on the reference panel P2. For the more elastic panels, P6 and especially P5, significant dynamics can be observed in the loading and response process. The maximum total load on P5 is more than 40 percent larger than the load on the stiff reference panel.

The different response of the panels is related to the natural frequencies of the elastic panels. These natural periods are related to the stiffness C of the spring, as well as the mass M and added mass A of the water according to:

$$T_n = \frac{2\pi}{\sqrt{\frac{C}{M+A}}} \quad (\text{II.1})$$

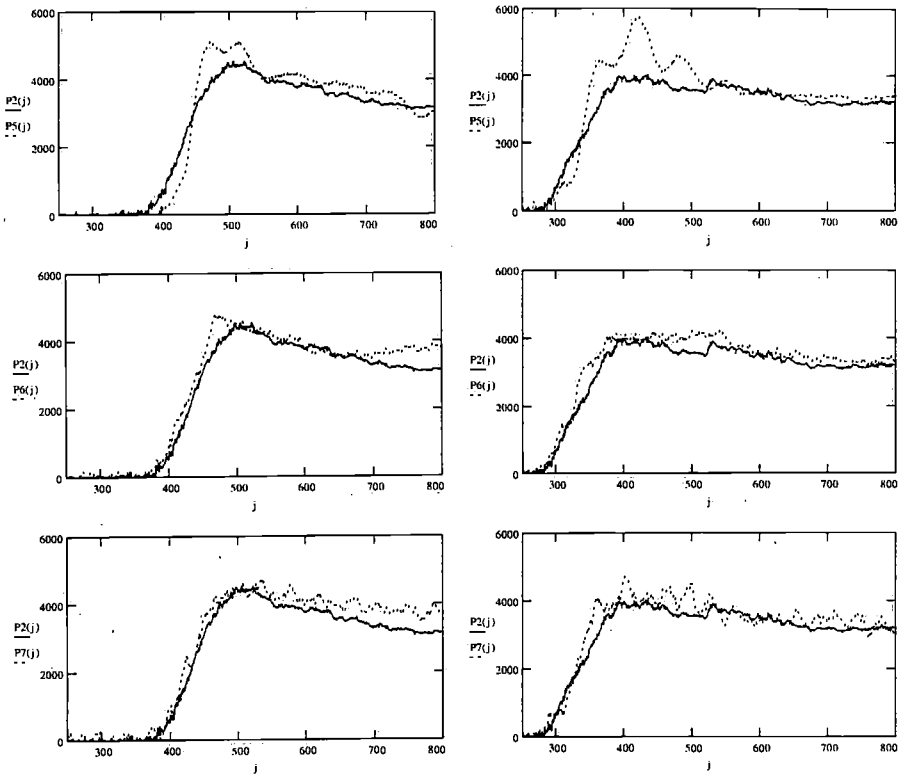


Figure II-7

Comparison of the pressure (in Pa) on the rigid force panel (P2, solid line) and the elastic panels P5, P6 and P7 (from top to bottom) for test 4485 (left) and 4657 (right). On the horizontal axis the sample numbers are given (sample time 2100 samples/second)

In Table II-2 the natural frequencies in air and water are summarised. For the total structural mass M the mass of the panel at model scale was taken (179.1 g), plus half the mass of the linear spring for each stiffness. The added mass was estimated as 620 g, based on an extensive evaluation of the decay tests in water for P5.

The added mass is very large compared to the weight of the panel. The added mass is approximately equal to the mass of a virtual horizontal cylinder in front of the circular transducer that has a length equal to its diameter (90 mm). For real structures the added mass will even be more important because the components that are used in the model test set-up are relatively heavy.

Table II-2
Characteristics of the flexible panels at model scale

Panel	Mass M	Added mass A	T _n in air	T _n in water
P5	242.5 g	620 g	0.021 s	0.039 s
P6	269.1 g	620 g	0.016 s	0.028 s
P7	329.5 g	620 g	0.011 s	0.018 s

The natural periods of the more elastic panels, which are closer to the rise time, result in a more dynamic response of the panels. The fact that the more elastic panels show dynamic behaviour does not imply directly that the process is hydro-elastic. It can simply be a dynamic response to an impulsive quasi-static loading. The loading is not affected per definition by the response. This will be discussed in the next section.

II.1 Simulation of dynamic response to impacts

The dynamic response of the applied linear elastic force panels to green water loading can be described by the behaviour of a single degree of freedom mass spring system:

$$(m + a) \ddot{x} + b \dot{x} + c x = F(t, x) \quad (\text{II.2})$$

In the case of static loading the velocity and acceleration forces are negligible and the green water force is independent on time and place. If dynamic response is observed without hydro-elastic effects, the structural response can be described with the equation of motion above when a constant damping and (added) mass are assumed. The quasi-static green water impact loading is only dependent on the time and independent of position. In the case of hydro-elastic loading the damping, added mass and green water load can be dependent on time and place and can be mutually coupled. In fact, it is not possible to distinguish between added mass, damping and loading effects in that case anymore.

The equation of motion can be solved with a standard integration method. To determine the amount of damping, first the free decay tests in air and water were simulated and compared with the model test results.

It was found that for the present set-up the mechanical damping was approximately 8% of the critical damping, with the critical damping defined as:

$$B_c = 2 \sqrt{(M + A) \cdot C} \quad (\text{II.3})$$

Because the spring coefficient, mass, added mass and damping are known now, the equation of motion can be solved. As input load F the load on the stiff panel P2 is used, which is independent of position.

Figure II-8 shows for tests 4487 and 4480 the input load P2, the measured load in transducer P5 and the simulated displacement multiplied by the stiffness.

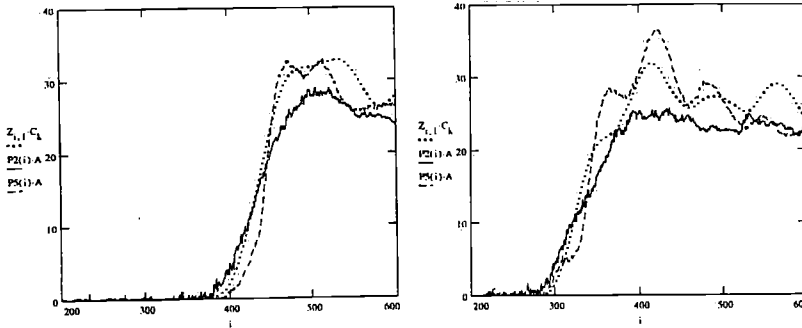


Figure II-8

Input load P2 (solid line), the measured load in transducer P5 (dashed line) and the simulated displacement multiplied by the stiffness (dotted line), all in N

The two figures show that the simulation with this stiffness has a similar dynamic behaviour as the measurement. A similar dynamic amplification and dynamic response is found and the oscillations have the same frequency. The observed differences can be due to the different positions of the panels and the related differences in loading. A significant variation is observed between the measurements in the two tests, which is predicted correctly in the simulations.

II.1 Conclusion on the effect of structural elasticity

These results indicate that the structural response to green water loading can be seen as the dynamic response to a quasi-static loading. No dominant hydro-elastic phenomena are observed which cannot be explained by the dynamics of a mass spring system with a prescribed input load from a measurement with a stiff panel.

APPENDIX A: PILOT TESTS TRADITIONAL FULL BOW (TEST SERIES A)

A.1 Main particulars, weight and stability data of model

Table A-1 gives an overview of the main particulars, weight and stability data of the model.

*Table A-1
Main particulars, weight and stability data of the model*

Length	260.34	m
Beam	47.10	m
Draft (even keel)	17.52	m
Freeboard	8.88	m
Depth	26.4	m
Displacement weight	183,053	t
CoG above base	14.22	m
CoG forward of midship	6.72	m
Longitudinal radius of gyration	65.1	m

A.2 Measurements

The following measurements were carried out:

*Table A-2
Overview of instrumentation and measurements during the tests*

Name	Description	Unit
R1-R7	Vertical wave resistance probes around the bow	m
RV1-RV3	Horizontal wave resistance probes at the deck edge	m/s
H1-H10	Vertical wave resistance probes at the deck	m
HV1, HV2	Horizontal wave resistance probes at the deck	m/s
F2-F4	Circular force panel with a stiff axial force transducer, measurements presented as integrated pressures over the total area of the panel (5.725 m ²)	kPa
F1	Circular force panel with spring between panel and axial force transducer, measurements presented as integrated pressures over the total area of the panel (5.725 m ²)	kPa
P1, P2	Strain gauge high-frequency local pressure transducers	kPa
FX, MY	Strain gauge force and moment transducers between structure and deck	kN and kNm
AX, AZ	Vessel fixed accelerometers at centre of structure at the bow	m/s ²
F-DECK	Circular force panel in deck, measurements presented as integrated pressures over the total area of the panel (5.725 m ²)	kPa
Angular motions	Gyroscope	degrees
Heave	Potentiometer	m

The force and pressure channels were recorded at a sampling rate of 2100 Hz, whereas all other signals were recorded at 150 Hz (model scale).

A.3 Basin set-up

To have a constant phase relation between the incoming waves and the ship behaviour for the comparison with future numerical simulations, it was decided to restrict the surge motions of the vessel for these theoretical tests. This was done by attaching the model to the basin carriage via a vertical cylinder with roller bearings. This cylinder was connected to the model at the centre of gravity.

A.4 Environmental conditions

The following regular wave tests were carried out:

Table A-3
Regular wave tests carried out

	Wave length (λ) to ship length (L) ratio	
	$\lambda/L=1.0$ ($\omega=0.487$ rad/s)	$\lambda/L=0.75$ ($\omega=0.562$ rad/s)
Height (first harmonic)	17.18 m	17.3 m (with and without current)
	-	15.76 m
	-	14.64 m

The following irregular wave tests were carried out (JONSWAP spectral shape, $\gamma=3.3$):

Table A-4
Irregular wave tests carried out

Significant wave height $H_s=13.5$ m	Spectral peak period (T_p)	
	12.9 s	12.9 s Current speed 2.0 m/s

Current is simulated by towing the model through the basin, considering the basin carriage as the earth-fixed reference.

APPENDIX B: COMPARATIVE TESTS TRADITIONAL FULL BOW AND ALTERNATIVE THIN BOW (TEST SERIES B)

B.1 Main particulars, weight and stability data of model

Table B-1 gives an overview of the main particulars, weight and stability data of the model with the traditional bow.

*Table B-1
Main particulars, weight and stability data of the traditional tanker model*

Length	260.34	m
Beam	47.10	m
Draft (even keel)	15.24	m
Freeboard	11.2	m
Depth	26.4	m
Displacement weight	159,187	t
CoG above base	14.22	m
CoG forward of midship	7.38	m
Longitudinal radius of gyration	65.1	m

Table B-2 gives an overview of the main particulars, weight and stability data of the models with the alternative thin bows.

Table B-2
Main particulars, weight and stability data of the alternative thin bow models

Length	260.34	m
Beam	47.10	m
Draft (even keel)	15.24	m
Freeboard	11.2	m
Depth	26.4	m
Displacement weight	143,246	t
CoG above base	14.22	m
CoG forward of midship	-2.76	m
Longitudinal radius of gyration	65.1	m

B.2 Measurements

The following measurements were carried out:

Table B-3
Overview of instrumentation and measurements during the tests

Name	Description	Unit
RI	Vertical wave resistance probe at bow centreline	m
H1	Vertical wave resistance probe at the deck, 28.6 m from fore perpendicular	m
HV1	Horizontal wave resistance probe at centreline of the deck	m/s
F1	Circular force panel with a stiff axial force transducer, measurements presented as integrated pressures over the total area of the panel (5.725 m ²) in a box type structure 33.6 m from the fore perpendicular	kPa
FXTOT	Total force between the ship and the linear soft mooring system	kN
Angular motions	Gyroscope	degrees
Translations	Optical tracking system	m

The force and pressure channels were recorded at a sampling rate of 2100 Hz, whereas all other signals were recorded at 150 Hz (model scale).

B.3 Basin set-up

The mooring system consisted of four horizontal linear springs, which gave the mooring system a stiffness of 224 kN/m in the x-direction. This is a realistic stiffness for a mooring system in the applied water depth of 150 m.

B.4 Environmental conditions

The following regular wave tests were carried out:

Table B-4
Regular wave tests carried out

	Wave length (λ) to ship length (L) ratio			
	$\omega=0.418$ rad/s	$\omega=0.483$ rad/s	$\omega=0.571$ rad/s	$\omega=0.698$ rad/s
H=100%	*	*	*	*
H=75%	*	*	*	*
H=25%	*	*	*	*

The 100% wave amplitude was chosen to investigate green water loading. The 75% and 25% wave amplitudes were chosen to have a good comparison of the motions and drift forces in high and low waves.

The following irregular wave tests were carried out (JONSWAP spectral shape, $\gamma=3.3$):

Table B-5
Irregular wave tests carried out

	Spectral peak period (T_p)
Significant wave height $H_s=13.2$ m	12.9 s

APPENDIX C: SYSTEMATIC TEST SERIES WITH DIFFERENT HULL SHAPES AND FLARE ANGLES (TEST SERIES C)

C.1 Main particulars, weight and stability data of model

All models were at even keel draft of $T=16.5$ m with no trim. For different flare angles or bulwark heights with the same underwater hull shape, the total mass, position of the centre of gravity and radius of gyration remained constant. This was achieved by having the weight and centre of gravity the same for all flare (and additional bulwark) parts. This was necessary for a direct comparison between the different flare angles.

Table C-1 gives an overview of the main particulars, weight and stability data of the model with full elliptical bow and traditional stern.

*Table C-1
Main particulars, weight and stability data of the model with full elliptical bow
and traditional stern*

Length	260.34	m
Beam	47.10	m
Draft (even keel)	16.50	m
Freeboard including bulwark (1.4 m)	10.5	m
Depth (to deck)	25.6	m
Displacement weight	168,870	t
CoG above base	14.14	m
CoG forward of midship	5.69	m
Longitudinal radius of gyration	69.80	m

Table C-2 gives an overview of the main particulars, weight and stability data of the model with full elliptical bow and full (barge type) stern.

*Table C-2
Main particulars, weight and stability data of the model with full elliptical bow
and full (barge type) stern*

Length	260.34 m
Beam	47.10 m
Draft (even keel)	16.50 m
Freeboard including bulwark (1.4 m)	10.5 m
Depth (to deck)	25.6 m
Displacement weight	182,836 t
CoG above base	14.83 m
CoG forward of midship	-1.53 m
Longitudinal radius of gyration	65.08 m

Table C-3 gives an overview of the main particulars, weight and stability data of the model with thin triangular bow and full (barge type) stern.

*Table C-3
Main particulars, weight and stability data of the model with thin triangular bow
and full (barge type) stern*

Length	260.34 m
Beam	47.10 m
Draft (even keel)	16.50 m
Freeboard including bulwark (1.4 m)	11.9 m
Depth (to deck)	27.0 m
Displacement weight	167,529 t
CoG above base	14.60 m
CoG forward of midship	-10.70 m
Longitudinal radius of gyration	65.08 m

C.2 Deck, bulwark and freeboard heights

All models were made with a flat deck without camber. A typical bulwark was applied around the bow with a constant vertical height of 1.4 m. It had the angle of the applicable flare. Freeing ports were placed in all bulwarks for water drainage from the deck.

Table C-4 gives an overview of the effective freeboard (including bulwark height of 1.4 m) for the even keel draft of 16.5 m for all tests:

Table C-4
Effective freeboard heights for all tests

	Effective freeboard bow	Effect freeboard stern and side
Thin triangular bow, full and flat stern	11.9 m	10.5 m
Full elliptical bow, Traditional stern	10.5 m	7.0 m
Full elliptical bow, full and flat stern	10.5 m	10.5 m

C.3 Structures at the deck

The following structures at the deck were modelled (all dimensions in metres full scale):

Squared structure (Structure 1)

With the instrumented squared structure with flat front (Structure 1), most of the tests in the main test program were carried out with the structure at 30 m from the forward perpendicular. The exception is the test with the full elliptical bow and flat stern, which was carried out with Structure 2 at the same position. The main program with Structure 1 was carried out to investigate the effect of the hull shape on the green water occurrence and loading. The loads on Structure 1 can therefore be considered as the base case for all investigations. It is shown with its instrumentation in Figure C-1.

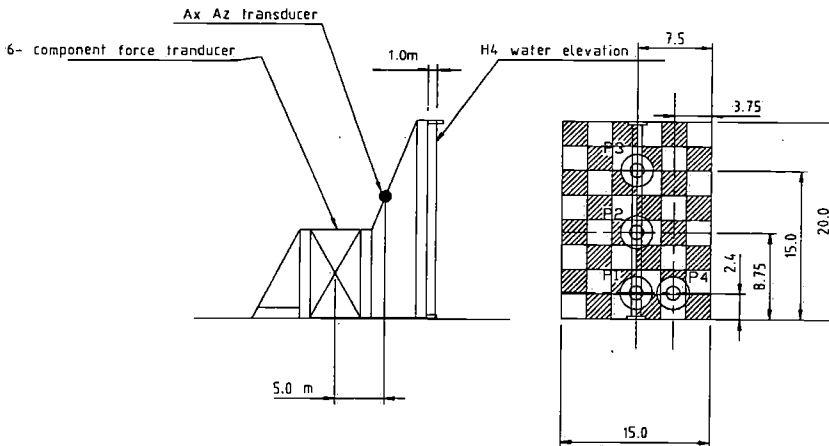


Figure C-1
Model and instrumentation of the squared structure (Structure 1)

Alternative squared structure (Structure 2)

The alternative squared deck structure with flat front (Structure 2) was prepared after the completion of the series of tests with the thin triangular bow. It is identical to Structure 1, except for its instrumentation. The position of the panel force transducers was changed, together with the size of the lowest panel force transducer in the centre (from 1.35 m to 2.7 m diameter). This is shown in Figure C-2.

This was done because of the fact that during this first series of tests it was found that the loads on the small panels were low compared to the relatively large unfiltered noise levels. This, combined with the fact that the load was concentrated at the lower part of the structure, resulted in the alternative squared structure (Structure 2).

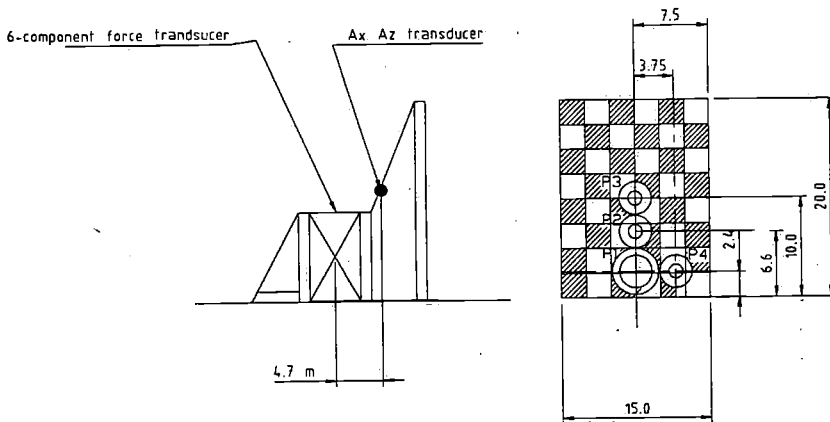


Figure C-2

Model and instrumentation of the alternative squared structure (Structure 2)

Tilted structure under angle with vertical (Structure 3)

Structural loading due to green water is a result of the momentum in the green water on the deck, which is destroyed per time step. If this momentum is destroyed more gradually, the loads can be reduced. Structure 3 was designed to investigate what the effect would be of a vertical deflection of the water. Structure 3 is shown with its instrumentation in Figure C-3.

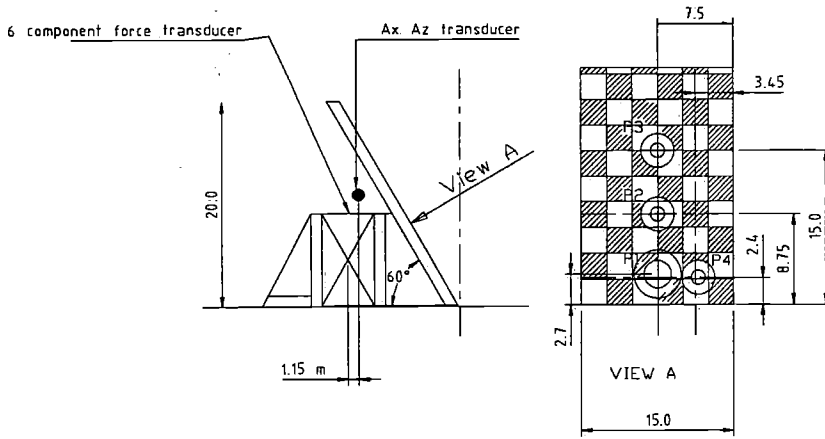


Figure C-3

Model and instrumentation of the tilted structure under angle with vertical (Structure 3)

Triangular structure with 45 degrees front (Structure 4)

Based on similar strategies as for Structure 3, the triangular structure with a 45 degrees front (Structure 4) was used to deflect the water 45 degrees instead of 90 degrees, but now in the horizontal direction. It is shown with its instrumentation in Figure C-4.

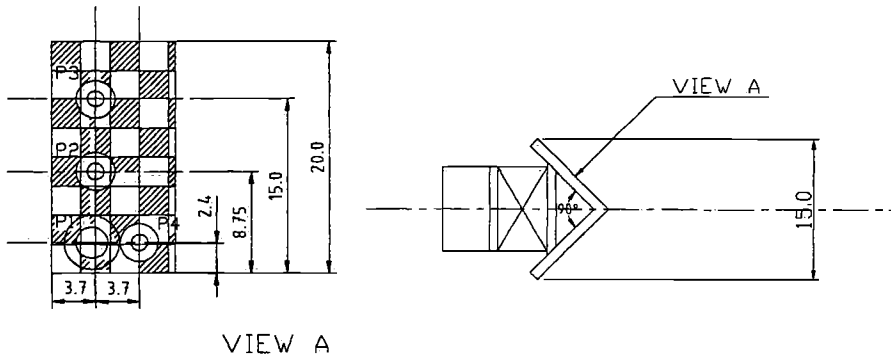


Figure C-4

Model and instrumentation of the triangular structure with 45 degrees front (Structure 4)

Triangular structure with 60 degrees front (Structure 5)

Structure 5 is equal to Structure 4, except that it is used to deflect the water 60 degrees instead of 45 degrees. It is shown with its instrumentation in Figure C-5.

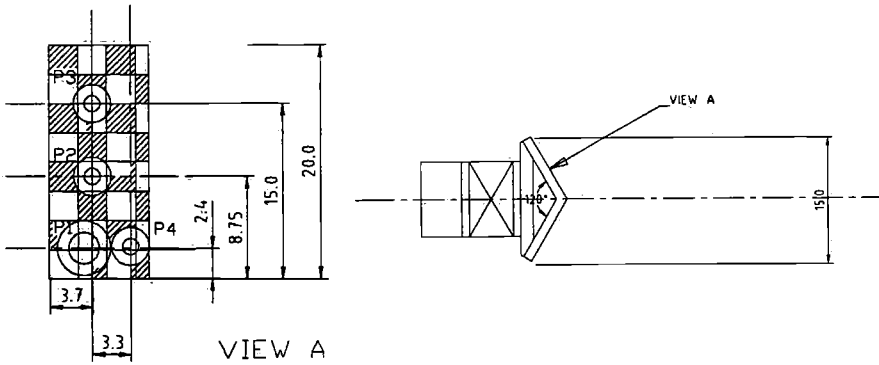


Figure C-5

Model and instrumentation of the triangular structure with 60 degrees front (Structure 5)

Structure with cylindrical front (Structure 6)

Structure 6 has a cylindrical front. It is shown with its instrumentation in Figure C-6.

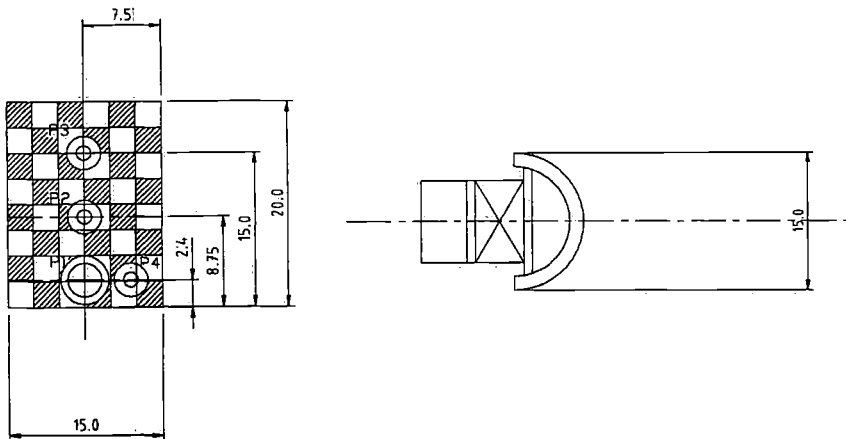


Figure C-6

Model and instrumentation of the structure with cylindrical front (Structure 6)

Squared structure knee support in front (Structure 7)

Structure 7 is equal to Structure 2 with only a wedge in front of Structure 2 to deflect the water more gradually. It is shown with its instrumentation in Figure C-7. Panel force transducer 1 is placed in the wedge (under an angle).

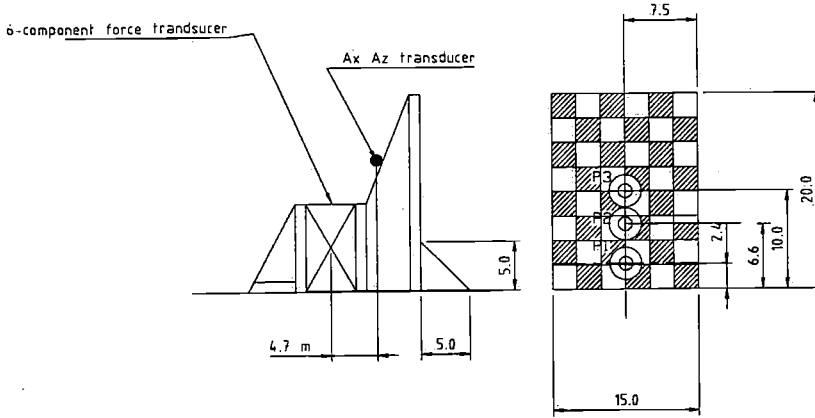


Figure C-7

Model and instrumentation of squared structure with knee support in front (Structure 7)

C.4 Breakwaters

In this study three different types of breakwaters were evaluated:

1. Traditional V-type breakwater (No. 1)
2. Vertical wall breakwater with its upper side tilting forward (No. 2)
3. Vane type breakwater (No. 3)

The different breakwater shapes are shown in Figure C-8. The shaded areas in the figures indicate the parts at which the local load is measured. Also the global load and moment on the complete breakwater were measured.

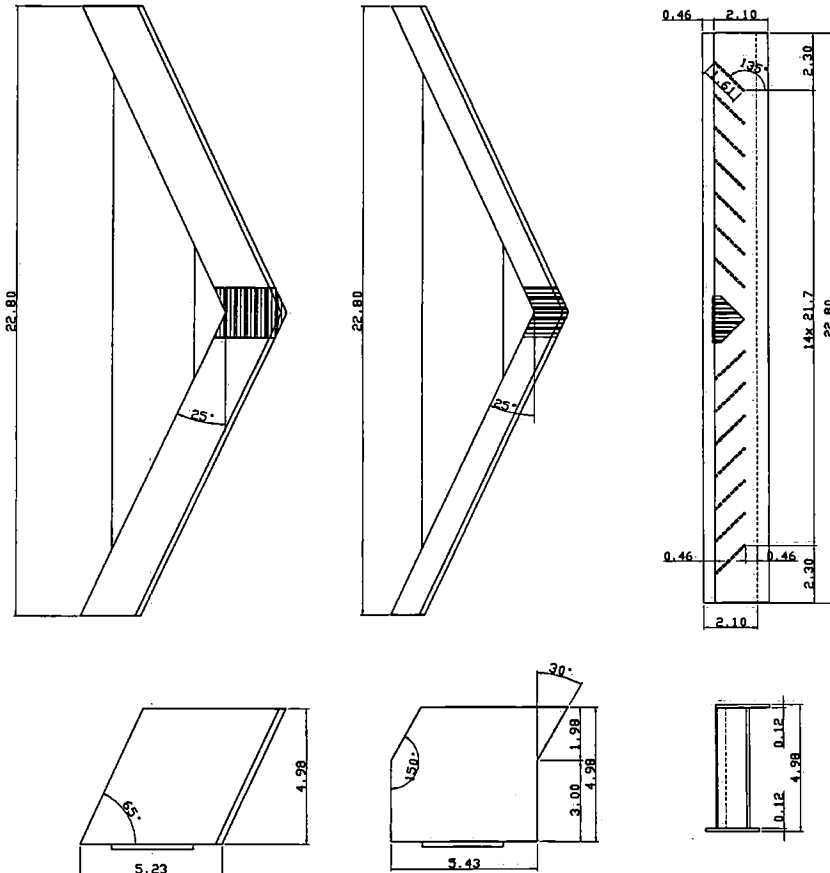


Figure C-8
 Traditional V-type breakwater, vertical wall breakwater and vane type breakwater
 (from left to right)

Table C-5 (cont'd)
Overview of instrumentation and measurements during the tests

Name	Description	Unit
PDECK1-3	Circular force panels in deck, measurements presented as integrated pressures over the total area of the panel (5.725 m ²)	kPa
FX LOC. BW FX TOT. BW MY BW	Strain gauge force and moment transducers between the breakwaters and the deck (moment transferred to deck level)	kN and kNm
FX FORE, FX AFT	Forces between the ship and the linear soft mooring system fore and aft	kN
Angular motions	Gyroscope	degrees
Translations	Optical tracking system	m

The characteristics of transducers in the actual set-up can affect the measurements because they act like mass spring systems. For this reason, the natural frequencies of the impact force transducers were determined with decay tests. To determine the natural frequencies, small impact loads were applied to the transducers. The following natural frequencies were found:

Table C-6
Natural periods of force transducers

	Natural frequency at prototype scale
Panel force transducers (PSTRUC)	110 Hz
Force on structure on deck (FX COR, MY DECK)	45 Hz

C.6 Data acquisition

Most of the signals were sampled at a rate of 150 Hz (model scale). This means that the time difference between two samples is equal to 0.0516 seconds full scale. This sampling rate is clearly sufficient for the following channels:

- motions
- wave probes for waves and relative motions
- wave probes for water heights on deck and water front/velocity over deck
- accelerations

High frequency sampling was applied for impact type channels at a sampling rate of 2100 Hz (model scale). The time difference between two samples is equal to 0.003688 seconds full scale.

C.7 Basin set-up

The mooring system consisted of four horizontal linear springs, which gave the mooring system a stiffness of approximately 430 kN/m in the x-direction. This is a realistic stiffness for a mooring system in the applied water depth of 150 m.

C.8 Environmental conditions

The following regular wave tests were carried out:

Table C-7
Regular wave tests carried out

	Wave length (λ) to ship length (L) ratio			
	$\lambda/L=1.25$ ($\omega=0.435$ rad/s)	$\lambda/L=1.0$ ($\omega=0.487$ rad/s)	$\lambda/L=0.75$ ($\omega=0.562$ rad/s)	$\lambda/L=0.50$ ($\omega=0.688$ rad/s)
H=140%	-	H140/ $\lambda 1.0$	-	-
H=130%	-	H130/ $\lambda 1.0$	-	-
H=115%	H115/ $\lambda 1.25$	H115/ $\lambda 1.0$	H115/ $\lambda 0.75$	-
H=100%	H100/ $\lambda 1.25$	H100/ $\lambda 1.0$	H100/ $\lambda 0.75$	-
H=85%	H85/ $\lambda 1.25$	H85/ $\lambda 1.0$	H85/ $\lambda 0.75$	-
H=70%	H70/ $\lambda 1.25$	H70/ $\lambda 1.0$	H70/ $\lambda 0.75$	-
H=50%	H50/ $\lambda 1.0$	H50/ $\lambda 1.0$	H50/ $\lambda 0.75$	H50/ $\lambda 0.5$

The adjusted regular waves were subjected to a harmonic analysis. This resulted in the following first harmonic amplitudes ζ_a for all waves:

Table C-8
Periods and first harmonic amplitudes of regular wave tests carried out

	Wave length (λ) to ship length (L) ratio			
	$\lambda/L=1.25$ ($\omega=0.435$ rad/s)	$\lambda/L=1.0$ ($\omega=0.487$ rad/s)	$\lambda/L=0.75$ ($\omega=0.562$ rad/s)	$\lambda/L=0.50$ ($\omega=0.688$ rad/s)
H=140%	-	H140/ λ 1.0 ($\zeta_a=10.26$ m)	-	-
H=130%	-	H130/ λ 1.0 ($\zeta_a=8.93$ m)	H130/ λ 0.75 ($\zeta_a=10.82$ m)	-
H=115%	H115/ λ 1.25 ($\zeta_a=1.45$ m)	H115/ λ 1.0 ($\zeta_a=7.63$ m)	H115/ λ 0.75 ($\zeta_a=8.73$ m)	-
H=100%	H100/ λ 1.25 ($\zeta_a=9.73$ m)	H100/ λ 1.0 ($\zeta_a=6.76$ m)	H100/ λ 0.75 ($\zeta_a=7.64$ m)	-
H=85%	H85/ λ 1.25 ($\zeta_a=8.10$ m)	H85/ λ 1.0 ($\zeta_a=5.80$ m)	H85/ λ 0.75 ($\zeta_a=7.07$ m)	-
H=70%	H70/ λ 1.25 ($\zeta_a=6.73$ m)	H70/ λ 1.0 ($\zeta_a=4.65$ m)	H70/ λ 0.75 ($\zeta_a=6.15$ m)	-
H=50%	H50/ λ 1.00 ($\zeta_a=4.76$ m)	H50/ λ 1.0 ($\zeta_a=3.25$ m)	H50/ λ 0.75 ($\zeta_a=4.71$ m)	H50/ λ 0.5 ($\zeta_a=4.48$ m)

A family of three survival wave spectra with constant significant wave height of 13.5 m, but with different peak periods of 12, 14 and 16 seconds, was used in the irregular wave tests. The JONSWAP spectral shape was used with $\gamma=3.3$.

Table C-9
Irregular wave tests carried out

	Spectral peak period (T0)		
	12 seconds	14 seconds	16 seconds
Significant wave height $H_s=13.5$ m	P12	P14	P16

A three hours sea state was adjusted in the basin that represented a typical survival storm duration:

Current is simulated by towing the model through the basin, considering the basin carriage as the earth-fixed reference. Both regular and irregular waves were tested with current:

Table C-10
Tests with current carried out

	Current speed 1.0 m/s	Current speed 2.0 m/s
Regular H100/ ω 1.0	H100/ ω 1.0/V1.0 ($\omega=0.465$ rad/s) ($\zeta a=6.79$ m)	H100/ ω 1.0/V2.0 ($\omega=0.446$ rad/s) ($\zeta a=6.70$ m)
Regular H100/ ω 0.75	H100/ ω 0.75/V1.0 ($\omega=0.533$ rad/s) ($\zeta a=7.61$ m)	H100/ ω 0.75/V2.0 ($\omega=0.509$ rad/s) ($\zeta a=7.79$ m)
Irregular P14	P14/V1.0	P14/V2.0

APPENDIX D: PILOT TESTS GREEN WATER FROM THE SIDE (TEST SERIES D)

D.1 Main particulars, weight and stability data of model

Table D-1 gives an overview of the main particulars, weight and stability data of the model with full elliptical bow and traditional stern.

*Table D-1
Main particulars, weight and stability data of the model with full elliptical bow
and traditional stern*

Length	260.34	m
Beam	47.10	m
Draft (even keel)	16.50	m
Freeboard including bulwark (1.4 m)	10.5	m
Depth (to deck)	25.6	m
Displacement weight	168,870	t
CoG above base	14.14	m
CoG forward of midship	5.69	m
Longitudinal radius of gyration	69.80	m

The effective freeboard for the even keel draft of 16.5 m was 7.0 m along the side of the vessel.

D.2 Measurements

Figure D-1 shows the position of the wave probes for this series of tests.

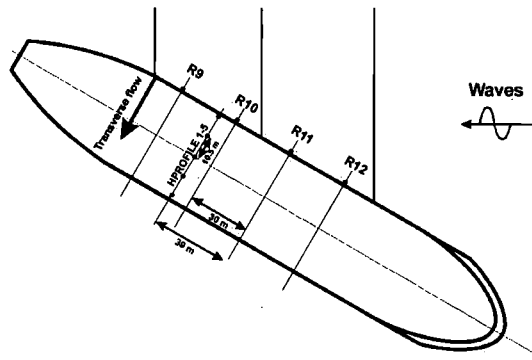


Figure D-1
Position of wave probes

The following measurements were carried out:

Table D-2
Overview of instrumentation and measurements during the tests

Name	Description	Unit
R9-R12	Vertical wave resistance probes around the ship	m
Hprofile1-5	Vertical wave resistance probes at the deck	m
Angular motions	Gyroscope	degrees
Translations	Optical tracking system	m

D.3 Basin set-up

The mooring system consisted of four linear springs, which gave the mooring system a stiffness of approximately 430 kN/m in the x-direction. This is a realistic stiffness for a mooring system in the applied water depth of 150 m.

The mooring system was rotated to achieve headings of 195 and 210 degrees (wave 15 and 30 degrees off the bow)

D.4 Environmental conditions

Tests were carried out in regular waves as well as in irregular wave spectra ($H_s=13.5$ m, $T_p=12, 14$ and 16 s). The JONSWAP spectral shape was used with $\gamma=3.3$.

REFERENCES

- Adegeest, L.J.M.: 1995**, *Non-linear Hull Girder Loads in Ships*, PhD thesis, Delft University of Technology.
- Andrew, R.N. and Lloyd, A.J.R.M.: 1980**, Full-scale Comparative Measurements of the Behaviour of Two Frigates in Severe Head Waves, *Transactions RINA 1981*.
- Arhan, M.K. and Plaisted, R.O.: 1981**, Non-linear Deformation of Sea-Wave Profiles in Intermediate and Shallow water, *Oceanologica Acta 1981*, Volume 4, No. 2, pp 107-115.
- Bagnold, R.A.: 1939**, Interim Report on Wave-Pressure Research, *Journal of ICE*.
- Bales, N.K.: 1979**, Minimum Freeboard Requirements for Dry Foredecks: A Design Procedure, *STAR Symposium SNAME*.
- Beck, F.R. and Loken, A.E.: 1989**, Three-dimensional Effects in Ship Relative-Motion Problems, *Journal of Ship Research*, Volume 33, No. 4, pp 261-268.
- Beynet, Pierre: 1994**, Personal communication on vane type breakwater.
- Blok, J.J. and Huisman, J.: 1984**, Relative Motions and Swell-Up for a Frigate Bow, *Transactions RINA*.
- Buchner, B.: 1994**, On the Effect of Green Water Impacts on Ship Safety (A Pilot Study), *Nav'94 Conference*, Rome.
- Buchner, B.: 1995a**, The Impact of Green Water on FPSO Design, *OTC paper 7698*, OTC 1995, Houston.

- Buchner, B.: 1995b**, On the Impact of Green Water Loading on Ship and Offshore Unit Design, *PRADS '95*, Seoul.
- Buchner, B.: 1996**, The Influence of the Bow Shape of FPSOs on Drift Forces and Green Water, *OTC paper 8073*, OTC 1996, Houston.
- Buchner, B. and Cozijn, J.L.: 1997**, An Investigation into the Numerical Simulation of Green Water, *BOSS'97*, Delft.
- Buchner, B. and Ballegoyen, G. van: 1997**, Joint Industry Project: F(P)SO Green Water Loading, Volumes A, B and C, *MARIN report No. 13644-1-ZT*, Wageningen.
- Buchner, B.: 1998**, A New Method for the Prediction of Non-Linear Relative Wave Motions", *OMAE98*, Lisbon.
- Buchner, B.: 1999**, Green Water from the Side of a Weathervaning FPSO, *OMAE'99*, St. Johns.
- Buchner, B. and Voogt, A.J.: 2000**, The Effect of Bow Flare Angle on FPSO Green Water Loading, *OMAE2000*, New Orleans.
- Buchner, B., Bunnik, T.H.J., Fekken, G. and Veldman, A.E.P.: 2001**, A Numerical Study on Wave Run Up on an FPSO Bow, *OMAE2001*, Rio de Janeiro.
- Buchner, B., Voogt, A.J., Duggal, A.S. and Heyl, C.N.: 2002**, Green Water Evaluation for FPSOs in the GoM, *OTC*, Houston.
- Cozijn, J.L.: 1995**, *Development of a Calculation Tool for Green Water Simulation*, Master's thesis, Delft University of Technology/MARIN.
- Cumberbatch, E.: 1960**, The Impact of a Water Wedge on a Wall, *Journal of Fluid Mechanics*, Vol. 7.
- Daalen, E.F.G. van: 1993**, *Numerical and Theoretical Studies of Water Waves and Floating Bodies*, PhD thesis, University of Twente.
- Dallinga, R.P. and Gaillarde, G.: 2001**, Hatch Cover Loads Experienced by M.V. Derbyshire during Typhoon Orchid, *International Workshop on Safety of Bulkcarriers*, Glasgow.

- Dillingham, J.:** 1981, Motions Studies of a Vessel with Water on Deck, *Marine Technology*, Vol. 18, No. 1.
- Drake, K.R.:** 2000, Transient Design Waves for Green Water Loading on Bulk Carriers, *Transactions of RINA*, Part C, pp 217-229.
- Drake, K.R.:** 2001, Wave Profile Characterisation of Green Water Loading Events from Model Test Data, *Applied Ocean Research*, 23, pp 187-193.
- Ersdal, G. and Kvitrud, A.:** 2000, Green Water on Norwegian Production Ships, *ISOPE2000*, Seattle.
- Faulkner, D.:** 2001, Survival Design of Cargo Hatch Structures, *RINA Conference Design and Operation for Abnormal Conditions II*, London.
- Fekken, G.:** 1998, *Numerical Simulation of Green Water Loading on the Foredeck of a Ship*, Master's thesis, RuG.
- Fekken, G., Veldman, A.E.P. and Buchner, B.:** 1999, Simulation of Green Water Flow Using the Navier-Stokes Equations, *Seventh International Conference on Numerical Ship Hydromechanics*, Nantes.
- Fukuda, J., Ikegami, K. and Mori, T.:** 1973, Predicting the Long Term Trends of Loads on Deck due to Shipping Water, *Journal of the West Japan Society of Naval Architects*, No. 45.
- Gerrits, J.:** 1996, *Three-dimensional Liquid Sloshing in Complex Geometries*, Master's thesis, RuG.
- Gerrits, J.:** 2001, *Dynamics of Liquid-Filled Spacecraft, Numerical Simulation of Coupled Solid-Liquid Dynamics*, PhD thesis, RuG.
- Gerrits, J., Loots, G.E., Fekken, G. and Veldman, A.E.P.:** 1999, Liquid Sloshing on Earth and in Space, *In: Moving Boundaries V* (B. Sarler, C.A. Brebbia and H. Power Eds.) WIT Press, Southampton, pp 111-120.
- Glimm, J.:** 1965, Solutions in the Large for Nonlinear Hyperbolic Systems of Equations, *Communications on Pure and Applied Mathematics*, Vol. XVIII, pp 697-715.
- Goda, K., Miyamoto, T. and Yamamoto, Y.:** 1976, A Study of Shipping Water Pressure on Deck by Two Dimensional Ship Model Test, *JSNA Japan*, Vol. 140.

- Greco, M., Faltinsen, O.M. and Landrini, M.: 2000**, A Parametric Study of Water on Deck Phenomena, *Nav2000*.
- Greco, M., Faltinsen, O.M. and Landrini, M.: 2000**, Basic Studies of Water on Deck, *23rd Symposium on Naval Hydrodynamics*, Val de Reuil.
- Greco, M., Faltinsen, O.M. and Landrini, M.: 2001**, Green Water Loading on a FPSO, *OMAE2001*, Rio de Janeiro.
- Gu, M., Miao, Q. and Gu, M.: 1993**, Prediction of Relative Motion and Deck Wetness Around Ship Bow, *Shipbuilding in China*, 1 (in Chinese).
- Hamoudi, B. and Varyani, K.S.: 1994**, Load Prediction due to Green Water on Deck Mounted Equipment for Floating Bodies, *CADMO'94*.
- Hansen, H.J.: 1972**, Über die Vorhersage von Deckbelastungen durch Grünes Wasser, *Schiff & Hafen* 24.
- Hellan, Ø., Hermunstad, O.A. and Stansberg, C.T.: 2001**, Design Tool for Green Sea, Wave Impact, and Structural Response on Bow and Deck Structures, OTC 13213, *OTC2001*, Houston.
- Hirt, C.W. and Nichols, B.D.: 1981**, Volume of Fluid (VOF) Method for the Dynamics of Free Boundaries, *Journal of Computational Physics*, 39, pp 201-225.
- Hoffman, D. and Maclean, W.M.: 1970**, Ship Model Study of Incidence of Shipping Water Forward, *Marine Technology*.
- Hong, S.Y., Lee, P.M. and Gong, D.S.: 1993**, Experimental Study on the Deck Wetting of a Container Ship in Irregular Head Waves, *Selected Papers of the Society of Naval Architects of Korea*, Volume 1, No. 1, pp 37-44.
- Huang, Z. and Hsiung, C-C.: 1996**, Nonlinear Shallow-Water Flow on Deck, *Journal of Ship Research*, Vol. 40, No. 4, pp 303-315.
- Huijsmans, R.H.M. and Dallinga, R.P.: 1983**, Non-linear Ship Motions in Shallow Water, *International Workshop on Ship and Platform Motions*, Berkeley.
- ISSC Committee II3 Report: 1979**, *Impacts From Liquid Cargo Sloshing*.
- Kawakami, M.: 1969**, On the Impact Strength of Ship due to Shipping Green Seas, *JSNA Japan*, Vol. 125.

-
- Kawakami, M. and Tanaka, K.: 1975**, On Shipping of Green Seas and Whipping Vibrations of a Large Full Ship, *Transactions of the West Japan Society of Naval Architects*, No. 50.
- Kawakami, M. and Tanaka, K.: 1977**, Stochastic Prediction of Impact Pressure due to Shipping Green Sea on Fore Deck of Ship, *Transactions of the West Japan Society of Naval Architects*, No. 53.
- Kriebel, D.L. and Dawson, T. H.: 1993**, Nonlinearity in Wave Crest Statistics, *2nd Int. Symposium on Ocean Wave Measurement and Analysis*, 6175.
- Lloyd, A.J.R.M.: 1983**, Deck Wetness Experiments, *20th American Towing Tank Conference*, Hoboken, New Jersey.
- Lloyd, A.J.R.M., Salsich, J.O. and Zselezky, J.J.: 1985**, The Effect of Bow Shape on Deck Wetness in Head Seas, *RINA*.
- Longuet-Higgins, M.S.: 1952**, On the Statistical Distribution of the Height of Sea Waves, *Journal of Marine Research*, Number 3.
- Longuet-Higgins, M.S.**, The Effect of Non-linearities on Statistical Distributions in the Theory of Sea Waves, *Journal of Fluid Mechanics*, Volume 17, pp 459-480.
- Loots, G.E.: 1998**, *Free Surface Flow in 3D Complex Geometries Using Enhanced Boundary Treatment*, Master's thesis, RuG.
- Maskew, B., Wang, M.L. and Troesch, A.W.: 1994**, Comparison of Calculated and Measured Loads on a Flared Body oscillating in a Free Surface, *20th Symposium on Naval Hydromechanics*, Santa Barbara.
- Maskew, B., Wang, M.L. and Troesch, A.W.: 1996**, Comparison of Two Different Mixed Eulerian-Lagrangian Schemes based on a Study of Flare-Slamming Hydrodynamics, *Transaction of ASME*, Volume 118, pp 174-183.
- Meskers, G.: 2002**, *Realistic Inflow Conditions for Numerical Simulation of Green Water Loading*, Master's thesis, Delft University of Technology/MARIN.
- Mizoguchi, S.: 1988**, Analysis of Shipping Water with the Experiments and the Numerical Calculations, *JSNA*, Japan, Volume 163.
- Mizoguchi, S.: 1989**, Design of Freeboard Height with the Numerical Simulation on the Shipping Water, *PRADS' 89*.

- Morris, W.D.M., Millar, J. and Buchner, B.: 2000**, Green Water Susceptibility of North Sea FPSO/FSUs, *15th Conference on Floating Production Systems (FPS)*, London.
- Nagai, S.: 1960**, Shock Pressures Exerted by Breaking Waves on Breakwaters, *Journal of the Waterways and Harbours Division*.
- Newton, R.N.: 1959**, Wetness Related to Freeboard and Flare, *Summer Meeting RINA*, Paper No. 3.
- Ochi, M.K.: 1964**, Extreme Behaviour of a Ship in Rough Seas Slamming and Shipping of Green Water, *Annual Meeting SNAME*.
- O'Dea, J.F. and Walden, D.A.: 1984**, The Effect of Bow Shape and Nonlinearities on the Prediction of Large Amplitude Motions and Deck Wetness, *15th Symposium on Naval Hydrodynamics*.
- Ogawa, Y., Taguchi, H. and Ishida, S.: 1998**, A Prediction Method for the Shipping Water Height and its Load on Deck, *PRADS'98*, The Hague.
- Oortmerssen, G. van: 1973**, *The Motions of a Moored Ship in Waves*, PhD thesis, Delft University of Technology, MARIN Publication No. 510.
- Ortloff, C.R. and Krafft, M.J.: 1997**, Numerical Test Tank: Simulation of Ocean Engineering Problems by Computational Fluid Dynamics, *OTC 8269*, OTC 1997, Houston.
- Pantazopoulos, M.S.: 1988**, Three Dimensional Sloshing of Water on Decks, *Marine Technology*, Vol. 25, No. 4.
- Pastoor, L.W.: 2002**, *On the Assessment of Nonlinear Ship Motions and Loads*, PhD thesis, Delft University of Technology.
- Pinkster, J.A.: 1980**, *Low Frequency Second Order Wave Exciting Forces on Floating Structures*, PhD thesis, MARIN Publication No. 600.
- Romate, J.E.: 1989**, *The Numerical Simulation of Nonlinear Gravity Waves in Three Dimensions using a Higher Order Panel Method*, PhD thesis, University of Twente.
- SNAME Panel HS2 'Impact Loading and Response': 1993**, Notes on Ship Slamming, *Technical and Research Bulletin 230*, SNAME.

- SNAME Panel HS1 'Hull Loadings': 1975**, Dynamic Slosh Induced Loads on Liquid Cargo Tank Bulkheads, *Technical and Research Bulletin R19*, SNAME.
- Song, W. and Maruo, H.: 1993**, Bow Impact and Deck Wetness: Simulations based on Nonlinear Slender Body Theory, *ISOPE93*, Singapore.
- Suhara, T., Hiyama, H. and Koga, Y.: 1973**, Shock Pressure due to Impact of Water Jet and Response of Elastic Plates, *Trans. of the West Japan Society of Naval Arch.*, No. 46.
- Stansberg, C.T. and Karlsen, S.I.: 2001**, Green Sea and Water Impact on FPSO in Steep Random Waves, *PRADS2001*, Shanghai.
- Stansberg, C.T., Hellan, Ø., Hoff, J.R. and Moe, V.: 2002**, Green Sea and Water Impact: Numerical Predictions Validated Against Model Tests, OMAE2002-28562, *OMAE2002*, Oslo.
- Stoker, J.J.: 1957**, *Water Waves, The Mathematical Theory With Applications*, Interscience Publishers.
- Tagaki, K. and Niimi, A.: 1990**, A Theoretical Approach to Bow Deck Wetness of a High-speed Ship, *Journal of Ship Research*, Vol. 34, No. 3.
- Takagi, K. and Naito, S.: 1993**, Deck Wetness and Influences of Above Water Hull Form at Bow, *J. Kansai Soc. N.A.*, Japan, No. 290 (in Japanese).
- Takaki, M. and Takaishi, Y.: 1993**, Development of Expression for Estimating Bow Freeboard and Assessment of the 1966 Load Line Convention, *Journal of the Society of Naval Architects Japan*, Vol. 174.
- Takezawa, S., Hagino, K., Kobayashi, K. and Sawada, K.: 1977**, On Deck Wetness and Impulsive Water Pressure acting on the Deck in Head Seas (in Japanese), *Journal of Zosen Kiokai*, SNAJ, Vol. 141.
- Tan, S.G.: 1969**, Observations Made on Board of Dutch Merchant Ships, *Int. Shipbuilding Progress*, Volume 16, No. 181, pp 259-276.
- Tasai, F.: 1961**, Wave Height at the Side of Two-Dimensional Body Oscillating on the Surface of a Fluid, *Report of the Research Institute for Applied Mechanics*, Kyushu University, Vol. 9, No. 35.

- Tasaki, R.: 1963**, On Shipment of Water in Head Waves, *Tenth ITTC*, London.
- Tayfun, M.A.**, Narrow Banded Nonlinear Waves, *Journal of Geophysical Research*, Vol. 85, No. C3, pp 1548-1552.
- Vermeer, H.: 1980**, Prediction of Amount of Shipping Water, *NMI Report R218*.
- Vestbøstad, T.M.: 1999**, Relative Wave Motions Along the Side of an FPSO Hull, *OMAE99*, St. Johns.
- Wang, Z., Juncher Jensen, J. and Xia, J.: 1998**, On the Effect of Green Water on Deck on the Wave Bending Moment, *PRADS'98*, The Hague.
- Wang, Z., Xia, J., Juncher Jensen, J. and Braathen, A.: 2000**, Prediction of Vertical-Plane Wave Loading and Ship Response in High Seas, *23rd Symposium on Naval Hydrodynamics*, Val de Reuil.
- Watanabe, I., Ueno, M. and Sawada, H.: 1989**, Effect of Bow Flare Shape to the Wave Loads of a Container Ship, *JSNA Japan*, Vol. 166.
- Watanabe, I.: 1990**, Remarks on Influence of Bow Flare Form on Deck Wetness, *Written discussion to the Seakeeping Committee Report of the 19th ITTC*.
- Westhuis, J.H.: 2001**, *The Numerical Simulation of Nonlinear Waves in a Hydrodynamic Model Test Basin*, PhD thesis, University of Twente.
- Zhou, Z.Q., De Kat, J.O. and Buchner, B.: 1999**, A Non-Linear 3-D Approach to Simulate Green Water on Deck, *Seventh International Conference on Numerical Ship Hydromechanics*, Nantes.

NOMENCLATURE

SEMI-EMPIRICAL DESIGN EVALUATION METHOD

A	= added mass or inertia
ar	= area in m^2
a	= fitting parameter
a_H	= coefficient in relation freeboard exceedance and water height on deck
a_u	= coefficient in relation freeboard exceedance and water velocity over deck
a_p	= coefficient in relation freeboard exceedance and pressure on structures
a_F	= coefficient in relation freeboard exceedance and global load on structures
a_s	= coefficient in expression for the pressure on different structural shapes
a_M	= coefficient in expression for the moment on different structural shapes
B	= damping
B_c	= critical damping
b	= fitting parameter
b_s	= coefficient in expression for the pressure on different structural shapes
b_M	= coefficient in expression for the moment on different structural shapes
C	= restoring term or spring stiffness
c	= fitting parameter
c_s	= coefficient in expression for the global load on different structural shapes
c_M	= coefficient in expression for the moment on different structural shapes
C_d	= drag coefficient
d	= fitting parameter
d_s	= coefficient in expression for the global load on different structural shapes
D	= diameter in m
e	= fitting parameter
FX	= global horizontal force in kN
F'	= force per metre length, breadth or height in kN/m
F''	= scaled breakwater load in kN
f	= fitting parameter
fb	= freeboard height from still waterline to top bulwark (if present) in m
g	= gravity (9.81 m/s^2)

H	=	water height on the deck in m
H_s	=	significant wave height in m
H_{10}	=	water height on deck at 10 m from fore perpendicular
h	=	exceedance of freeboard by relative motions in m
h'	=	initial height of dam before theoretical dam breaking problem
$H(\omega)$	=	Response Amplitude Operator (RAO)
hb	=	actual breakwater height in m
hb'	=	reference breakwater height in m (= 4.98 m)
I	=	force impulse per metre length, breadth or height in kNs/m
i	=	index
j	=	fitting parameter
k	=	fitting parameter
L	=	ship length in m
l	=	moment arm in m
m	=	mass in kg or t
M	=	moment in kNm
M''	=	scaled breakwater moment with respect to deck level in kNm
M_θ	=	wave exciting moment in kNm
M_g	=	green water moment in kNm
N	=	number of extremes
N_l	=	number of extremes based on T_l from linear calculations
N_n	=	number of extremes in non-linear calculations
o_a	=	amplitude of output signal
p	=	pressure in kPa (kN/m^2)
p_a	=	atmospheric pressure in kPa
p_{ref}	=	reference pressure on impact panel P1 in kPa
$p(r)$	=	probability of occurrence in percent/100
P	=	probability of exceedance in percent/100
$Q(\omega)$	=	quadratic transfer function for mean drift force in kN/m^2
r	=	relative wave motion in m
r'	=	relative wave velocity in m/s
r_0	=	relative wave motion due to ship motions and undisturbed wave in m
r_s	=	relative wave motion including dynamic swell-up in m
r_l	=	relative wave motion from linear theory in m
R	=	extreme value in relative motions in m
R_{MPM}	=	Most Probable Maximum value of relative motions in m
s	=	standard deviation
$S_\zeta(\omega)$	=	wave spectrum
$S_o(\omega)$	=	spectrum output signal

t	= time in s
T_p	= peak period of wave spectrum in s
T_1	= mean period of wave or output spectrum in s
u	= water (front) velocity in m/s
U	= current or water velocity in m/s
V	= entrance velocity for wedge entry in m/s
w	= vertical velocity of the deck (ship bound) in m/s
W	= width of water flow over deck in m
x	= longitudinal position or motion in m
y	= transverse position or motion in m
z	= vertical position or motion in m
α	= wedge angle in degrees, non-linearity parameter
β	= non-linearity parameter
γ	= bow flare angle with vertical in degrees (measured perpendicular to the fully loaded waterline for the full elliptical bow and transverse to the ship longitudinal for the triangular bow)
δ	= dynamic amplification
η	= multiplication factor for number of extremes
θ	= pitch angle
λ	= deep water wave length as function of current speed and frequency
μ	= scale factor
τ	= factor in expression for probability of exceedance
ρ	= density of seawater in t/m^3
ζ	= wave elevation in m
ζ_0	= undisturbed wave amplitude
ζ_i	= radiating waves due to the ship motions in the i -th degree of freedom
ζ_7	= reflected (diffracted) waves against the vessel hull
ζ_a	= undisturbed (first harmonic) wave amplitude in m
ζ^n	= n -th harmonic wave amplitude in m
ω	= wave frequency in rad/s
ω_n	= frequency of n -th harmonic amplitude in rad/s

NUMERICAL METHODS

a	= acceleration
G	= influence function
g	= gravitational acceleration
h	= cell width or height
ΔL	= panel length
n_{ξ}	= normal
\bar{x}	= collocation point position vector
\bar{R}	= combined convective, diffusive and body force vector
S	= surface
t	= time
Δt	= time step
\bar{u}	= velocity of fluid particle
u_n	= normal velocity of fluid particle
u_t	= tangential velocity of fluid particle
u	= velocity in x-direction
v	= velocity in y-direction
w	= velocity in z-direction
x	= x-position
y	= y-position
z	= z-position
λ	= water height on the deck
Φ	= potential
Ω	= fluid domain
$\bar{\xi}$	= source point position vector
ρ	= fluid density
∇	= gradient operator
σ	= surface tension
κ	= surface curvature
ρ	= density
p	= pressure
Δ	= Laplace operator
ν	= kinematic viscosity
τ	= tangential stress

ABBREVIATIONS

- FPSO = Floating Production Storage and Offloading unit
RAO = Response Amplitude Operator
MPM = Most Probable Maximum
SUC = Swell-Up Coefficient
COG = Centre of Gravity

SUMMARY

'Green Water on Ship-type Offshore Structures'

In heavy storms, the waves and ship motions can become so large that water flows onto the deck of a ship. This problem is generally known as 'green water loading'. On ship-type offshore structures green water loading can result in risk for the ship, its crew and its sensitive equipment. Therefore, it should be taken into account in the design of such structures.

Based on a historical overview of green water research it was concluded that there is limited insight in the physics of the complex green water problem, which results in a wide range of assumptions in prediction methods. Existing research was also not focussed on moored offshore structures in extreme environmental conditions ('100 year storms') and there is very limited insight in the loading process on structures on the deck. Finally, the important problem of green water loading from the side of the vessel has not been studied before. Therefore, the main objective of this study was to develop methods for the evaluation of green water on ship-type offshore structures based on a clear description of the green water physics.

To achieve this objective, first the physics of the green water process on the bow were studied using two series of initial model tests. Based on these tests this process was described in the following phases:

1. Motions and relative wave motions
2. Water flow onto the deck
3. Water behaviour and loading on the deck
4. Green water impact on structures

It was concluded that in all phases of the green water problem non-linear and highly complex phenomena occur. Consequently, the green water problem cannot be predicted with existing linear prediction methods. New numerical methods still need significant further development, integration and validation before they can be used to

predict the green water as a whole within a reasonable timeframe. Therefore, a semi-empirical design evaluation method was proposed, to predict the green water problem from the input (extreme relative wave motions) to the output (predicted load levels) based on a clear description of the green water physics.

This semi-empirical design evaluation method has been developed using a systematic series of model tests. The building blocks of the method and their relations are presented in detail in the thesis and based on the phases in the green water process. The problem of green water loading from the side of the ship is taken into account as well. The development of the method is completed with a review, together with recommendations for its application in relation with metocean (wind, wave and current) data and structural response analysis.

Finally, the numerical prediction of green water loading is discussed. A number of methods have been evaluated based on the specific requirements related to the physics of green water loading. A numerical method for the prediction of green water loading should be able to deal with:

- Water entry of a flared bow structure.
- Complex flow onto the deck, including the discontinuity at the deck edge.
- 'Hydraulic jump'-type shallow water flow on a moving ship deck.
- Meeting water flows on the deck.
- Short duration water impact on a structure.
- Overturning flow after run-up of the water in front of the structure.

The evaluation of a Modified-VOF (Volume Of Fluid) method based on these requirements has shown its ability to simulate the complex green water problem, although a number of numerical details need significant further development and validation. The description of the physics and the model test results presented in this thesis, can provide detailed validation material for this process.

Bas Buchner, November 2002
(*b.buchner@MARIN.NL*)

SAMENVATTING

'Groen Water op Scheepsvormige Offshore Constructies'

In zware stormen kunnen de golven en scheepsbewegingen zo groot worden dat water op het dek van het schip stroomt. Dit wordt in het algemeen het 'groen water' probleem genoemd. Op scheepsvormige offshore constructies is groen water een risico voor het schip, haar bemanning en haar hoogwaardige apparatuur. Het probleem moet daarom in het ontwerp van de constructie worden meegenomen.

Gebaseerd op een historisch overzicht van het groen water onderzoek is geconcludeerd dat er een beperkt inzicht is in de fysica van het complexe groen water probleem. Dit heeft geresulteerd in voorspellingsmethoden op basis van een ruime variatie van aannamen. Verder is het onderzoek tot nu toe niet gericht geweest op afgemeerde offshore constructies in extreme stormcondities ('100 jarige stormen') en is er weinig inzicht in het belastingsproces op constructies op het dek. Tot slot is het probleem van groen water vanaf de zijkant van het schip tot nu toe niet bestudeerd. Daarom was de hoofddoelstelling van deze studie: het ontwikkelen van evaluatiemethoden voor groen water belasting op scheepsvormige offshore constructies gebaseerd op een duidelijke beschrijving van de groen water fysica.

Om deze doelstelling te bereiken, wordt eerst de fysica van het groen water proces op de boeg bestudeerd op basis van twee series initiële modelproeven. Gebaseerd op deze proeven wordt het proces beschreven in de volgende procesfasen:

1. Bewegingen en relatieve golfbewegingen
2. Stroming op het dek
3. Gedrag en belasting van het water op het dek
4. Groen water belasting op constructies op het dek

Op basis hiervan wordt geconcludeerd dat in alle fasen van het groen water probleem niet-lineaire en sterk complexe verschijnselen voorkomen. Als gevolg hiervan kan het probleem niet worden voorspeld met bestaande lineaire berekeningsmethoden.

Nieuwe numerieke rekenmethoden moeten nog verder worden ontwikkeld, geïntegreerd en gevalideerd voordat ze het probleem als geheel kunnen voorspellen binnen een redelijke rekentijd. Daarom wordt een semi-empirische ontwerp evaluatiemethode gepresenteerd om het groen water probleem van begin (extreme relatieve golfbewegingen) tot eind (belastingniveaus op constructies) te voorspellen op basis van een duidelijke beschrijving van de groen water verschijnselen.

Deze semi-empirische ontwerp evaluatiemethode is ontwikkeld op basis van een systematische serie modelproeven. De bouwstenen van de methode en de relaties tussen de verschillende grootheden worden in detail gepresenteerd op basis van de verschillende fasen in het groen water proces. Ook het probleem van groen water over de zijkant van het schip wordt hierbij meegenomen. De ontwikkeling van de methode wordt afgesloten met een evaluatie, waarbij aanbevelingen worden gedaan voor het gebruik in relatie met de omgevingscondities (wind, golven en stroom) en voor de analyse van de dynamische reactie van constructies op groen water belastingen.

Tot slot wordt de numerieke voorspelling van groen water belasting besproken. Een aantal rekenmethodes is geëvalueerd op basis van de specifieke voorwaarden voor de beschrijving van het groen water probleem. Een numerieke methode voor de voorspelling van groen water moet de volgende aspecten kunnen beschrijven:

- Het in het water komen van een uitwaaiende boegvorm.
- Complexe stroming op het dek, inclusief de discontinuïteit van de scherpe dekrand.
- 'Hydraulische schok'-achtige ondiep water stromingen over een bewegend dek.
- Elkaar ontmoetende waterstromen op het dek.
- Kortdurende belastingen op een constructie.
- Overslaande stroming nadat het water tegen de voorkant van een constructie is omhoog gestroomd.

De evaluatie van een aangepaste-VOF (Volume Of Fluid) methode op basis van deze voorwaarden, heeft de mogelijkheden ervan voor het voorspellen van het complexe groen water probleem aangetoond. Wel is een significante verdere ontwikkeling en validatie van een aantal numerieke details van de methode noodzakelijk. De beschrijving van de fysica en de modelproef resultaten zoals gepresenteerd in dit proefschrift, kunnen dit proces van gedetailleerd validatie materiaal voorzien.

Bas Buchner, november 2002
(*b.buchner@MARIN.NL*)

ACKNOWLEDGEMENTS

Looking back, I wonder how it finally came to this thesis. In any case it is clear that it is not without the help and support of a lot of other people. Some of them I would like to thank here specifically.

First my father: for his love for ships, which he passed on to me without pushing. Our joint visit to the model basin at Delft University of Technology made the decision for me to become a Naval Architect. Both my parents always showed their interest in my study and work, which was really stimulating!

My first project at MARIN was directly related to the subject of this thesis: a study on the green water problem on S-class frigates of the Royal Netherlands Navy. But the real breakthrough came after a telephone call from Peter Poranski of (FMC) Sofec in 1993 with the simple question 'what do you know about green water?' My work on the 'Liuhua' FPSO as a result of that and Peter's continuous support for the investigations on the subject over the years were very important for me.

MARIN is acknowledged for funding the work and allowing me to publish the results as part of this thesis. I would like to thank Johan Wichers for strongly stimulating this research in the beginning, when the importance of the green water problem was not directly obvious to all in the offshore industry. At a later stage Peter Tan's reminders were a great help in making the decision to finally start writing the thesis itself. Gert van Ballegoyen was of real importance for the accurate data analysis of all model test results, resulting in almost a metre of data volumes.

The participants of the Joint Industry Project 'F(P)SO Green Water Loading' are acknowledged for their support of the research on this subject and the interesting discussions of the results: ABB Offshore Technology, Bluewater Engineering, BP, Chevron, Conoco, Exxon, FMC Sofec, Germanischer Lloyd, Health & Safety Executive in the UK (HSE), Maersk Contractors, Mobil, Samsung Heavy Industries, SBM, Gusto Engineering, Shell and Texaco.

Sverre Haver of Statoil Exploration and Production is acknowledged for his inspiring discussions on the subject of green water loading from the side during the green water investigations on the Norne FPSO.

The co-operation with the people of the University of Groningen (RuG) was very important for my personal development and the numerical part of the work. Professor Arthur Veldman has made it clear to me that numerical simulations are more than bookkeeping. I would like to thank him for his enthusiastic support for my work. Geert Fekken of RuG and Tim Bunnik of MARIN are really acknowledged for performing the actual simulations presented in this thesis.

The comments of my colleagues René Huijsmans and Geert Kapsenberg after reading earlier versions of this thesis are really appreciated and helped to improve the contents and structure of the final version. Ingrid Wolfs' critical eye on my English and the resulting suggestions were very useful and much appreciated (the remaining errors are all mine and put in afterwards). Liselotte van Zaanen and Mariëtte Drinóczy were indispensable in the final editing of this thesis and getting it printed.

I would like to thank my promotor Professor Jo Pinkster for the opportunity to write this thesis under his supervision. His support and stimulation in recent years were very important to finalise this 'project'.

Finally, I would like to thank my wife Hilda and my daughters Els, Heleen and Karen. They are for me like the brave fisherman's women on the cover of this thesis: supporting from the shore their man in the storm! Hilda supported the idea of writing this thesis (and me) from the beginning to the end. For both of us the work had in any case one advantage: the nice lunches at home together for some time! The girls are thanked for their time and patience, but also for their support to get the job done. "Haven't you finished yet?" I just heard.

CURRICULUM VITAE

Bas Buchner was born on November 29, 1966 in Sliedrecht (The Netherlands). He attended the Atheneum of the 'Gereformeerde Scholengemeenschap Rotterdam' (GSR) from 1979 to 1985. In 1985 took up the study of Naval Architecture at Delft University of Technology. He completed this in 1991 with a study on the 'Evaluation of the shallow draft diffraction theory', performed in a co-operation between Delft University of Technology (Hydrodynamics, Prof. dr. ir. J.A. Pinkster) and Marine Structure Consultants (MSC, ir. J.A. van Santen). After obtaining his Master's degree, he joined the offshore research department of the Maritime Research Institute Netherlands (MARIN) in 1991. At present he is Manager Offshore of MARIN.

